THE PHYSICS OF METALS AND METALLOGRAPHY

FIZIKA METALLOV I METALLOVEDENIE

VOLUME 5 No. 3 1957

CONTENTS

	PAGE
Thermodynamics of Irreversible Polarization Processes in Magneto-Elastic Media, Part II K. B. VLASOV	1
Calculation of the X-Ray Emission Spectrum Structure of Ordered-Solution-Forming Alloys A. N. ORLOV and A. V. SOKOLOV	7
Excited States of an Atomic Semiconductor in the Many-Electron Model S. V. VONSOVSKII and A. N. KUSHNIRENKO	12
The Criterion of the Semi-Metallic State of Matter, According to the Many-Electron Theory E. N. AGAFONOVA and N. P. KONTOROVICH	20
Theory of Galvanomagnetic Phenomena in Metals F. G. BASS, M. I. KAGANOV and V. V. SLEZOV	24
Magnetic Properties of Magnetically Anisotropic Specimens made from Ferromagnetic Powders—I. Magnetization Curves and Individual Hysteresis Loop Cycles E. V. SHTOL'TS, YA. S. SHUR and G. S. KANDAUROVA	31
Magnetic Properties of Magnetically Anisotropic Specimens made from Ferromagnetic Powders—II. Dependence of Magnetization Curves on the Method used for bringing about a Demagnetized State YA. S. SHUR, E. V. SHTOL'TS and G. S. KANDAUROVA	38
Effect of Annealing Regime on the Thermomagnetic Ageing of Permanent Magnets from the Alloy Magnico A. M. MOROZOVA and F. I. FEIGINA	44
X-ray Structure Investigation of Metals after Electric Spark Treatment K. F. STARODUBOV and B. P. KOLESNIK	49
Research on the Detection of Railway Line Defects in Moving Magnetic Fields—1. Some of the Problems of Electromagnetic Detection of Rail Defects V. V. VLASOV	56
The α—β Transformation in Zirconium from Electron Field Emission Observations A. P. KOMAR and V. N. SHREDNIK	65
Study of the Physical Factors Determining the Hardening of Alloyed Iron V. M. GOLUBKOV, V. A. IL'INA, V. K. KRITSKAIA, G. V. KURYUMOV and M. D. PERKAS	77
Calculation of Diagrams of True Stresses of a Cold-Hardened Metal G. P. ZAITSEV	93
The Effect of Frozen-in Strains of the Crystal Lattice on the Mechanical Properties of Alloys of Aluminium with Magnesium—I. Dependence of the Yield Strength and Tensile Strength on the Temperature and Rate of Deformation A. V. GRIN, V. A. PAVLOV and I. A. PERETURINA	101
Effect of Magnesium on the Mechanism of Plastic Deformation of Alumino-Magnesium Alloys V. I. SYUTKINA and E. S. YAKOVLEVA	108
The Effect of Phase Transformation in a Solid Solution on Plastic Deformation—1. "Uniform" Deformation N. F. SIUTKIN	116
On the Acceleration of the Ageing Process in Alloys of Aluminium with Magnesium under the Influence of Small Admixtures of Silver and Zinc. On the Question of the Causes of the Effects of Small Admixtures on the Kinetics of the Ageing of Alloys III V. I. ARKHAROV, I. P. BERENOVA and L. M. MAGAT	123

[*Continued inside back cover*]

Printed in Great Britain by The Compton Printing Works (London) Ltd.

VOL. 5 1957

FIZIKA METALLOV I METALLOVEDENIE

Chief Editor:
S. V. VONSOVSKII

Deputy Chief Editor:
V. I. ARKHAROV

EDITORIAL BOARD:

A. F. IOFFE
S. T. KONOBEEVSKII
V. D. KUZNETSOV
G. V. KURDYUMOV
B. G. LAZAREV
V. A. PAVLOV
YU. B. RUMER
V. D. SADOVSKII
I. G. FAKIDOV
YA. S. SHUR

VOLUME 5 No. 3 **CONTENTS**—*Continued* 1957

PAGE

Study of the Properties and Structure of Invar Alloys Alloyed with Molybdenum, Chromium and Niobium — A. Z. IVANUSHKINA and B. G. LIVSHITS — 134

Excess Vacancies in an Electrolytic Metal — YA. E. GEGUZIN — 142

Letters to the Editor

Contribution to the Theory of Surface Tension in Liquid Metals — P. S. ZYRIANOV — 149

On the Theory of Excitonic Dispersion and Light Absorption — V. I. CHEREPANOV and V. S. GALISHEV — 152

Contribution to Spin Wave Statistics — M. S. SVIRSKII and B. KH. ISHMUKHAMETOV — 154

Theory of Stark Effect in Excitons. Part 1 — G. G. TALUTS and S. A. SHULYATEV — 157

The *S-D* Exchange Model of Transition Metals — A. A. BERDYSHEV and IU. A. IZIUMOV — 159

The Effect of Short Range Order on the Electrical Resistance of Alloys in the State of Ordering — A. F. POLESIA and B. N. FINKELSHTEIN — 162

On Determination of the Ponderomotive Force of Interaction Between Magnet and a Ferromagnetic Material — V. L. SHMARTS — 165

The Effect of Pressure on the Young's Modulus of Certain Metals — A. D. EKHLAKOV, V. A. GLADKOVSKII and K. P. RODIONOV — 169

The Thermodynamics of the Ferromagnetic State at Low Temperatures — M. I. KAGANOV and V. M. TSUKERNIK — 172

On the Nature of Expansion of Cast Iron Castings Prior to Final Contraction — V. P. CHERNOBROVKIN — 175

The Diffusion of Silicon in Transition Metals — G. V. SAMSONOV and L. A. SOLONNIKOVA — 177

The Nature of Etch-Figures in an Ageing Al-Zn-Cu Alloy — N. N. BUINOV and T. V. SHCHEGOLEVA — 180

ERRATA — 182

VOL
5
195

VOL.
5
1957

VOL
5
195

THERMODYNAMICS OF IRREVERSIBLE POLARIZATION PROCESSES IN MAGNETO-ELASTIC MEDIA, Part II *

K.B. VLASOV
Institute of Metal Physics Urals Filial, Academy of Sciences, SSSR
(Received 27 June 1957)

As has been shown by Viswanathan [1, 2] and Laval [2], on the basis of calculations based on microscopic observation of crystal lattices, the mechanical stress tensor σ_{ij} is non-symmetrical in the general case, and the elastic properties of crystalline media of minimum symmetry are defined not by 21 constants, but by 45. According to [1], the potential energy of an elastic medium is equal to $2U = d'_{ijkl}\, u_{ij}\, u_{kl}$ where $u_{ij} = \partial u_i/\partial u_j$ and u_i are components of the displacement vector. For the constants d'_{ijkl}, in the general case, there is only the following relationship: $d'_{ijkl} = d'_{klij}$. For quasi-statistical equilibrium processes, the mechanical stress tensor σ_{ij}, according to [1], is connected with U_{kl} by the relationship

$$\sigma_{ij} = \frac{\partial U}{\partial u_{ij}} = d'_{ijkl}\, u_{kl}\ .$$

VOL. 5 1957

In the case when an elastic medium also possesses magnetic and magneto-mechanical properties, it will be characterized, for reversible processes by the following equations of state (for the case when the difference between $h_{ij,m}$ and $h^*_{n,kl}$ is neglected, [4]):

$$\begin{aligned} \sigma_{ij} &= d'_{ijkl}\, u_{kl} + h'_{ij,m} I_m, \\ H_n &= h'_{n,kl}\, u_{kl} + \gamma'_{nm}\, I_m, \end{aligned} \tag{1}$$

where H_n and I_n are components of the vectors of magnetic field intensity and magnetization respectively.

With non-equilibrium processes [5], for the case where the deviation of the system from the initial state is small and determined only by I_m and u_{ij}, the following relationship holds:

$$\begin{aligned} I_m &= L_{mn}(H_n - \overline{H}_n) + L_{m,\,ij}(\sigma_{ij} - \overline{\sigma}_{ij}), \\ u_{kl} &= L_{kl,\,n}(H_n - \overline{H}_n) + L_{klij}(\sigma_{ij} - \overline{\sigma}_{ij}), \end{aligned} \tag{2}$$

where H_n and σ_{ij} are the magnetic field intensity and the mechanical stress respectively, and $\overline{H}_n$, $\overline{\sigma}_{ij}$ are determined from equation (1).

Consider as an example an isotropic magneto-elastic medium, polarized in the initial condition by magnetic field H_0 (i.e. with polarization magnetization I_0), directed along the z axis. For this case the Onsager relationship for the kinetic coefficients takes the form [6]:

---

* *Fiz. metal. metalloved.* 5, No. 3, 385-389, 1957.

$$L_{mn}(H_0) = L_{nm}(-H_0);\ L_{m,ij}(H_0) = -L_{ij,m}(-H_0);$$
$$L_{ijkl}(H_0) = L_{klij}(-H_0). \tag{3}$$

Moreover, equation (1) must be invariant with respect to the operation of rotation about an axis parallel to the polarization magnetization, through any angle $L_\infty^{\parallel}$ and to the operation $RL_2^{\perp}$, where operation R denotes a reversal in direction of the magnetic field intensity and magnetization vectors, and a change in sign of time [6] and $L_2^{\perp}$ a 180° rotation about an axis perpendicular to the polarization magnetization. In contrast to equations (1), equations (2) remain invariant only with respect to operation $L_\infty^{\parallel}$. As a result of taking into account (3), together with considerations of symmetry, we find that the following constants differ from zero:

$$L_{22} = L_{11};\ L_{33};\ L_{21} = -L_{12}.$$
$$L_{2,13} = -L_{13,2} = L_{23,1} = -L_{1,23};\ L_{2,31} = -L_{31,2} = L_{32,1} = -L_{1,32}.$$
$$L_{3,21} = -L_{21,3} = L_{12,3} = -L_{3,12};\ L_{3,22} = L_{22,3} = L_{11,3} = L_{3,11}$$
$$L_{33,3} = L_{3,33};\ L_{2,32} = L_{32,2} = L_{31,1} = L_{1,31};\ L_{2,23} = L_{23,2} = L_{13,1} = L_{1,13};$$
$$L_{2222} = L_{1111};\ L_{3333};\ L_{2211} = L_{1122};\ L_{2233} = L_{3322} = L_{3311} = L_{1133};$$
$$L_{1313} = L_{2323};\ L_{3131} = L_{3232};\ L_{3113} = L_{1331} = L_{3223} = L_{2332};$$
$$L_{2121} = L_{1212};\ L_{2112} = L_{1221};\ L_{2221} = -L_{2122} = L_{1211} = -L_{1112};$$
$$L_{2212} = -L_{1222} = L_{2111} = -L_{1121};\ L_{3321} = -L_{2133} = L_{1233} = -L_{3312};$$
$$L_{1332} = -L_{3213} = L_{3123} = -L_{2331};\ L_{1323} = -L_{2313};\ L_{3132} = -L_{3231}; \tag{4}$$

whilst:

$$L_{1221} = L_{1111} - L_{1122} - L_{1212}.$$

It also follows from considerations of symmetry that constants of the type:

$$L_{11};\ L_{33};\ L_{1,23};\ L_{1,32};\ L_{3,12};\ L_{1111};\ L_{3333};\ L_{1122};\ L_{1133};$$
$$L_{2323};\ L_{3232};\ L_{2332};\ L_{1212} \text{ и } L_{1221}$$

are even functions of H_0 (or I_0) and are not zero when $H_0 = 0$ (or $I_0 = 0$). In fact:

$$L_{33}(0) = L_{11}(0);\ L_{1,23}(0) = -L_{1,32}(0) = L_{3,12}(0)$$
$$L_{3333}(0) = L_{1111}(0);\ L_{1133}(0) = L_{1122}(0);\ L_{3232}(0) = L_{2323}(0) =$$
$$= L_{1212}(0);\ L_{2332}(0) = L_{1221}(0). \tag{5}$$

The constants of type L_{12}; $L_{3,11}$; $L_{3,33}$; $L_{1,31}$; $L_{1,13}$; L_{1112}; L_{1121}; L_{3312}; L_{2331}; L_{2313} and L_{3231} are odd functions of H_0 (or I_0) and are zero when $H_0 = 0$ (or $I_0 = 0$). For the constants γ'_{nm}; $h'_{n,kl}$; $h'_{ij,m}$

and d'_{ijkl} the same relationships are valid, as are the same conclusions regarding the nature of their dependence on H_0 (or I_0), as for the corresponding constants l_{mn}; $L_{m,ij}$; $L_{kl,n}$ and L_{ijkl}, with the exception that constants of the type γ'_{12}; $h_{1,23}$; $h'_{1,32}$; $h'_{3,12}$; d'_{1112}; d'_{1121}; d'_{3312}; d'_{2331}; d'_{2313} and d'_{3231} are equal to zero.

Solving the set of equations (2), taking (1) into account with regard to H_m and σ_{kl} and assuming that I_n and u_{ij} vary periodically in time with angular frequency ω, we obtain the following system of equations:

$$\begin{aligned} H_m &= \gamma_{mn} I_n + h_{m,ij} u_{ij} \\ \sigma_{kl} &= h_{kl,n} I_n + d_{klij} u_{ij}, \end{aligned} \tag{6}$$

where constants γ_{mn}; $h_{m,ij}$; $h_{kl,n}$ and d_{klij} are already complex magnitudes. For them the same relationships are valid as those in (4) for the constants:

$$L_{mn};\ L_{m,ij};\ L_{kl,n} \text{ and } L_{klij}\ .$$

VOL. 5 1957

The strain and rotation tensors are introduced according to the known formulae:

$$\varepsilon_g = \frac{1}{2}(u_{ij} + u_{ji}) \text{ and } \omega_q = \frac{1}{2}(u_{ij} - u_{ji}).$$

Moreover, taking into account the fact that the stress tensor σ_{ij}, as can be seen from equations (6) and the relationships between the components of constants γ_{mn}; $h_{m,ij}$; $h_{kl,n}$ and d_{ijkl}, is non-symmetric * we convert it into symmetric and anti-symmetric parts of the stress tensor (the latter gives the moment of the force acting on unit volume):

$$\sigma_f = \frac{1}{2}(\sigma_{kl} + \sigma_{lk});\quad T_p = \frac{1}{2}(\sigma_{kl} - \sigma_{lk}).$$

Indices f and g take the values 1, 2 ...., 6, whilst for example,

$$\varepsilon_1 = u_{11},\ \ldots,\ \varepsilon_6 = \frac{1}{2}\quad (u_{12} + u_{21}),$$

and indices p and q take the values 4, 5 and 6, whilst, for example,

$$\omega_4 = \frac{1}{2}(u_{23} - u_{32}),\ \ldots.\ T_6 = \frac{1}{2}(\sigma_{12} - \sigma_{21}).$$

As a result we obtain the following system of equations:

---

* The non-symmetric nature of tensor σ_{ij} in a magnetic medium was also pointed out in private conversation by N.N. Andreev.

$$H_m = \gamma_{mn} I_n + h_{mg} \varepsilon_g + \overset{\bullet}{h}_{mq} \omega_q ,$$
$$\sigma_f = h'_{fn} I_n + c_{fg} \varepsilon_g + \overset{\bullet}{c}_{fq} \omega_q , \tag{7}$$
$$T_p = \overset{\bullet\prime}{h}_{pn} I_n + \overset{\bullet\prime}{c}_{pg} \varepsilon_g + \overset{\bullet\bullet}{c}_{pq} \omega_q ,$$

where

$$\gamma_{11} = \gamma_{22} = \gamma'_{11} + i\omega\gamma''_{11};\ \gamma_{33} = \gamma'_{33} + i\omega\gamma''_{33};\ h_{33} = h'_{33} = h'_{3,33} + i\omega h''_{3,33};$$
$$h_{31} = h_{32} = h'_{13} = h'_{23} = h'_{3\ 11} + i\omega h''_{3,11};\ h_{15} = h_{24} = h'_{51} = h'_{42} =$$
$$= \frac{1}{2}(h'_{1,31} + h'_{1,13}) + \frac{1}{2} i\omega (h''_{1,31} + h''_{1,13});$$
$$c_{11} = c_{22} = d'_{1111} + i\omega d''_{1111};\ c_{12} = c_{21} = d'_{1122} + i\omega d''_{1122};\ c_{13} =$$
$$= c_{23} = c_{31} = c_{32} = d'_{1133} + i\omega d''_{1133};$$
$$c_{33} = d'_{3333} + i\omega d''_{3333};\ c_{44} = c_{55} = \frac{1}{4}(d'_{2323} + d'_{3232} + 2d'_{2332}) +$$
$$+ \frac{1}{4} i\omega (d''_{2323} + d''_{3232} + 2d''_{2332});$$

$$c_{66} = \frac{1}{2}(c_{11} - c_{12}); \tag{8}$$

$$\overset{\bullet}{c}_{44} = -\overset{\bullet}{c}_{55} = \overset{\bullet\prime}{c}_{44} = -\overset{\bullet\prime}{c}_{55} = \frac{1}{4}(d'_{2323} - d'_{3232}) + \frac{1}{4} i\omega (d''_{2323} - d''_{3232});$$
$$\overset{\bullet\bullet}{c}_{44} = \overset{\bullet\bullet}{c}_{55} = \frac{1}{4}(d'_{2323} + d'_{3232} - 2d'_{2332}) + \frac{1}{4} i\omega (d''_{2323} + d''_{3232} - 2d''_{2332}); \tag{9}$$
$$\overset{\bullet\bullet}{c}_{66} = d'_{1212} + i\omega d''_{1212} - c_{66};$$

$$h_{15} = -h_{24} = \overset{\bullet}{h}_{51} = -\overset{\bullet}{h}_{42} = \frac{1}{2}(h'_{1,31} - h'_{1,13}) + \frac{1}{2} i\omega (h''_{1,31} - h''_{1,13}). \tag{10}$$

$$\gamma_{12} = -\gamma_{21} = i\omega\gamma''_{12} \tag{11}$$

$$h_{14} = -h_{25} = -h'_{41} = h'_{52} = \frac{1}{2} i\omega (h''_{1,23} + h''_{1,32}),$$
$$\overset{\bullet}{h}_{14} = \overset{\bullet}{h}_{25} = -\overset{\bullet\prime}{h}_{41} = -\overset{\bullet\prime}{h}_{52} = \frac{1}{2} i\omega (h''_{1,23} - h''_{1,32}), \tag{12}$$

$$h^{\cdot}_{36} = -h^{\cdot\cdot}_{63} = i\omega h^{\cdot}_{3,12}$$

$$c_{16} = -c_{26} = -c_{61} = c_{62} = \frac{1}{2}\, i\omega (d^{\cdot}_{1112} + d^{\cdot}_{1121})$$

$$c^{\cdot}_{16} = c^{\cdot}_{26} = -c^{\cdot\cdot}_{61} = -c^{\cdot\cdot}_{62} = \frac{1}{2}\, i\omega (d^{\cdot}_{1112} - d^{\cdot}_{1121});\ c^{\cdot}_{36} = -c^{\cdot\cdot}_{63} = i\omega d^{\cdot}_{3312}$$

$$c_{45} = -c_{54} = \frac{1}{4}\, i\omega (d^{\cdot}_{3231} + d^{\cdot}_{2313} + 2d^{\cdot}_{2331});\ c^{\cdot\cdot}_{45} = -c^{\cdot\cdot}_{54} = \tag{13}$$

$$= -\frac{1}{4}\, i\omega (d^{\cdot}_{3231} + d^{\cdot}_{2313} - 2d^{\cdot}_{2331})$$

$$c^{\cdot}_{45} = c^{\cdot}_{54} = -c^{\cdot\cdot}_{45} = -c^{\cdot\cdot}_{54} = \frac{1}{4}\, i\omega (d^{\cdot}_{3231} - d^{\cdot}_{2313})$$

The constants denoted by an index of two dashes are in this case expressed by completely determinate relationships through the kinetic coefficients (4). From these relationships, (4), and from considerations of the even nature of the kinetic coefficients with respect to H_0 (or I_0) for the constants denoted by an index of two dashes, it follows that they obey the same relationships as do the kinetic coefficients (4). The nature of their dependence on H_0 (or I_0) is the same as that of the kinetic coefficients (4). Thus for an isotropic (unpolarized) magneto-elastic medium, the only constants which differ from zero are those of the type:

$$\gamma_{33}(0) = \gamma_{11}(0) = \gamma'_{11}(0) + i\omega\gamma^{\cdot}_{11}(0);\ c_{33}(0) = c_{11}(0) = d'_{1111}(0) + i\omega d^{\cdot}_{1111}\ (0);$$

$$c_{13}(0) = c_{12}(0) = d'_{1122}(0) + i\omega d^{\cdot}_{1122}(0);\ c_{44}(0) = c_{66}(0) = \frac{1}{2}\,(c_{11}(0) - c_{12}(0));$$

$$c^{\cdot\cdot}_{44}(0) = c^{\cdot\cdot}_{66}(0) = d'_{1212}(0) + i\omega d^{\cdot}_{1212}(0) - c_{66}(0);\ h^{\cdot}_{14}(0) = h^{\cdot}_{36}(0) = i\omega h^{\cdot}_{1,23}(0).$$

The physical nature of constants (8) – (13) can be found only on the basis of observation of the microscopic kinetic processes occurring in a magneto-elastic medium. Not having gone into detailed analysis of this problem, we can only state, for example, that the imaginary terms of constants (8) take into account the energy loss due to relaxation processes; that constants (9) are the rotary moduli, introduced and discussed in [1, 2]; that constant h^*_{15} takes into account the non-symmetric nature of the mechanical stress tensor, due to the non-agreement between the directions of I and H, and considered in [7]; that constants (11) – (13) differ from zero only under dynamic conditions, whilst constants of the type γ_{12} are due to the phenomena of magnetic resonance; that constants h^*_{14}; h^*_{36} and h_{14} are due to gyromagnetic phenomena, whereas constants c_{16}; c^*_{16}; c^*_{36}; c_{45}; c^*_{45} and c^{**}_{45} take into account the possibility, for example, of the existance of Lorentz forces in a non-compensated charge.

From (7) and (8) – (13) it follows that the relationships given in [5] refer only to the symmetric part of the stress tensor.

Translated by E. Bishop

REFERENCES

1. K.S. Viswanathan, *Proc. Indian. Acad. Sci.*, 41A, 98 (1955).
2. C.V. Raman and K.S. Viswanathan, *Proc. Indian Acad. Sci.* 42A, 51 (1955).

VOL. 5 1957

3. J. Laval, *C.R. Paris*, 232, 1947 (1951).
4. K.B. Vlasov, *Fiz. metal. metalloved.*, 3, 55 (1956).
5. K.B. Vlasov, *Fiz. metal metalloved.*, 4, 542 (1957).
6. L. Landau and E. Livshits, *Statisticheskaya fizika (Statistical physics)*, Gostekhizdat, Moscow-Leningrad (1951).
7. W.F. Brown, *Rev. Mod. Phys.*, 25, 131 (1953); *Amer. J. Phys.*, 19, 290 and 330 (1951).

VOL
5
195

CALCULATION OF THE X-RAY EMISSION SPECTRUM STRUCTURE OF ORDERED-SOLUTION-FORMING ALLOYS*

A.N. ORLOV and A.V. SOKOLOV

Institute of Metal Physics Urals Filial, Academy of Sciences, SSSR

(Received 26 December 1956)

Within the framework of the one-electron theory of ordered-solution-forming body-centred cubic alloys, a calculation has been made of the intensity of X radiation emitted when electrons are transferred from the conduction band to the L-level.

VOL. 5 1957

1. The energy spectrum of an electron in the crystal lattice of a binary ordered-solution-forming alloy of any concentration has been discussed elsewhere [1]. It was established that when ordering occurs in some structures, e.g. in the body-centred cubic lattice, a range of forbidden energies arises in the conduction band, the width of which depends on the degree of long-range order η. Depending on the extent to which the conduction band is filled with electrons, this range may lie above or below the Fermi boundary. The form of the iso-energy surfaces, and in particular of the Fermi surface, also depends on η. Consequently, those physical properties of the crystal which are basically due to the behaviour of the conduction electrons must depend on the degree of long-range order.

Smirnov, in a series of papers [1, 2], has discussed the relationship between η and electrical conductivity and galvano-magnetic effects, i.e. phenomena connected with the behaviour of electrons on the Fermi slope. The results obtained agree qualitatively with available experimental data. The effect of ordering on the state of electrons with less than limiting energy is exhibited in crystal properties such as the binding energy [3] and elasticity [4]. However, the fullest information on the structure of the entire energy spectrum and in particular on that of the conduction band, can be obtained by optical measurements over a wide range of frequencies. As applied to the infra-red and visible regions of the spectrum, this problem has been discussed theoretically [5, 6].

In the present paper, a qualitative study is made of the effect of ordering on the structure of X-ray emission spectra in binary alloys, within the framework of the one-electron theory, and to the strong-bond approximation.

2. Let the concentration of A atoms in an alloy $A_c\,B_{1-c}$ equal C, and the probability for an interchange of A and B atoms at lattice site types 1 and 2 equal:

$$p_A^1 = c + (q-c)\eta, \quad p_B^1 = 1 - c - (q-c)\eta, \quad p_A^2 = c - (q-c)\eta,$$
$$p_B^2 = 1 - c + (q-c)\eta,$$

where $q = 2c$ for $c < \frac{1}{2}$ and $q = 1$ for $c > \frac{1}{2}$. Then the intensity $I(\nu)\,d\nu$ for X-radiation of frequency in the interval between ν and $\nu + d\nu$, emitted by atoms of type M ($M = A$ or B), when an electron transfers from state ψ_k to state ψ_0, is defined by the formula [7]:

$$I_M(\nu)\,d\nu = d\nu \frac{h^3 e^2 \nu^2}{6\pi^3 m^2 c^3} \sum_i^M \sum_{k} \iint_{\nu=\nu_{k0}} \left[\left| \frac{\partial E}{\partial k_1} \right|^{-1} \left| \int \psi_k^* \frac{\partial \psi_0^M}{\partial x} d\tau \right|^2 \right] dk_2 dk_3, \qquad (1)$$

---

* *Fiz. metal. metalloved.* 5, No. 3, 390-394, 1957.

where $h\nu_{k_0}$ is the energy difference between states ψ_k and ψ_0. $E(\vec{k})$ is the energy of a conduction electron of wave vector $\vec{k}$. $\sum_i^M$ denotes summation over all lattice sites occupied by type M atoms.

It will be assumed that the conduction electrons are in the s-state (since this is the only case for which the relationship between E, c and η is known, and it is required in the calculation of $\partial E/\partial k$). Then, by the selection principle, the ψ_0 state must be the p-state. Thus, we confine ourselves to considering only the L-band.*

According to [1], the electron wave function in the body-centred cubic lattice of a partially ordered alloy is of the form:†

$$\psi_\kappa = \sum e^{i\vec{k}\vec{R}_s}[b_1(f_s^1 + \varphi_1\omega) + b_2(f_s^2 + \varphi_2\omega)], \tag{2}$$

where $f_s^i = f(\vec{r} - \vec{R}_s - \vec{h}_i)$ is the electron wave function in the effective atom situated at site i (i = 1 or 2) of the s-th unit cell;
ω is a small increment to f_s^i, found from excitation theory formulae and independent of c and η;
b_1 and b_2 are constants:

$$\varphi_1 = c - 1/2 + (q - c)\eta, \quad \varphi_2 = c - 1/2 - (q - c)\eta \tag{3}$$

and $\vec{h}_i$ is a vector directed from the zeroth site of the cell to the ith site.
Substitute (2) in (1) and write:

$$\int (f_s + \varphi_i\omega)\frac{\partial\psi_{ot}}{\partial x}\,d\tau = J_M + \varphi_i l_M, \quad (s = t), \tag{4}$$

if $f_s + \phi_i\omega$ and ψ_{ot} refer to a single lattice site, and

$$\int (f_s + \varphi_i\omega)\frac{\partial\psi_{ot}}{\partial x}\,d\tau = i_M + \varphi_i\lambda_M, \quad (s \neq t), \tag{5}$$

if $f_s + \phi_i\omega$ and ψ_{ot} refer to adjacent lattice sites (overlapping of the wave functions for more distant atoms is regarded as a phenomenon of a higher order of smallness). Integrals l_M and i_M are of the first order of smallness, since i_M contains a product of slightly overlapping functions, and l_M a small value of ω. Integral λ_M is of a second order of smallness, since it contains both these indications of smallness at the same time; it will be neglected from now on. In expressions (4) and (5) the integrals over k_2 and k_3, given in (1), can be introduced, to an accuracy of terms of a higher order of smallness, in the form:

$$\iint \frac{\left|(f_s + \varphi_i\omega)\frac{\partial\psi_{ot}}{\partial x}\,d\tau\right|^2}{|\partial E/\partial k_1|}\,dk_2dk_3 = J_M^2\iint\frac{\partial k_2\,\partial k_3}{|\partial E/\partial k_1|} + \tag{6}$$
$$+ 2J_M i_M\iint\frac{G(k)\,dk_2\,dk_3}{|dE/dk_1|} + 2\varphi_1 J_M l_M\iint\frac{dk_2\,dk_3}{|\partial E/\partial k_1|},$$

* To calculate the fine structure of absorption spectra, it is necessary to know the wave functions and energy levels for the unfilled bands of high energy. In view of the marked overlapping of bands, effects due to the distortion of the iso-energy surfaces as a result of ordering are less pronounced than in the conductivity band. Experiment on Au Cu_3 alloys [8] give minor changes in the absorption spectrum as a result of ordering.

† As is known [10], in X-ray transitions fairly substantial changes occur in the energy spectrum of the metal and particularly in the inner levels of the atom in which the transition takes place. In some cases it is possible to eliminate local levels from the bottom of the conductivity band, electrons which occupy these levels screening vacancies in the X-ray level. In other cases the screening of vacancies originates at the expense of conductivity band electrons. In neither case does the presence of vacancies in the X-ray level lead to significant displacement of the Fermi boundary.

where, in the sum $G(k) = \sum e^{-ikRs}$, account is taken of cells into which fit the nearest neighbours of the atom under consideration.

Substituting (6) in (1) and completing the summation over all sites occupied by type M atoms, we find

$$I_M(\nu) = \text{const} \cdot \nu^2 \iint \frac{W_M}{|\nabla_k E|} dS, \tag{7}$$

where

$$W_A = [J_A^2 + 2J_A i_A G(k)]c + 2J_A l_A (\varphi_1 P_A^1 + \varphi_2 P_A^2) =$$
$$= J_A^2 c + 2J_A i_A G(k) c + 4J_A l_A [c(c - 1/2) + (q-c)^2 \eta^2], \tag{8}$$

$$W_B = J_B^2 (1-c) + 2J_B i_B G(k)(1-c) + 4J_B l_B [(1-c)(c-1/2) - (q-c)^2 \eta^2]. \tag{9}$$

VOL. 5 1957

3. We now turn to a consideration of the relationship between c and η and the integral,

$$F = \iint \frac{ds}{|\nabla_k E|},$$

appearing in (7).

According to Smirnov [1], the electron energy in the alloy lattice under consideration takes the form

$$E = W + \varepsilon_* + (c - 1/2)\chi \pm \left[(q-c)^2 \eta^2 \chi^2 + 64\varepsilon_0^2 \cos^2 \frac{k_x a}{2} \cdot \right.$$
$$\left. \cos^2 \frac{k_y a}{2} \cos^2 \frac{k_z a}{2}\right]^{1/2}. \tag{10}$$

Here W, ϵ_*, χ and ϵ_0 are constants, independent of c and η to this approximation. When this structure becomes ordered, an additional boundary is formed to the Brillouin zones,

$$\frac{k_x a}{2} = \frac{k_y a}{2} = \frac{k_z a}{2} = \frac{\pi}{2}.$$

The iso-energy surfaces do not pass beyond this boundary, and the energy suffers a discontinuity at it to the extent of $2(q-c)\eta\chi$. Inside the discontinuity, the density of energy levels $n(E)$ is equal to zero. If the conductivity band is exactly half filled, the Fermi energy will lie inside the discontinuity and the crystal is an insulator [1]. If the degree of filling is greater and the Fermi level lies in the upper half-band, the presence of a range of forbidden energies must reveal itself in the form of a drop in intensity in the emission band.

For simplicity, we introduce the following calculated expressions

$$W + \varepsilon_* + (c - 1/2)\chi = C, \quad (q - c)^2 \chi^2 \eta^2 = \alpha, \quad 64\varepsilon_0^2 = \beta,$$
$$[(E-C)^2 - \alpha]/\beta = C_1^2, \quad \frac{k_x a}{2} = \xi, \quad \frac{k_y a}{2} = \eta_1, \quad \frac{k_z a}{2} = \zeta.$$

Then (10) assumes the form

$$E = C \pm [\alpha + \beta \cos^2 \xi \cos^2 \eta \cos^2 \xi]^{1/2}, \tag{11}$$

whence we obtain for F

$$F = \iint \frac{\partial S}{|\nabla_k E|} = \frac{2\sqrt{\alpha + \beta C_1^2}}{\beta C_1} \iint \frac{d\xi d\eta}{\sqrt{\cos^2 \xi \cos^2 \eta - C_1^2}}. \tag{12}$$

The integral in (12) is not amenable to analytical solution. However, a number of qualitative conclusions can be drawn, starting from the general properties of the sub-integral functions. To illustrate this, we shall consider an actual example, with the following values for the constants:

$$c = \tfrac{1}{2},\ C = 20,\ \chi = 2,\ \beta = 8.$$

In this case, the lower boundary of the energy band, when $\eta = 1$, lies at $E = 20 - 3 = 17$, and the upper at $E = 23$. The forbidden zone ranges from $E = 19$ to $E = 21$. The degree of filling of the band (number of conduction electrons is selected so that when $\eta = 1$, the Fermi energy $E_F = 21.5$.

The relationship between E_F and η is found from the condition that the volume enclosed within the Fermi surface is unchanged when ordering takes place. According to (11), the equation for the constant energy surface is of the form

$$\cos^2 \xi \cos^2 \eta \cos^2 \zeta = C_1^2. \tag{13}$$

Consequently, the volume enclosed with the surface E = const. is determined by the value of C_1 and remains constant when ordering takes place, if the change in η is balanced by a change in E_F according to the relationship

$$E_F = C + \sqrt{C_1^2 \beta + \alpha}.$$

For the selected values of the constants, $C_1^2 = 0.15625$, whence $E = 20 + \sqrt{1.25 + \eta^2}$.

Numerical integration of (12), for the given values of the constants, was carried out at $\eta = 0$, 0.5 and 1.0. The results are given in Fig. 1.

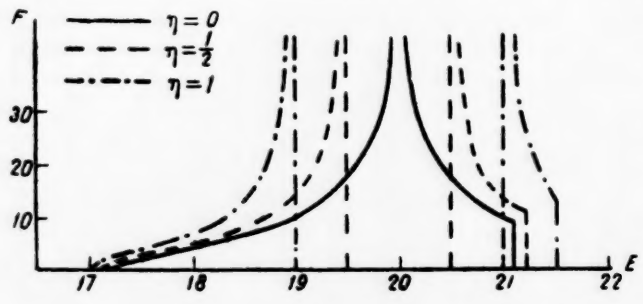

FIG. 1.

4. Thus, the relationship of I to c and η is determined both by the probability W_M of transition and by the structure of the energy spectrum of the conduction electrons. As can be seen by comparing Fig. 1 with formulae (8) and (9), the second factor is more sensitive than the first to changes of η. Since integrals i_M and l_M are one order smaller than j_M, it can be taken that the $I - \eta$ relationship is mainly determined by the F factor. This leads to the following features (cf. Fig. 1) of the change in the emission L-band due to ordering.

(a) the long-wave boundary of the band is displaced to longer wavelengths;

(b) the short-wave boundary of the band is displaced in the opposite direction;

(c) if the alloy has more than one conduction electron per atom, a forbidden band of energy levels is formed, with a corresponding drop in the emission band.

These conclusions are independent of the values of the constants selected in the example discussed above.*

As shown previously [1], in the weak-bond approximation the energy discontinuity as a result of ordering, predicted by formula (10), is not obtained. Possibly, in the emission spectrum of a real crystal, this effect will only reveal itself in a certain loss of intensity at the middle of the conduction band. It must also be noted that Fig. 1 does not show the full relationship of I to c, η and E, predicted by theory, since neither W_M nor the factor ν^2 enter into F.

It is of interest to verify experimentally the conclusions formulated above, on alloys of the β-brass type. Since in β-brass the degree of long-range order cannot be frozen in by quenching, it is necessary to make exposures at temperatures near the Curie point; at the same time that part of the temperature relationship of the fine structure of the emission band which is independent of η may lead to distortion of the predicted effect.

Thanks are expressed to Shepelova for carrying out the numerical computations.

Translated by E. Bishop

REFERENCES

1. A.A. Smirnov, *Zh. eksp. teor. fiz.*, 17, 730 (1947); 17, 743 (1947.
2. A.A. Smirnov, *Zh. teor. fiz.*, 18, 153 (1948).
3. A.A. Smirnov, *Trud. I.F.M. UFAN*, 12, 40, (1949).
4. A.N. Orlov, *Fiz. metal. metalloved.*, 5, 212 (1957).
5. S.V. Vonsovskii, A.A. Smirnov and A.V. Sokolov, *Dokl. Akad. Nauk. SSSR* 80, 353 (1951).
6. A.V. Sokolov and V.I. Cherepanov, *Zh. eksp. teor. fiz.*, 22, 493 (1952).
7. A. Wilson, *Kvantovaya teor. metal. (Quantum theory of metals)*, Gostekhizdat, Chap. 4. (1941).
8. R. Smoluchowski, Phys. 2. 95, 588 (1935).
9. H. Jones, N.F. Mott and H.W.B. Skinner, *Phys. Rev.* 45, 379 (1934).
10. J. Friedel, *Phil. Mag.*, 43, 153 (1952).

* Consideration of the case in which ψ_{ot} describes the s-state, requires knowledge of the $E(\vec{k})$ relationship for the conduction band electrons, as described by the p-functions. This problem leads to a secular equation of high order (8 in the general case) the solution to which does not provide a simple $E(\vec{k})$ relationship. As is known [9], the emission band in this case assumes another form, but it can be expected that the effect of ordering on the form of this band, connected with the formation of additional Brillouin surfaces and with the displacement of the conduction band boundaries, will resemble the changes in the L-band found above.

VOL. 5 1957

EXCITED STATES OF AN ATOMIC SEMICONDUCTOR IN THE MANY-ELECTRON MODEL *

S.V. VONSOVSKII and A.N. KUSHNIRENKO

Institute of Metal Physics, Urals Filial, Academy of Sciences, SSSR

(Received 8 April 1957)

The many-electron model of an atomic semiconductor without impurities is considered in the configuration-space representation. In each lattice site of the crystalline lattice in the normal state there are two valency electrons, with anti-parallel spin projections in the non-degenerate orbital *s*-state. In addition, the first excited *p*-state, also regarded as non-degenerate, is taken into account. In a crystal of this type, two kinds of collective elementary excitation are possible: (*a*) excitations of the "Frenkel exciton" type, in singlet or triplet states, and (*b*) excitations of the "conduction electrons" and "holes" type, also in singlet or triplet states. Type (*a*) excitations are not connected with transfer of electrical charge, whereas type (*b*) excitations are responsible for the intrinsic electrical conductivity of the semiconductor. Similar studies have also been carried out previously for the model with one valency electron [1–4], and also for the model used in the present paper, but without taking into account the type (*b*) excitations [5].

1. ELEMENTARY EXCITATIONS OF THE FRENKEL CURRENT-LESS EXCITON TYPE

1. We shall assume that at each of N crystal lattice sites in an atomic semiconductor in the ground state there are two valency electrons with anti-parallel spin projections, in the non-degenerate orbital *s*-state (in addition to the closed ionic electron shells, the effect of which will from now on be neglected †). The intrinsic function of each of these electrons in the isolated atom k will be denoted by

$$\phi_{k\sigma}\,(\vec{r}_k^{(l)}\ S_k^{(l)}),\text{where}\ \vec{r}_k^{(l)}$$

is the electron radius vector, and $S_k^{(l)}$ its spin co-ordinate, $l = 1$ or 2 and the symbol σ takes the value α for "right-hand" spin and β for "left-hand." An abbreviated notation,

$$\vec{r}_k^{(l)}\ S_k^{(l)} = x_k^{(l)}.$$

is introduced below. The wave function of the h-site electron in the excited *p*-state (which is regarded as non-degenerate) is denoted as

$$\chi_{h\sigma}\,(x_h^{(l)}).$$

The second valency electron at this site is in the ground state.

---

* *Fiz. metal. metalloved.*, 5, No. 3, 395-401, 1957

† This omission is equivalent to the assumption that the dielectric constant $\epsilon = 1$; in actual cases ϵ considerably exceeds unity.

The wave function of the system of $2N$ electrons with one excited site, in the neighbourhood of zero, is written in the form of a Slater determinant:

$$\psi_h^{\alpha\alpha'} = [(2N)!]^{-1/2} \sum_P (-1)^P P \chi_{h\alpha}(x_h^{(1)}) \varphi_{h\beta}(x_h^{(2)}) \cdot$$

$$\varphi_{k_1\alpha}(x_{k_1}^{(1)}) \varphi_{k_1\beta}(x_{k_1}^{(2)}) \cdots \varphi_{k_{h-1}\beta}(x_{k_{h-1}}^{(2)}) \varphi_{k_{h+1}\alpha}(x_{k_{h+1}}^{(1)}) \cdots \varphi_{k_N\beta}(x_{k_N}^{(2)}), \tag{1.1}$$

where P is an operator on pair permutations. Here four types of spin distribution are possible in the excited site, namely:

$$\psi_h^{\alpha\beta},\ \psi_h^{\beta\alpha},\ \psi_h^{\alpha\alpha},\ \psi_h^{\beta\beta}.$$

Consequently, there are one singlet and three triplet states [5]:

$${}^{(1)}\psi_h = 2^{-1/2}[\psi_h^{\alpha\beta} - \psi_h^{\beta\alpha}];\ {}^{(3)}\psi_h = \begin{matrix} \psi_h^{\alpha\alpha} & (m_s = -1) \\ 2^{-1/2}[\psi_h^{\alpha\beta} + \psi_h^{\beta\alpha}] & (m_s = 0) \\ \psi_h^{\beta\beta} & (m_s = 1) \end{matrix} \tag{1.2}$$

Ignoring magnetic (spin) interactions, the (1.2) states of various multiplicities do not intercombine. Therefore, the wave functions for states of the system with different multiplicities (M = 1.3) can be represented, to a first approximation, in the form of a series:

$$\psi^{(M)} = \sum_h a(h)^{(M)} \psi_h. \tag{1.3}$$

The wave equation for determining (1.3) and the energy E^M of the system takes the form:

$$\hat{H}\psi^{(M)} = E^{(M)}\psi^{(M)}, \tag{1.4}$$

and operator $\hat{H}$ in (1.4) is given by the expression

$$\hat{H} = -\frac{h^2}{2\pi\, 2m}\sum_{q=1}^{2N}\Delta_q + \sum_{q=1}^{2N}\sum_{t=1}^{N} u_t(\vec{r}_q) + \sum_{q<q'}^{2N}\Phi(|\vec{r}_q - \vec{r}_{q'}|), \tag{1.5}$$

Here $2\pi h$ is the Planck constant, m the mass of an electron, Δq the Laplace operator, acting at the co-ordinates of the qth electron, $u_t(\vec{r}_q)$ the potential energy of electron q in the field of ion t, and $\phi(|\vec{r}_q - \vec{r}_{q'}|)$ the interaction energy of the electron pair q and q'.

Multiplying the left-hand side of (1.4), term by term, by M_{ψ_h}, integrating over the co-ordinates of the electrons (summing over the spins) and using (1.3) we obtain the secular equation for determining the wave functions in the h: $a(h)$ representation and the intrinsic values for the energy of the system

$$\sum_{h'} a(h') \sum_{s} \int^{(M)} \psi_h^* H^{(M)} \psi_h \, d\tau = E^{(M)} \sum_{h'} a(h') \sum_{s} \int^{(M)} \psi_h^{*(M)} \psi_{h'}^* \, d\tau, \tag{1.6}$$

Here dr is an element of volume in space of $6N$ dimensions. Using the condition for ortho-normalization of the single-particle functions, it is easy to see that (1.6) will assume the form

$$\sum_{h'} a(h') A_{hh'}^{(M)} = E^{(M)} a(h). \tag{1.7}$$

Clearly, the solution to (1.7) can be written in the form

$$a(h) = a \exp[i(\vec{k} \cdot \vec{R}_h)], \tag{1.8}$$

where $\vec{k}$ is the quasi-impulse of the excited state of the system, the possible values of which fill the first Brillouin zone, corresponding to the reciprocal lattice. Therefore the dispersion relationship for the energy of the excited state of the crystal will take the form

$$E^{(M)}(\vec{k}) = A_{hh}^{(M)} + \sum_{h' (\neq h)} \exp i(\vec{k} \cdot (\vec{R}_{h'} - \vec{R}_h)) \cdot A_{hh'}^{(M)}, \tag{1.9}$$

where

$$A_{hh}^{(M)} = \sum_{s} \int^{(M)} \psi_h^* \hat{H}^{(M)} \psi_h \, d\tau$$

are the diagonal and

$$A_{hh'}^{(M)} = \sum_{s} \int^{(M)} \psi_h^* \hat{H}^{(M)} \psi_{h'} \, d\tau -$$

the non-diagonal matrix elements of the energy operator (1.5), and $\vec{R}_h$ the radius-vector of lattice site h. The diagonal matrix element in both states ($M = 1.3$) equals the sum of twice the "zero" energies of the isolated atoms, $2NE_0$, the excitation energies of the p-state of an isolated atom ΔE and the quasi-coulomb interaction C of all the valency electrons in the various sites. The non-diagonal matrix elements differ substantially for the states of different multiplicities. Thus, in the singlet state we have

$$A_{hh'}^{(1)} = \frac{1}{2} \sum_{s} \int^{(1)} \psi_h^* \hat{H}^{(1)} \psi_{h'} \, d\tau =$$

$$= \int \chi_h^*(\vec{r}) \varphi_{h'}^*(\vec{r}) \Phi(|\vec{r} - \vec{r}'|) \varphi_h(\vec{r}) \chi_{h'}(\vec{r}') \, d\vec{r} \, d\vec{r}' - \tag{1.10}$$

$$- \int \chi_h^*(\vec{r}) \varphi_{h'}^*(\vec{r}') \Phi(|\vec{r} - \vec{r}'|) \chi_{h'}(\vec{r}) \varphi_h(\vec{r}') \, d\vec{r} \, d\vec{r}' = B_{hh'} - J_{hh'},$$

where $B_{hh'}$ is the "quasi-coulomb" integral and $J_{hh'}$ the "volume" integral. The latter is essentially dependent on the overlapping of orbits of different lattice sites and as a rule small compared with the first, even for the sites of the nearest neighbours. In the triplet state we have

$$A^{(3)}_{hh'} = -J_{hh'}. \tag{1.11}$$

Merely from what has been said it follows that the width of the triplet exciton energy band, as determined by the value of the volume integral $J_{h,h'}$ will be considerably narrower than the width of the corresponding singlet band, as determined by the value of $B_{hh'}$. As has already been pointed out [5], this difference in the width of the exciton energy bands for different multiplicities can have considerable importance for the nature of the optical properties of the exciton states of semiconductors.

It can easily be seen from formula (1.9), that it can be generalized without difficulty to cover also the case of many elementary excitations, i.e. to the case of an exciton "gas". The only condition which must be fulfilled is that excitation shall be weak; the number of excitons must be considerably less than the number of lattice sites.

2. We shall now show that states of the Frenkel exciton type do not involve a current. To prove this, we shall consider the expression for the components of the quantum current vector:

$$I_j^{(M)} = \frac{eh}{2mi}\sum_{q=1}^{2N}\int(\psi^{(M)*}\nabla_j^{(q)}\psi^{(M)} - \psi^{(M)}\nabla_j^{q}\psi^{(M)*})\,d\tau, \tag{1.12}$$

where $j = 1,2$ or 3. Substituting functions (1.3) in (1.12) we obtain

$$I_j^{(M)} = \frac{eh}{2mi}\sum_{h\neq h'}[a^*(h)a(h') - a(h)a^*(h')]\int^{(M)}\psi_h^*\Big[\sum_{q=1}^{2N}\nabla_j^{(q)}\Big]^{(M)}\psi_{h'}\,d\tau. \tag{1.13}$$

The matrix elements appearing in (1.13) differ from those for the secular equation (1.7) in that in place of the operator (1.5), they contain an additive operator

$$\hat{I}_j = \sum_{q=1}^{2N}\nabla_j^{(q)}. \tag{1.14}$$

It can be seen from (1.13) that only the non-diagonal matrix elements of operator (1.14) make a non-zero contribution to the current, but in this operator there are no binary terms, so that all its non-diagonal elements are zero and consequently the resultant current (1.13) is also zero for excited crystal states of the Frenkel exciton type.

2. CURRENT-CARRYING ELEMENTARY EXCITATIONS IN ATOMIC SEMICONDUCTORS

We shall now consider the other type of elementary excitations in the system. Let there be, surrounding one site f of the lattice, two electrons with opposite spin projections in the s-state, and a third electron with any value of spin projection in the p-state (which as before is considered as non-degenerate). Around any second site, g, there is, in addition to the filled electron shells of the ion, only one valency electron, with any value of spin projection in the s-state. All other (N-2) lattice sites have two valency electrons each in the s-state. The intrinsic function for such an excited state, by analogy with (1.1) assumes the form:

$$\psi_{fg}^{\alpha\alpha'} = [(2N)!] \sum_{P} (-1)^{P} P \varphi_{f\alpha}(x_f^{(1)}) \varphi_{f\beta}(x_f^{(2)}) \chi_{f\alpha}(x_g^{(1)}) \varphi_{g\alpha'}(x_g^{(2)}) \varphi_{1\alpha}(x_1^{(1)}) \varphi_{1\beta}(x_1^{(2)}) \ldots$$
$$\ldots \varphi_{f-1\beta}(x_{f-1}^{(2)}) \varphi_{f+1\alpha}(x_{f+1}^{(1)}) \ldots \varphi_{g-1\beta}(x_{g-1}^{(2)}) \varphi_{g+1\alpha}(x_{g+1}^{(1)}) \ldots \varphi_{N\beta}(x_N^{(2)}). \tag{2.1}$$

Here again, four types of spin distribution are possible in the excited sites:

$$\psi_{fg}^{\alpha\beta}, \ \psi_{fg}^{\beta\alpha}, \ \psi_{fg}^{\alpha\alpha}, \ \psi_{fg}^{\beta\beta}.$$

Consequently, as before, there are one singlet and three triplet states of excitation of the type under consideration:

$$^{(1)}\psi_{fg} = 2^{-1/2} [\psi_{fg}^{\alpha\beta} - \psi_{fg}^{\beta\alpha}]; \quad \psi_{fg}^{(3)} = 2^{-1/2} [\psi_{fg}^{\alpha\beta} + \psi_{fg}^{\beta\alpha}] \quad \begin{matrix} \psi_{fg}^{\alpha\alpha} & (m_s = -1) \\ & (m_s = 0) \\ \psi_{fg}^{\beta\beta} & (m_s = 1). \end{matrix} \tag{2.2}$$

The solution to the wave equation assumes the form:

$$\psi^{(M)} = \sum_{fg} b(fg)^{(M)} \psi_{fg}. \tag{2.3}$$

The corresponding secular equations are written as:

$$\sum_{f'g'} b(f'g') \sum_{s} \int \psi_{fg}^{*(M)} \hat{H}^{(M)} \psi_{f'g'} d\tau = E^{(M)} \sum_{f'g'} b(f'g') \sum_{s} \int \psi_{fg}^{*(M)} \psi_{fg}^{(M)} d\tau. \tag{2.4}$$

Using the ortho-normalization of the single-particle functions, we have in place of (2.4):

$$\sum_{f'g'} b(f'g') A_{fg,f'g'}^{(M)} = E^{(M)} b(fg). \tag{2.5}$$

The solution to (2.5) has the form:

$$b(fg) = b \exp \{i [(\vec{k}_1 \vec{R}_f) + (\vec{k}_2 \vec{R}_g)]\}, \tag{2.6}$$

where $\vec{k}_1$ and $\vec{k}_2$ are the quasi-impulses of the elementary excitations of the "trio" or "conduction electron" type and "unit" or "hole" respectively; the possible values of these quasi-impulses fill the first Brillouin zone of the corresponding reciprocal lattices. The dispersion relationship in this case is of the form:

$$E^{(M)}(\vec{k}_1 \vec{k}_2) = A_{fg,fg}^{(M)} + \sum_{f'g'} \exp i [\vec{k}_1 (\vec{R}_{f'} - \vec{R}_f) + \vec{k}_2 (\vec{R}_{g'} - \vec{R}_g)] \cdot A_{fg,f'g'}^{(M)}. \tag{2.7}$$

Here terms with $f' = f$, $g' = g$ and $f' = g'$ must be omitted from the summation. As in the case of current-less excitons, (2.7) gives two types of band, for singlet and triplet excitations respectively. Moreover, different bands are obtained for conduction electrons and for holes. The result obtained is again easily generalized to cover large numbers of electron-hole pairs, with the condition that this number is considerably less than the number of crystal lattice sites (the case of weak excitation).

It is also important to point out that side by side with solutions of the type of (2.6) for free electrons and holes, propagating independently through the crystal, there are solutions for "bound" electrons and holes forming a single neutral complex (see for example, analogous states in [6]) which propagate through the crystal as a single whole. It can be shown [6] that the corresponding solution of (2.4) will be of the form:

$$b(fg) = b_1 \exp\left[i\vec{k}(\vec{R}_f + \vec{R}_g)\right] b_2(|\vec{R}_f - \vec{R}_g|), \tag{2.8}$$

where $\vec{k}$ is the quasi-impulse of the neutral electron-hole complex whilst function $b_2(|\vec{R}_f - \vec{R}_g|)$ decreases with increasing distance $|\vec{R}_f - \vec{R}_g|$ between the sites. It can readily be seen that these excitations merely represent another variety of Frenkel current-less exciton.

2. We shall now show that the elementary "electron-hole" excitations found above involve a current. By analogy with (1.13) we have:

$$I_i^{(M)} = \frac{eh}{2\pi 2mi} \sum_{fg,\, f'g'} \left[b^*(fg)\, b(f'g') - b(fg)\, b^*(f'g')\right] \cdot \sum_s \int \psi^{*(M)}_{fg} \left(\sum_{q=1}^{2N} \nabla_j^{(q)}\right)^{(M)} \psi_{f'g'}\, d\tau. \tag{2.9}$$

In (2.9) matrix elements appear which are of the same type as in the secular equations (2.4), but with an impulse operator in place of an energy operator. Of these matrix elements those which differ from zero are the elements of the type:

$$\left.\begin{aligned} (I_j')_{lg} &= -(I_j'')_{gl} = \sum_s \int \varphi_l^*(x_l^{(1)})\, \nabla_j^{(l)}\, \varphi_g(x_l^{(1)})\, d\vec{x}_l^{(1)}, \\ (I_j'')_{fl} &= -(I_j'')_{lf} = \sum_s \int Z_f^*(x_\kappa^{(1)})\, \nabla_j^{(g)} Z_l(x_\kappa^{(1)})\, d\vec{x}_\kappa^{(1)} \end{aligned}\right| \tag{2.10}$$

Using (2.10) and (2.6), we find

$$I_j^{(M)} = \frac{2eh}{m} |b|^2 \sum_{l=1}^{N-2} \left\{ \left| \sum_g \sin\left[\vec{k}_2(\vec{R}_l - \vec{R}_g)\right] (I_j')_{gl} + \left[\sum_l \sin\left|k_1(\vec{R}_l - R_j)\right| (I_j'')_{fl}\right| \right. \tag{2.11}$$

Thus, the states of (2.6) in fact possess current. The first sum on the right-hand side of (2.11) gives the hole current, and the second the pair current.

3. CONCLUSION

The importance of the results obtained in the present paper is primarily the fact that we have succeeded in finding, within a unified scheme, various types of elementary collective electron excitations for those systems the ground state of which is saturated with respect to spin and to charge (the singlet state of closed quantum shells). The paper shows that the essence of the excitations and their collective nature result from strong electron interactions in the system. One of the types of excitation found is of the current-less exciton variety and the other – current-carrying excitation – of the conduction-electron and hole variety. The classification of the various types of excitation can be compared with the various terms in the "expansion" of the quantum electron density. To oscillations of the quasi-classical zero term of this expansion correspond the so-called "plasma oscillations" of the electron system in the crystal. To the term containing transitions into excited states, but without a "discontinuity" due to oppositely-charged fluctuations of electron density correspond the current-less excitations,i.e. various types of exciton. To the term with quantum transitions and with a "discontinuity" between the oppositely-charged density fluctuations, correspond the current-carrying excitations, i.e. conduction electrons and holes. To the terms of the interchange process type correspond, not charged excitations, but "spin excitations", of the electron system, e.g. ferromagnons or spinons, etc.

A further important advantage of the many-electron treatment is that it shows that there is no essential physical difference between the so-called Frenkel and Mott excitons. In both cases we are dealing with a phenomenon of collective, but current-less, excitation, belonging to the crystal as a whole.

It is also essential, that in the many-electron model used, account can be taken, in a completely correct form, of the spin characteristics of the electron excitations examined, e.g. of the degree of multiplicity.

It is of course a fact that the concrete form of the dispersion relationships (1.9) and (2.7) can only be regarded as a very rough scheme, which is very far from an accurate picture of the dispersion relationships for the electron energy spectrum of real crystals of atomic semiconductors. It must, for example, be emphasized that in real crystals the nature of the exciton excitations may be immensely more complex, so that such excitations can be approximated only in the neighbourhood of zero by the atomic wave functions of the excited p-state, and even then degeneration is neglected. An essential role in this respect may also be played by internal excitations of the ionic islands, which may be closely connected with the polarizability of the latter in real atomic semiconductor crystals.

Further practical development of this model will be found in another paper by the authors in collaboration with Irkhin and Turov [7] (see also [8]) and also in a paper [9] by these two authors.

Translated by E. Bishop

REFERENCES

1. Ya. I. Frenkel, *Phys. Rev.*, 37, 17 (1931).
2. S.V. Vonsovskii, *Zh. eksp. teor, fiz.*, 8, 1104 (1938).
3. V.S. Galishev, Candidates dissertation, Sverdlovsk, (1953).
4. V.S. Galishev and S.V. Vonsovskii, *Fiz. metal. metalloved.*, 3, 395 (1956).
5. R.E. Merrifield, *J. Chem. Phys.*, 23, 402 (1955).
6. S.P. Shubin, and S.V. Vonsovskii, *Phys. Z. Sowjet.*, 10, 348 (1936).
7. S.V. Vonsovskii, Yu. P. Irkhin, A.N. Kushnirenko and E.A. Turov, *Fiz. metal. metalloved.*, 3, 385 (1956).
8. S.V. Vonsovskii, *Zh. tekh. fiz.*, 25, 2023 (1955).
9. E.A. Turov and Yu. P. Irkhin, *Fiz. metal. metalloved.*, 4, 9 (1957).

VOL
5
195

10. V.L. Bonch-Bruevich, *Nauk. zap. L'vovsk. Univ.*, 33, 59 (1955).
11. K.D. Tovstyuk, *Dissertation Chernovtsy*, (1956).

VOL.
5
1957

THE CRITERION OF THE SEMI-METALLIC STATE OF MATTER ACCORDING TO THE MANY-ELECTRON THEORY*

E.N. AGAFONOVA and N.P. KONTOROVICH

Ural State Gor'kii University

(Received 20 December 1956)

The mean energy of atomic semiconductors with impurities is determined within the framework of the many-electron theory. For the sake of simplification, it is assumed that the impurities are minor and do not distort the crystal lattice. In the model of the atomic semiconductor with closed spin shells, the criterion is obtained for the semi-metallic state of matter, as a result of assuming the energy-wise viability of the "polarized" state of matter. This state is characterized by the fact that a constant, temperature-independent, small number of current carriers is formed, equal to the number of impurities.

1. The name of semi-metal is applied to substances in which the electrical conductivity falls off with increasing temperature, in the low temperature range (as with metals), but increases at high temperatures, as with semiconductors, i.e. the temperature coefficient of electrical conductivity changes sign at a certain temperature (the "transition temperature"). To this class of solid substances belong silicon and germanium with certain impurities, PbS, PbSe, MnFe, SiC, grey tin and many others. The presence of impurities of one sort or another is a necessary condition of the semi-metallic state.

In the one-electron theory there are two points of view regarding the energy spectrum of semi-metals. The more widely accepted view assumes that in a semi-metal, the impurity levels – donors and acceptors – are disposed not in the forbidden band but in the conductivity band. In this case, even at low temperatures, the material is electrically conducting, i.e. the conductivity band contains a constant number, independent of temperature, of electrical current carriers, equal to the number of impurities.

The other attempt at a theoretical interpretation of the temperature relationship of semi-metals proceeds from the fact that in semi-metals, the impurity atoms create their own impurity band of energy, which is located in the forbidden band below the conductivity band. In the impurity levels there is a certain number of electrons, independent of temperature, and equal to the number of impurity atoms. Electrical conductivity exists at low temperatures because of the electrons which, in the impurity band, behave in a similar way to the conductivity band electrons in a metal.

However, within the terms of reference of the one-electron theory, it seems to us, it is difficult to formulate a quantitative condition to cover semi-metallic conductivity. Within the framework of the many-electron theory, which takes into account interactions between electrons, on the other hand, it is possible to obtain a condition for the existence of the semi-metallic state, and to formulate it quantitatively.

The problems before this paper include the determination of the mean energy of a semiconductor with impurities and the setting-up of a criterion for the semi-metallic state on the many-electron basis.

2. As the starting model for the description of an atomic semiconductor with impurities, we shall take the polar-exciton model, with closed spin shells [1-3]. The lattice contains N sites, of which N_1 are occupied by atoms of the major constituent (type "A" atoms) and N_2 sites by impurity atoms (type "B" atoms); $N_1 + N_2 = N$. The number of external valency electrons in the crystal is thus $2N$.

The wave equation for the system of electrons in a semiconductor with impurities can be written in the following form:

---

* *Fiz. metal. metalloved.*, 5, No. 3, 402-405, 1957.

$$\left\{-\frac{\hbar^2}{2m}\left(\sum_{1\leqslant k\leqslant 2N_1}\Delta_{q_k}+\sum_{1\leqslant k'\leqslant 2N_2}\Delta_{q_{k'}}\right)+\sum_{1\leqslant k<l\leqslant 2N_1}F(q_k, q_e)+\sum_{1\leqslant k'\leqslant l'\leqslant 2N_2}F'(q_{k'}, ql')+\right.$$
$$\left.+\sum_{k,\,k'}F''(q_k q_{k'})+\sum_{\substack{1\leqslant l\leqslant N\\ 1\leqslant k\leqslant 2N_1}}U_f(q_k)+\sum_{\substack{1\leqslant l'\leqslant N\\ 1\leqslant k'\leqslant 2N_2}}U_{l'}(q_{k'})\right\}\psi(q_1 s_1 \ldots q_{2N} s_{2N})=E\psi(q_1\ldots s_{2N}), \tag{1}$$

where $U_f(q_k)$ is the electrostatic potential energy of the k-th electron in the field of the f-th site, $F(q_k q_l)$ the energy of electrostatic repulsion between the k-th and l-th electrons, E the energy of the system, $\psi(q_1,\ldots S_{2N})$ the wave function for the system of 2N electrons, and q_k and S_k the space and spin co-ordinates respectively of the k-th electron. Dashed superscripts refer to impurity sites and electrons and the undashed terms to the major constituent.

Using the method of secondary quantization developed in papers by Bogolyubov and Tyablikov [4,5] we obtain the energy operator in the following form:

$$\hat{H}=\sum_{(\alpha\alpha')}L(\alpha,\alpha')a_\alpha^+ a_{\alpha'}+\sum_{(\alpha\alpha')}L'(\alpha,\alpha')b_\alpha^+ b_{\alpha'}+$$
$$+\frac{1}{2}\sum_{(\alpha_1\alpha_2\alpha_1'\alpha_2')}F(\alpha_1\alpha_2\alpha_1'\alpha_2')\,a_{\alpha_1}^+ a_{\alpha_2}^+ a_{\alpha_2'} a_{\alpha_1'}+$$
$$+\frac{1}{2}\sum_{(\alpha_1\alpha_2\alpha_1'\alpha_2')}F'(\alpha_1\alpha_2\alpha_1'\alpha_2')\,b_{\alpha_1}^+ b_{\alpha_2}^+ b_{\alpha_2'} b_{\alpha_1'}+ \tag{2}$$
$$+\frac{1}{2}\sum_{(\alpha_1\alpha_2\alpha_1'\alpha_2')}F_1''(\alpha_1\alpha_2\alpha_1'\alpha_2')\,a_{\alpha_1}^+ b_{\alpha_2}^+ b_{\alpha_2'} a_{\alpha_1'}+$$
$$+\frac{1}{2}\sum_{(\alpha_1\alpha_2\alpha_1'\alpha_2')}F_2''(\alpha_1\alpha_2\alpha_1'\alpha_2')\,b_{\alpha_1}^+ a_{\alpha_2}^+ a_{\alpha_2'} b_{\alpha_1'}.$$

where a_α and b_α are the Fermi amplitudes relative to the solvent and impurity atoms respectively, L and F matrix elements with the same significance as [4] L' and F' matrix elements similar to the last but referring to the impurity system, and F'' "mixed" matrix elements characterizing interaction between the solvent and impurity systems.

The indices α and α' replace a trio of terms, namely f, the number of the site, λ the principal and orbital quantum numbers, and S the spin quantum number of the electron.

Using the commutation relationships for the Fermi operators a_α and b_α, taking into account in the energy operator the s-state and one of the p-states (the non-degenerate case) and carrying out a straighforward transformation into the Hamiltonian form (bearing in mind that $N_2 \ll N_1$), it is not difficult to obtain, to the nearest neighbour approximation, an expression for the mean energy of the crystal, for the case of complete polarization of the impurities, in the following forms:

$$E_1 = 2I(f0\,f0)N_1 + 2F(f_1 0\,f_2 0\,f_1 0\,f_2 0)N_1 + 2F(f0\,f0\,f0\,f0)N_1 +$$
$$+ I'(f0\,f0)N_2 + I'(f1\,f1)N_2 + F'(f1\,f0\,f1\,f0)N_2 + 2F''(f_1 0\,f_2 0\,f_1 0\,f_2 0)N_2 +$$
$$+ 2F''(f_1 0\,f_2 1\,f_1 0\,f_2 1)N_2 - F''(f_1 0\,f_2 1\,f_2 1\,f_1 0)N_2 -$$
$$- F(f_1 0\,f_2 0\,f_2 0\,f_1 0)N_1 - F''(f_1 0\,f_2 0\,f_2 0\,f_1 0)N_2, \tag{3}$$

VOL. 5 1957

where $L\,(f0f0)$, $L'\,(f0\,f0)$ and $L'\,(f1\,f1)$ are the mean energies from corresponding terms of the additive part of the Hamiltonian, whereas the terms F_1, F' and F'' are the mean energies of electrostatic and volume interaction between electrons in the main constituent and impurity systems. (It can be shown, e.g. by considering, using the same method, molecules composed of two different atoms, that F denotes the mean energy of electrostatic and volume interaction between a main-constituent in one atom and the electrons of neighbouring atoms, F'' the energy of interaction of an impurity-atom electron with the electrons of neighbouring main-constituent atoms, and F' the energy of interaction between the electrons of impurity atoms.

If it is taken into account that polarization does not occur in either main-constituent or impurity sites, the expression for the mean energy of the crystal, under the simplifying assumption made above, assumes the form:

$$\begin{aligned} E_2 = {} & 2L\,(f0\,f0)N_1 + 2F\,(f_10\,f_20\,f_10\,f_20)\,N_1 + 2F\,(f0\,f0\,f0\,f0)N_1 + \\ & + 2L'\,(f0\,f0)\,N_2 + 2F'\,(f0\,f0\,f0\,f0)\,N_2 + 4F''\,(f_10\,f_20\,f_10\,f_20)N_2 - \\ & - F\,(f_10\,f_20\,f_20\,f_10)N_1 - 2F''\,(f_10\,f_20\,f_20\,f_10)N_2. \end{aligned} \tag{4}$$

If it is admitted that some impurities may be spontaneously polarized on interacting with atoms and electrons of the main constituent, then in this case $E_2 > E_1$, i.e.

$$\begin{aligned} & \Delta E N_2 + F'\,(f1\,f0\,f1\,f0)N_2 - 2F''\,(f_10\,f_20\,f_10\,f_20)\,N_2 + F''(f_10\,f_20\,f_20\,f_10)\,N_2 + \\ & + 2F''\,(f_10\,f_21\,f_10\,f_21))N_2 - F''\,(f_10\,f_21\,f_21\,f_10)N_2 < 2F'\,(f0\,f0\,f0\,f0)N_2, \end{aligned} \tag{5}$$

where $\Delta E = L'\,(f1\,f1) - L'\,(f0\,f0)$ is the excitation energy for an electron in an impurity atom, $2F''\,(f_10\,f_21\,f_10\,f_21) + F'\,(f1\,f0\,f1\,f0) - F''\,(f_10\,f_21\,f_21\,f_10)$ is the energy of electrostatic and volume interaction for an electron, excited in the impurity atom A^* (to the nearest neighbour approximation), and $2F''\,(f_10\,f_20\,f_10\,f_20) - F''\,(f_10\,f_20\,f_20\,f_10) + 2F'\,(f0\,f0\,f0\,f0)$ is the energy of interaction of a non-excited electron in an impurity atom with electrons in the same site and electrons of the main constituent in neighbouring sites (A_B).

Thus, condition (5) can be rewritten in abbreviated symbols as follows,

$$\Delta E + A^* < A_B, \tag{6}$$

i.e. spontaneous polarization is possible in the system of interacting electrons of an atomic semiconductor with impurities, if the energy of interaction of an electron in an impurity atom (to the nearest neighbour approximation) exceeds the sum of the excitation energy of an electron in an impurity atom and the interaction energy of the excited electron (exciton). In this case the crystal must have the properties of a semi-metallic substance, since conduction electrons exist, however low the temperature.

Exactly the same result is also obtained using the quasi-classical approximation, analogous to that applied [6] to the study of polar states. In this connexion it is shown that the band of states in the presence of polarized lattice sites (i.e. the impurity sites) overlaps the non-polar band in the case where condition (6) is satisfied.

The transition temperature of a semi-metal to the normal semiconductor state is clearly determined by the condition that the number of electrons arising from spontaneous polarization of impurities (equal to the number of impurities) should equal the number of electrons arising from thermal ionization, i.e.

$$N_2 = N_1 e^{-\frac{\Delta E_0}{kT_n}}. \tag{7}$$

In experiments by Fritzsche and Laik-Horovitz [7] for germanium semiconductors with small amounts of impurity, the transition temperature was found to be near 50°K, rising with increasing impurity content. Substituting in (7) the experimental values of N_1, N_2 and ΔE_0, we obtain $T_n \simeq 33$°K for $N_2 \sim 10^{15}$ cm^{-3} and $T_n \simeq 44$°K for $N_2 \sim 10^{16}$ cm^{-3}.

Translated by E. Bishop

REFERENCES

1. S.V. Vonsovskii, *Zh. tekh. fiz.*, 25, 12 (1958).
2. A.N. Kushnirenko, *Avtoref. dissertation, Sverdlovsk* (1955).
3. E.N. Agafonova, *Fiz. metal. metalloved.*, 2, 391 (1956).
4. N.N. Bogolyubov, *Lektsii po kvantovoi statistike (Lectures on quantum statistics)* (1949).
5. S.V. Tyablikov, *Zh. tekh. fiz.*, 23, 715 (1953).
6. S.P. Shubin and S.V. Vonsovskii, *Phys. Z. Sowjet.* 7, 3 (1953).
7. H. Fritzsche and K. Laik-Horovitz, *Physica*, 20, 834 (1954).

VOL.
5
1957

THEORY OF GALVANOMAGNETIC PHENOMENA IN METALS*

F.G. BASS, M.I. KAGANOV and V.V. SLEZOV

Physico-technical Institute, Academy of Sciences, Ukrainian SSR

(Received 16 October 1956)

Expressions are obtained for the resistivity and Hall constant in arbitrary magnetic fields, for the two-zone model of a metal with a quadratic, anisotropic dispersion law.

1. The newly developed theory of galvanomagnetic phenomena [1] has shown that measurement of the asymptotic value (in a strong magnetic field) of the components of the conductivity tensor can help to elucidate the topology of the isoenergy surfaces near the Fermi surface and to determine the value $n_1 - n_2$ (n_1 is the number of electrons and n_2 the number of "holes"). In this connexion a single-valued interpretation of the experimental data obtained will only be possible for the case when it is obvious that the magnetic field is sufficiently intense and the measured values of the components of the conductivity tensor are in fact asymptotic values. A possible criterion of this is "stable" saturation of resistivity for $n_1 \neq n_2$ or a "stable" secondary quadratic resistivity relationship, if $n_1 = n_2$.

However there is a lack at present not only of any kind of complete data on all the components of the conductivity tensor in a strong magnetic field, for any of the metals, but even of detailed studies of the anisotropy of the Hall "constant" in a strong field; thus, we cannot at present tell whether open isoenergy surfaces exist or whether the major rôle in all metals is played by closed surfaces (cf. [1]). On the other hand there is a large number of experimental papers [2] in which, by selecting the constants describing the electron gas (mobility, effective masses), attempts are made to describe the curves of resistivity and the Hall field against magnetic field. In this connexion it has occurred to the authors, in order to resolve this difficulty, to resort to the assumption that there are large numbers of groups of current-carriers of different sign. Since the introduction of each fresh group yields two additional parameters, it is in fact satisfactory to describe the curve by two comparatively monotonic curves. Notwithstanding the obviously arbitrary nature of construction of such a type, they appear to us to possess a definite significance: it can be hoped that they (such constructions) will provide a theoretical understanding of the behaviour of the resistivity and the Hall constant in the intermediate range of magnetic fields $\Omega\tau \sim 1$†. In particular, they may give us more precise information on the linear portion of the curve relating resistivity to magnetic field (Kapitsa's law). Many features of this phenomenon are up to now unclear. For instance, it is difficult to explain why in practice all metals in the transition zone, where one would expect the relationship to be more complicated, such strict monotonicity, approximating closely to a linear relationship, is observed.

The aim of the present paper is to find out what conclusions are derivable from the assumptions that the electron spectrum is of a two-zone nature and that the relationship of the electron and "hole" energy to the wave-vector is quadratic. The isotropic case and special cases of anisotropy have been considered previously [3,5].

Our problem is to elucidate the effect of any anisotropy of the effective masses and mean free path times (see below).

---

* *Fiz. metal. metalloved.*, 5, No. 3, 406-411, 1957.

† $\Omega = eH/mc$ is twice the Larmor frequency, τ — the mean free path time.

2. We shall consider the kinetic equation for the electron distribution function* in a single zone having the dispersion law:

$$\varepsilon = \frac{1}{2}\left(\frac{1}{m}\right)_{ik} p_i p_k, \tag{1}$$

where $(1/m\ ik)$ is the reciprocal effective mass tensor,

$$\frac{e}{c}\frac{\partial f_1}{\partial \vec{p}}[\vec{v}, \vec{H}] + \left(\frac{\partial f_1}{\partial t}\right)_{cm} = -\frac{\partial f_0}{\partial \varepsilon} e(\vec{E}\,\vec{v}). \tag{2}$$

As is known, the basic relationship of the kinetic coefficients of metals to temperature, both with and without a magnetic field present, is connected with the relationship to temperature of the mobility and not with the deviation of the equilibrium Fermi function from its value when $T = 0$. Thus we can assume that:

$$-\frac{\partial f_0}{\partial \varepsilon} = \delta(\varepsilon - \varepsilon_0), \tag{3}$$

where ϵ_0 is the limiting Fermi energy.

The collision integral, broadly speaking, is an integral operator which, at sufficiently low temperatures, when the major rôle is played by collisions with impurities, can (at least in the isotropic case) be replaced by the expression f_1/r, where r is the relaxation time for the electron gas. Thus the solution to kinetic equation (2), in the light of (1), can be written in the form:

$$-e\frac{\partial f_0}{\partial \varepsilon}\vec{A}\,\vec{v}, \tag{4}$$

where $\vec{A}$ is a constant vector (independent of the electron impulses).

In order to take into account anisotropy, which the collision integral may introduce, we shall assume that

$$\left(\frac{\partial f_1}{\partial t}\right)_{cm} = -\frac{\partial f_0}{\partial \varepsilon} eA_i\left(\frac{1}{\tau}\right)_{ik} v_k, \tag{5}$$

where $(1/r)ik$ is the "tensor" of the mean free path time. We note that in this connexion, as usual,

$$f_1 = -\frac{\partial f_0}{\partial \varepsilon}\vec{e}\vec{v}\vec{A}.$$

* More correctly, for the linear increment (owing to the electrical field) to the equilibrium Fermi function.

Actually, if expression (4) is substituted into equation (2), taking (5) also into account, then v_i is eliminated and an algebraic equation is obtained for vector A_i, containing no terms dependent on the electron impulse (on the assumption that τ_{ik}, m_{ik}, etc. are constants for the metal*).

To study galvanomagnetic properties we must obtain an expression for current density:

$$\vec{j} = \frac{2e}{h^3} \int \vec{v} f_1 (d\vec{p}).$$

From (4), (3) and (1) it follows that

$$j_l = \frac{2e^2V}{h^3} A_l \left(\frac{1}{m}\right)_{ll}, \tag{6}$$

where V is the volume of the ellipsoid in impulse space occupied by the electrons, and $2V/h^3 = n$, the number of electrons. If we are dealing with a completely filled zone, then

$$\varepsilon = \varepsilon_1 - \frac{1}{2}\left(\frac{1}{m}\right)_{ik} p_i p_k, \tag{7}$$

and expression (6) retains its form (in this case $2V/h^3$ plays the rôle of number of "holes").
When $H = 0$

$$A_l = E_k \tau_{kl},$$

so that

$$j_l = \frac{2e^2V}{h^3} E_k \tau_{kl} \left(\frac{1}{m}\right)_{ll}.$$

Hence

$$\sigma_{ik} = ne^2 \left(\frac{1}{m}\right)_{ll} \tau_{kl} \tag{8}$$

a natural, generalized expression, valid in the isotropic case

$$\left(\sigma = \frac{ne^2\tau}{m}\right).$$

* They may depend on the energy, but in connexion with (3) not significantly.

Using formulae (1), (3), (4), (6) and (8) we average equation (2) over all the impulses, first multiplying it by $2ev_i/h^3$. After simple manipulations we obtain

$$j_i = \sigma_{ik}\left\{E_k + \frac{1}{ecn}[\vec{j}\,\vec{H}]_k\right\}. \text{ (electrons)} \tag{9}$$

If instead of expression (1) we use the dispersion law (7), the sign in front of the second term in equation (9) is reversed:

$$j_i = \sigma_{ik}\left\{E_k - \frac{1}{ecn}[\vec{j}\,\vec{H}]_k\right\} \text{ (holes)} \tag{10}$$

When there are several zones, then

$$j_i = \sum j_i^{(\mu)}, \tag{11}$$

where the superscript μ denotes the number of the zone. Each of the partial currents j_i^{μ} satisfies the equation

$$j_i^{(\mu)} = \sigma_{ik}^{(\mu)}\left\{E_k \pm \frac{1}{ecn^{(\mu)}}[\vec{j}^{(\mu)}, \vec{H}]_k\right\}. \tag{12}$$

Here $\sigma_{ik}^{(\mu)}$ is the partial conductivity, and $n^{(\mu)}$ the number of particles of the μ-th type. The sign of the second term is determined by whether we are dealing with electrons (+) or holes (–).

This discussion indicates that if there is a quadratic dispersion law (1) then it is unnecessary, for a consideration of galvomagnetic phenomena, to solve the kinetic equation: we can use averaged equations of the type of (8). This assertion, of course, results from the assumptions noted above (on the form of the collision integral (5) and the degeneration of the electron gas (3)).

3. Before discussing the two-zone model in detail, we note that in the presence of a single zone the resistivity and Hall constant are completely independent of the magnetic field (apart from their dependence on anisotropy). In fact, from the definition of resistivity

$$\rho = \frac{E_i j_i}{j^2}. \tag{13}$$

From (9) (or (10)):

$$E_i = \rho_{ik} j_k \pm \frac{1}{ecn}[\vec{j}\,\vec{H}]_i, \tag{14}$$

where ρ_{ik} is the resistivity tensor for $H = 0$. If the last expression is projected on the current axis we can satisfy ourselves that the magnetic field is entirely eliminated. From the same expression (14) it

follows that the Hall "constant" is actually a constant in this case:

$$R = \pm \frac{1}{enc} \text{ ((–) for electrons, (+) for holes).}$$

4. We now turn to consideration of the two-zone model. To calculate the resistivity tensor it is necessary to express current in terms of the field $\vec{E}$. From (12) we have:

$$j^{(\mu)} = \frac{\hat{\sigma}^{(\mu)}\vec{E} \pm \frac{1}{cn^{(\mu)}c}\|\sigma^{(\mu)}\|\left[\vec{E}, \hat{\rho}^{(\mu)}\vec{H}\right] + \frac{1}{e^2n^{(\mu)2}c^2}\vec{H}(\vec{E}\vec{H})}{1 + \frac{1}{e^2n^{(\mu)2}c^2}\|\sigma^{(\mu)}\|(\vec{H}\hat{\rho}^{(\mu)}\vec{H})} \tag{15}$$

Here $\hat{\sigma}\vec{E}$ signifies $\sigma_{ik}E_k \ldots$; $\|\sigma\|$ is a determinant consisting of the elements of matrix σ_{ik}, and $\hat{\rho} = \hat{\sigma}^{-1}$. The total current is in fact a sum of similar expressions. Writting the expression for total current in the form

$$j_i = \sigma_{ik}(\vec{H})j_k,$$

we can find all the components of the resistivity tensor in a magnetic field. The reciprocal tensor $\rho_{ik}(\vec{H}) = \sigma^{-1}_{ik}(\vec{H})$ can be calculated according to the general rules.

Omitting some cumbersome manipulations, we write the expression for resistivity (13) and Hall "constant"

$$R = \frac{\rho_{xy}(\vec{H}) - \rho_{xy}(-\vec{H})}{2H} \tag{16}$$

(the z-axis is directed along the magnetic field, and the x-axis coincides with the current direction). Thus, in the case of two zones ($n_1 \neq n_2$):

$$\rho = \rho_0 \frac{1 + \frac{b^2|c|^{(1)}|_{xx}|c^{(2)}|_{zz} + a^2|c^2|_{xx}\sigma^{(1)}_{zz} + b^2\|\sigma^{(2)}\|\sigma^{(1)}_{yy} + a^2\|\sigma^{(1)}\|\sigma^{(2)}_{yy} - 2ab|\sigma^{(1)}|_{xz}|\sigma^{(2)}|_{xz}}{|c^{(1)} + c^{(2)}|_{xx}}H^2}{1 + (a-b)^2 \cdot \frac{\|\sigma^{(1)}\| \cdot |\sigma^{(2)}|_{zz} \cdot \|\sigma^{(2)}\| \cdot |\sigma^{(1)}|_{zz}}{\|c^{(1)} \cdot c^{(2)}\|}H^2},$$

$$R = R_0 \frac{1 + ab(b-a)\frac{(\|c^{(1)}\| \cdot |c^{(2)}|_{zz} + \|\sigma^{(2)}\| \cdot |\sigma^{(1)}|_{zz})H^2}{a(\|\sigma^{(1)}\| + \sigma^{(2)}_{zi}\|c^{(1)}|_{iz}) - b(\|\sigma^{(2)}\| + \sigma^{(1)}_{zi}|\sigma^{(2)}|_{iz}}}{1 + (a-b)^2 \cdot \frac{\|\sigma^{(1)}\| \cdot |\sigma^{(2)}|_{zz} + \|\sigma^{(2)}\| \cdot |\sigma^{(1)}|_{zz}}{\|\sigma^{(1)} + \sigma^{(2)}\|}H^2} \tag{17}$$

Here $|\sigma^{(\mu)}|_{ik}$ is the corresponding minor;

$$a = \frac{1}{n_1ec}; \quad b = \frac{1}{n_2ec};$$

$\rho_0 = \rho\ (0)$ and R_0 is the Hall "constant" in weak fields.
If the number of electrons equals the number of "holes", $a = b = 1/nec$.

$$\rho = \rho_0 \left[1 + \frac{|\sigma^{(1)}|_{xx}\sigma^{(2)}_{zz} + |\sigma^{(2)}|_{xx}|\sigma^{(1)}|_{zz} - 2\sigma^1|_{xz}|\sigma^{(2)}|_{xz} + \|\sigma^{(2)}\sigma^{(1)}_{yy} + \sigma^{(1)}\sigma^{(2)}_{yy}}{|\sigma^{(1)} + \sigma^{(2)}|_{yy}} \left(\frac{H}{nec}\right)^2 \right]$$

$$R = \frac{1}{nec} \frac{\sigma^{(1)}\| + \sigma^{(2)}_{zz}|\sigma^{(1)}|_{iz} - \|\sigma^{(2)}\| - \sigma^{(1)}_{zz}|\sigma^{(2)}|_{iz}}{\|\sigma^{(1)} + \sigma^{(2)}\|}$$

Thus we see that the introduction of anisotropy in the effective masses and mean free path times does not fundamentally alter the relationships of resistivity and Hall "constant" to the magnetic field, as compared with the isotropic case. In particular, the discussion gives a single quadratic relationship for resistivity:

$$\rho = \rho_0 \left(1 + \frac{H^2}{H_0^2}\right),$$

which leaves no room for Kapitsa's law. It is of interest to note that the addition of a third group of current carriers, e.g. electrons

$$n_1^{(1)} + n_1^{(2)} = n_2^{(3)}$$

leads to different quadratic relationships in weak and strong fields. This fulfils a rule which is true of all the metals examined [4], namely that the coefficient of H^2 in weak fields is greater than the coefficient of H^2 in strong fields. Actually, in this case*

$$\rho \sim \rho_0 + \frac{u_1 u_2 u_3 (H/c)^2}{n_1^{(1)}(u_2 u_3 + u_2 u_1) + n_1^{(2)}(u_1 u_3 + u_1 u_2)} \left\{ 1 + \right.$$

$$\left. + \frac{n_1^{(1)} n_1^{(2)} n_2^{(3)} (u_1 - u_2)^2 (u_1 + u_3)^2 (u_2 + u_3)^2}{u_1 u_2 u_3 \left[n_1^{(1)}(u_1 + u_3) + n_1^{(2)}(u_2 + u_3) \right]} \right\}, \quad (H \ll H_0);$$

$$\rho \sim \frac{u_1 u_2 u_3 (H/c)^2}{n_1^{(1)}(u_2 u_3 + u_2 u_1) + n_1^{(2)}(u_1 u_3 + u_1 u_2)} \quad (H \gg H_0).$$

In this case $H_0 \sim c/eu$.

In conclusion the authors express their thanks to E.S. Borovik and I.M. Lifshits, for useful discussions.

Translated by E. Bishop

* We have confined ourselves for the sake of simplicity, to the isotropic case: $u_i = \tau_i/m_i$, the mobility, u_1 and u_2 are electron mobilities and u_3 the "hole" mobility.

VOL. 5 1957

REFERENCES

1. I.M. Lifshits, M.Ya. Asbel' and M.I. Kaganov, *Zh. eksp. teor. fiz.*, No. 7 (1956).
2. E.S. Borovik, *Izv. Akad. Nauk SSSR*, 19, 429 (1955).
3. A. Wilson, *Theory of Metals*.
4. E.S. Borovik, *Zh. eksp, teor. fiz.*, 23, 91 (1952).
5. E.S. Borovik, *Fiz. metal. metalloved.*, 2, 33 (1956).

VOI
5
19

MAGNETIC PROPERTIES OF MAGNETICALLY ANISOTROPIC SPECIMENS MADE FROM FERROMAGNETIC POWDERS 1. MAGNETIZATION CURVES AND INDIVIDUAL HYSTERESIS LOOP CYCLES*

E.V. SHTOL'TS, YA.S. SHUR and G.S. KANDAUROVA

Institut Fiziki Metallov Ural'skogo Filiala Akad. Nauk SSSR

(Received 17 May 1957)

The dependence of the nature of anisotropy of magnetization curves for magnetically textured specimens, made from fine MnBi-alloy powders, on the grade of powder has been established. In the case of certain grades of powder, a peculiarity is observed in longitudinally textured specimens during the process of technical magnetization, in that the magnetization to saturation is attained in fields which are weaker than the maximum value of magnetization and coercive force.

On the basis of results obtained an assumption is made about the nature of the magnetic structure of fine-grained powders (transition structure).

VOL. 5 1957

As is known, the magnetic properties of ferromagnets depend on their magnetic structure. This relationship has been thoroughly studied in magnetically soft materials, which possess an inherently multi-domain magnetic structure. In magnetically hard ferromagnets this relationship has been studied extremely little. There is every reason to assume that in fine-grained powders, and also in heterogenous alloys, where the small ferromagnetic particles formed are isolated from each other by non-ferromagnetic layers, there is only one domain within each ferromagnetic particle [1, 2]. At certain definite ferromagnetic particle sizes a transitional magnetic structure can arise which, under certain conditions, appears as mono-domain structure, and under other conditions as multi-domain [3]. There can be no doubt that a transition to such a type of structure, as well as to a mono-domain one, is bound to influence the magnetic properties of ferromagnets in a definite way. Hence, the present work is devoted to the elucidation of this relationship. It must be said that in view of the great experimental difficulties involved it has not yet been possible to correlate the magnetic structure, observed in separate particles by visual methods, with its magnetic characteristics. Therefore, for the solution of the given problem we confined ourselves to testing the magnetic properties of magnetically textured specimens made from powders of a MnBi alloy of varying dispersion. Qualitative conclusions can be made about the changes in magnetic structure of the ferromagnet from the nature of the change in magnetic properties of the specimens with decrease in powder particle size. The alloy MnBi was chosen as the object for investigation because it can be made, due to its high magnetic anisotropy constant, to assume a transitional and even mono-domain structure [3] in comparatively coarse particles. Besides, this alloy possesses magnetic uniaxiality, as a result of which a distinct anisotropy in magnetic properties is evident in magnetically textured specimens. The use of magnetically textured powder specimens enables the peculiarities of the magnetic structure of fine-grained powders to be elucidated even more fully.

In the present work, magnetization curves and individual hysteresis loop cycles were studied.

SPECIMENS FOR INVESTIGATION

The alloy MnBi was made by sintering powders of manganese and bismuth at 550°C for 2 hours. The coercive force H_c of the alloy was 80 oersted. MnBi powders were made by mechanical grinding, followed by sorting into fractions according to particle size.

The mean diameter of the particles in the various fractions varied from 1.2 mm to 3 μ. The test specimens had a cylindrical shape and were made in the following way: the powder was thoroughly mixed with a binder, the mixture thus obtained was rammed into an appropriate die and placed between the poles of an electromagnet; then compacting of the powder particles was carried out in the magnetic field. The

* *Fiz. metal. metalloved.*, 5, No. 3, 412-420, 1957.

angle between the axis of texture and the axis of the specimen is called ϕ.

Investigations were carried out on three types of specimen which were made a) with the magnetic field placed along the specimen axis ($\phi = 0°$, longitudinally textured specimens); b) without application of a magnetic field (isotropic); c) with the magnetic field being applied perpendicular to the specimen axis ($\phi = 90°$, cross-sectionally textured specimens). The proportion of ferromagnetic phase in the specimens was about 20 per cent.

Testing of magnetic properties was carried out by a ballistic method of throwing down. Prior to plotting elementary magnetization curves* the specimens were demagnetized in a constant field of opposite sign.

Investigations have established the fact that no anisotropic magnetic properties are observed in specimens made of coarse powders of MnBi alloy [4]. Therefore only specimens made of fine powders, 7 and 3μ were used for detailed study. Besides, some tests were also carried out on specimens made from powder of particle size 63μ. The magnitudes of coercive force and relative residual magnetism of the specimens investigated are given in the Table.

mens in which the texture axis is perpendicular to the specimen axis ($\phi = 90°$).

TEST RESULTS

(a) Magnetization curves.

In Figs. 1, 2 and 3 magnetization curves, obtained by various methods of magnetization, are reproduced for textured specimens with particle sizes 63, 7 and 3 μ, respectively. The magnetizing field strength is plotted along the axis of the abscissae, and the relationship between actual magnetism and magnetization to saturation, along the axis of the ordinates.

As can be seen from Fig. 1, the anisotropy between magnetization curves for specimens with a particle size of 63 μ is small; the magnetization curve for the longitudinally textured specimen (curve 1) reaches higher than that for the isotropic (curve 2).

From Fig. 2, in which magnetization curves of textured and isotropic specimens, made from powder of particle size 7 μ, are shown, it can be seen that in this case the magnetization curve for the longitudinally textured specimen (curve 1) is very steep,

TABLE 1. Coercive force and relative residual magnetism of specimens made from powders of the alloy MnBi.

Texture / Size, μ	$\varphi = 0°$		Isotropic		$\varphi = 90°$	
	H_c	I_r/I_s	H_c	I_r/I_s	H_c	I_r/I_s
3	9000	0.93	5600	0.61	1600	0.15
7	3500	0.90	2500	0.46	2000	0.26
63	1000	0.30	950	0.24	850	0.21

As can be seen from the Table, the nature of anisotropy of the coercive force and relative residual magnetism is independent of particle size. At all powder particle sizes, specimens in which the texture axis coincides with the specimen axis ($\phi = 0°$), possess a maximum coercive force and residual magnetism. In isotropic specimens the corresponding factors are lower. A minimum coercive force and relative residual magnetism is observed in speci-

and magnetization to saturation is reached in a field of about 5000 oersted. The magnetization curve for the isotropic specimen (curve 2) is more sloping and reaches saturation only in a field of 16,000 oersted. To magnetize a cross-sectionally textured specimen (curve 3) is even more complicated*.

Thus, as the particle size decreases to 7 μ, the nature of anisotropy of magnetization curves is preserved, but the difference between the paths

* In future these will simply be called magnetization curves.

* It should be stated that in the fields at our disposal for

(continued on next page)

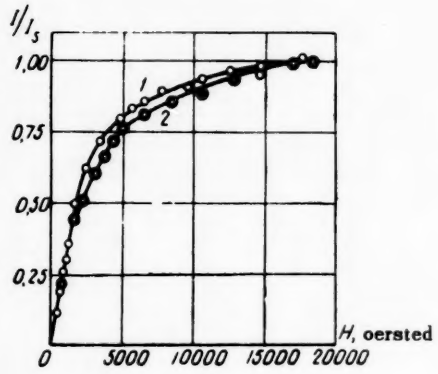

FIG. 1. Magnetization curves for specimens made from powder of particle size 63 μ:
1 – longitudinally textured,
2 – isotropic.

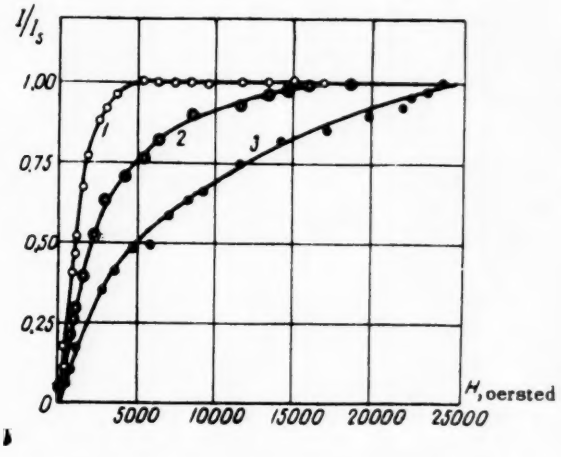

FIG. 2. Magnetization curves for specimens made from powder of particle size 7 μ:
1 – longitudinally textured,
2 – isotropic,
3 – cross-sectionally textured.

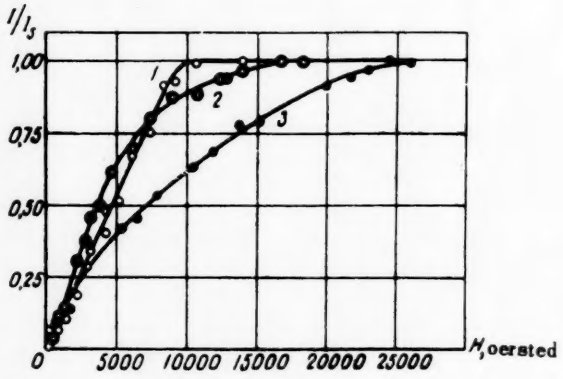

FIG. 3. Magnetization curves for specimens made from powder of particle size 3 μ:
1 – longitudinally textured,
2 – isotropic
3 – cross-sectionally textured.

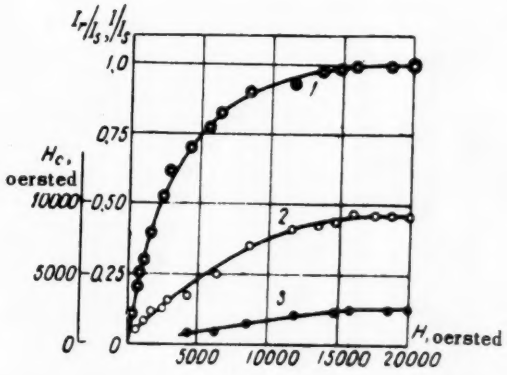

FIG. 4. Dependence of degree of magnetization (curve 1), residual magnetism (curve 2) and coercive force (curve 3) on the magnitude of the magnetizing field of an isotropic specimen.
Powder particle size 7 μ.

(continued from previous page)
cross sectionally textured specimens, magnetization to saturation was not attained. For I_s a magnetization in a field of 24,500 oersted is assumed.

travelled by the magnetization curves considerably increases. With further decrease in particle size the nature of anisotropy of magnetization curves changes, as can be seen from Fig. 3, in which magnetization curves for specimens made of powder of 3 μ particle size are reproduced. Namely, the magnetization curve for the longitudinally textured specimen (curve 1) in weak fields passes below the corresponding curve for the isotropic specimen (curve 2); in a field of 8,000 oersted they cross, and only in stronger fields does the magnetization curve for the longitudinally textured specimen (curve 1) pass above the analogous curve for the isotropic specimen (curve 2). The path of the magnetization curve for the cross-sectionally textured specimen (curve 3) is less steep, i.e. this specimen is more difficult to magnetize.

Thus, the anisotropy of the magnetization curves for specimens made of coarse powders (larger than 50 μ) is not very pronounced. A decrease in particle size leads to an increase in the extent of anisotropy of the magnetization curves, but its characteristics are preserved. However, a further decrease in particle size (to 3 μ) makes magnetization of longitudinally textured specimens more difficult, and hence leads to a change in the nature of anisotropy of magnetization curves.

(*b*) *Individual hysteresis loop cycles.*

In Figs. 4-8 the relationship between the relative magnitude of magnetization (curve 1), residual magnetism (curve 2), as well as coercive force (curve 3) and the amplitude of the magnetizing field for specimens with different powder coarseness is given.

As can be seen from Fig. 4, saturation in the magnetization curve and a maximum value for the coercive force and relative residual magnetism for an isotropic specimen, made from powder with a particle size of 7 μ is attained in the same fields at about 16,000 oersted. With a cross-sectionally textured specimen made from powder of the same mesh (Fig. 5), maximum values for coercive force and relative residual magnetism are attained in approximately the same fields (about 17,000 oersted): however, considerably stronger fields are required for magnetization to saturation.

A particular type of regularity is observed for individual hysteresis cycles in a longitudinally textured specimen made from powder of the same mesh (7 μ). As can be seen from Fig. 6, magnetization (curve 1) reaches saturation in fields of the order of 5000 oersted, although the residual magnetism and coercive force are still far from their maximum values in this field ($I_r/I_s = 0.57$, $H_c = 1200$ oersted). A further increase of the magnetic field, without changing the degree of magnetization, leads to an increase in residual magnetism and coercive force, which reach their maxima in a field of about 10,000 oersted. The maximum relative residual magnetism in this case is 0.90.

Let us now consider corresponding curves plotted for longitudinally textured specimens made from powder of different particle size. In Fig. 7 analogous curves are given for a longitudinally textured specimen made from powder with a particle size of 63 μ. In this case the magnetic fields in which magnetization to saturation and maximum relative residual magnetism and coercive force is attained, practically coincide. It should be noted that the maximum value of the relative residual magnetism of this specimen is extremely low ($I_r/I_s = 0.30$).

In Fig. 8 analogous curves, plotted for a longitudinally textured specimen, made from powder with a particle size of 3 μ, are reproduced. The maximum relative residual magnetism in this case is close to unity, i.e. the residual magnetism is nearly equal to magnetization to saturation. The curve representing the relationship between residual magnetism and magnetic field (curve 2) is close to the magnetization curve (curve 1). A maximum for both residual magnetism and coercive force is attained in the same fields as magnetization to saturation. This field is about 10,000 oersted strong.

Thus, in longitudinally textured specimens made from fine powders of various particle sizes, a peculiarity is observed during magnetization in that magnetization to saturation of the specimen is attained in weaker fields than the maximum for residual magnetism and coercive force.

ANALYSIS OF RESULTS

As can be seen from the test results given, the magnetic properties of both magnetically anisotropic specimens can change in an extremely complex manner with change in powder mesh. There can be no doubt that these changes in magnetic characteristics are directly associated with changes of the magnetic structure of the ferromagnet.

First of all it should be noted that magnetic anisotropy becomes pronounced only in specimens made from fine powders (see Table, Figs. 2-3); it is not observed in specimens made from coarse powders (see Table, Fig. 1). This is due to the fact that, with our method of making an alloy for investigation, the coarse powders, as a rule, consist of a few grains of MnBi alloy with random crystallographic orientation. Therefore, it is impossible to

VOL 5 195

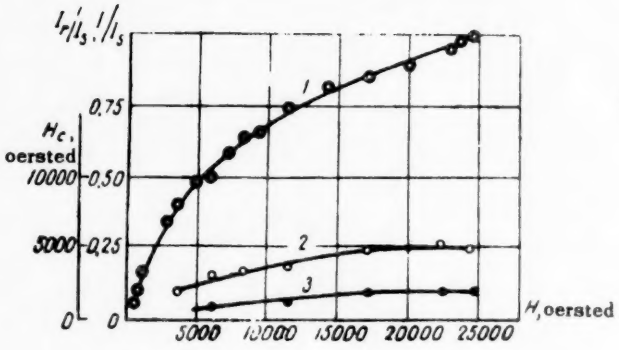

FIG. 5. Same as Fig. 4 for a cross-sectionally textured specimen. Powder particle size 7 μ.

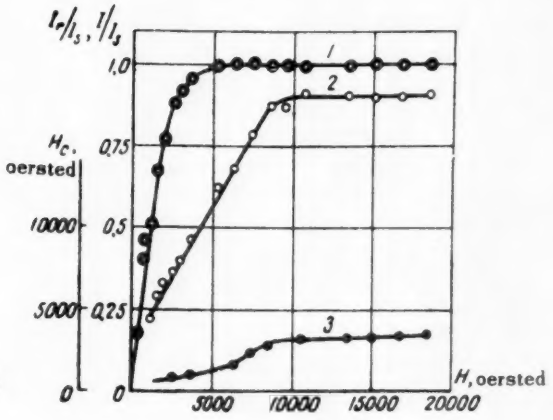

FIG. 6. Same as Fig. 4 for a longitudinally textured specimen. Powder particle size 7 μ.

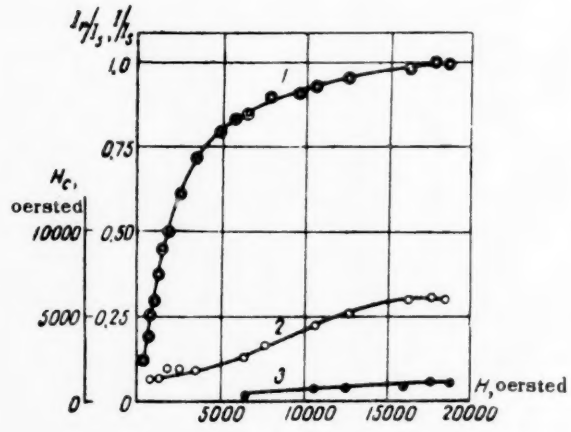

FIG. 7. Same as Fig. 4 for a longitudinally textured specimen. Powder particle size 63 μ.

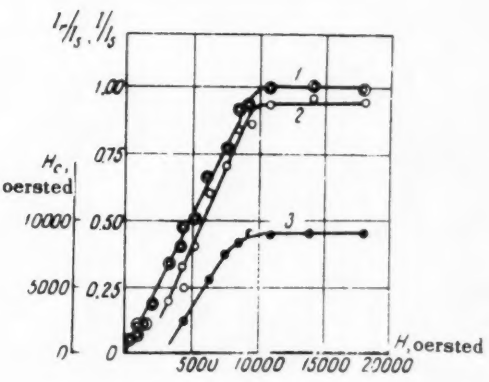

FIG. 8. Same as Fig. 4 for a longitudinally textured specimen. Powder particle size 3 μ.

bring about a sizeable magnetic texture in specimens made from grains of powder of such dimensions. As the alloy particle size is decreased, there is an increasing tendency for the formation of compacts consisting of one crystal (i.e. monocrystals). After exposing such monocrystal compacts to a magnetic field a specimen is obtained in which separate powder grains possess axes of easy magnetization in one direction. In this case a distinct anisotropy in magnetic properties can be expected, as the specimen represents a magnetically uniaxial pseudo-crystal with an enormous anisotropy constant, inherent in the MnBi alloy. The nature of anisotropy in such specimens, it appears, must vary with the type of magnetic structure of the separate grains of powder. From Fig. 2 it can be seen that in specimens with grains of 7 μ an anisotropy in magnetization curves is observed, which is in-

herent in magnetically soft material. Namely, the curve for the longitudinally textured specimen (curve 1) passes, in all fields, above the analogous curves for both the isotropic and cross-sectionally textured specimen. In magnetically soft material the type of anisotropy under consideration is associated with its multi-domain magnetic structure. It appears that in the present case the magnetic structure of fine powders is multi-domain. The magnetization curves for specimens from powder with a particle size of 3 μ (Fig. 3) have some similarity to analogous curves plotted for magnetically textured specimens made from the strongly coercive alloy Alnico [1], which appears to possess an essentially mono-domain structure. Probably, therefore, the intersection of curves 1 and 2 in our case is associated with the fact that there occurs, in separate powders, a mono-domain or close to mono-domain structure.

An approach to the mono-domain structure can be expected to occur for various magnetic characteristics at somewhat different powder grain sizes. Thus, a maximum degree of magnetization, residual magnetism and coercive force in a longitudinally textured specimen, made from powder with particle size of 63 μ, in which the mono-domain structure predominates, is attained at the same field stength (Fig. 7).

However, in a longitudinally textured specimen made from powder with a particle size of 7 μ the maximum value of the characteristics indicated is attained at different field strengths (Fig. 6). Here, the residual magnetism and coercive force reach a maximum at field strengths close to each other (10,000 oersted); the strength of this field is considerably greater than that at which the magnetization curve reaches saturation (5000 oersted).* These mechanisms may be understood if it is assumed that there exists, at a given powder particle size, in the original condition, a magnetic structure of the following form: a separate grain of powder consisting of one region, at the boundaries of which there are situated closely adjoining regions † (Fig. 9b). Such a magnetic structure will be a transitional one between a multi-domain (Fig. 9a) and a mono-domain (Fig. 9c). When a magnetic field is applied (in the given case parallel to the orientation of magnetization in the basic region) a decrease in the size of the adjoining regions occurs, the I_s of which is opposite to the field direction. The volume of the basic region at the same time increases.

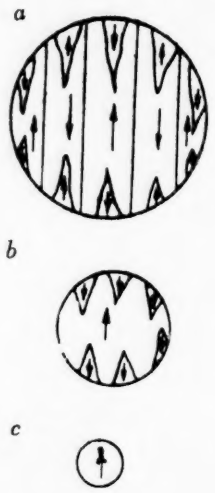

FIG. 9. Lay-out of the domain structure of magnetically uniaxial particles:
a – multi-domain,
b – transitional,
c – mono-domain.

In fields of 5000 oersted, the whole volume of the powder particles, in the presence of the field, becomes magnetized in the direction of the field; the adjoining regions are still preserved, but their volume is negligible. Therefore, from the appearance of the magnetization curve it can be assumed that saturation is reached. When the field is applied, the adjoining regions grow (they play the role of a kind of seed crystal of remagnetization), as a result of which the residual magnetism as well as coercive force remain negligible. On magnetizing in a strong field (10,000 oersted) the adjoining regions disappear, and they do not reappear when the field is removed. Hence, the magnitude of the residual magnetism is close to that of the magnetization to saturation. The coercive force also reaches a maximum. Remagnetization can be brought about by a

* A similar mechanism was first noticed by Guillaud [7].

† As indicated before [5], the expression "closely adjoining regions" is conventional.

process of rotation. A difference between the values of magnetization to saturation and residual magnetism may be due to the specimen not having a fully magnetic texture, the easy magnetization directions of separate powder grains not being entirely parallel to each other.

We have confirmed the existence of a transition structure by investigating the domain structure of a MnBi alloy by the method of powder shapes [5].

In even finer powders a greater approach to the mono-domain structure can be expected. Here, there is only one basic region in individual particles; adjoining regions are absent. Such a structure leads to saturation having to occur in stronger fields. At the same time, the magnetization curve, residual magnetism and coercive force must attain saturation at the same field strength.

Such a mechanism can be observed in curves of Fig. 8, which have been obtained for a longitudinally textured specimen made from powder of particle size 3 μ.

CONCLUSIONS

On the basis of examinations of magnetization curves and individual hysteresis cycles for isotropic and magnetically textured specimens, made from a manganese-bismuth alloy of varying dispersion, it has been found that a transitional magnetic structure from multi-domain to mono-domain, as well as a mono-domain structure can exist in fine powders.

Translated by G. Isserlis

VOL. 5 1957

REFERENCES

1. L.A. Shubina, Ya.S. Shur, *Zh. tekh. fiz.* 19, 88, (1949).
2. V.I. Drozhzhina, M.G. Lushinskaya, Ya. S. Shur, *Zh. tekh. fiz.* 19, 95, (1949).
3. D.A. Shturkin, Ya. S. Shur, *Zh. tekh. fiz.* 19, 235, (1949); 20, 1393, (1950).
4. Ya. S. Shur, E.V. Shtol'ts, G.S. Kandaurova, *Fiz. metal. metalloved.* 2, 569, (1956).
5. E.V. Shtol'ts, Ya. S. Shur, *Dokl. Akad. Nauk SSSR*, 95, 781, (1954).
6. Ya. S. Shur, E.V. Shtol'ts, G.S. Kandaurova and L.V. Bulatova, *Fiz. metal. metalloved.* 5, 234, (1957).
7. C. Guillaud, *Journ. Phys. radium*, 12, 492, (1951).

MAGNETIC PROPERTIES OF MAGNETICALLY ANISOTROPIC SPECIMENS MADE FROM FERROMAGNETIC POWDERS II DEPENDENCE OF MAGNETIZATION CURVES ON THE METHOD USED FOR BRINGING ABOUT A DEMAGNETIZED STATE*

YA. S. SHUR, E. V. SHTOL'TS and G. S. KANDAUROVA

Institut Fiziki Metallov Ural'skogo Filiala Akad. Nauk SSSR

(Received 17 May 1957)

Study of the dependence of return curves for magnetically anisotropic specimens made from MnBi alloy powders on powder particle size. The appearance of magnetization curves for specimens along their texture axis has been studied in relation to the method used for bringing about demagnetization and to the coarseness of the powder. The results obtained confirm the assumption made that there exists a transitional magnetic structure in fine particles of MnBi alloys.

As shown [1], certain peculiarities occur in magnetically anisotropic specimens, made from fine powders, in the course of technical magnetization processes. In the explanation of these peculiarities the assumption was said to have been made that they are caused by the emergence of a particular type of magnetic structure, different from both multi-domain and mono-domain (transitional magnetic structure). These assumptions about the transitional magnetic structure must be more closely defined. For this purpose it is essential that new experimental results on magnetic properties of specimens made from fine powders should be obtained. With this in mind, the present work has been carried out, which is concerned with the study of demagnetization curves and the relationship between magnetization curves and the method by means of which the initial demagnetized state of specimens, made from powders of MnBi alloy of variable dispersion, is brought about.

SPECIMENS FOR INVESTIGATION AND TESTING METHODS

The MnBi alloy was made by sintering manganese and bismuth powders at a temperature of 320°C for 2 hours. The coercive force of this material is 1000 oersted, $4\pi I_s = 4000$ G and the relative residual magnetism $I_r/I_s = 0.30$.

The concentration of ferromagnetic phase in the alloy is 50 per cent. The powders were made by mechanical grinding, followed by sieving into fractions according to particle size. The average particle diameter of separate fractions varied from 1.2 mm to 4 μ.

From these powders disk shaped specimens (15 mm diameter, 2 mm thick) were made. The magnetic texture was induced in these specimens by the following method: the powder was thoroughly mixed with a binder, the mixture thus obtained transferred to a disk-shaped mould, which was placed between the poles of an electromagnet and heated until the binder was molten ($\sim$ 60°C). Then the specimen was cooled in a magnetic field, which fixed the powder particles in position. Let ϕ be the angle between the direction of the orientating magnetic field during the making of the specimen (axis of texture) and the direction of the magnetic field during the testing of magnetic properties.

The magnetic properties of the specimens were tested by a ballistic method. Before plotting magnetization curves the specimens were first demagnetized. Demagnetizing of fine powder specimens presents considerable difficulties. At room temperature it was impossible to bring about demagnetization of magnetically anisotropic specimens by a smooth decrease of the amplitude of an alternating magnetic field or of the commutating permanent magnetic field. Demagnetization of the specimens was brought about by three methods. First, fine powder specimens were demagnetized by an alternating magnetic field at the temperature of liquid nitrogen, where the coercive force is small, owing to the low value of the constant of anisotropy (case "*a*"). Secondly, demagnetization of the specimens was brought about at room temperature by a reverse magnetic field. In this case it was necessary to choose, for each specimen, a reverse magnetic field of such

* *Fiz. metal. metalloved.* 5, No. 3, 421-427, 1957.

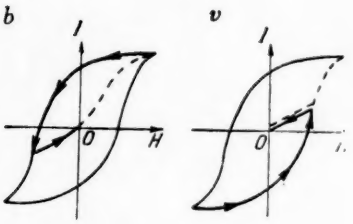

FIG. 1. Method for attaining the demagnetized state with the help of a reverse field (full line) and corresponding magnetization curves (dashed line).

field in which the magnetization curve is plotted; *v*) on the other hand, the field which previously demagnetized the specimen now coincides in sign with the field in which the magnetization curve is plotted.

TEST RESULTS

a) Demagnetization curves

In Fig. 2 demagnetization arms of hysteresis curves and return curves are shown, which were obtained at various angles to the texture axis of a specimen made from powder with a particle size of 4 μ. In the direction $\phi = 0°$ (Fig. 2a) the return curves are nearly completely horizontal, i.e magneti-

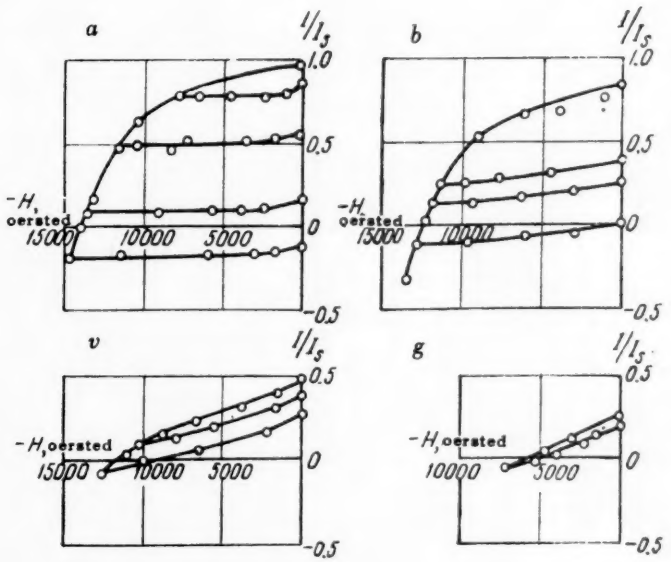

FIG. 2. Demagnetization arms of hysteresis loops and return curves for a textured specimen of particle size 4 μ in the directions:
a – $\phi = 0°$,
b – $\phi = 30°$,
v – $\phi = 60°$ and
g – $\phi = 75°$.

magnitude as to cause the specimen to be demagnetized when this field was disconnected. A graphic representation of the magnetization of the specimens attained with this method of demagnetizing is given in Fig. 1. As can be seen from the figure, two cases are possible: *b*) the field which demagnetizes the specimen is opposite in sign to the

zation does not change with decrease in field strength. Only in weak fields is a small change in magnetization observed. In the directions $\phi = 30°$ and $\phi = 60°$ (Fig. 2b and 2v) the horizontal portion disappears in return curves, i.e. as the field decreases, an increase in magnetization is observed in return curves. However, the curves have an

VOL. 5 1957

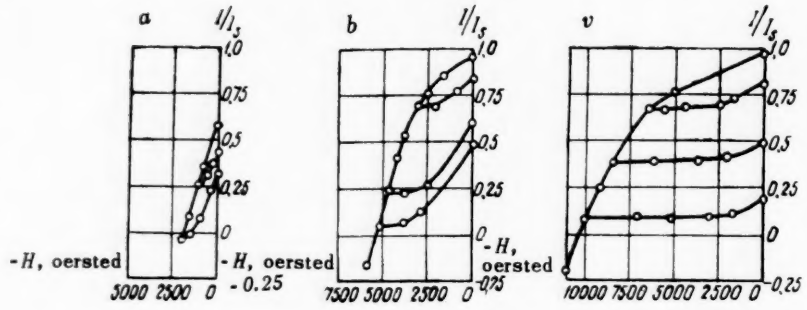

FIG. 3. Demagnetization arms of hysteresis loops and return curves for the direction $\phi = 0°$ of textured specimens with particle sizes:
$a = 250\ \mu$,
$b = 25\ \mu$,
$v = 6\ \mu$.

unusual appearance, namely, the curvature of these curves is in the downward direction. In the direction $\phi = 75°$ (Fig. 2 g), where the magnitude of residual magnetism and coercive force are low and the demagnetization arm is a straight line, the return curve goes comparatively steeply upwards as the field strength is increased, and practically overlaps with the hysteresis loop. All recovery curves are reversible.

In Fig. 3 demagnetization arms of the hysteresis loop and return curves along the texture axis for specimens made from powder of various mesh are given. In the case of a specimen made from powder of particle size 250 μ (Fig. 3 a), the magnetism on return curves changes with change in field strength over the whole field range. As the particle size decreases, so the nature of return curves changes, a horizontal portion making its appearance on them, i.e. within a certain range of field strength the magnetism is independent of the field strength. In a specimen made from powder of particle size 25 μ (Fig. 3 b) no change in magnetism is observed within a small field strength range; on further lowering of field strength an increase in magnetism is observed. In a specimen made from powder of particle size 6 μ (Fig. 3 v) the horizontal position of return curves continues to fields of about 2000 oersted, and an insignificantly small increase in magnetism is observed only in weaker fields.

Thus, an anomalous shape of return curves is observed in magnetically textured specimens made from fine powders in the direction of the texture axis. This anomaly becomes more pronounced as the fineness of the powder increases.

b) Magnetization curves along the textured axis of specimens after their demagnetization by various methods.

In Fig. 4 magnetization curves for the direction $\phi = 0°$ of a specimen, made from powder of 25 μ mean particle size, after a demagnetized state had been attained by using the three above methods, are given. As can be seen from the diagram, magnetization is most easily carried out when the first method of demagnetization is applied (curve *a*). After demagnetizing by the second method the path of magnetization curves depends on the sign of the demagnetizing field relative to the field in which the magnetization curve is plotted. If the demagnetized state has been obtained by method "*b*", then magnetization is easy to carry out, and the field in which magnetization to saturation can be attained need be only a little stronger (curve *b*) than that required after application of the first method for demagnetizing (curve *a*). If the demagnetized state was obtained by method "*v*", then magnetizing is more difficult (curve *v*), the magnetization curve has a step-like appearance, and the primary portion of the magnetization curve coincides with the return curve.

In Fig. 5 magnetization curves for specimens with varying particle size are given, where the demagnetized state had been obtained by the first method (case "*a*"). As can be seen from the curves in Fig. 5, as the particle size decreases, the magnetization

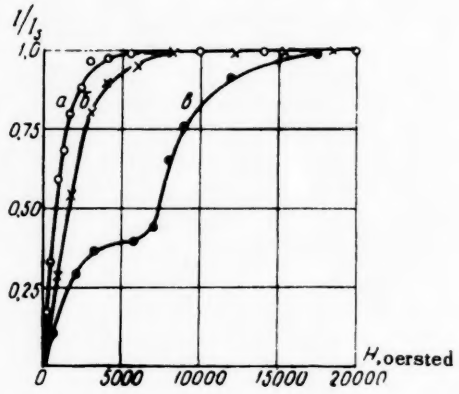

FIG. 4. Magnetization curves for the direction $\phi = 0^0$.
a – after demagnetization by an alternating field at a temperature of – 196°C;
b and *v* – after demagnetization by a reverse direct field at room temperature (see Fig. 1).
Powder particle size = 25 μ.

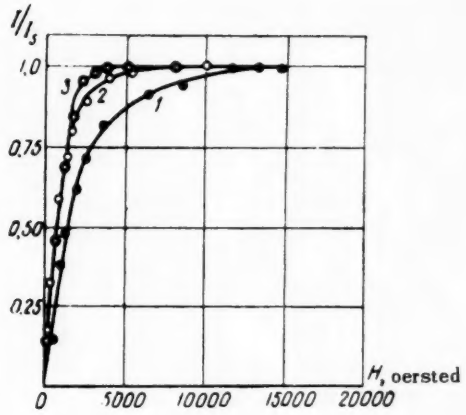

FIG. 5. Magnetization curves for the direction $\phi = 0^0$
after demagnetization by an alternating field at a temperature of – 196°C.
Powder particle sizes:
1 = 250 μ, 2 = 25 μ and 3 = 6 μ.

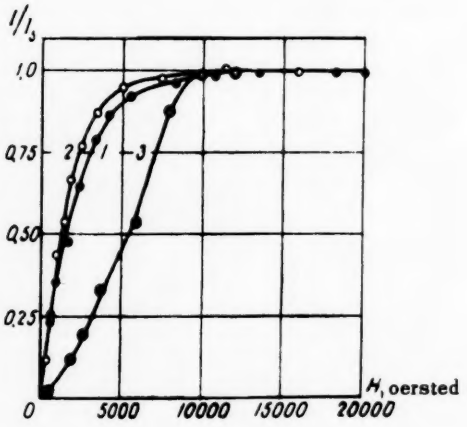

FIG. 6. Magnetization curves for the direction $\phi = 0^0$ after demagnetization by a reverse direct field (see Fig. 1 (b)) at room temperature.
Powder particle sizes:
1 = 250 μ, 2 = 25 μ and 3 = 6 μ.

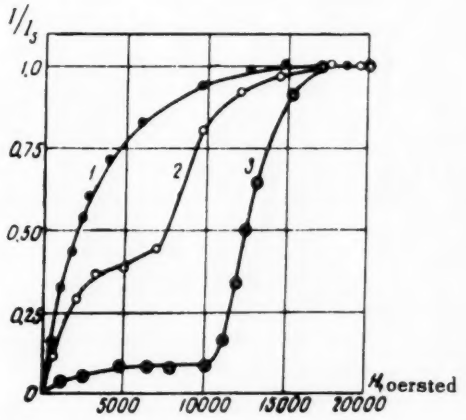

FIG. 7. Magnetization curves for the direction $\phi = 0^0$ after demagnetization by a reverse direct field at room temperature.
Powder particle sizes:
1 = 250 μ, 2 = 25 μ, 3 = 6 μ.

curves become steeper, and curves 3 and 2 (6 and 25 μ respectively) differ markedly from curve 1 (250 μ). The difference in the paths of magnetization curves 2 and 3 is not great, and becomes apparent only in the vicinity of saturation.

In Fig. 6 magnetization curves for specimens with different powder particle sizes, after demagnetizing by method "*b*", are given (see Fig. 1 b). As can be seen from the curves in Fig. 6, magnetizing a specimen made from powder of particle size 25 μ

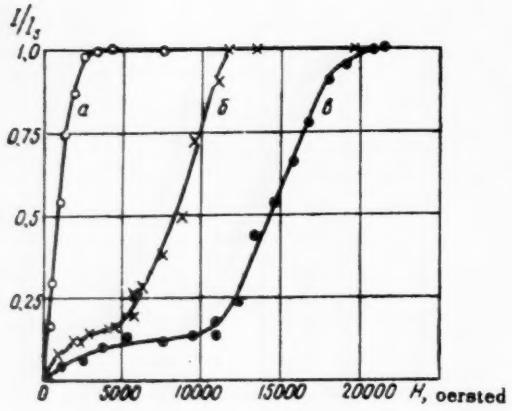

FIG. 8. Magnetization curves for the direction $\phi = 0°$:
a — after demagnetization by an alternating field at a temperature of — 196°C;
b and *v* — after demagnetization by a reverse direct field at room temperature (see Fig. 1).
Powder particle size = 4 μ.

(curve 2) is easier than one made of coarser powder (curve 1). However, with further decrease in particle size, magnetization is observed to become more difficult, and the curve 3 (6 μ) passes considerably below curve 1 (250 μ) and curve 2 (25 μ).

In Fig. 7 magnetization curves are given for specimens with various powder particle sizes, after being demagnetized by method "*v*" (see Fig. 1 v). After such a demagnetization the magnetization process, on changing to specimens with a smaller particle size, only becomes more difficult: the finer the powder, the lower down does the magnetization curve pass. For specimens of fine powders (25 and 6 μ, curves 2 and 3) the magnetization curve assumes a step-like appearance. In curve 3 the "step" extends up to field strengths of the order of the coercive force, and magnetization is attained only about within 0.1 of the value of magnetization to saturation. With further increase in field strength a sharp growth in magnetization takes place.

In Fig. 8 magnetization curves are given for the direction $\phi = 0°$ of a specimen made from even finer powder (4 μ). Demagnetization of the specimen was carried out by the three above mentioned methods. As can be seen from the diagram, the magnetization curve, after demagnetizing at the temperature of liquid nitrogen (curve *a*) is steep, attaining saturation in a field of about 4000 oersted. Magnetization curves after demagnetizing in a constant field at room temperature are step-like in appearance. A considerable increase in magnetization is observed in curve *b* in a field of around 6000 oersted, and in curve *v* in a field of 11,000 oersted. When comparing the curves of Figs. 4 and 8, we see that the curve of type "*b*" approaches that of type "*v*" as the powder particle size decreases.

Thus, in textured specimens made from fine powders of MnBi alloy a number of peculiarities is observed in the direction $\phi = 0°$ during the process of technical magnetization. A change of demagnetization method leads not only to a change in the appearance of magnetization curves, but also to a change of the nature in the relationship between these curves and the particle size of the powder. Also, the magnetization curve obtained after demagnetizing by method "*b*", in the case of coarse powders, is close to the magnetization curve obtained after demagnetizing by method "*a*". As the particle size decreases, the magnetization curves obtained after demagnetizing by method "*b*" increasingly approach magnetization curves obtained after demagnetizing by method "*v*".

ANALYSIS OF RESULTS

As has been established earlier, on the basis of investigations of certain peculiarities in magnetic properties of specimens made from fine powders of MnBi alloy [1], as well as by visual inspection of the domain structure of fine particles of this alloy [2], the transition to fine powders is accompanied by a change in magnetic structure of a ferromagnet. There is no doubt that these changes in magnetic structure are the reason for the peculiarities, discovered in the present work, of the paths of return curves and for the dependence of magnetization curves on the method of demagnetization. The most interesting result, obtained in the course of studying return curves, is their unusual path obtained when testing specimens made of fine powder along the axis of texture. The peculiarity of the path of return curves observed appears to be due to the presence of a transitional magnetic structure in small particles. After excluding the magnetic field which takes the specimen to saturation, there is, in the state of residual magnetism, only one basic domain within separate particles. Besides, adjacent regions arise, the volume of which, however, is extremely small. The last assumption is confirmed by the fact that the magnitude of the residual magnetism of such a specimen is nearly equal to that of magnetization to saturation (Fig. 2 a). If a field of opposite sign is included and gradually increased in strength, a decrease in magnetization takes place while there is a growth in the volume of adjacent domain, part of

VOL
5
195

which act as nuclei for remagnetization. It appears that the growth of nuclei of remagnetization is irreversible, which is also the reason for unaltered magnetization when the strength of the opposite field is lowered; hence the horizontal portion on the return curve. The reasons for such irreversibility in a large range of magnetic fields are as yet not clear, and require additional study.

The second important result is that there is a close dependence of magnetization curves on the conditions under which the initial demagnetized state is attained. This difference is associated with the fact that when we apply different methods of demagnetization, we create, in different types of specimens a basic magnetic structure, which then determines the conditions of magnetization of a ferromagnet.

On demagnetizing in an alternating field at a temperature of liquid nitrogen, a multi-domain structure is formed even in specimens made from fine powders (a few μ). This is due to the critical dimension for the onset of the mono-domain structure (and, hence, also of the transition structure) decreasing with lowering of the anisotropy constant. On heating such a demagnetized specimen to room temperature, a change takes place in its magnetic structure. However, the multi-domain structure formed persists, and for this reason magnetization processes proceed with relative ease under the influence of the external field, which is shown by the attainment of saturation in relatively weak fields.

On demagnetizing in a direct field, using method "*b*" and "*v*", a transitional magnetic structure is formed in the powder particles. The finer the powder, the more different will be the structure obtained from a multi-domain structure resulting from treatment by method "*a*", and therefore the more different will be the magnetization curves "*b*" and "*v*" from curves "*a*" (see Figs. 4 and 8).

The difference between magnetization curves plotted after demagnetizing the same specimen by methods "*b*" and "*v*" indicates that the conditions for the development of remagnetization nuclei are different in these cases. It appears that the magnetizing process in the case "*v*" approaches the magnetizing process of a mono-domain structure to a greater extent than in the case "*b*", which is responsible for the step-like path travelled by the magnetization curves (e.g. curve 3, Fig. 7). The exact mechanism of change of domain structure in this case requires more detailed study.

CONCLUSIONS

The investigations carried out have confirmed that there arises a transitional magnetic structure in fine MnBi alloy powders. In the presence of such a structure in a direction along the texture axis of magnetically anisotropic specimens the hysteresis of formation and growth of remagnetization nuclei plays a particular role in the process of technical magnetizing.

Translated by G. Isserlis

REFERENCES

1. E.V. Shtol'ts, Ya. S. Shur and G.S. Kandaurova, *Fiz. metal. metalloved.* 5, 412, (1957).

*2. Ya. S. Shur, E.V. Shtol'ts, G.S. Kandaurova and L.V. Bulatova, *Fiz. metal. metalloved.* 5, 234 (1957).

* See errata on last page of this issue.

EFFECT OF ANNEALING REGIME ON THE THERMOMAGNETIC AGEING OF PERMANENT MAGNETS FROM THE ALLOY MAGNICO*

A.M. MOROZOVA and F.I. FEIGINA

State Scientific Research Institute of the Radiotechnical Industry

(Received 19 September 1956)

Experimental research has been conducted into the thermomagnetic ageing of permanent magnets from the alloy magnico as a function of the annealing regime with the object of establishing the conditions under which stability is increased.

It was established that the annealing regime affects thermomagnetic ageing. Both an increase in the duration of the tempering at 580°C and staggered tempering under a special regime make it possible to increase the stability of permanent magnets without changing the magnitude of their coercive force.

The thermomagnetic ageing of permanent magnets depends to a considerable extent on the type of alloy, the magnitude of the demagnetization factor and the magnitude of the coercive force. It is known that the greater the magnitude of the coercive force, the more stable is the magnet of the given alloy. The magnitude of the coercive force depends on the thermal treatment, in particular on the annealing. Earlier, the annealing of the alloy magnico had been studied with the object of getting the optimum magnetic properties, but the stability of the alloy was not also investigated. The present paper sets out to study the effect of the annealing regime on the stability of the alloy magnico so as to establish the conditions under which the stability of permanent magnets is increased.

METHOD OF INVESTIGATION

For the investigation samples of the alloy magnico of the following composition were selected: 15 per cent nickel, 24 per cent cobalt, 8.5 per cent aluminium, 3 per cent copper, the rest iron. The samples of a cross-section of 15 x 15 mm had a length of from 30 to 180 mm (l/d from 10.8 to 1.7); twelve samples of one melt were examined, two samples for each value of l/d.

After the usual thermomagnetic treatment (heating to 1300°C and cooling in a magnetic field at optimum speed) the samples were subjected to three different annealing regimes.

I annealing regime: 580°C, 24 hr; every four hr the annealing was interrupted, the coercive force was measured and the samples were subjected to thermomagnetic ageing.

II annealing regime: 580°C, 4 hr; 640°C, 2 hr; 580°C, 4 hr, after which the coercive force was measured and the samples were subjected to thermomagnetic ageing.

III annealing regime: 700°C, 15 min; 650°C, 30 min; 600°C, 1 hr; 580°C, 2 hr; 550°C, 2 hr. The total duration of the anneal was 5 hr 45 min; after that the coercive force was measured and the samples were subjected to thermo magnetic ageing.

To avoid the effect of deviations from the chemical composition every examined annealing regime was conducted on the same samples which were first once more subjected to thermomagnetic treatment.

The effect of the annealing regime on thermomagnetic ageing was verified by measuring the flux to the neutral of the samples during a cyclical change of temperature from + 20 to − 60°C.

For the cooling of the magnets to the temperature − 60°C a cryostat with dry ice (solid carbon dioxide) was used.

Before the temperature cycles the magnets were magnetized to saturation at room temperature. During the temperature cycles the flux to the neutral of the sample was measured in the disconnected state consecutively at temperatures of + 20, − 60 and + 20°C. The flux was measured in one and the same ballistic setting under identical conditions; the error of measurement did not exceed 0.5 per cent. The coercive force was measured by the ballistic method.

With cyclical variation of the temperature of the

* *Fiz. metal. metalloved.* 5, No. 3, 428-433, 1957

VOL
5
195

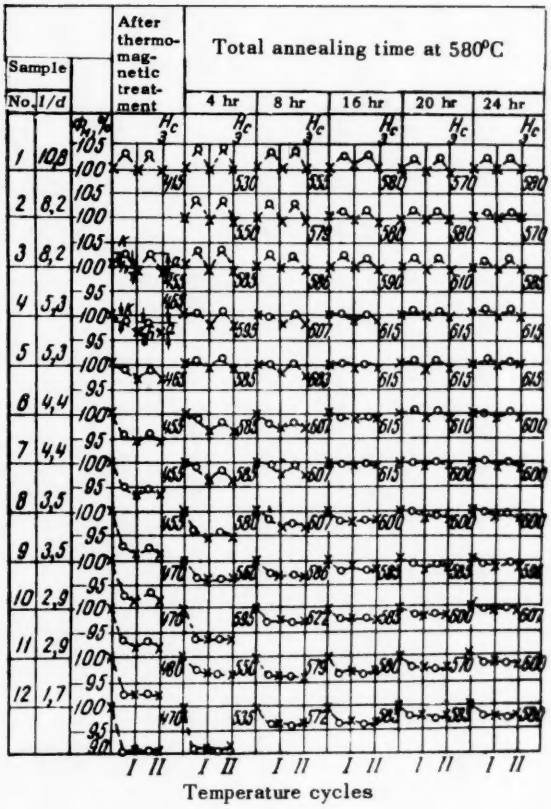

FIG. 1. Effect of annealing time at 580°C on the magnitude of the flux (ϕ_H) to the neutral of the magnets with different demagnetization factors at cyclic variation of the temperature from + 20 (x) to − 60°C (o).

permanent magnets thermomagnetic ageing is observed which can be characterized by three parameters of instability: the irreversible change h and the reversible changes a of the magnetic characteristics (in our case of the flux to the neutral) and the change K of the magnetic characteristic under the influence of the first cooling or heating (Fig. 1).

Where ϕ^H_{+20}, ϕ^H_t is the initial magnitude of the flux or other characteristic at + 20° and at the first action of the investigated temperature t; ϕ^k_{+20}, ϕ^k_t the magnitude of the flux or other characteristic at the investigated temperature t when the process is established.

The magnitude of the temperature coefficient,

$$h = \frac{(\Phi^K_{+20} - \Phi^N_{+20})}{\Phi^N_{+20}} \cdot 100; \quad a = \frac{\Phi^K_t - \Phi^K_{+20}}{\Phi^N_{+20}} \cdot 100;$$

$$K = \frac{(\Phi^N_t - \Phi^N_{+20})}{\Phi^N_{+20}} \cdot 100,$$

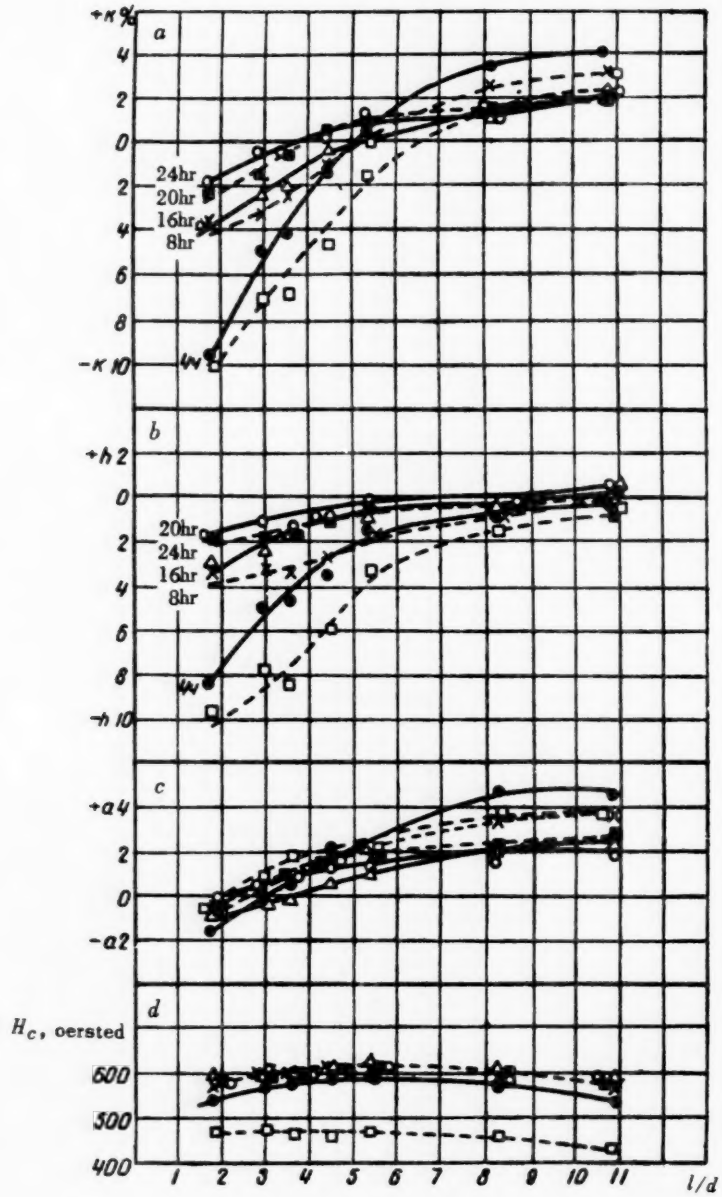

FIG. 2. Effect of annealing time at 580°C on the magnitude of the parameters of instability (K, h, a) of magnets with different demagnetization factors at cyclic variations of temperature from + 20 (x) to – 60°C (o):

□·····□ before annealing; ●——● 4 hr annealing ×·····× 8 hr;
△——△ 16 hr; ■·····■ 20 hr; ○——○ 24 hr.

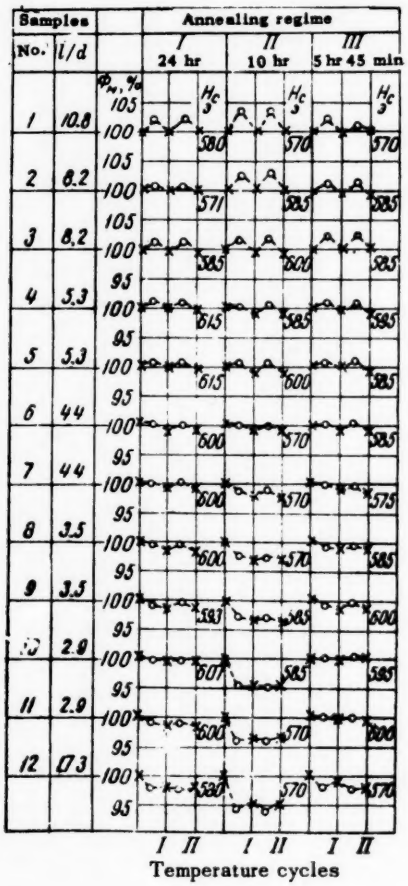

FIG. 3. Effect of the annealing regime on the magnitude of the flux (ϕ_H) to the neutral of the magnets with different demagnetization factors at cyclic temperature changes from + 20 (x) to − 60°C (o).

magnetic treatment (before tempering) and after tempering at 580°C for 4, 8, 16, 20 and 24 hr. Near every curve the corresponding value of the coercive force of the sample has been written in. The curves drawn show that when the annealing time is increased to more than 8 hr the relative changes of the flux decrease in all samples although their coercive force does not grow. For samples with a small demagnet-

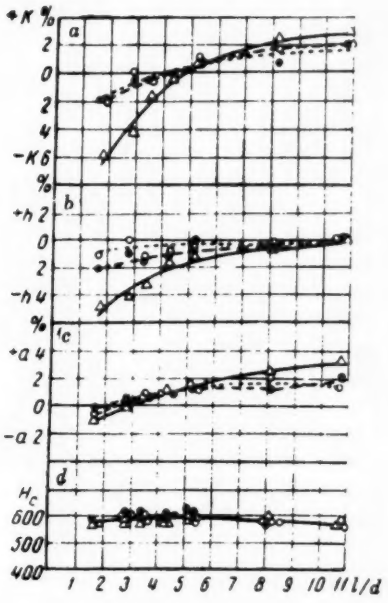

FIG. 4. Effect of the annealing regime on the magnitude of the parameters of instability (K,h,a) of magnets with different demagnetization factors at cyclic variations of temperature from + 20 (x) to − 60°C (o).
Tempering regime: •·····•— I;
∠——△— II;; ○ ····○ — III.

which reflects only reversible changes, cannot sufficiently fully characterize the process of thermomagnetic ageing. Therefore, we have in this investigation used the three above named parameters to describe the process of thermomagnetic ageing.

RESULTS OF INVESTIGATION

Fig. 1 shows the results of the measurement of the flux to the neutral with cyclic variation of the temperature from + 20 to − 60°C for samples with different demagnetization factors after thermo-

ization factor ($l/d \sim 10.8$ to 8.2), the flux increases with the first cooling. With the increase in annealing time the increase in flux diminishes. For example, in sample No. 3 ($l/d = 8.2$) the increase in flux decreases from 3.5 per cent after 4 hr annealing to 1 per cent after 24 hr, while the coercive force is the same. With increasing demagnetization factor the increase in flux on first cooling decreases and beginning with samples where l/d is 5.3 a decrease in flux is becoming noticeable which grows more and more. In samples with $l/d = 1.7$ the decrease in flux before tempering is 10 per cent. With

VOL. 5 1957

increasing annealing time from 8 to 24 hr the decrease in flux decreases for samples with $l/d = 5.3$ to 1.7, although the magnitude of the coercive force of the samples remains constant (for samples with $l/d \sim 3.5$ to 1.7 the decrease in flux decreases from 2 to 4 per cent to 0.5 to 2 per cent, for samples with $l/d = 4.4$ from 2.5 per cent to zero, and for samples with $l/d = 5.3$ the flux even begins to increase by 1 to 2 per cent). These changes in flux are on first cooling characterized by the parameter $K \pm$ which is shown in Fig. 2 as a function of the demagnetizing factor and annealing time. This also shows the two other parameters of instability: the irreversible change h and the reversible change a as well as the change in the coercive force.

From the curves of Fig. 2 it is evident that the annealing time has the greatest effect on the parameter K, that is on the rise or fall of the flux on first cooling, and on the parameter h, the irreversible change, although the coercive force ceases to increase already after over 8 hr annealing time. The greater the demagnetization factor of the sample, the stronger is the effect of annealing. In samples with $l/d > 5.3$ the effect of annealing on the magnitude of the parameters h and K is less significant. The magnitude of the irreversible changes a, on the contrary, is more affected by annealing in samples with a relatively small demagnetization factor ($l/d \geq 5.3$) and hardly at all in samples with large demagnetization factors ($l/d \leq 3.5$).

Figs. 3 and 4 give data on the thermomagnetic ageing of permanent magnets which have been annealed under regimes I, II and III. From the curves given for the parameters of instability K, h and a it is evident that the third and first regimes give very close and the best results although the magnitudes of the coercive force of the samples subjected to annealing under all three regimes hardly differed at all.

CONCLUSIONS

1. The annealing regime affects the thermomagnetic ageing of permanent magnets made from the alloy magnico: the parameters of instability K, h and a can be of different magnitude with one and the same magnitude of their coercive force close to its maximum.

2. At large magnitudes of the demagnetization factor ($l/d \leq 5.3$; $4\pi/N \leq 28$) the annealing regime has the greatest effect on two parameters of instability: on the parameter K which characterizes the first effect of cooling, and on the irreversible change h which is connected with it.

At relatively small values of the demagnetization factor ($l/d > 5.3$; $4\pi/N > 28$) the annealing regime has its greatest effect on the magnitude of the reversible changes, the parameter a.

3. The thermomagnetic ageing of permanent magnets depends on the magnitude of their coercive force until it reaches a value close to the maximum, at which the stability of magnets is in the main determined by the annealing regime.

4. The stability of permanent magnets made from the alloy magnico can be raised by means of increasing the annealing time at 580°C or by staggered annealing, for example under regime III.

Translated by B. Ruhemann

VOL 5 195

X-RAY STRUCTURE INVESTIGATION OF METALS AFTER ELECTRIC SPARK TREATMENT *

K.F. STARODUBOV and B.P. KOLESNIK

Institute of Ferrous Metallurgy Academy of Sciences, U.S.S.R.

(Received 4 June 1956)

Experimental data are given on the phase composition and microhardness of the surface layers of over 100 combinations of V, Mn, Zr, Nb with C, Al, Fe, Ni, Cu, Zn, Cd, Sn, Pb, Bi after electric spark treatment.

VOL. 5 1957

The electric spark treatment of metals proposed by the Soviet scientists B.R. and N.I. Lazarenko [1] has received wide application in industry for the hardening of tools and machine parts.

The physicochemical processes which occur in electric spark treatment are, however, insufficiently investigated because of their complexity and the shortness of the time they take. It is known [1 to 6] that the specific nature of these processes consists in that they cover small volumes and occur at very high temperatures (8,000 to 12,000°) in the course of very small time intervals (10^{-4} to 10^{-6} sec). After that the melted thin surface layers are cooled down with tremendous speed by the main cold mass of the whole piece.

Of very great theoretical and practical interest is the question of the interaction between different metals under the conditions of electric spark hardening.

Palatnik [2] has on the basis of an experimental study of 18 chemical elements as treated electrodes in various combinations with 9 treated metals (in all about 100 combinations) established the laws of interaction between the electrodes during electric spark hardening. In the literature this law is known as the "criterion of interaction". According to this law the composition of the vapour phase in the space between the electrodes is approximately described by the formula:

$$\frac{x_2}{x_1} \cong \frac{\tau_1}{\tau_2} \cong \frac{c_1 \rho_1 \lambda_1 (T_1 - T_0)^2}{c_1 \rho_2 \lambda_2 (T_2 - T_0)^2},$$

where x is the concentration of the vapours of the electrode material in the vapour phase, τ the time which precedes the beginning of the vaporization of the electrode material; c, ρ and λ respectively the specific heat, density and coefficient of heat conductivity of the electrode material; T the temperature field; T_0 the initial electrode temperature; magnitudes with index (1) refer to one electrode, with index (2) to the other. If $\tau_1 \cong \tau_2$ interaction and the formation of solid solutions, compounds and phases takes place on the surface of the electrodes. If $\tau_1 \gg \tau_2$ a transfer of metal 2 to electrode 1 takes place, but if $\tau_1 \ll \tau_2$ metal 1, on the contrary, is transferred to electrode 2.

Using the criterion of interaction, one can foresee the nature of the interaction between any electrodes if their thermal constants are known.

Starting from a theoretical analysis of the thermal conditions of electric spark hardening, Gusev [6] has shown that since the criterion of interaction is qualitative, it correctly describes the phenomena of interaction in electric spark hardening in the first approximation.

In the previous quoted paper [2], however, the combinations of the elements with such important metals as V, Mn, Zr and Nb, with which steel and other alloys are frequently alloyed, were not investigated.

It is known that small additions of V, Zr and Nb have a strong effect on the properties of steel [7, 8]. The great importance of the use of carbide forming elements for obtaining surfaces with very great microhardness in electric spark hardening was noted in the paper by Krasyuk [4].

Therefore, to find out whether or not the criterion of interaction is valid for these metals, too, is of great interest, since, in the first place, it enables one to show the general validity of the criterion of

* *Fiz. metal. metalloved.* 5, No. 3, 434-441, 1957.

TABLE 1. Phase composition of the surface layers of metals (on the cathode) after electric spark treatment with various elements from X-ray structure analysis data.

Treated metal (cathode)	Treating electrode (anode)													
	C Graphite	Al	V	Mn	Fe	Ni	Cu	Zn	Zr	Nb	Cd	Sn	Pb	Bi
Al	Al_4C_3	Al_2O_3	$\gamma_1\gamma_2\gamma_3^{\bullet}$ α V_2O_5	γ_1 $MnAl_6$ Mn	FeAl Fe_2Al_5 $FeAl_3$	NiAl $NiAl_2$ $NiAl_3$	γ $CuAl_2$		γ*ψ $ZrAl_3$ ZrO_2	γϑτ Al_2O_3 NbO_2				
V	VC V_2C α	$\gamma_3^{\bullet}\alpha_1^{\bullet}\alpha_2^{\bullet}$ Al_2O_3 V_2O_5	V_2O_5 V_2O_5	α ν* MnO	$\alpha_1\alpha_2\beta$ V_2O_5 Fe_3O_4	$\alpha_2^{\bullet}$ γ_1	α γ CuO	V+Zn V_2O_5 ZnO	α β* ϑ	β* NbO	Cd CdO	Sn	ı b	Bi Bi_2O_3
Mn	Mn_3C γ—Mn	$\gamma_1\gamma_2^{\bullet}\eta$ $MnAl_6$ MnO	α β—Mn V_2O_5	β—Mn MnO	γ* νω Fe_3Mn	$\gamma_1\gamma_2^{\bullet}$ Ni_3Mn MnO	τ,ω MnO	γMn+Zn MnO ZnO	ντ,ω ψ	ν ω $\alpha_2^{\bullet}$ τ	Cd CdO	Sn SnO_2	Pb PbO	Bi
Fe	Fe_3C	FeAl Fe_3Al_5	β α_2	γ* ω Fe_3Mn	γ FeO	α $\gamma_1\gamma_2$ FeO	Cu+Fe FeO		α Zr_2Fe_2 ZrO_2	α φ Fe_3O_4				
Ni			$\alpha_1\alpha_2^{\bullet}$ $\gamma_3^{\bullet}$	γ_1 ω MnO					γ*β ZrO_2 NiO	$\alpha_1^{\bullet}\alpha_2^{\bullet}$ γ_1 NbO				

VOL 5 195

VOL. 5 1957

TABLE 1. (*continued*)

Treated metal (cathode)	Treating electrode (anode)													
	C Graphite	Al	V	Mn	Fe	Ni	Cu	Zn	Zr	Nb	Cd	Sn	Pb	Bi
Cu	Cu + graphite	γ Al_4Cu_9	α* CuO	γ ω MnO	α+Cu FeO	γ τ	Cu		γ* ZrO_2	α γ Cu_2O				
Zn			Zn	Zn ZnO MnO					Zn	Zn ZnO				
Zr	ZrC	ψ γ* $ZrAl_3$ ZrO_2	τ* α* κ V_2O_3	τ MnO	β Zr_3Fe_3 FeO ZrO_2	ψ β γ* ZrO_2	ψ β γ* α ZrO_2	Zn+Zr ZnO	β—Zr ZrO_2	ψ β α	Cd CdO	Sn	Pb PbO	Bi
Nb	NbC	α γ ϑ Al_2O_3 NbO	α β NbO V_2O_3	α_1 α_2^* ε	α* τ NbO_2	α_1^* α_2^* γ_1 γ_2^* NbO_2	λ CuO NbO_2	Nb+Zn ZnO	ψ α NbO ZrO_2	Nb NbO NbO_2	Cd CdO	Sn	Pb PbO	Bi
Cd			Cd	Cd CdO MnO_2					Cd ZrO_2	Cd				
Sn			Sn	Sn SnO					Sn	Sn SnO_2				
Pb			Pb	Pb PbO MnO					Pb	Pb				
Bi			Bi	Bi					Bi	Bi				

Note. Greek letters denote solid solutions; an asterisk supersaturated solutions; the positive sign corresponds to the formation of a mechanical mixture of the materials of anode and cathode in the surface layer of the cathode.

TABLE 2. Microhardness of samples before and after electric spark hardening H^{20}_{KhB}, kg/mm³.

Treated metal (cathode)	Microhardness of cathode before treatment	Treating electrode (anode)													
		C Graphite	Al	V	Mn	Fe	Ni	Cu	Zn	Zr	Nb	Cd	Sn	Pb	Bi
Al	60	500	85	500	765	360	500	400		420	580				
V	370	1200	820	500	580	600	630	750	190	900	880	60	20	18	17
Mn	400	900	740	500	310	540	500	460	230	850	610	85	32	24	20
Fe	145	925	370	760	500	300	400	170		920	760				
Ni	180			600	340					650	850				
Cu	70	130	670	460	600	120	220	110		580	670				
Zn	50			150	140					100	95				
Zr	300	1300	530	850	540	870	800	760	320	500	850	80	20	30	24
Nb	310	1230	670	1030	670	700	860	600	160	880	570	40	32	14	22
Cd	32			75	60					75	45				
Sn	15			24	20					24	26				
Pb	10			25	30					27	20				
Bi	18			23	20					33	24				

interaction and to extend this law to all metals of Mendeleyev's periodic system; secondly, the study of this question makes it possible to design new electrodes which heighten the effect of electric spark hardening.

METHOD OF INVESTIGATION

Samples were treated in an apparatus built on the usual scheme for electric spark hardening proposed by B.P. and N.I. Lazarenko [1].

The apparatus had a gas filled, two phase rectifier. In order to get constant electric parameters for the regime of electric spark hardening, particularly for the degree of condenser discharge, a special device was used which automatically regulated the process. To control the electric parameters of the process we used an electronic oscillograph of EO-5 type. The combination of the automatic regulation of the process with uninterrupted control of the electric regime made it possible to ensure a constant regime and reproducibility of the conditions of treatment for all samples.

All the samples investigated were electric spark hardened under the following regime: capacity 30 μF, voltage 80 V, strength of the short-circuiting current 1.4 A. The automatic device was so adjusted that the degree of condenser discharge was 100 per cent.

Technically pure elements graphite, Al, V, Mn, Fe, Ni, Cu, Zn, Zr, Nb, Cd, Sn, Pb and Bi were chosen as samples. From these elements polished surfaces were prepared for the purpose of X-ray structure analysis and for the electrodes.

The basic method of investigation was X-ray structure analysis, since at present this is the most effective method of investigating surface layers obtained as a result of electric spark hardening.

The merit of this method is that it is possible to investigate the composition and structure of various phases, including a number of quite new ones, which appear with the hardening on the surface of the treated article. The photographs were taken in a camera of DK-1 type [9] with a drum radius of 114.6 mm and with chromium radiation. All samples were tested for microhardness in a PMT-3 apparatus with a load of 20 g.

The results of the X-ray structure analysis of the surface layers of the various metals after their electric spark treatment with various elements in air are given in Table 1. Table 2 gives the data for the micohardness of the surface layers of the samples.

DISCUSSION OF THE RESULTS OBTAINED

1. For the elements V, Mn, Zr, Nb, which under conditions of electric spark hardening were treated in various combinations with graphite, Al, Fe, Ni, Cu, Zn, Cd, Sn, Pb, Bi three kinds of interactions were observed:

(1) Formation on the cathode surface of solid solutions, chemical and intermetallic compound between the elements of the cathode and anode:

(2) Formation on the cathode of a "covering" layer of the anode material which does not react with the element of the cathode;

(3) Transfer of the cathode material to the anode (the anode material is not transferred to the cathode). In this case so-called "reverse transfer" occurs.

The first form of interaction was observed with electric spark hardening between V, Mn, Zr, Nb, Al, Fe, Cu, Ni and graphite in various combinations. In this case the microhardness of the surface layer of the sample (the cathode) increases greatly compared with the microhardness of the initial elements of the anode and cathode.

The second form of interaction appears in the electric spark hardening of vanadium, manganese, zirconium, niobium with zinc, cadmium, tin, lead, bismuth. In this case the microhardness of the surface layer of the cover is greater than the microhardness of the original anode material, but not much.

The third form of interaction was observed in the treatment of zinc, cadmium, tin, lead, bismuth with vanadium, manganese, zirconium, niobium. In this case also a small increase is observed in the microhardness of the surface layer of the cathode compared with the microhardness of the original cathode material. This phenomenon of the small increase of the microhardness in the second and third forms of interaction can evidently be explained by the thermal stresses which arise as a result of the rapid cooling of the melted metal of the surface layer of the cathode by the main cold mass of the sample.

Hence, for Vn, Mn, Zr, Nb in various combinations with other elements the same forms of interaction and a similar functional relation between the forms of interaction and the microhardness are observed as for the other, already investigated combinations of elements [2]. This allows us to conclude that the above mentioned law is a general one for all metals.

It should be noted that the microhardness of samples of V, Mn, Zr and Nb in combination with other elements and with each other reaches considerable magnitudes. Thus, in the electric spark hardening of iron with niobium or vanadium the microhardness of the sample is 760 kg/mm², and with zirconium or graphite 920 kg/mm². Even higher figures are observed in the hardening of niobium with vanadium: 1030 kg/mm². In the treatment of vanadium with niobium and zirconium with graphite the hardness increases to 1200 – 1300 kg/mm². Therefore to obtain surfaces of great hardness the combined treatment of the surfaces with these electrodes is to be recommended.

2. As can be seen from Table 1, supersaturated solid solutions, high temperature phases and compounds are observed after electric spark hardening in the surface layer of a large number of samples. These metastable phases are of considerable stability: they do not dissociate at room temperature for a long time. With the usual methods of thermal treatment it is difficult or even impossible to obtain these compounds and solutions. Thus, e.g. carbides of aluminium, β and γ manganese, β zirconium-γ iron, supersaturated solid solutions of the systems Al-V, Fe-Mn, Mn-Al, Nb-Ni, V-Zr, Ni-Zr, etc. are formed after electric spark hardening. The formation of such stable metastable phases, compounds and solid solutions is explained by the conditions of electric spark hardening: great speed and high temperature of heating, great speed of cooling (quenching) of the surface layer of the cathode which is melted during the discharge.

3. In all the examined combinations of V, Mn, Zr, Nb with graphite, Al, Fe, Ni, Cu, Zn, Cd, Sn, Pb, Bi (more than a hundred new combinations) complete agreement is noted between the experimentally observed forms of interaction and those found according to the criterion of interaction by calculation from the thermal constants of the electrode materials [2]. This shows that the criterion of interaction correctly reflects the law of the interaction processes between the electrodes in electric spark hardening

VOL. 5 1957

and is valid for all the metals of Mendeleyev's periodic system which have been investigated.

4. On the effect of polarity on the direction of the transfer of electrode material there are contradictory reports. Some authors believe that the direction of the transfer of electrode material during electric spark hardening is governed by polarity [1], others maintain that the transfer of material is of a purely thermal nature and that the polarity of the electrodes has no marked influence [2, 4, 6].

As a result of the comparative analysis of more than a hundred combinations of elements which differ from each other only by the polarity of the circuit during the electric spark treatment we have come to the conclusion that in the combinations of V, Mn, Zr, Nb with the other elements which were examined, there is no correspondence between the polarity of the electrodes and the direction of the transfer of material.

The direction of transfer is governed in the main by the thermal constants of the electrode materials and a change of polarity does not change that direction.

It should be noted that the shape of the electrode also has a certain effect on the direction of transfer. It has been established [5] that the smaller the diameter of the electrode, the more metal of that electrode is in the vavour phase. Therefore with comparable thermal constants of the electrodes there will be more of the anode than of the cathode element in the vapour phase. When the thermal constants of the electrodes are very different, the effect of the shape on the transfer of material is slight and may not even be observed at all.

5. The great firmness with which the covering layer clings to the basic material of the cathode in the second form of interaction, despite a possibly greater difference between the atomic radii of the elements of the sample and cover, attracts attention. The reason for this is evidently the mixing of the anode and cathode materials in the liquid state on the cathode surface and the extremely rapid cooling which follows. It is evident that in the transitional layer of this cover stresses arise which are caused by the great difference in atomic radii between the elements of the sample and the cover. These stresses, added to the thermal ones, undoubtedly have an effect on the strengthening of the covering layer.

6. In the surface layer of the majority of samples oxides of both the anode and the cathode material are to be found after electric spark hardening. There are more oxides formed of the element of which more is contained in the vapour phase of the discharge. Therefore quite often one finds more oxides of the anode than of the cathode on the cathode. This can be explained by the pointed shape of the anode which causes a greater quantity of the anode element than of the flat cathode to enter the vapour.

In the investigation which was made into the phase composition of the surface layers of more than a hundred elements, nitrogen or nitrogen containing phases and compounds were not found.

CONCLUSIONS

1. In the present paper various combinations of V, Mn, Zr, Nb with graphite, Al, Fe, Ni, Cu, Zn, Cd, Sn, Pb and Bi were examined which hitherto have not been investigated in the conditions of electric spark hardening. The phase composition and microhardness of the surface layers of the samples and the forms of interaction were investigated, the connexion between the microhardness and the form of the interaction was established and the criterion of interaction was shown to be valid for these combinations.

The results obtained show that the combinations examined interact during electric spark hardening in the same way as those previously investigated [2].

2. The polarity of the electrodes does not affect the direction of the transfer of material. The direction of transfer is determined by the thermal constants of the material and to a smaller degree by the form of the electrodes.

3. With the second form of interaction a firm clinging of the covering layer to the material of the sample is always observed.

4. On the majority of samples oxides are formed. It was noticed that more oxides of the anode than of the cathode element are formed. This is a result of the pointed shape of the anode and also confirms the thermal nature of the processes between the electrodes.

5. In the investigation made into the phase composition of the surface layers of different combinations of elements nitrogen containing phases or compounds was not observed in a single case.

Translated by B. Ruhemann

REFERENCES

1. B.R. and N.I. Lazarenko, *Electric erosion of metals*, 1944, 1st Ed; 2nd Ed. 1946. *The physics of the spark method of treating metals;* Ts. B.T.I.M.E.P. U.S.S.R.,

(1946). *Electric Spark Treatment of Metals*, Gosenergoizdat (1950).

2. L.S. Palatnik, *Izv. Akad. Nauk. U.S.S.R.*, Physical Series, 15, 80, 469 (1951); D.A.N. U.S.S.R. 89, 455 (1953).
3. I.V. Arkharov, Z.P. Kichigina and A.A. Spiridonova D.A.N. U.S.S.R. 78, 673 (1951).
4. B.A. Krasyuk, Investigation of certain processes which occur in the electric spark treatment of metals, dissertation for doctor's degree, Institute of Metallurgy, Akad. Nauk. U.S.S.R. (1950).
5. L.S. Palatnik and A.N. Lyulichev, *Zh. tekh. fiz.* 26, 832, 839 (1956); *Izv. Akad. Nauk. U.S.S.R.*, physical series, 18, 259 (1954).
6. G.V. Gusev, *Zh. tech. fiz.* 25, 763 (1955).
7. M.A. Filyand and E.I. Semenova, *The properties of rare metals*. Metallurgizdat, Moscow (1953).
8. M.P. Slavinskii, *The physicochemical properties of the elements*. Metallurgizdat, Moscow, (1952).
9. I. Kh. Varivoda, D.G. Kurilekh and L.P. Kurilekh, Zav. lab. 20, 4 (1954).

VOL.
5
1957

RESEARCH ON THE DETECTION OF RAILWAY LINE DEFECTS IN MOVING MAGNETIC FIELDS*

1. SOME OF THE PROBLEMS OF ELECTROMAGNETIC DETECTION OF RAIL DEFECTS

V.V. VLASOV

Institute of Physics of Metals of the Ural Branch of the Academy of Sciences, USSR

(Received 21 August 1957)

It is a known fact that railway lines are subjected to very complex influences of considerable dynamic and static stress during the passage of trains over them. The service life of a rail depends on the quality of the metal and the conditions of its operation. On our railways we have rails which are dozens of years old, but sometimes they become useless within a matter of years or even weeks after they have been laid on the track. They go out of service as a result of wear or owing to the development in them of various macroscopic defects – fissures [1-3]. Rail wear is a normal phenomenon and is comparatively safe. But the presence of rails on the track which are riddled with defects is completely inadmissible, as they can cause accidents which sometimes have serious consequences and cause prolonged interruptions of rail traffic. Experience has shown that such defects develop both in light rails which have lain on the track for a considerable time, and in heavy rails which are everywhere replacing the former.

Longitudinal fissures, in particular vertical and horizontal stratification of the rail head, form a wide-spread group of comparatively dangerous defects. The chief reason for the vertical stratification lies in the peculiarities of metal deformation in the rail head. Starting inside the rail, the vertical fissures at the appropriate stage of development appear on the rail surface and near the web of the rail. Horizontal fissures in the rail head are started by various defects of metallurgical origin. Generally they start inside the head of the rail and then break through the lateral face of the rail head or become continuous. Longitudinal fissures develop also where the web joins the rail head. It must be noted that in the rail base there occur very fine longitudinal fissures, called shatter cracks, which progressively develop under the action of trains.

Transverse fissures in the rail head are extremely dangerous. As a rule, they are produced by various micro – and macro-defects in the metal. For the most part transverse fissures are formed inside the rail head. Then they gradually develop and appear on the surface as very fine fissures, which are rather difficult to see with the naked eye. Sometimes transverse fissures arise simultaneously in several sections in rail length. Quite frequently these defects are caused by nicks in the rail head and longitudinal horizontal fissures. Moreover transverse fissures arize from small rail burn fissures, which are formed on the surface of the rail head as a result of wheel skidding when the brakes are applied. The fine longitudinal fissures in the rail base, mentioned above, comparatively quickly become transverse. Certain other defects occur in rails also.

The timely discovery of defective rails and their withdrawal from the track greatly increases the safety of travel. For this purpose it is of great importance to use non-disrupting methods of testing. To discover defective rails electromagnetic and ultrasonic detectors are used.

The electromagnetic detection of defects in ferromagnetic products is based essentially on the resistance of the defect to magnetic flux or an electric current. A distortion in the form of an additional field arises in the vicinity of the defective section of the rail when it is magnetized. An analogous distortion appears when the rail is surrounded by an electric current. Moreover, in the latter case an additional electric field intensity is set up on the surface of the rail. The presence of defects in the rails is indicated by the presence of one distortion or the other.

The first attempt to use electromagnetic phenomena for detecting rail defects was made by Berrouz in 1916. Later on quite a number of designs for rail detectors were suggested. Only a few of the systems, however, have practical application; for instance,

* *Fiz. metal. metalloved.* 5, No. 3, 442-451, 1957.

Karpovyi's rail detectors and some others were not used [4,5]. Nowadays electromagnetic detectors of rail defects are wide-spread as a means of testing rails. They enable rail head defects to be detected, but their sensitivity to web and base defects is practically nil.

As regards design, rail detector cars belong either to a light or heavy class. Detector cars of the light class are intended for testing rails at a speed of up to 4 km/hr, whereas the heavy class detectors are for greater speeds.

In the light detector cars quite a wide use was made of the method of detecting defects by means of eddy currents, induced in the rails by a comparatively weak alternating magnetic field of audible frequency. This method is made use of in the rail detector car DS-13, developed by the Siberian Physical Engineering Institute [6-8], in the single-thread detector designed by D'iakov and Ryshikov [9] and in the detector RDP-56 MPS, designed by Trakhtenberg [10]. The latter detectors differ from the first only in construction. The search systems in these detectors respond to distortions of the magnetic field, which arise as a result of surrounding the defect with eddy currents. A milliammeter and a telephone are used as indicators. The deflection of the milliammeter needle and a sound in the telephone indicate the presence of a defect in the section of rail on which the detector is placed. Detectors working in an alternating magnetic field respond satisfactorily to fissures which appear on the surface. However, internal defects occurring at a depth of several fractions of a millimetre – irrespective of their size – are not discovered by the detector. This is due to the strongly pronounced surface effect.

Effective means of detection are to be found in systems in which small highly sensitive electromagnetic elements, called ferro-probes are used as a search system. In this case, the search system responds to an additional magnetic field, produced by the defect. The work of the detector is based on the non-linear dependence of magnetic induction on the field. This type of detector is used in the light magnetic rail detector car MRD-52 TsNII MPS [11]. The defect field in this case is formed on account of the magnetism created in the rail section under test by a U-shape electromagnet. A milliammeter and a telephone are used as indicators.

This particular detector reveals transverse fissures in the rail head, which appear on the surface, as well as internal defects which occur quite deep. It detects defects inside light rails to a depth of 6-8 mm and in heavy rails to a depth of 4 mm. The explanation of the difference of working when testing light and heavy rails is given in the work [12].

The detector responds to defects both when moving and when it is stationary. This is very valuable as it enables the exact position of the defect to be determined. Generally speaking, the detector works most effectively on light rails; when testing heavy rails there are numerous wrong conclusions about the defectiveness of the rails. The detector does not reveal relatively well developed defects which appear under the rail head, but do not fall within the limits of the above states depths, at which defects can be discovered. Moreover, it is impossible to detect defects in sections of rail where there is a change from tempered metal to normal metal. This is due to the fact that in the relatively weak field used in the detector, distortions from structural irregularities in the metal considerably exceed the field from dangerous defects. It must be noted that rails have sections at the ends with a tempered surface.

Ultrasonic rail testing is very effective. It is carried out by transmitting a sound wave into the rail from above and the defects are detected on the basis of the reflection, scattering or absorption of sound energy. With this it is possible to detect various defects in any part or at any height of the rail within the limits of the web breadth. The working of the light detector car for testing rails where there are joints including fish plates is based on the principle of sound energy reflection. In the detector cars used on our railways [13, 14], the reflection from the defect is picked up and shown visually on an oscillograph screen. The absence of a reflection returning from the rail base and the appearance of another indicates the presence of a defect on the rail. The working of a portable detector [15], intended for testing rails along their whole length, is based on the scattering and absorption of sound energy by the defect. A telephone is used in this detector as an indicator. Apart from the light detectors for testing rails already discussed here, heavy ultrasonic detectors are used which are described below.

Heavy detector devices are mounted in a carriage or on a trolley. This permits, if we bear in mind rail testing in a magnetic field, the use of more powerful field sources in comparison with detector cars, which is a definite advantage. In heavy detectors electric currents of considerable power can be used. This fact was used by Sperry [16, 17] in his detector for testing rails at a speed of up to 12 km/hr. In this detector an electric current of several thousand amperes is forced into the rail section

VOL. 5 1957

under test. A low voltage d.c. generator is used as a source of current. The first version of the detector was equipped with a search potentiometer which responds to a difference of potential. For several reasons it was necessary to give up using this search device. At the present time a search device is used in the detector which responds to the defect field [18]. The potentiometer method, called the voltage drop method, is used abroad as an auxiliary testing device in addition to the magnetic rail detectors.

The induction method using a continuous external field is used comparatively widely in rail detectors. The first detector based on this method was designed by Suzuki [19, 20]. The detection of defects in this case is by the distortions set up by the magnetism in the rail. For this purpose the rail section under test is magnetized by means of a U-shaped electromagnet fed with direct current. A small coil placed over the rail midway between the poles of the electromagnet acts as a search device. A temporary e.m.f. is induced in the coil as it passes over a defective section of rail. The outline of these impulses is recorded on tape by means of a pen. Testing speed using this detector was about 4 km/hr. It has now been replaced by a more advanced detector which travels at a far higher speed. [21].

It was suggested that residual magnetism should be used for testing [22]. Certain foreign detectors make use of residual magnetism for rail testing [23, 25]. In these detectors a demagnetizing device in the form of an electromagnet, fed by an alternating current of audible frequency is mounted between the electromagnet creating a constant magnetic field and the search device. The rails are demagnetized by this on account of the strong surface effect to a certain depth, whereas the defect field remains essentially invariable. Demagnetizing rails obviously eliminates part of the obstacles caused by various irregularities of the metal in the surface layers.

The testing speed of these detectors [23-25] is up to 13 km/hr. The defects are recorded on tape by the appropriate electromagnetic signs. Working with these detectors appropriate sections of the track are run over a second time. Then doubtful rail sections are subjected to additional examination by a testing detector. The latter works by the voltage drop method. For this purpose an electric current up to 1500 amperes is passed through the rail.

At one time the detector station TsNII NKPS [26] was used on our railways. This detector works on the principle analogous to Suzuki's detector described above, but it differs from it in construction. In particular, defects in the detector station were recorded on a tape by means of electromagnetic signs. It enabled rail testing to be carried out at a speed of up to 20 km/hr. but it had many disadvantages. Later on the detector was perfected by the staff of the Institute of Physics of Metals of the Ural branch of the Academy of Sciences, USSR, in collaboration with workers on rail detection on the Sverdlovsk railway [27]. As a result the "detector car" was produced [28]. With this it was possible to raise the rail testing speed to 30-35 km/hr. and to manage with a single run instead of the triple run recommended for the detector station [29]. However, attempts to overcome other faults in rail defect detection were not successful at the increased speed. All the same, detector cars from the Sverdlovsk railway were used on tracks in the Urals and in Siberia.

Comparatively recently an ultrasonic detector appeared, for testing the whole rail at a speed of 26 km/hr. [30], at somewhat faster speed. [31]. They work on the basis of the reflection of ultrasonic energy by the defects. It is interesting to note that in the more advanced detector [31] sound waves are directed at the rail from various angles to the surface of the rail head. Defects in this case are recorded on photographic paper by a special device. The detector enables defects to be discovered in any part or height of the rail. The disadvantage of the detector lies in the fact that defects – transverse, longitudinal or slanting – which are situated in that part of the rail head just out from the web and does not come within the area bordered by the continuation of the web, are not discovered by the detector. The comparatively low speed of the ultasonic detectors and the difficulties associated with their use in winter constitute real disadvantages in this type of detection.

PRINCIPAL TASKS IN THE ELECTROMAGNETIC DETECTION OF RAIL DEFECTS

One of the principal problems involved in detecting defects is that of increasing the speed of testing rails which make up a track. In view of the considerable extent of the railway network and the high density of traffic this is a matter of the utmost importance. Generally speaking it is desirable that the speed of the detector should be such that its work does not hinder the normal passage of trains.

We consider that electromagnetic detection has not yet been used to the full in testing rails. In connexion with this we think it useful to study rail defect detection by means of a constant magnetic field. In doing so it is generally necessary to take

VOL 5 195

into account the presence of eddy currents induced in objects when a magnetic field source and the object magnetized by it are in a state of relative motion.

Electrical phenomena arising in conducting bodies as a result of their motion in a constant magnetic field were discovered by Faraday and Arago [32], and in a moving magnetized body by Faraday [33]. The electrical polarization of a moving body was explained only at the beginning of this century on the basis of the theory of relativity [34]. The electrical polarization of bodies moving in a magnetic field is called "unipolar induction". This phenomenon has practical application in unipolar machines which give a d.c. electric current of considerable power [35]. The term "unipolar induction" is not satisfactory and sometimes it is invested with a meaning different from that generally accepted [36]. Later on we shall use this term in the general sense, but we will agree to call eddy currents which are developed in bodies unipolar-induction currents. These terms are used in some works on the detection of defects in metal objects.

The idea of using these currents for defect detection was first advanced by Buturlinskii [37]. It is attractive for the following reasons. The electrical conductivity of the medium inside a defect-fissure is practically nil, while the magnetic permeability of that same medium is not of infinitely small magnitude. The electric current flows round a defect, while the magnetic flux is subject to only a minor distortion as the greater part of it passes through the defect. Consequently the sensitivity of the apparatus to defects detected by a current must be higher than in the case of detection by means of a magnetic flux, other things being equal. In this case induced currents are also an important factor. In principle this permits detection at any speed.

In connexion with this it is necessary to consider works on the study of electromagnetic phenomena, when the magnetic field source and the body magnetized by it are in a state of relative motion. The general theory of such phenomena can be found in text-books on the theory of relativity [38] and the theory of electricity [39]. Without stopping for an exposition of the general theory, we will note the following. We are interested in the velocity v of the magnetic field source relative to the rail, which is non-relativistic, as in this case $v/c \ll 1$, where c – is the speed of light. Eddy currents in conducting bodies moving relative to the field source with non-relativistic speed can be satisfactorily explained within the fremework of the pre-relativistic theory of Hertz [40]. Electromagnetic phenomena in the case of non-relativistic velocities has been studied in general terms by Hinteregger [41].

There is quite a wide field of literature on unipolar machines [35, 42-44]. However it is devoted exclusively to the description of details and design of these machines, in other words to questions which are completely irrelevant to our own specific problems.

Electromagnetic phenomena in bodies moving in a magnetic field were studied analytically only in the case of geometrically simple bodies. Thus the problem of the sphere rotating in a constant magnetic field was investigated by Herz [45] and Hans [46]. Currents in a lamina with a magnetic dipole rotating above it were described by Smait [47]. The theory of currents induced in an infinitely extended lamina when it moves in a transverse magnetic field were elaborated in the works of Rudenberg [48], Steidinger [49], Sycheva [50, 51], and Sapozhnikov [52]. The electrical polarization of a cylinder, moving along its axis in a transverse magnetic field was determined by Sommerfeld [53], and then investigated in detail by Hinteregger [54]. However, all these investigations, unfortunately, are far from the conditions under which a rail is magnetized in a moving field source.

The first qualitative experimental investigations of eddy currents, induced in rails by a moving local transverse magnetic field, were carried out by Matveev and Trakhtenberg [55]. More detailed investigations in the particular case of a rail, magnetized by a relatively weak transverse field travelling at low speed, were carried out by Polivano [56]. Comparatively intensive currents are induced in rails magnetized under these conditions, according to his assessment. From the qualitative experiments of Khalileev and Vlasov [57, 58] on the magnetizing of ferromagnetic bodies at high speed in a relatively strong magnetic field, it also follows that currents in rails magnetized under the latter conditions of motion must be quite intense. However an attempt to use eddy currents, induced in rails by a moving magnetic field for the purpose of rail defect detection was unsuccessful [59, 60]. In this case, as we see it, certain mistakes caused by insufficient study of eddy currents were allowed to go uncorrected.

The concept of intense currents in rails magnetized in motion is not generally recognized. Thus Sycheva [50, 51] ascertained that strong unipolar-induction currents arise in non-magnetic bodies but in magnetic bodies the currents are comparatively weak. Sapozhnikov [52], summarizing the investigations on unipolar induction carried out in the

Siberian Physical Technical Institute, made the following statements. The surface magnetic effect for unipolar-induction currents will be comparatively weak in objects such as rails. For this reason the conditions of rails magnetized by stationary or moving electromagnets will be approximately the same. The comparatively weak force of unipolar-induction currents is a factor which reduces the value of the idea of using these currents for the detection of defects. These conclusions, it seems to us, are the result of incorrect inferences drawn from results of theoretical and experimental investigations into comparatively strong fields used in rail defect detection which were carried out with application to weak fields.

Thus rail defect detection presents problems of increasing the speed of detecting apparatus and the application for detection of those eddy currents which undoubtedly exist in the rails as a moving source of magnetic field. Moreover, there is the problem of separating useful signals.

The fact is that electromagnetic detectors respond both to dangerous defects and to various harmless flaws in the rail head. Under this heading are scabs on the metal and fissures in them, traces of blows from a spiking maul, small chips in the lateral face of the rail head etc. This is not important when the testing apparatus is moving at slow speed, as it is always possible to stop and ascertain whether some harmless fault in the rail head caused the apparatus to operate. When the detector is travelling at high speed the utmost importance is attached to the problem of separating the signals. In our opinion it can be solved because the eddy currents induced in the rails by a moving source of magnetic field participate in the formation of the defect field.

With a view to the practical detection of rail defects, it is interesting to study the problem of magnetizing these objects in motion, of the intensity of eddy currents produced in rails, of the possibility of using the latter for detection, and also of the problems of separating useful signals. In connexion with the problems of magnetizing rails in motion, it is necessary to study the mathematical description.

MATHEMATICAL FORMULATION OF THE PROBLEM

Electromagnetic phenomena in quiescent bodies are shown by the system of Maxwell's equations:

$$\operatorname{rot}\vec{E}+\frac{\partial\vec{B}}{\partial t}=0,\qquad \operatorname{rot}\vec{H}-\frac{\partial\vec{D}}{\partial t}=\vec{\delta}, \tag{1}$$

$$\operatorname{div}\vec{B}=0,\qquad \operatorname{div}\vec{D}=q,$$

$$\vec{B}=\mu\mu_0\vec{H},\qquad \vec{D}=\varepsilon\varepsilon_0\vec{E}$$

$$\vec{\delta}=\gamma\vec{E},$$

where $\vec{E}$ and $\vec{H}$ – are the intensities of the electric and magnetic fields; $\vec{B}$ and $\vec{D}$ – magnetic and electrical induction; ϵ_0 and μ_0 – electric and magnetic permeability of a vacuum; ϵ and μ relative electric and magnetic permability; q – quantity of electric charge; $\vec{\delta}$ – amount of electric current and γ – electrical conductivity.

Electrical phenomena in moving bodies at non-relativistic speeds can be described, as was shown above, on the basis of pre-relativistic conceptions, in particular within the framework of Hertz's theory. The latter is not strictly consistent, but in relation to currents in conducting bodies, it leads to results which are in accordance with modern theory and practice, and in consequence of its comparative simplicity, it is used nowadays in electrical engineering [6]. However, considering the mathematical side of the problem we are interested in, we will proceed from the general system of relativistic electrodynamics, disregarding the second and higher degrees of the relationship v/c.

In the problem we are considering the rail is magnetized by a moving field source. In principle, obviously, the field source can be considered as stationary, with the rail moving relative to it but in the opposite direction. This treatment of the problem is completely permissible as the motion is relative and consequently the fact that it moves is not important: the field source in relation to the body, or on the other hand, the body relative to the field source. This being so we must bear in mind that the description of electromagnetic phenomena depends on what system we consider them in, the moving or quiescent. This is explained, as is known, by the fact that the division of the electromagnetic field into an electric and a magnetic field is relative.

Electromagnetic phenomena in moving bodies are described in general by the system of Minkowski's equations, which under the conditions stated above have the following form:

$$\operatorname{rot}\vec{E}+\dot{\vec{B}}=0,\qquad \operatorname{rot}\vec{H}-\dot{\vec{D}}=\vec{\delta},$$
$$\operatorname{div}\vec{B}=0,\qquad \operatorname{div}\vec{D}=q, \tag{2}$$

VOL 5 195

$$\vec{B} - \frac{1}{c^2}[\vec{v}\vec{E}] = \mu\mu_0\vec{H}^*, \quad \vec{D} + \frac{1}{c^2}[\vec{v}\vec{H}] = \varepsilon\varepsilon_0\vec{E}^*$$
$$\vec{\delta} = \gamma\vec{E}^* + q\vec{v}.$$

The magnitude of the reading in the moving system as well as in the body is marked here by an asterisk, while the magnitudes without asterisks refer as before to the system at rest. $\vec{B}$ and $\vec{D}$ are determined by the relation:

$$\vec{\rho} = \frac{\partial\vec{P}}{\partial t} + \vec{v}\,\mathrm{div}\,\vec{P} - \mathrm{rot}\,[\vec{v}\vec{P}],$$

where by $\vec{P}$ is understood B or $\vec{D}$.

The resolution of vectors of the field on changing from one system of reading to another are determined by the equation:

$$\vec{E}^* = \vec{E} + [\vec{v}\vec{B}], \quad H^* = \vec{H} - [\vec{v}\vec{D}],$$
$$\vec{B}^* = \vec{B} - \frac{1}{c^2}[\vec{v}\vec{E}], \quad \vec{D}^* = \vec{D} + \frac{1}{c^2}[\vec{v}\vec{H}]. \tag{3}$$

Electrical phenomena in a system which is moving with the body are given by the Maxwell equations. Consequently, we have:

$$\mathrm{rot}\,\vec{E}^* + \frac{\partial B^*}{\partial t} = 0, \quad \mathrm{rot}\,\vec{H}^* - \frac{\partial\vec{D}^*}{\partial t} = \vec{\delta}^*,$$
$$\mathrm{div}\,\vec{B}^* = 0, \quad \mathrm{div}\,D^* = q^*,$$
$$\vec{B}^* = \mu^*\vec{H}^*, \quad \vec{D}^* = \varepsilon^*\vec{E}^*, \tag{4}$$
$$\vec{\delta}^* = \gamma\vec{E}^*.$$

Thus the equation of the resolution of the vectors of the field have the form:

$$\vec{E} = \vec{E}^* - [\vec{v}\vec{B}^*], \quad \vec{H} = \vec{H}^* + [v\,D^*]$$
$$\vec{B} = \vec{B}^* + \frac{1}{c^2}[v\vec{E}^*], \quad \vec{D} = \vec{D}^* - \frac{1}{c^2}[vH^*]. \tag{5}$$

Some of the reduced equations for the resolution of vectors of the field in the condition of the problem we are considering can be simplified if we take into account the following factors. For instance it is not difficult to show that in the case we are interested in these conditions are fulfilled.

$$\frac{1}{c^2}[\vec{v}\vec{E}] \ll \vec{B}, \quad [\vec{v}\vec{D}] \ll \vec{H}$$

On the basis the equation of resolution in the first line (3) can be written down in the form.

$$\vec{B}^* = \vec{B}, \quad \vec{H}^* = H. \tag{6}$$

Comparing the expressions for the dependence of the magnetic induction on the field (1) and (4) with the calculation (6) it follows that

$$\mu^* = \mu\mu_0. \tag{7}$$

Consequently, in the case we are considering of the induction $\vec{B}$ the field $\vec{H}$ and the magnetic permeability in a system at rest and one moving with a body, they have exactly the same value.

In the case when the source of the constant magnetic field and the body magnetized by it are in a state of relative motion, free electric charges are absent and consequently $q = 0$. This being so, from the expressions for the amount of electric current in (2) and (4) with the equation for the resolution of the electric field intensity in (3) we have

$$\vec{\delta} = \vec{\delta}^* = \gamma(\vec{E} + [\vec{v}\vec{B}]). \tag{8}$$

In conclusion we will consider the differential equation for the eddy current intensity induced in a ferromagnetic body by a moving magnetic field. This equation will be indispensable in future work.

Since the external field and the velocity are constant, then it follows that

$$\frac{\partial\vec{B}}{\partial t} = 0.$$

In this case from the first equation in (1) it follows that rot $\vec{E} = 0$. Taking this into account, we can, on the basis of (8) write the relation

$$\mathrm{rot}\,\vec{\delta} = \gamma\,\mathrm{rot}\,[\vec{v}\vec{B}].$$

VOL. 5 1957

This expression according to the laws of vector algebra, since div $\vec{B} = 0$, can be written in the following form:

$$\text{rot}\,\vec{\delta} = \gamma\{(\vec{B}\,\text{grad})\,\vec{v} - (\vec{v}\,\text{grad})\,\vec{B} - \vec{B}\,\text{div}\,\vec{v}\}.$$

Confining ourselves to the case where the velocity is constant in magnitude and size, we have div $\vec{v} = 0$ and $(\vec{B}\,\text{grad})\,\vec{v} = 0$. Calculating these relations we get the well-known equation for the amount of current

$$\text{rot}\,\vec{\delta} = \gamma\,(\vec{v}\,\text{grad})\,\vec{B}.$$

If we take $\vec{B} = \text{rot}\,\vec{A}$, it is easy to show that the expression for the amount of current, can be written in the form

$$\vec{\delta} = \gamma\,(\vec{v}\,\text{grad})\,\vec{A}. \qquad (9)$$

The significance of this expression is that the amount of current is proportional to the product of the speed and the derived vector potential in its direction [62].

We must note that ferromagnetic bodies being tested for defects are surrounded by air, that is a non-magnetic medium. The vector potential in the general case [63], taking into consideration the absence of a magnetized medium surrounding the body, can be written in the following form

$$\vec{A} = \frac{\mu_0}{4\pi}\left\{\int \frac{\text{rot}\,\vec{I}}{R}\,d\tau - \int \frac{[\vec{n}\vec{I}]}{R}\,ds + \int \frac{\vec{\delta}}{R}\,d\tau\right\}, \qquad (10)$$

where $\vec{I}$ – the magnetism brought about by the resulting field; $\vec{n}$ – is the vector of the external normal to the surface of the body; $d\tau$ and ds – are surface and volume elements; R – the distance from the element of volume or surface to the point of observation of the vector potential.

In expression (10) the surface integral is connected with the demagnetizing field and in rail defect detection, generally speaking, is comparable in order of magnitude with the volume integral from magnetization.

Thus the problem of the intensity of eddy currents in objects magnetized by a moving field source comes down to an integral-differential equation. When solving equations (9) and (10) the initial and limiting conditions must be taken into account and we will not write them out here.

CONCLUSION

In connexion with demands for the practical detection of defects in railway lines, it is essential to study the electromagnetic phenomena in them in the presence of moving external magnetic fields.

Translated by J. Murray

REFERENCES

1. R.S. Nikolaev, *Prichini polomol detalei podvizhnogo sostava i rel'sov (Reasons for the break down of rail and rolling stock components)* Transzheldorizdat, (1954).
2. A.I. Skakov, *Kachestvo zheleznodorozhnykh rel'sov (The quality of railway lines)* Metallurgizdat, (1950).
3. *Spravochnaya knizhka zheleznodorozhnika (The railway man's reference book)* Transzheldorizdat pp. 305, (1956).
4. I.G. Nartov, *Mekhanicheskie defectoskopy sistemy izobretatelya F.M. Karpova (Mechanical detectors on the system of the inventor F.M. Karpova)* Transzheldorizdat, pp. 42 (1937).
5. *Vremennaya instruktsiya po ukhodu i obsluzhivaniya velo-defectoskopov sistemy izobretatelya F.M. Karpova (Provisional instructions on the care and maintenance of velo-detectors on the system of the inventor F.M. Karpov)* Transzheldorizdat, (1940).
6. P.N. Bol'shakov, V.F. Ivlevn, B.P. Kashkin and A.B. Sapozhnikov, *Trud. Sib. fiz. tekh. inst.* Tomsk, No. 5 (1938).
7. A.B. Sapozhnikov, *Opisanie defectoskopov s'emnogo tipa modelei 7, 4, 11. (Description of portable detectors of the type 7, 4, 11.)* Tomsk, (1941).
8. *Rukovodstvo po obsluzhivaniya i rabote s defectoskopnoi telezhkoi Sib. fiziko-tekh. inst., Model' No. 13 (DS-13), (Handbook on the servicing and working of the detector trolley of the Sib. fiz-tekh. inst. Type No. 13 (DS-13).* Transzheldorizdat, (1947).
9. F.S. D'iakov and E.I. Ryzhikov, *Radiotekhnicheskaia apparatura v narodnom khozyaistve (Radio engineering equipment in the national ecnonomy)* Gosenergoizdat, Part 2, p. 24, (1953).
10. M.V. Trakhtenberg, *S"emnyi rel'sovyi defectoskop na peremennon pole tipa RDP-56 TsNII. (Portable rail detector in a variable field model*

RDP-56 TsNii) Transzheldorizdat, (1956).

11. *Rel'sovyi defectoskop (MRD)-52) (Rail detector (MRD-52 of the system TsNII MPS),* Transzheldorizdar, (1952).
12. V.V. Vlasov and L.Z. Piatigorskaia, *Fiz. metal. metalloved.* vol V. No. 2. (1957).
13. Iu. N. Shtremer *Zavodskaya laboratoriia (Works laboratory),* 7, 855, (1952).
14. M.E. Mokeev and Iu. N. Shreemer, *Ul'trazvukovoi rel'sovyi defectoskop (Ultrasonic rail detector) (URD-52) TsNII MPS,* Transzheldorizdat (1953).
15. V.B. Kozlov, *Put'i putevoe khozyaistvo (Track and economy)* 2, 39, (1957).
16. I.A. Gorodinskii, *Magni tyne i elektricheskie metody ispytanii metallov (Magnetic and electrical methods of testing metals)* Gosplanizdat, (1940).
17. See [1] [4], pp. 9-26.
18. R.C. McMaster, *Proc. Amer. Soc. Test. Meter,* 52, 617, (1952).
19. M. Suzuki, *Si. Rep. Tohoku Jmp. Univ.,* 15, 479, (1926).
20. M. Suzukia, *Anniversary Volume dedicated to Professor Kotaro Honda Tohoku,* 309, (1936).
21. H. Kithara, *Nondestructive Test; July-August 17,* (1954).
22. See [16] pp. 134.
23. *Mod. Railroads,* 5, 6, 193, (1950).
24. *Maintenance Engineering,* May, 459 (1950).
25. M. Deutsch, *Rev. gen. Chem-de-Fer,* 5, 257 (1954).
26. A. Gorelik, V. Smirnov and S. Samarin, *Vest. metal. prom. (Metal Industry News)* 9, 67 (1939).
27. T.G. Bul'ba, B.P. Dovnar, V.V. Vlasov, P.A. Khalileev and P.I. Ianus, Vagon-defectoskop Sverdlovskoi Zh. d., (Detector car of the Sverdlovsk railway) *Sverdlovsk, Urals Fil. Akad. Nauk,* reports (1948).
28. *Tekhnicheskii spravochnik zheleznodorozhnika (Railwayman's technical handbook)* Transzheldorizdat, vol. 5, p. 502. (1951).
29. Vremennaya instruktsia o poryadke vyyavleniia defectov v rel'sakh. lezhashchikh v puti. defectoskopnoi stantsii NIIPS NKPS i pravil ee ekspluatatsii (Provisional instructions on the method of detecting defects in rails on the track by the detector station NIIPS NKPS and rules for its operation). *Sverd. zh. d.* (1943).
30. *Rly Age.* 138, 26, 46 (1955).
31. E. Martin and K. Werner, *Eisentb. tech. Rdsch.,* H. 12, 487 (1957).
32. M. Faraday, *Eksperimental'nye issledovaniya po elektrichestvu (Experimental investigations on electricity)* Published by Acad. Sciences, U.S.S.R. p. 42 (1947).
33. See (32) p. 94.
34. R. Nekker, *Elektronnaya teoriya (Electronic Theory)* pp. 329-332 (1936).
35. M.P. Kostenko, *Elektricheskie mashiny (Electrical machines)* General section Moscow., p. 53, (1944).
36. H. Hinteregger, *Acta Phys. Aust.,* 7, 1, 1. (1953).
37. A.P. Buturlinskii, *Avtorskoe evidetel'stvo (Author's testimony)* No. 64820, (1928).
38. See V. Pauli *Teoriia otnositel'nosti (Theory of Relativity)* p. 147, United Scientific and Technical Publishing House (1947).
39. See H. Thirling *Hd. d. Phys.,* 22, 325 (1927).
40. See (39) p. 329
41. H. Hinteregger, *Acta Phys. Austr.,* 7, 4, 337, (1953).
42. *Unipoliarnye mashiny i primenenie prosteishikh magnitov v electro-mashinostroenii (Unipolar machines and the use of simple magnets in electrical machine construction)* Published by the Acad. of Sciences of the U.S.S.R. (1940).
43. L. Slepian, *Izv. Petrogr. Polit. inst. otd. tekh. est. i mat.,* 22, 55, (1914).
44. V.M. Mitkevich, *Magnitnyi potok i ego preobrazovaniya (Magnetic flux and its transformation)* Published by the Academy of Sciences, U.S.S.R. p. 213.
45. H. Herz, *Ges. werke, Braunschw.,* 37 (1896).
46. R. Hans, *Arch. Elektrotech.,* 9, 413, (1921).
47. V. Smait, *Elektrostatika and elektrodinamika (Electrostatics and electrodynamics)* p. 398, Moscow (1954).
48. R. Rudenberg, *Energie der Wirbelstrome* (1906).
49. W. Steidinger, *Arch. Electrotech.,* 22, 153, (1923).
50. T.M. Sycheva, *Zh. tekh. fiz.,* 25, 6, 1132 (1955).
51. T.M. Sycheva, *Tr. Sib. fiziko-tekh. inst. Tomsk,* No. 35. p. 75 (1956).
52. A.B. Sapozhnikov, *Osnovy elektromagnitnoi defectoskopii metallicheskh tel. Tomsk. (Principles of the electromagnetic detection of defects in metal bodies)* Tomsk, thesis (1952).
53. A. Sommerfeld, *Vorl. uber. teoret. phys.,* 3, 355 (1948).
54. H. Hinteregger, *Acta Phys. Austr.,* 7, 2, 129 (1953).
55. A.N. Matveev, M.V. Trakhtenberg, Usovershenstvoyanie metodov defectoscopii (Developments in methods of detection of defects) *TsNII zh. d. transp. report.* (1944).
56. K.M. Polivanov, *Problemy ferromagnetizma i magnetodinamiki (Problems of ferromagnetizm and ferrodynamics)* Academy of Sciences of the U.S.S.R. p. 147 (1946).
57. P.A. Khalileev, V.V. Vlasov, *Zavodskaya*

VOL. 5 1957

laboratoriya (Workshop laboratory) 7-8, 695 (1945).

58. P.A. Khalileev and V.V. Vlasov, *Trud. inst. fiz. metallov Urals Fil. Akad. Nauk Sverdlovsk* No. 7, p. 81 (1948l.

59. A.N. Mateev and M.V. Trakhtenberg, Skorostnoi rel'sovyi vagon-defectoskop (Rapid rail detector car) *zh. d. trans. Union Central Scientific Research Institution. report* (1949).

60. A.N. Matveev and M.V. Trakhtenberg, Rel'sovyi vagon-defectoskop (Rail detector car) *TsNII, zh. d., transp. report* (1950).

61. I.E. Tamm. *Osnovy teorii elektrichestva (Basis for the theory of electricity)* Moscow p. 553. (1954).

62. I.E. Kochin, *Vektornoe ischislenie i nachalo tenzornogo ischisleniya (Calculus of vectors and elementary tensor)* London-Moscow p. 131 (1954).

63. See (61) pp. 286, 289.

THE $\alpha \rightleftarrows \beta$ TRANSFORMATION IN ZIRCONIUM, FROM ELECTRON FIELD EMISSION OBSERVATIONS*

A.P. KOMAR and V.N. SHREDNIK

Leningrad Physico-technical Institute, Academy of Sciences of the U.S.S.R.

(Received 9 November 1956)

A study was made of the $\alpha \rightleftarrows \beta$ phase transformation in zirconium, for single crystals of the order of a micron in size. The electron gun method facilitated visual observation of the crystals during transformation, at magnifications of up to 100,000 diameters. Emission pictures were obtained of crystals of both cubic (β – zirconium) and hexagonal (α – zirconium) symmetry. The Burgers' orientational relationships were confirmed. During transformation, as a rule only one of the possible orientations of the new phase relative to the original was produced; this is connected with the substantial part played by surface energy for crystals of small size. Indications were revealed of dislocations in the zirconium crystals, the origin of which may be associated with the diffusionless transformation mechanism.

VOL. 5 1957

1. INTRODUCTION

Numerous X-ray investigations of phase transformations in pure metals and alloys have revealed the important geometrical laws governing these transformations and have made it possible to state a number of conclusions regarding the mechanism underlying the orientational interdependence between the lattices of different phases. It must be pointed out, however, that as yet ideas on this mechanism are by no means complete and lucid. Not all the observed phenomena can be explained by means of these concepts. It is obvious that in order to build up a completely adequate picture of phase transformations in metals and alloys, and in particular a picture of the transformation kinetics, data are required on the processes which take place in very small regions of crystals. To observe the latter, a new experimental technique is required. It seems to us that the electron and ion gun method is just such a new technique [2]. The great advantage of the electron gun in the study of phase transformations in substances possessing metallic conductivity is the possibility of visually observing transformation in very small crystallites (recording down to 180-200Å) with a high resolving power (down to 20Å) [3] and very considerable magnification (up to 10^6 diameters). Observations can usually be made without particular difficulty on crystallites with linear dimensions of the order of 10^{-5} cm, and at magnifications of 250-300 thousand diameters.

In the case of the ion gun the attainable resolving power is 4 Å [3], and it is possible to witness the migration of small groups of atoms over the surface of the crystal.

The present research was planned* for the purposes of:

(1) evaluating the capabilities of the electron gun technique for the study of phase transformations;

(2) checking by means of this method the crystallographic relationships between the α and β zirconium lattices, found by Bergers [5] by an X-ray study of macroscopic specimens;

(3) elucidating the role of crystallite shape and size in determining the type of mutual orientation between α and β-phase lattices.

In planning the work it was not overlooked that the study of zirconium by means of the electron gun is also of great interest from the viewpoint of experimental technique [6]. Up to now no one has obtained regular pictures, showing the crystal symmetry, by field emission from zirconium. Even in the highest vacuum, irregular field emission pictures have usually been obtained, due apparently to various impurities on the crystal surface ([6] p. 319).

2. EXPERIMENTAL METHOD, TECHNIQUE AND MATERIALS

An ordinary Muller electron field emission microscope [6] was used in the present work. The anode used was a layer of "conducting glass" on the

* *Fiz. metal. metalloved.* 5, No. 3, 452-464, 1957.

* This research was initiated prior to the publication of Brock's investigation on titanium [4].

inside of a spherical glass vessel, over which was placed a coating of luminophor (willemite). Work was carried out both on continuously evacuated guns and on sealed guns (containing tantalum as a getter).

It is known that zirconium oxides, nitrides and carbides, which have formed on the surface of a single crystal needle, cannot be removed by heating *in vacuo*, even close up to the melting point of zirconium, 1845°C [7]. Their melting points are considerably in excess of the melting point of zirconium and they neither vaporize nor dissociate at temperatures below 1845°C. Thus, obtaining field emission pictures of pure zirconium involves obtaining a very complete vacuum. The partial pressures of gases such as N_2, O_2 and hydrocarbons must be below 10^{-8} mm Hg. Consequently, careful outgassing of the glass vacuum equipment and the metallic parts of the gun – the tantalum lead and holder and the zirconium needle brazed on the latter – is essential. The needle was heated by thermal conduction from this holder, which was heated by an electric current.

To obtain the high vacuum, use was made of a mercury diffusion pump, with three series-connected glass traps, filled with liquid nitrogen. During evacuation of the gun vessel, the vessel itself, and not only that but also a considerable part of the vacuum line including one of the traps, were heated for 60-70 hr at up to 490°C. After heating and evacuation, a vacuum better than 5×10^{-8} mm Hg was reached, according to the ionization gauge readings. Thereupon, the tantalum holder with the brazed-on needle of zirconium was heated for 1-2 min to a temperature of 1400°C. This short-period heating was sufficient to outgas completely the holder and needle, since they were made from fine Ta and Zr wire respectively, which had previously been well out-gassed under vacuum conditions better than 5×10^{-8} mm Hg. In guns containing tungsten needles, evacuated in exactly the same way and then sealed off after spraying with getter, partial pressures below 10^{-11} mm Hg have successfully been reached, for gases which "poison" the emission. We emphasize that that was the partial pressure of emission "poisons" and not the total pressure [9]. The pressure limit of 5×10^{-8} mm Hg was fixed from the rate of contamination of a needle when held for a certain time without heating. The contamination of a tungsten surface can be calculated as a function of pressure, on the basis of gas kinetics considerations [10] and can be observed from field emission pictures. Since the field emission current for a "smooth point" depends greatly on the work function, whilst the latter in turn depends on the extent to which the surface is covered with electro-negative impurities, the best indicator of pressure changes in the gun must be the field emission current at a fixed voltage after a certain exposure of the needle in the vacuum.

Unfortunately we did not obtain smooth points on the zirconium needles, but invariably ribbed shapes (see Fig. 7, *a* to *f*), with well-developed separate facets. The emission current distribution over such a needle is primarily a function of its shape, i.e. of the increased local fields in the vicinity of the ribs, and depends little on the work function. Nevertheless an indication of pressure changes was obtainable both from the current and from the general appearance of the field emission picture of the zirconium needle. In our experiments no substantial change was observed after holding a zirconium needle for many days without heating, in either the appearance of the picture of the field emission current at a voltage fixed to an accuracy of 1 per cent. This indicates that the vacuum was better than 10^{-8} mm Hg.

The temperature of the zirconium tip was measured by means of an optical pyrometer, with corrections for the difference between colour temperature and true temperature and for absorption in the glass. The difference between the needle tip temperature and that of the area coinciding with the pyrometer filament, which can be ignored for tungsten, is by no means negligible in the case of zirconium. In view of the latter having a lower thermal conductivity than tungsten, at temperatures above 1200°C, considerable errors (up to 10 per cent) can be encountered. The needle tip temperature was calculated by a method described in a paper [11] which takes into account the temperature gradient along the needle.

The radius of curvature of the needle tip was determined from the field emission current by means of a graph, and corrected for work function by a method described in [12]. In view of the faceted shape of the crystal the tip radius (r_0) could not be determined accurately. For the majority of needles it varied from 0.5 to 1.5 μ. The magnification was calculated from the formula

$$m = \frac{1}{\gamma} \frac{R}{r_0}, \qquad (1)$$

where R is the gun radius (usually 5 cm), and γ is the compression factor (see Section 3), $\gamma \approx 1.5$. Thus, magnifications between 20,000 and 70,000 diameters were used. The electrical field strength

VOL 5 195

at the crystal surface was calculated from the emission current-voltage relationship, under the assumption that field strength E is directly proportional to voltage V:

$$E = aV. \quad (2)$$

Wire * of diameter 0.15 mm, made from iodide zirconium [13] was used to prepare the needles.

3. METHOD OF IDENTIFYING AND INDEXING THE ZIRCONIUM CRYSTAL FACET EMISSION IMAGES

The identification and indexing of the separate crystal facets on an emission picture did not present great difficulties. Since to a first approximation the shape of the needle tip in a gun can be regarded as hemispherical and since the size of the tip radius is considerably less than the spherical radius of the gun, the electrical field between the tip and the gun sphere can, to a certain approximation, be regarded as the field of a spherical condenser in which electrons will move along radii of the gun sphere. On falling on the willemite screen, the electrons will cause the screen to scintillate and will give, on the gun sphere, an orthogonal projection of the crystal facets and ribs. On this projection it is easy to pick out the centres of the facets which can be regarded as spherical projections of the normals to the facets. It is obvious that this spherical projection of the normals can be readily brought into correspondence with the gnomo-stereographic projection of the crystal. This correspondence also affords a means of deciphering the field emission picture.

When the emission picture of a crystal, on a strictly spherical gun screen, is photographed at natural size on flat film, one obtains an orthogonal projection of the spherical gun screen and of the crystal emission image. Obviously, this plane projection of the crystal image can also be brought into correspondence with the gnomo-stereoscopic projection of the crystal. By using the known crystal gnomo-stereographic projections, we can beforehand draw up the position of the centres of the individual facets, in the form in which they will appear on the photograph used in spherical gun experiments. By placing this drawing on the field emission picture it is possible, when the latter is symmetrical, to identify and index the facets with ease. If the emission picture is not symmetrical, the symmetrical theoretical picture is rotated about a given axis, until the new rotated pole figure coincides with the experimental picture. The described method of deciphering has been idealized, since under real conditions it must be taken into account that the field at the tip is not a spherical field and the electrons do not move exactly along radii of the gun sphere. In actual fact the electrical field at the tip must be regarded as the sum of a spherical field and that of a hyperboloid of rotation [12]. By virtue of this, the trajectory deviates from the needle (gun) axis by an increasing amount as the angle between the gun axis and the electron path direction is increased. If the intersection of the needle axis with the sphere of the gun or the plane of the photographic film is regarded as the centre of the image, then points on this image will be displaced along a radius towards this centre, as compared with points on an "ideal" image in a spherical condenser. The real image is compressed along the radii, to an extent increasing with the length of the radii. To simplify the further work on deciphering, we can introduce a coefficient of angular compression:

$$\gamma = \frac{\theta \text{ ideal}}{\theta \text{ experimental}}.$$

Up to angles of $\theta_{\text{ideal}} \leq 60°$, γ is constant. For angles $\theta_{\text{ideal}} > 60°$, γ increases markedly with increasing θ_{ideal}. To solve the majority of deciphering problems, the field emission picture can be confined to the constant γ region. The value of γ is readily determined experimentally from field emission pictures of crystals in which the angles between the normals to the facets are known previously, the actual identification of the facets being carried out directly from a knowledge of the crystal symmetry. Thus, for example, it is well known that the angle between the normals to the cube and dodecahedron faces in cubic system crystals is 45°, whilst the angle between the normals to the prism faces $(\bar{1}2\bar{1}0)$,$(\bar{1}\bar{1}00)$ $(2\bar{1}\bar{1}0)$, $(10\bar{1}0)$, $(11\bar{2}0)$ and $(0\bar{1}\bar{1}0)$ in hexagonal crystals is 30°. Knowing the value of γ it is possible beforehand to distort the "theoretical" pole figure of the Wulff grid analogue for given gun dimensions and photographic conditions. With the described method of deciphering, the angles between the normals to facets were determined to an accuracy

* We express our sincere thanks to V.S. Emel'ionov (corr:-member, Acad. Sci. U.S.S.R.) for kindly providing us with samples of this wire.

VOL. 5 1957

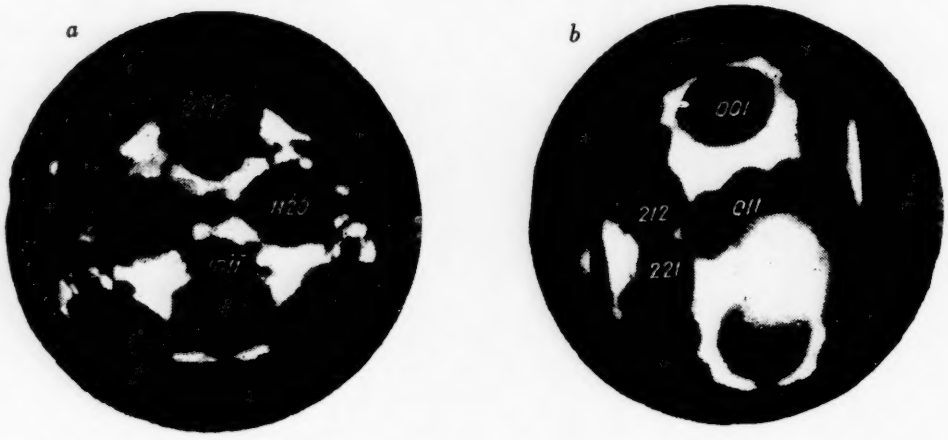

FIG. 1. Typical emission pictures of zirconium single crystals on the tip of the needle.
a – hexagonal micro-crystal. The [0001] axis is normal to the plane of the paper.
$T = 20°C$; $r_0 = 0.8\ \mu$.
b – cubic micro-crystal. $T = 1060°C$; $r_0 = 1.5\ \mu$.
Illumination from the holder can be seen.

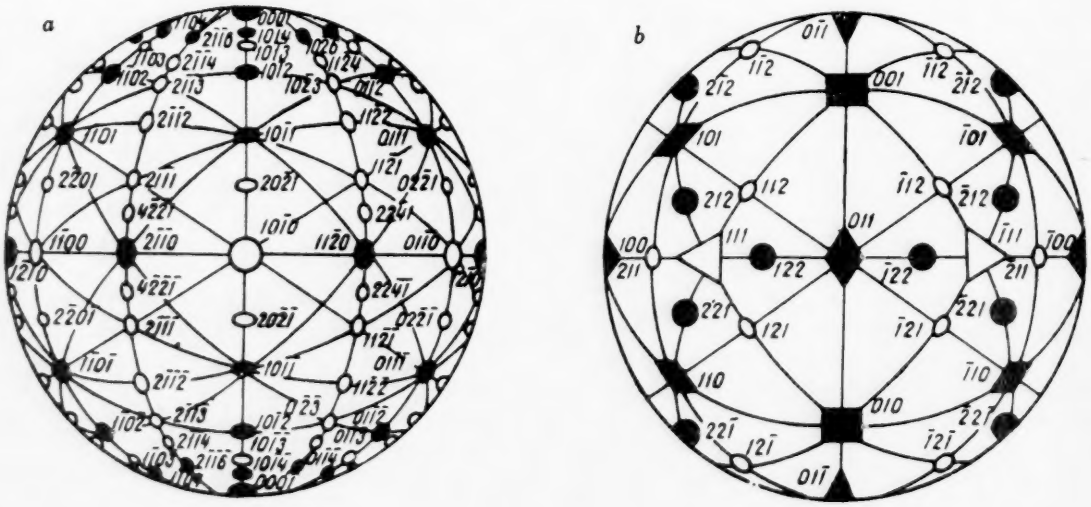

FIG. 2. Projections of the main faces and zones of:
a – a hexagonal crystal,
b – a cubic crystal.
Faces commonly observed on Zr field emission pictures are shaded.

of approximately ± 5°, for $\theta_{ideal} \leq 60°$.

4. EXPERIMENTAL RESULTS

a) Structure of facet surfaces and field emission

In Figs. 1a and b are shown field emission pictures of single crystals of zirconium, of the hexagonal and cubic modifications respectively; they are typical of the present work. In Figs. 2a and b are reproduced the special pole figures for crystals of the same symmetry and corresponding orientation. The indices of the most well-developed facets have been inserted directly in Figs. 1a and b on the dark images of these facets. Near the centre of Fig. 1b there is a good image of the (011) facet, which is characteristic of field emission pictures of crystals with the body-centred cubic lattice. As follows from a comparison of the pole figure in Fig. 2a and the field emission image in Fig. 1a, the (0001) face of the hexagonal crystal is arranged parallel to the needle axis. Around all the indexed faces in Figs. 1a and b there is a well defined bright border. This is particularly well developed around the (001) face in Fig. 1b. This border is due to emission from the stepped ribs of "skyscraper" structure, where the potential gradient is considerably higher than on the comparatively flat face. It can be assumed that the dark areas on the figure are essentially plane faces, having roughness due only to the size and shape of the atoms. The ribs however are very rough, because of the irregular stacking of certain atoms in various areas. We have often observed this type of roughness in the ion gun [14] and it has probably been most clearly observed in Müller's helium gun [3]. Since the current density on the ribs is not less than 10^6 A/cm², at the most conservative estimates, the coulomb repulsion of the electrons plays an important part and the rib images become blurred.

The formation of faces on a crystal (Fig. 1b) can be related in the first place to the "rearrangement" of the surface [15] when the needle is heated in the electrical field, which cannot be avoided if the high-temperature phase of zirconium is to be studied.* However, the pronounced development of the cube faces {001} in β-zirconium, as compared with the dodecahedron faces (which is by no means typical of pure tungsten, having the same body-centred cubic lattice, see Fig. 4) indicates that the β-zirconium crystal is bounded by equilibrium faces which do not correspond to the normal surface of the metal. The identical emission from the {001} and {011} faces in β-Zr despite the fact that the first are undoubtedly the rougher and according to Stranski and Suhrmann [16] must emit more strongly, leads us to suggest that the cube faces in β-Zr are "smoothed" by nitrogen atoms, which fill the gaps between the zirconium atoms (Fig. 5). With this type of interpolation the interatomic bonds are strengthened and an extremely strong "skin" is formed on the surface. Actually, one such crystal (Fig. 3a), held at a temperature of 1200°C for 60 hr in a sealed vessel, had such a strong surface that no amount of pre-heating in the comparatively weak field used for the observations could alter it. From the type of image in Fig. 3a it is quite difficult to decide on the symmetry. Comparison of Fig. 3a with a number of β-Zr, images (not reproduced in the paper) led to the conclusion that the crystal is a pseudomorph having hexagonal structure in bulk and the faces of two regularly oriented cubic crystals on the surface.

Elucidation of the internal structure of the crystal only proved possible by using the device of heating the needle with a superimposed high positive potential (a "reverse" field). Heating in a strong "reverse" field leads to layer by layer destruction [17] of the crystal surface. With "reverse" fields of 150-160 MeV/cm, the possibility is not excluded on the rapid "evaporation", due to the field, of lattice atoms and the desorption of foreign atoms. The effectiveness of this method is illustrated in the series of photographs, Figs. 3a to f (Fig. 1a belongs in the same series, coming between Figs. 3d and 3e). The conditions under which the needles were treated are stated in the figure captions. Besides providing indisputable evidence of the hexagonal bulk structure of the crystal, heating in a reverse field made it possible to produce a series of interesting forms, such as Fig. 3e, with developed type {11$\bar{2}$2} faces, and a series of forms with well developed large steps, Figs. 3b-d and 3f.

The α-Zr crystallite in Fig. 1a (the same as in Fig. 3) underwent no transformation at the high temperatures attainable for observation in the gun (up to 1300°C; at higher temperatures observations were upset by thermal emission background). This was associated with the fact that during prolonged heating, although it took place in a very high vacuum, the crystallite absorbed a certain amount of nitrogen from the residual gases, which led to a marked rise of transformation temperature [7, 18].

As an alternative method of obtaining a relatively pure surface on a zirconium crystallite, use was

* The transformation temperature for pure zirconium is 862°C.

VOL. 5 1957

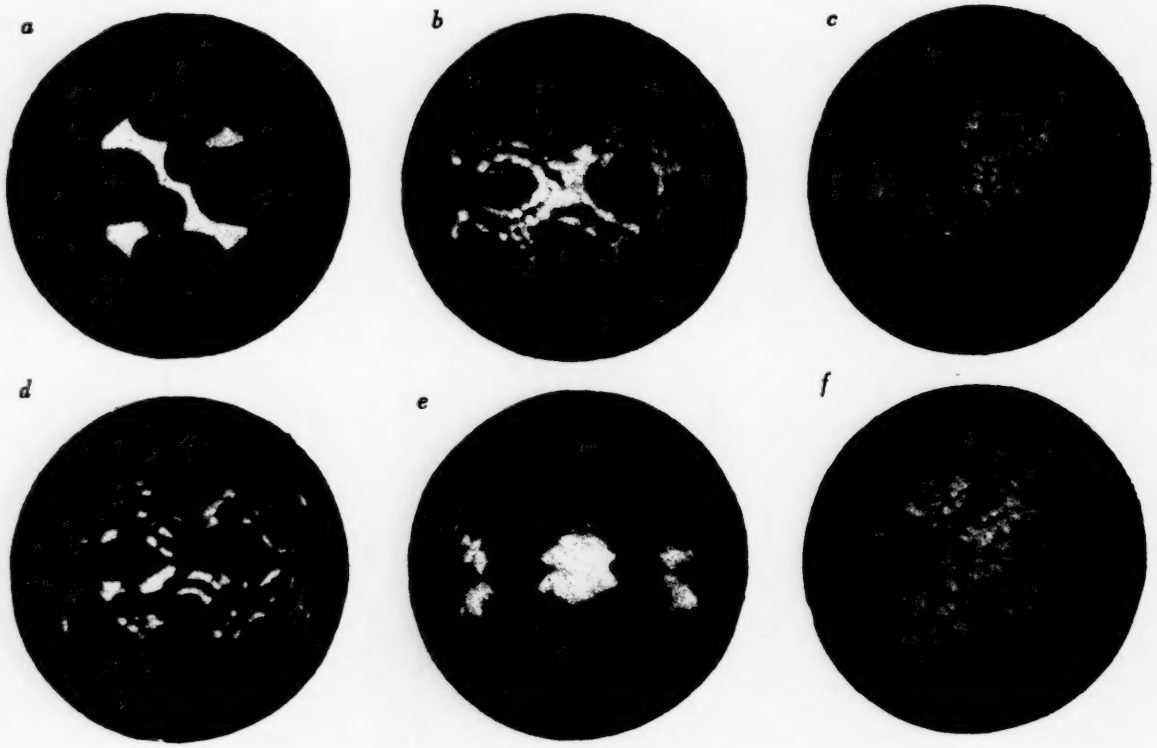

FIG. 3. Surface changes in a crystal during heating in a reverse field.
a — Zr crystal after heating 60 hr at 1200°C, without field,
b — after treatment at a temperature of 1140°C in reverse fields up to 140 mV/cm,
c — after 3 min at 1200°C in a reverse field of 130 mV/cm,
d — after heating 1 hr at 1200°C, without field (see Fig. 1a for appearance after a further 14 hr at the same temperature),
e — after 10 min in a reverse field of 150 mV/cm at 1220°C, followed by 4 min heating at 1220°C without field,
f — after 1 min in a reverse field of 160 mV/cm at 1220°C.
All photographs taken with the needle at room temperature.

made of the condensation on a heated zirconium needle of large amounts of zirconium, evaporated from an external source under high vacuum. The low volatility of the oxides and carbides of zirconium guaranteed the extreme purity of zirconium evaporated under such conditions. Fig. 6 illustrates the capabilities of this method. Fig. 6a shows the image of one face $(10\bar{1}2)$ of a large hexagonal crystallite, formed after transformation from the β-phase. Heating with and without a field, led to no improvement of the image. Then the needle (Fig. 6a), heated to red heat (below the transformation temperature) was coated with a large amount of zirconium. After some further heat treatment, in a field up to 4×10^7 V/cm, and without a field, an extremely perfect hexagonal crystal was obtained (Fig. 6b). The pronounced rib formation is apparently associated with the causes already described as producing ribbing in the crystal (Fig. 1a).

b) The field emission picture and the $\alpha \rightleftarrows \beta$ transformation in zirconium

Figure 7a shows the field emission picture taken

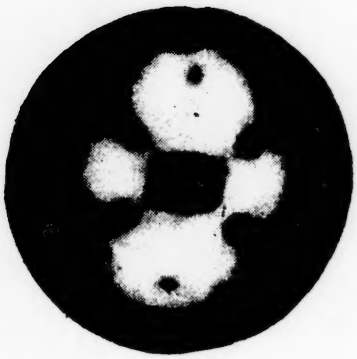

FIG. 4. The emission picture from a "smoothed" pure tungsten needle.

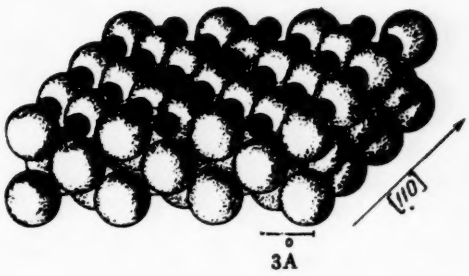

FIG. 5: Packing of nitrogen atoms on the (001) face of β-Zr.

VOL. 5 1957

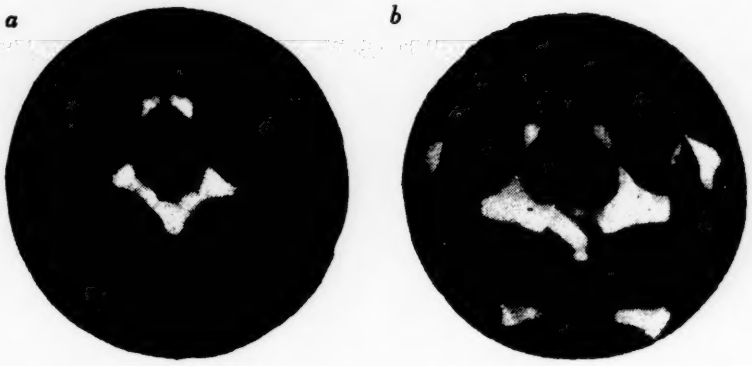

FIG. 6. Formation of the surface of an α-Zr crystal when Zr is deposited on it:
a – the $(10\bar{1}2)$ face of a hexagonal crystal after its transformation from the β-phase,
b – after 5 hr deposition of Zr on the same crystal and some thermal and field treatment.

at a temperature of 1040°C on a cubic crystal of zirconium, obtained by heating in a field of 2×10^7 V/cm at a temperature of 1100°C. The heated holder, to which the zirconium needle was brazed, can be well seen in this picture. The image of the holder can be used as an independent indicator of the crystallographic orientation of the needle and the direction of the axis of the photographic object lens.

Fig. 7b shows the image of a crystal, distorted as a result of the phase transformation. The deformation commenced at a temperature of about 1000°C. This form of image was also retained on cooling the needle to room temperature. On the assumption that this was a case of pseudomorphism in the hexagonal modification, we tried to bring out indications of the hexagonal symmetry, by heating the needle below 1000°C, but without success. Heating the needle for a few minutes to a temperature higher than the transformation temperature (1100°C), led to a change in the picture shown in Fig. 7b. At 1060°C the picture shown in Fig. 7c was obtained, with a single cube face, surrounded by a bright fringe with arcuate

FIG. 7. Phase transformations between $\alpha \rightleftarrows \beta$ Zr ($r_0 = 1.5\ \mu$):
a – β-Zr crystal, $t = 1040°C$,
b – after cooling below 1000°C,
c – after heating a few minutes at 1100°C, without field; $T = 1060°C$,
d – after heating to a higher temperature in a field; $T = 1080°C$,
e – the $(10\bar{1}2)$ face in place of (001) at $T = 1040°C$,
f and *g* pictures showing simultaneous existence of elements of both α and β-Zr, at temperatures of 1130 and 1040°C,
h – a well-developed α-Zr crystal, $T = 800°C$.

segments, evidence of the presence of facets with {122} indices. On continuing to heat the needle for a few minutes in a "direct" electrical field (needle at negative potential) at a temperature above 1100°C, the picture shown in Fig. 7d, taken at $T = 1080$°C, was obtained as a result of the well known phenomenon of "rearrangement" in an electrical field [15]. Besides the single cube faces, very similar to the cube face in Fig. 7a, the lower half of the picture showed the outlines of the ribs of a second cube face. The new crystal formed at the tip of the needle as a result of heating, appeared to be oriented slightly differently from the crystal in Fig. 7a. When the crystal which had given Fig. 7d was cooled to 1040°C, it underwent a phase transformation at this temperature. The outline of the (001) face of the cubic crystal became subdivided into three very bright areas, and the picture shown in Fig. 7e was obtained. The well-developed face in Fig. 7e is the $(10\bar{1}2)$ pyramid face of a crystal of hexagonal symmetry. When the crystal was repeatedly taken through the transformation point, accurate reproducibility was attained, for the pictures shown in Figs. 7e and 7d for $T < T_{trans}$ and $T > T_{trans}$ respectively. During repeated heating, the transformation temperature gradually increased up to 1200°C, above which observation became difficult, due to strong illumination from the holder and to thermal emission.

Heating the needle at a temperature of 1250°C in the presence of a reverse field of 3×10^7 V/cm caused, first, the formation of a cubic crystal face (Too) on the hexagonal $(1\bar{1}20)$ face (see Fig. 7f). The same crystal at room temperature gave the picture shown in Fig. 6a. After condensing zirconium at red heat on the needle which had given Fig. 6a, the picture shown in Fig. 7g was obtained at a temperature of 1040°C. This picture confirms that the crystal at the needle tip was not holomorphic. Facets can be seen in Fig. 7g which appertain simultaneously to crystals of cubic and of hexagonal symmetry. Thus, for example, the $(10\bar{1}2)$ face of the crystal of hexagonal symmetry is well developed. At the same time a face can be seen which is equally reminiscent of the $(\bar{1}00)$ cube face and the $(11\bar{2}0)$ prism face. Thus, the crystal which gave Fig. 7g appears to be of intermediate form, and is most probably a pseudomorph. The crystal form appearing in Fig. 7g must be unstable. Heat treatment in a direct field was in fact able to change it to the form giving the field-emission picture shown in Fig. 7h. This picture comes from a crystal of hexagonal symmetry, with well-developed $\{10\bar{1}2\}$ pyramid faces. In the upper part of the photograph the basal face (0001) stands out clearly, and is surrounded by $\{10\bar{1}4\}$ faces.

It should be noted that all the changes associated with phase transformations (see Figs. 7a → 7b, 7d ⇄ 7e, and the indications of a new phase appearing in Figs. 7f and 7g) took place instantaneously at a definite temperature. On the other hand, changes associated with changes in form, for example rearrangement in a field (see Figs. 7c → 7d) took place gradually over a wide range of temperatures.

The increase in transformation temperature referred to, as the duration of heating of the needle was increased, is apparently associated with the absorption of residual gases (N_2, O_2), and indicates their very strong adsorption by zirconium, in a vacuum of the order of 10^{-8} mm Hg. Calculations based on the data in [18] indicate that, for a needle of radius 0.2 μ, the solution, in the mass of the hemispherical needle tip, of a monomolecular layer of oxygen covering the hemisphere, will raise the transformation temperature by 30°C. At a coefficient of adhesion of 1, a monomolecular layer is formed within one minute at $p = 10^{-8}$ mm Hg.

5. DISCUSSION OF RESULTS

The relationships between the orientations of the α-and β-phase lattices, according to Burgers [5] are such that

$$(0001)_\alpha \parallel (011)_\beta \text{ and } [1\bar{1}20]_\alpha \parallel [\bar{1}\bar{1}1]_\beta \quad (4)$$

As a consequence of these relationships it can be deduced that in the $\beta \rightarrow \alpha$ transformation, 12 orientations of the new phase can correspond to a given orientation of the original phase, and in the $\alpha \rightarrow \beta$ transformations, 6 orientations.

In our experiments, with various β-phase orientations, only one α-phase orientation was observed in every case (Fig. 7), apparently corresponding to a minimum in surface energy. It makes sense, therefore to examine the possible orientations in the $\alpha \rightarrow \beta$ transformations only. The 6 possible orientations of the β-phase relative to the α-phase in zirconium, following the α-β transformation, are shown according to Burgers's relationships on the pole figures in Figs 8a-c, in which the normal to the $(10\bar{1}0)$ face is placed at the centre. The striking feature in considering the pole figures is the closeness of orientation of the daughter cubic phases, which differ one from the other by a 10°32′ orientation about the [0001] direction. It is, in all probability, not possible to distinguish between these close orientations on faces of crystals.

VOL. 5 1957

The general observation can be made, that the probability of obtaining cubic symmetry of one orientation or another, as a result of the transformation of the crystallite at the tip, in view of its microscopic dimensions, will be greater, the smaller the change in surface energy to which the setting up of the given orientation corresponds. This observation must be particularly valid, if the results given in [19, 20] are taken into account, for those orientations for which well-developed low-index faces in both phases remain approximately parallel. Our results indicate that this is in fact so. Thus, for example, it can be seen from Fig. 7a that the dodecahedral face (011) is approximately parallel to the $(1\bar{1}00)$ face in Fig. 7h. In Fig. 7d the cube face is approximately parallel to the $(10\bar{1}2)$ face in Fig. 7e. In Fig. 7g, the $(1\bar{0}0)$ and $(01\bar{0})$ cube faces are parallel to faces $(11\bar{2}0)$ and $(\bar{1}\bar{1}02)$ respectively. To the basal (0001) plane of the hexagonal crystal there corresponded in every case one or another plane of type {011}. It is not difficult to see that the β-phase orientations observed all fall into the 3 groups (with 2 in each) of orientations as shown in the pole-figures in Fig. 8. Thus Figs. 7a, 7f and 7g correspond to the pole figure in Fig. 8c, Fig. 7d to Fig. 8b and Fig. 3a (an α-phase pseudomorph) to Figs. 8a and 8c simultaneously. On the basis of this it can be accepted that orientational relationships between the α and β-phase lattices, shown in [4], are confirmed by the present observations. Brock [4] reached analogous conclusions in respect of titanium, which exhibits a similar transformation. At the same time it can be noted that in the case of the small crystals used in the gun, only those few daughter phase orientations occur which do not lead to any substantial increase in the surface energy of the crystals. This observation is in complete accord with the results of paper on cobalt and thallium [19, 20].

Great interest attaches to the crystallites of pseudomorphic habit, which gave the field emission pictures shown in Figs. 7f and 7g. The simultaneous existence on these crystallites of faces appertaining to both modifications is evidence, in our opinion, of the diffusionless, coherent transformation of the parent phase crystal to the daughter phase crystal, with partial retention of the external form of the parent phase crystal. Transformations of this nature have been observed under special conditions on microscopic crystals of copper-aluminium-nickel alloy [21]. The image on Fig. 7f can be regarded as the field emission picture of a cubic crystal, partly retaining the hexagonal crystal habit, Similarly Fig. 7g is the field emission

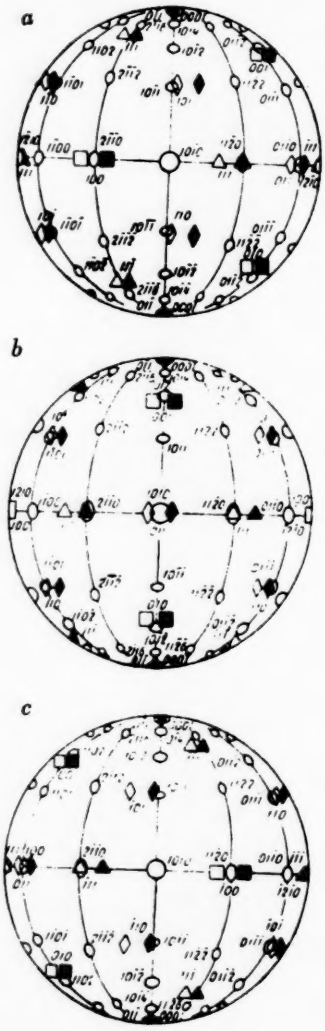

FIG. 8. Pole figures of the faces of a hexagonal crystal and the important faces of possible cubic crystals, which satisfy the conditions of the Burgers relationships:

$\{011\}_\beta \parallel \{0001\}_\alpha$ and

a – light: $[\bar{1}11]_\beta \parallel [\bar{1}2\bar{1}0]_\alpha$

dark: $[111]_\beta \parallel [11\bar{2}0]_\alpha$

b – light: $[\bar{1}11]_\beta \parallel [11\bar{2}0]_\alpha$

dark: $[111]_\beta \parallel [\bar{2}\bar{1}10]_\alpha$

c – light: $[111]_\beta \parallel [2\bar{1}\bar{1}0]_\alpha$

dark: $[111]_\beta \parallel [1\bar{2}10]_\alpha$

picture of a hexagonal crystal, partly retaining the cubic crystal habit. The presence in Fig. 7f of a

cube face within the $(11\bar{2}0)$ face of the hexagonal crystal is evidence of the effort on the part of the new phase to bound itself by faces which correspond to its lattice symmetry. The considerable surface mobility of the atoms creates conditions under which this effort can occur. Since the photograph reproduced in Fig. 7f was obtained after annealing the needle at a temperature of 1250°C, it is quite natural that a cube face was able to form.

Layer-by-layer destruction in a reverse field, which can be regarded as crystal growth in the negative direction, must reveal any dislocations in the crystal [17]. In accordance with the theory of crystal growth [22] growth spirals (and in our experiments decomposition spirals) can be observed on planes normal to the axes of screw dislocations. In Ref. [17] and in our experiments (Fig. 3), the dislocations axes were found to be oriented perpendicular to the most closely packed equilibrium crystal faces. This could be deduced from the location of the centres of decomposition (revealed by the concentric stepping which surrounded them) in Figs. 3b and 3f. In Fig. 3b centres of decomposition are clearly noticeable on the $(\bar{2}1\bar{1}0)$ and $(11\bar{2}0)$ faces, the latter are also showing a well developed decomposition spiral. Fig. 3f, in addition to the latter, revealed decomposition centres on faces of types $\{10\bar{1}1\}$ and $\{10\bar{1}2\}$.

In metals which do not undergo phase transformations the presence of dislocations is associated with the strain history of the crystal. In the case of a Zr crystallite (Fig. 3), as we suppose, the presence of dislocations is associated with the transformation history it has undergone. Consideration of the pole-figures (Fig. 8) indicates that the β-phase lattice planes of types $\{100\}$ and $\{110\}$, corresponding to the adjacent pairs of orientations which can be formed during the $\alpha \rightarrow \beta$ transformation, can be arranged equally nearly parallel to the $\{1\bar{1}20\}$, $\{10\bar{1}1\}$ and $\{10\bar{1}2\}$ faces of the α-phase. Since in the reverse $(\beta \rightarrow \alpha)$ transformation, the same hexagonal crystal can be formed from material of cubic symmetry with the very near lattice orientations referred to (Fig. 8), it is very probable that diffusionless transformation can give rise to the dislocations which are observed during layer-by-layer destruction. In fact, two decomposition centres, separated by an angular distance of about 10°, are clearly discernible on the $(11\bar{2}0)$ face in Fig. 3f. The corresponding angle between the $\{100\}$ lattice plane orientations (see Fig. 8c) is 10°32′, in strict fulfilment of Burgers's second condition, which according to more recent work [23], is correct to an accuracy of 2°. We do not yet regard our hypothesis as fully proven. No doubt further experiments and calculations are required to prove it. We considered it important to point out the possibility of the existence of dislocations in the centres of the hexagonal crystal faces.

CONCLUSIONS

1. Using an electron emission microscope, it is possible from the faces bounding the crystals in the needle to determine the orientational relationships between the lattices of the individual phases in polymorphic transformations. For the case of zirconium, the orientational relationships between the α- and β-phase lattices, previously determined by the X-ray method by Burgers, has been confirmed.

2. The polymorphic transformation of zirconium, in the case of crystallites with linear dimensions of the order of a micron, takes place by a diffusionless mechanism throughout the crystallites.

3. A polymorphic pseudomorph crystal of the daughter phase, given considerable surface mobility of the atoms, will go over to an equilibrium form, such that low-index faces in the parent and daughter crystals remain exactly or approximately parallel.

4. For the case of the Zr crystallites examined, with linear dimensions around 1 μ, those possible orientations are realized on transformation, which require a minimum change in surface energy.

5. The polymorphic transformation temperature for zirconium depends greatly on the amount of nitrogen and oxygen absorbed by the zirconium, and increases with increase in their concentration.

6. The faces observed on zirconium crystals of cubic symmetry are not the equilibrium faces for pure zirconium, but the equilibrium faces for crystals of a solid solution of nitrogen in zirconium, in the presence of a strong electrical field and at high temperatures.

7. Layer by layer spiral decomposition of crystallites of hexagonal symmetry in a reverse electrical field commences from the centres of the $(11\bar{2}0)$, $(10\bar{1}2)$, $(\bar{1}0\bar{1}2)$ and $(\bar{2}1\bar{1}0)$ faces, which is possibly associated with the presence of screw dislocations, the axes of which are parallel to the normals to the corresponding planes of atoms in the hexagonal lattice.

Translated by E. Bishop

REFERENCES

1. Ia. S. Umanskii, B.N. Finkel'shtein, *et al* *Fizicheskoe metallovedenie (Physical metallurgy)*, 502, (1955).

VOL. 5 1957

2. *Elektronnaia mikroskopiia (Electron microscopy)*, Ed. A.A. Lebedev, GITTL, p. 333 (1954).
3. E.W. Müller, *Z. Naturf.*, 11-a, 88, (1956).
4. E.G. Brock, *Phys. Rev.*, 100, 1619, (1955).
5. W.G. Burgers, *Physica*, 7, 561 (1934).
6. E.W. Müller, *Ergebn. exakt. Naturw.*, 27, 290-360 (1953).
7. G.L. Miller, *Tsirkonii (Zirconium)*, Foreign Literature Publishing House (1955).
8. R.E. Aitchison, *Aust. J. Appl. Sci.*, 5, 10 (1954).
9. D. Alpert and R.S. Buritz, *J. Appl. Phys.*, 25, 202 (1954).
10. F. Ashworth, *Advanc. Electron.*, 3, 1, (1951).
11. E.W. Müller, *Z. Phys.*, 126, 642 (1949).
12. M. Drechsler and E. Henkel, *Z. angew. Phys.*, 6, 341, (1954).
13. V.S. Emel'ianov, P.D. Bystrov and A.I. Evstiukhin, *Atomnaia energiia*, No. 3, 122 (1956).
14. A.P. Komar and Iu. A. Selitskii, *Dokl. Akad. Nauk SSSR*, 46, 957 (1954).
15. I.L. Sokol'skaia, *Zh. tekh. fiz.*, 26, 177 (1956).
16. I.N. Stranski and R. Suhrmann, *Ann. Phys.*, 1, 153 (1947).
17. M. Drechsler, G. Pankow and R. Wanselow, *Z. Phys. Chem.*, 4, 249 (1955).
18. R.F. Domagala and D.J. McPherson, *J. Metals*, 6 (2), Sect. 2, 238 (1954);
book *"Tsirkonii" (Zirconium)*, 2, Foreign Literature Publishing House,
40, 1 (1955).
19. U. Dehlinger, *Metallwirtschaft*, 11, 223 (1932).
20. U. Dehlinger, R. Osswald and H. Bumm, *Z. Metallk.*, 25, 62 (1933).
21. G.V. Kurdiumov and L.G. Khandros, *Voprosy fiziki metallov i metallovedenie (Problems of metal physics and metallography)*, 2, 56, (1950).
22. A.R. Verma, *Crystal Growth and Dislocations*, London, (1953).
23. E.O. Hall, *Twinning and Diffusionless Transformations in Metals*, London (1954).

VOL
5
195

STUDY OF THE PHYSICAL FACTORS DETERMINING THE HARDENING OF ALLOYED IRON*

V. M. GOLUBKOV, V. A. IL'INA, V. K. KRITSKAIA, G. V. KURYUMOV and M. D. PERKAS

Institute of Metallography and the Physics of Metals Ts.N.I.I.Ch.M.

(Received 4 December 1956)

It is known that by means of plastic deformation and heat treatment it is possible to obtain metals and alloys in a hardened state. This state is metastable and when the temperature is raised the metals or alloys change into the state of equilibrium (softening).

X-ray investigations have shown the fundamental difference in the diffraction picture for metals and alloys in the hardened and softened state. Thus, for X-ray photos obtained from deformed samples broadening and weakening of the diffraction lines is characteristic which is conditioned by the existence of displacements of the second and third kind and the areas of coherent scattering are small.

Although as a result of a number of investigations [1-26] the properties and many details of the structure of metals and alloys in the hardened state have been studied, the data available at present never-the-less does not make it possible to establish the role of the various physical factors in the change of the properties of metals and alloys when they are hardened, with complete certainty.

To understand the nature of the hardening of metals and alloys it is important to find out with what changes in the microcrystal structure the changes of the mechanical properties are connected and to establish the connexion between the changes which occur in the micro-areas and the properties of the macrovolume.

The present paper is devoted to the study of the physical factors which determine the hardening of α-iron alloyed with various elements.

Further on the hardening which is entirely due to the changes in the microstructure of the α-solid solution without changes in its chemical composition will be considered.

VOL. 5 1957

THE MATERIAL INVESTIGATED AND ITS TREATMENT

Iron alloyed with various elements was used for the investigation. The chemical composition of the binary alloys of the iron is given in Table 1. The alloys were smelted in a high frequency furnace. The total weight of the ingots was 25 kg. All ingots were subjected to diffusion annealing at 1200° for 20 hr. After homogenization annealing the ingots were forged into squares of 50 x 50 mm. The majority of the ingots were after the forging subjected to annealing to obtain uniform grain size.

After forging and annealing the samples were subjected to cold rolling with a total compression to 80 per cent. From the ribbon obtained by rolling flat samples were cut for X-ray analysis, the measurement of the hardness and also samples for micromechanical tests.

The alloys Fe + 3% Mn, Fe + 4% Ni, Fe + 8% Cr were also hardened by annealing. The heating of the samples for this purpose was done in a salt bath at 1000°, the cooling in a 10 per cent solution of NaOH.

The effect of various degrees of deformation on the changes in the characteristics of the micro structure was studied for the alloys Fe + 3% Mn, Fe + 0.5% Ti, Fe + 0.6% W and for unalloyed iron. The samples, which in the original state had the dimensions 70 x 15 x 8 mm, were subjected to cold deformation (in a laboratory rolling mill) with compression by 5, 10, 15, 20, 30, 50, 80 and 90 per cent.

The characteristics of the microstructure were also studied for filings obtained from the alloys Fe + 1.84% Co, Fe + 1.8% Mo, Fe + 2.28% V, Fe + 3% Mn, Fe + 4% Ni, Fe + 8% Cr.

Defects of the third kind and the characteristic temperature were mainly determined on samples prepared from powders.

METHODS OF INVESTIGATION

The main methods for the study of the effect of the alloying elements on the hardening of ferrite

* *Fiz. metal. metalloved.* 5, No. 3. 465-483, 1957.

TABLE 1. Chemical composition of the alloys

Alloy*)	Contents of elements, % weight												
	C	Mn	Cr	Ni	W	V	Ti	Co	Nb	Si	Mo	S	P
Armco iron	0.02	0.05	—	—	—	—	—	—	—	0.03	—	0.023	0.017
Fe+2%Cr	0.017	сл.	1.97	—	—	—	—	—	—	0.012	—	0.020	сл.
Fe+8%Cr	0.014	сл.	8.54	—	—	—	—	—	—	—	—	0.011	сл.
Fe+4%Ni	0.02	сл.	—	4.0	—	—	—	—	—	0.05	—	0.016	0.001
Fe+0.6%W	0.02	0.02	—	—	1.8	—	—	—	—	сл.	—	0.017	0.001
Fe+2.28%V	0.02	0.23	—	—	—	2.28	—	—	—	0.18	—	0.013	0.007
Fe+0.5%Ti	0.025	0.05	—	—	—	—	0.39	—	—	сл.	—	0.001	0.01
Fe+1.84%Co	0.035	—	—	—	—	—	—	1.95	—	сл.	—	0.014	0.006
Fe+0.8%Nb	0.03	0.09	—	—	—	—	—	—	1.25	0.01	—	0.01	0.005
Fe+6%Si	0.02	0.11	—	—	—	—	—	—	—	3.0	—	0.014	сл.
Fe+0.6%Mo	0.02	сл.								0.01	1.0	0.008	0.007
Fe+1.8%Mo	0.02	0.03	—	—	—	—	—	—	—	0.04	3.02	0.026	0.005
Fe+3%Mn	0.02	2.90	—	—	—	—	—	—	—	0.02	—	0.017	0.003
Fe+1.5%Mn	0.015	1.47	—	—	—	—	—	—	—	0.03	—	0.017	сл.

*) In this column the content of the alloy element is given in atomic %.

were the methods of X-ray structure analysis and mechanical tests.

(*a*) The study of the width of the diffraction lines of alloyed iron after hardening by cold plastic deformation and quenching was done in an ionization apparatus URS-50I with automatic registration of the intensity distribution curve in Fe K_α radiation. The width of the lines (110) and (220) was measured. The width of the lines (110) and (220) obtained from highly tempered iron samples was taken as standard. To make the correction for the geometry of the arrangement it was necessary to know the intensity distribution of both the investigated line and the standard. Calculations showed that the intensity distribution is best described by the function $e^{-\alpha x^2}$ (Fig. 1). Data obtained by Fourier analysis showed that the curve of the true intensity distribution of the line (110) of the deformed sample is also described by the function $e^{-\alpha x^2}$.

The true width of the line β was calculated by the formula

$$\beta = \sqrt{B_0^2 - b^2},$$

where B_0 is the width of the line corrected for radiation inhomogeneity; b the width of the standard line. The magnitude of the defects of the second order $\Delta a/a$ and the size of the areas of coherent scattering (D) were determined from the expression

$$\frac{\Delta a}{a} = \frac{n}{4R\tan\vartheta}, \quad D = \frac{\lambda}{m \cdot \cos\vartheta},$$

where m and n are the broadening on account of D and $\Delta a/a$. The method of differentiating the effects of the widening of the line on account of the small size of the blocks and the displacements of the second kind are described in papers [6, 26, 27].

(*b*) The characteristic temperature was determined by measuring the X-ray diffraction with Mo-radiation at two temperatures (liquid air and room temperature) [13].

(*c*) The magnitudes of static displacement of the lattice, caused by the presence of the atoms of the solute element or by plastic deformation, were determined on powders from the weakening of the intensity of the X-ray reflections with Mo-radiation, taking into account the change in the characteristic temperature [17, 18]. In the alloys investigated there was no extinction effect [38].

The micromechanical tests were made in a RF-2 machine with photographic registration of the elongation pattern on a photographic plate [28]. From the elongation pattern σ_s and σ_B were determined.

(*d*) The hardness was determined in a Vickers device at 10 kg load. For every state two samples were taken and on every sample three measurements were made.

RESULTS OF EXPERIMENTS *

(*a*) *Width of diffraction lines*

As has been noted above in the X-ray photographs, taken with samples subjected to cold plastic deformation, a broadening of the diffraction lines is observed.

(Footnote on the next page)

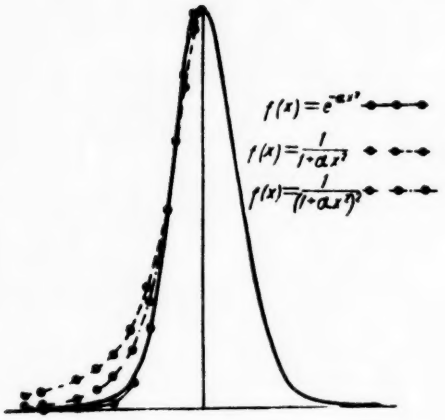

FIG. 1. *a*. Intensity distribution curves for Line (110).

in unalloyed iron.

The study of the width of the line (220) in filings (see Table 2) showed that after this deformation the lines become much more strongly broadened than after the deformation by rolling to 80 per cent. The greatest broadening of the lines in powders was observed in the alloys Fe + 3% Mn, Fe + 4% Ni and Fe + 8% Cr.

Hardening by means of quenching ("phase freezing") was studied for the binary alloys Fe + 3% Mn, Fe + 8% Cr, Fe + 4% Ni and for unalloyed iron. For the first two alloys the broadening of the line after hardening became greater than for samples deformed to 80 per cent, and somewhat less than for powders. (Table 2).

(*b*) *Magnitude of the displacements of the second kind* $\Delta a/a$

The differentiation between the effect of the broadening of the X-ray diffraction lines on account of

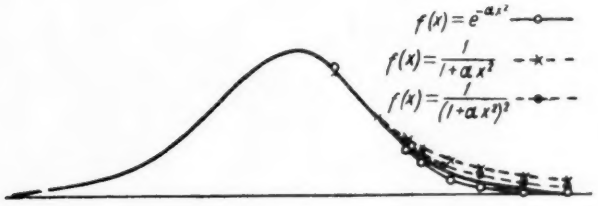

FIG. 1. *b*. Intensity distribution curves for Line (220).

Table 2 gives the widths of the diffraction lines (110) and (220) in milliradians obtained for the investigated alloys after hardening by cold plastic deformation to 80 per cent. The width of the diffraction line (220) varies for different alloys after one and the same degree of plastic deformation within wide limits, from 21 to 38 x 10^{-3} rad. The smallest width of the line after deformation is shown by the alloy Fe + 0.5% Ti, the greatest by the alloy Fe + 6.0% Si.

It was established that in certain binary alloys of iron, namely Fe-Ti, Fe-V, Fe + 2% Cr, Fe-Co the width of the line (after one and the same degree of cold plastic deformation) is less than in unalloyed iron. In the other binary alloys of iron the width of the line obtained from samples subjected to cold plastic deformation (to 80 per cent) was greater than the presence of defects of the second kind and those caused by the smallness of the blocks made it possible to determined the magnitude of the displacements of the second kind and the dimensions of the blocks.

In the alloys investigated one and the same degree of cold plastic deformation (80 per cent) leads to differences in the magnitude of the displacements of the second kind (Table 3). The greatest $\Delta a/a$ after deformation was observed in the ferrite alloyed with silicon: $\Delta a/a$ = 2.07 x 10^{-3}. The displacements of

(Footnote from previous page)

* The following diploma students took part in conducting the experiments: B.M. Barbalat, L.I. Mirkin, L.V. Tikhonov, I.G. Gladkova and V.S. Sichinskaya.

TABLE 2. Width of the lines (110) and (220) of iron alloyed with various elements after hardening by quenching, after cold plastic deformation (80%) and in filings

Treatment	Crystal plane	Armco iron	Fe + 4% Ni	Fe + 1,5% Mn	Fe + 3% Mn	Fe + 2% Cr	Fe + 8% Cr	Fe + 0,6% Mo	Fe + 1,8% Mo	Fe + 2,3% V	Fe + 1,8% Co	Fe + 0,6% W	Fe + 0,5% Ti	Fe + 0,8%Nb	Fe + 6,0% Si
After 80% deformation	110	9,48	10.7	9,25	9,90	8,5	8,3	8,2	9,95	8,06	8,55	9,5	6,75	8,9	9,44
	220	30,5	36,8	29,6	32,8	25,0	31,0	25,4	34,2	22,8	27,3	36,0	21,2	29,9	38,2
Filings	110	12,1	12,5	—	14,0	—	13,6	—	12,5	12,6	10,8	—	—	—	—
	220	41,0	49,0	—	49,0	—	48,0	—	44,1	38,0	32,3	—	—	—	—
After quenching	110	—	10,18	—	11,45	—	11,0	—	—	—	—	—	—	—	—
	220	—	34,4	—	44,47	—	44,2	—	—	—	—	—	—	—	—

TABLE 3. $\Delta a/a$, D for various alloys after different hardening treatments

Material / Treatment	Armco iron	Fe + 4% Ni	Fe + 1,5% Mn	Fe + 3% Mn	Fe + 2% Cr	Fe + 8% Cr	Fe + 0,6% Mo	Fe + 1,8% Mo	Fe + 2,3% V	Fe + 1,84% Co	Fe + 0,6% W	Fe + 0,5% Ti	Fe + 0,8% Nb	Fe + 6,0% Si
Second kind displacements, $\Delta a/a$. 10^{-3}														
After 80% deformation	0,68	1,35	0,93	1,15	—	1,46	0,5	1,31	—	—	1,8	0,72	1,1	2,07
Filings	1,78	2,6	—	2,1	—	2,4	—	—	—	—	—	—	—	(7)
After quenching	0,48	1,16	—	2,35	—	2,5	—	—	—	—	—	—	—	—
Size of the blocks, D. 10^{-6}														
After 80% deformation	3.0	2.8	3,4	3,1	4,0	5,35	3.7	3.0	4,3	2,35	3,8	7.7	3,7	4.0
Filings	2,42	2,4	—	—	—	2,17	—	2.2	2.0	—	—	—	—	—
After quenching	—	3.0	—	2,8	—	2,96	—	—	—	—	—	—	—	—

the second kind in unalloyed iron proved to be 0.68 x 10^{-3}. In the alloys Fe + 2.3% V and Fe + 1.84% Co after deformation to 80 per cent the displacements of the second kind were so small that they are virtually impossible to determine. In this case the broadening of the line is conditioned in the main by the small dimensions of the areas of coherent scattering.

In filings the displacements of the second kind were greater than in samples which were rolled to 80 per cent. Thus, for filings of unalloyed iron the quantity $\Delta a/a$ proved to be 1.8 x 10^{-3}, for the alloy Fe + 8% Cr 2.4 x 10^{-6}, in the alloy Fe + 4% Ni 2.6 x 10^{-3}.

After hardening the alloys by quenching the displacements of the second kind were in magnitude close to the value of $\Delta a/a$ obtained for filings (see Table 3).

(*c*) *Size of the blocks* (D)

Determination of the dimensions of the areas of

TABLE 4. Static displacements and characteristic temperature for alloys after different hardening treatments

Material	Unhardened state			After plastic deformation		After quenching	
	Annealing temperature, °C	Characteristic temperature Θ,°	$\sqrt{\overline{u^2_{cm}}}$, Å	Θ°,	$\sqrt{\overline{u^2_{cm}}}$, Å	Θ°,	$\sqrt{\overline{u^2_{cm}}}$, Å
Armco Fe	680	430	—	430	0,100	—	не обнаружены
Fe + 4,0% Ni	600	540	0,092	460	0,108	430	0,092
Fe + 3% Mn	610	630	0,091				
	750	470	0,070				
	800	430	0,065	430	0,111	430	0,065
Fe + 1,8% Mo	700	500	0,090	500	0,110	—	—
Fe + 0,5% Ti	800	440	0,073	440	0,073	—	—
Fe + 2,28% V	800	400	0,040	400	0,103	—	—
Fe + 1,84% Co	650	470	0,053	—	—	—	—
Fe + 0,8% Nb	800	570	0,121	—	—	—	—
Fe + 0,6% W	650	560	0,108	—	—	—	—
	750	540	0,096	-	—	—	—
	820	490	0,106	490	0,113	—	—
Fe + 6,0% Si	600	430	0,106	430	—	—	—

VOL. 5 1957

coherent scattering showed that as a result of cold plastic deformation (to 80 per cent) the size of these areas is for the majority of the solid solutions within the limits of 3 to 4 x 10^{-6} cm.

In filings the size of the blocks as a rule proved a little less than after deformation to 80 per cent.

(d) Displacements of the third kind

The study of the displacements of the third kind which arise as a result of cold plastic deformation (or martensite transformations) in solid solutions are considerably more complex than in pure metals. This, as investigation has shown, is conditioned not only by the presence of static displacements in the lattice of the annealed solid solution, caused by the atoms of the solute element, but also by changes in the bonds (dynamic defects) [32, 33]. The situation is complicated still further by the fact that for solid solutions the characteristic temperatures may change materially as a result of plastic deformation. Thus, the plastic deformation of solid solutions leads not only to a change in the static but also in the dynamic displacement of the atoms. This makes it necessary to take the photographs at two temperatures after each treatment of the alloy for the calculation of the changes in the dynamic displacement. The static displacement was determined by comparing the relative intensities of the diffraction maxima of the investigated samples with the relative intensities of the same lines for iron after the dynamic displacement had been eliminated [13, 17, 18].

Table 4 gives the results of the determination of the magnitudes of the static displacement of the atoms $\overline{u^2}_{cm}$ of the investigated alloys after different treatment. It also gives the data for the value of the characteristic temperature determined by means of photographs taken at two temperatures [13, 18]. After heating at a temperature above 600° the alloys were in the softened state. Therefore, the static displacement was conditioned only by the presence of "foreign" atoms in the lattice. The quantity $\overline{u^2}_{cm}$ did not, however, remain constant when the annealing temperature was changed, which was also observed for the magnitude of the characteristic temperature Θ. The reasons for this phenomenon are considered in a paper on the investigation of the bonds [35].

After plastic deformation the static displacement of the atoms increase. The increase in the quantity $\overline{u^2}_{cm}$ is, however, different for different alloys. Table 4 shows that they are the smaller the greater the quantity $\overline{u^2}_{cm}$ on account of the solute atoms in the annealed solid solution. After strong plastic deformation (filings) a value close to $\overline{u^2}_{cm}$ is obtained for various alloys and pure iron.

It should be noted that the hardening as a result of martensite transformation is not accompanied by an increase in the quantity $\overline{u^2}_{cm}$ which remains the

TABLE 5. Hardness Hv for alloys after different hardening treatments

Composition of the alloys	Hardness (Hv)		
	Equilibrium solid solution (after annealing at 850°C)	After 80% deformation	After quenching
Armco Fe	78	218	220
Fe+4% Ni	113	270	240
Fe+1.5% Mn . .	94	245	—
Fe+3.0% Mn . .	123.8	250	310
Fe+2.0% Cr . .	72	195	—
Fe+8.0% Cr . .	120	330	350
Fe+0.6% Mo . .	85	210	—
Fe+1.8% Mo . .	120	281	—
Fe+2.3% V . . .	73	172	—
Fe+1.8% Co . .	77	206	—
Fe+0.6% W . .	100	300	—
Fe 0.5% Ti .	68	203	—
Fe+0.8% Nb . .	101	260	—
Fe+6.0% Si . . .	186	340	—

same as for the non-hardened state (alloys with manganese and nickel) which was already observed in paper [12] for iron-chrome alloys.

In connexion with this it was interesting to study the question of the origin of the displacements of the third kind with hardening by quenching to martensite in a material in which in the non-hardened state static displacement is absent. Specially made experiments showed that under certain conditions pure iron can be quenched to martensite [34]. By measuring the intensities of the reflections it was established that the displacements of the third kind do not arise in this process, although hardening reaches the same magnitude as after cold deformation to 80 per cent.

(e) *Bonds in crystalline ferrite alloyed with various elements*

As has been observed before, the magnitude of the bonds in ferrite crystals alloyed with various elements was estimated by means of measuring the temperature factor of the intensity. The characteristic temperatures and the amplitudes of the thermal oscillations were determined.

Table 4 gives the values of the characteristic temperatures for ferrite alloyed with various elements [29]. After deformation or quenching the magnitude of the characteristic temperatures for the majority of the binary alloys of iron is close to the value of the characteristic temperature of unalloyed iron and equal to 430°. For the binary alloys Fe + 1.8% Mo and Fe + 0.6% W, Θ proved a little higher and for the binary alloy Fe + 2.3% V a little lower than for unalloyed iron.

(f) *Mechanical characteristics*

Of the mechanical properties the hardness Hv, the yield strength σ_s and the tensile strength σ_B are determined. The majority of the alloyed elements in solution in iron harden it. The greatest hardening was obtained in alloying ferrite with 6% Si and 0.6% W.

Some alloy elements decrease the hardness of ferrite a little in the state of equilibrium. This was observed for alloys of iron with 2.3% V and 0.5% Ti. The results of the measurements of the hardness of binary alloys of iron in the state of equilibrium (after annealing at 800 to 850°C) after cold plastic deformation to 80 per cent and after quenching are given in Table 5. As the data there given shows, one and the same degree of cold plastic deformation leads to different hardening in different alloys. The greatest hardening resulting from cold hardening was obtained in the alloys Fe + 6% Si, Fe + 0.6% W (hardness respectively 340 and 300 Hv).

The binary alloys Fe + 2.3% V, Fe + 0.5% Ti and Fe + 2% Cr are in the process of plastic deformation hardened less than unalloyed ferrite (172 Hv). The hardness of unalloyed ferrite after the same degree of deformation is 218 Hv.

After hardening by quenching the hardness of the binary alloys proved to be virtually of the same magnitude as after deformation to 80 per cent. An exception is the alloy Fe + 3% Mn the hardness of which after quenching became a little greater. (See Table 5).

TABLE 6. σ_S and σ_b for alloyed ferrite after annealing at 850°C, after 80% deformation and after quenching

Composition of the alloys	σ_S, kg/mm²			σ_S, kg/mm²		
	In equilibrium (after annealing at 850°C)	After 80% deformation	After quenching	In equilibrium	After deformation	After quenching
Armco Fe	15.0	65	—	31.0	65.0	—
Fe+4% Ni	24.0	78.0	76.0	41.0	78.0	76.0
Fe+1.5% Mn	22.0	86.0	—	—	88.0	—
Fe+3.0% Mn	26.0	86.0	86.0	49.0	86.0	90.0
Fe+2.0% Cr	21.5	62.0	—	32.0	68	—
Fe+8.0% Cr*	22.0	100	95	—	—	—
Fe+0.6% Mo	18.0	70	—	33.8	71.0	—
Fe+1.8% Mo	20.0	85	—	38	85	—
Fe+2.3% V	10.0	54.0	—	30.0	59.0	—
Fe+1.8% Co	18.4	78.0	—	30.0	77.0	—
Fe+0.6% W	22.5	90.0	—	37.0	90.0	—
Fe+0.5% Ti	17.0	54.0	—	30.0	59.0	—
Fe+0.8% Nb	12.0	74.0	—	43	80.0	—
Fe+6.0% Si	40.0	113.0	—	54	113.0	—

*) after annealing at 800°.
(this note refers to the alloy Fe + 8% Cr)

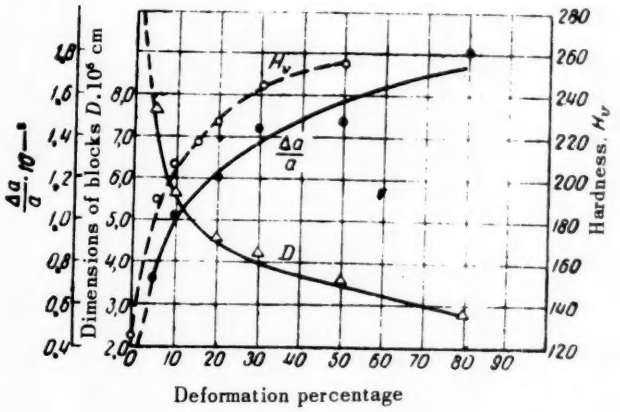

FIG. 2. Change of $\Delta a/a$, D and H_V as a function of the degree of cold deformation for the binary alloy Fe + 0.6% W.

The data for the magnitudes σ_S, σ_B for the investigated alloys after the different treatments are given in Table 6.

(g) *Effects of different degrees of deformation on the change of the characteristics of the microstructure and the mechanical properties*

The effects of different degrees of cold plastic deformation were studied for the binary alloys Fe + 0.6% W, Fe + 0.5% Ti, Fe + 3% Mn and unalloyed iron.

The binary alloy Fe + 0.6% W was subjected to deformation by rolling to 5, 10, 15, 20, 30, 50 and 80 per cent. The results of the experiments showed that the greatest hardening occurs at relatively low

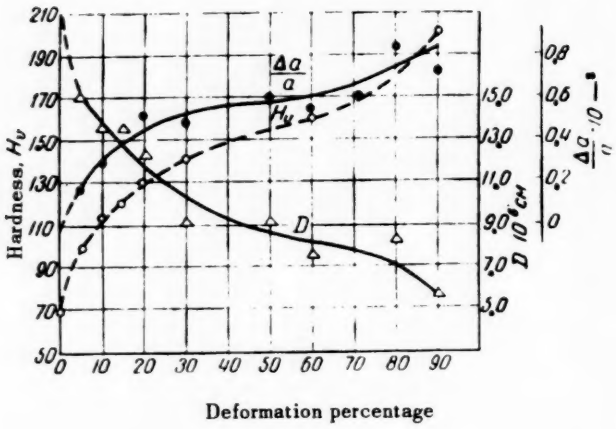

FIG. 3. Change of $\Delta a/a$, D and H_V as a function of the degree of deformation for the binary alloy Fe + 0.5% Ti.

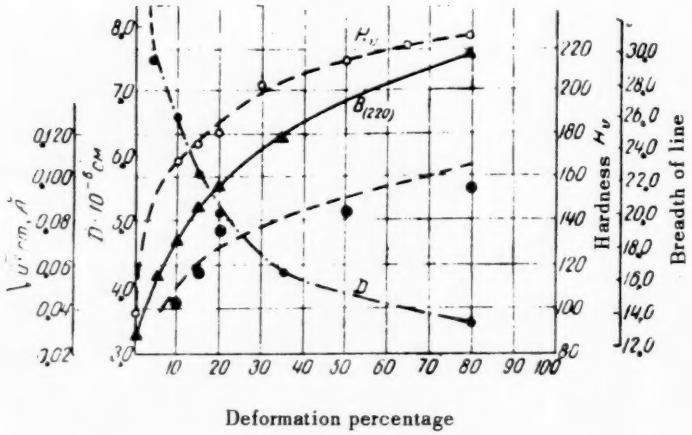

FIG. 4. Change of D, $\sqrt{u^2_{cm}}$ and H_V as a function of the degree of cold deformation for unalloyed iron.

degrees of deformation (up to 30 per cent). After this deformation the hardness increases from 110 to 240 H_V (Fig. 2). A further increase in the degree of cold plastic deformation causes an additional hardening of the alloy, but not as great as occurs at small degrees of deformation. Thus, the increase in the degree of deformation from 30 to 80 per cent increases the hardness from 240 to 300 H_V.

The study of the broadening of the diffraction lines is of considerable interest as a function of the degree of cold deformation. The differentiation between the broadening effects on the lines due to the smallness of the blocks and of displacements of the second kind made it possible to establish the nature of the changes of the microstructure. The results of the experiments showed that at relatively small degrees of deformation the blocks are greatly diminished. After deformation to 30 per cent the dimensions of the blocks reached a size of the order of 4×10^{-6} cm. A further increase in the

degree of deformation causes a comparatively smaller additional diminution of the blocks. A similar change with the degree of deformation is shown by the displacements of the second kind. As the degree of deformation increases, the displacements of the second kind increase parallel with the hardness.

For unalloyed iron the change in the displacements of the third kind were also investigated as a function of the degree of deformation (Fig. 4). It was established that when iron is deformed 10 per cent (when the greatest hardening occurs) the displacements of the third kind are small and amount to

$$\sqrt{u_{cm}^2} = 0.04 \text{ Å}$$

With the further increase in the degree of cold deformation the defects of the third kind increase and at 80 per cent deformation are

$$\sqrt{u_{cm}^2} = 0.09 \text{ Å}.*$$

DISCUSSION OF THE RESULTS

1. The experimental data obtained shows that the presence of solute elements in iron has a considerable effect both on the characteristics of the microcrystal structure, resulting from cold plastic deformation or martensite transformation, and on the magnitude of the hardening brought about by these processes. The presence of solute elements can substantially alter also the properties of iron in the state of equilibrium (annealed).

The yield strength of the annealed alloys investigated by us was in the range of from 10 kg/mm² for the alloy with 2.3% V to 26 kg/mm² for the alloy with 3% Mn, while the armco iron which served as the basis had a yield strength of 15 kg/mm². Only the alloy with 6 atomic per cent silicon distinguished itself sharply with a yield strength of 40 kg/mm². Much greater differences in the yield strength were found in the alloys after hardening. After 80 per cent cold deformation σ_s varies from 54 kg/mm² for the iron-vanadium alloy to 100 kg/mm² for the iron-chrome alloy (for the iron-silicon alloy it was 113 kg/mm².

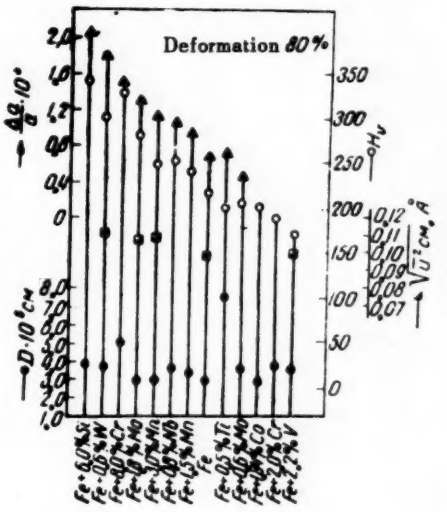

FIG. 5. $\Delta a/a$, D, $\sqrt{u_{cm}^2}$ and Hv for ferrite alloyed with various elements after plastic deformation to 80 per cent.

Thus the presence of solute elements has a particularly large effect on the hardenability of iron. Tables 5 and 6 show that for annealed alloys the presence of alloy elements has a considerably greater effect on the hardness than on the yield strength. This is explained by the fact that the hardness depends on the yield strength and on the coefficient of hardening, and, hence, characterizes not only the initial state.

2. The difference in the properties of the investigated alloys and the considerable difference in the magnitude of the tensile strength of the alloys in the hardened states makes it possible to draw certain conclusions on the laws of the changes of the microcrystal structure and the hardness characteristics, which occur as the result of the hardening of metals.

First of all it should be noted that there is a definite link between the magnitude of the displacements of the second kind of alloys in the hardened state and the characteristics of resistance to deformation (Fig. 5, Table 3, 5, 6). For 80 per cent deformation the greatest magnitude of the hardness and yield strength is possessed by the alloy with 6 atomic per cent of silicon (Hv = 340, σ_s = 113kg/mm². For the same alloy the largest value for $\Delta a/a$ was obtained: 2.1 x 10^{-4}. The alloy with 2.3% V shows the least resistance to deformation (Hv = 172, σ_s = 54 kg/mm²). The displacements of the

* The displacements of the third kind as a function of the degree of deformation was determined on bulk samples in iron and cobalt radiation; the intensities of lines (110) and (220) were compared. For absolute magnitude the values obtained cannot be compared with the magnitudes of the displacements of the third kind obtained with molybdenum radiation [30, 31].

VOL. 5 1957

second kind here proved to be small and could not be reliably measured ($\Delta a/a < 0.4 \times 10^{-3}$). Alloys which (after deformation to 80 per cent) had a greater hardness than that of iron also showed a greater magnitude of the displacements of the second kind $\Delta a/a$, that is more than 0.7×10^{-3}. For alloys with smaller hardness than iron the quantity $\Delta a/a$ as a rule was of small magnitude.

The parallel course of the change in hardness and the magnitude $\Delta a/a$ occurs also when the degree of plastic deformation is increased. Usually at deformations of more than 30 per cent the increase in hardness with the increase in the degree of deformation is greatly slowed down, which is also observed for the magnitude $\Delta a/a$. A new increase in the hardness and the displacements of the second kind is observed at deformations higher than 70 to 80 per cent.

The hardening of metals, both by cold plastic deformation and as a result of martensite transformation is always accompanied by a great diminution of the areas of coherent scattering (the blocks). With that the size of the blocks for all alloys in the hardened state varies usually between 2 and 4×10^{-6} cm. A higher value was obtained for the alloy of iron with titanium (7.5×10^{-6} cm).

In the process of plastic deformation, a considerable diminution of the blocks occurs even at small deformations. After deformation to 5 per cent the size of the blocks becomes 10×10^{-6} cm. As the degree of deformation increases the decrease in the size of the blocks proceeds more and more slowly and at deformations over 30 per cent becomes slight. The same feature is shown by the growth of the displacements of the third kind when the degree of deformation is increased.

In the discussion of the role of various features of the microcrystal structure in hardened metals one must take into account the following facts. When the resistance of an alloy in the hardened state to deformation is very different from that for pure iron the main difference in the microstructure is not the size of the blocks but the size of the displacements of the second kind; for instance, for the alloys iron-silicon, iron-tungsten and iron-chrome, where the resistance to deformation has the highest magnitude, the size of the blocks is not only not less than in iron, but even a little greater. The greater broadening of the lines for these alloys is determined by the greater magnitude of the displacements of the second kind. In alloys with 8% Cr the size of the blocks is considerably greater than in iron, although the alloy has a greater hardness than iron.

In the case of hardening by quenching we obtain blocks of a size close to that of the deformed alloys. The very great deformation in filing usually produces a greater broadening of the lines than the 80 per cent deformation. The blocks here are of a slightly smaller size, in the main, however, the increase in the broadening of the diffraction lines is due to the increase in the quantity $\Delta a/a$. Particularly pronounced is the dependence of the displacements of the second kind on the presence of solute elements in tempered steel, as is well known. The quantity $\Delta a/a$ increases rapidly with the increase in the carbon concentration in martensite. Already at 0.1% C it increase several times over that of pure iron [37] and becomes very big for martensite with 1% C, reaching 8×10^{-3} [6, 8]. At the same time the blocks for martensite with 1% C are of a size of about 2.5×10^{-6} cm, that is their size differs little from that of the blocks in quenched pure iron. The hardness characteristics of tempered steel, as is well known, change greatly with increased carbon content. Thus, the available data shows that great changes in the hardness of hardened states correspond to great changes in the quantity $\Delta a/a$. The size of the blocks however, remains at the same level.

3. Now let us see how the hardness characteristics are linked with the displacements of the third kind. We have noted that the quantity $\overline{u^2}_{cm}$ increases with the increase in the degree of deformation. However, the size of the displacements of the third kind which occur in plastic deformation depends on the magnitude of the static displacements of the lattice of the annealed alloy, which is conditioned by the presence in the lattice of the atoms of the solute elements.

Table 4 shows that $\overline{u^2}_{cm}$ after deformation increases most in pure iron in which before the deformation it was zero. For alloys in which before the deformation $\overline{u^2}_{cm}$ is already of a considerable size on account of the presence of solute atoms, the increase in $\overline{u^2}_{cm}$ on account of the deformation is considerably less. Table 4 shows that this increase is the smaller the greater the static displacements of the lattice on account of the solute atoms in the annealed solid solution.

Attention is attracted by the fact that for a considerable deformation the total magnitude $\overline{u^2}_{cm}$, including both the displacements of account of the foreign atoms and the displacements which arise as a result of plastic deformation has for all alloys a similar value which does not differ much from $\overline{u^2}_{cm}$ for pure iron. An exception is the alloy with titanium in which the magnitude of $\overline{u^2}_{cm}$ did not change as a result of plastic deformation and remained considerably smaller than that for iron.

VOL 5 195

Most important is the fact that with hardening by means of quenching the magnitude of $\overline{u^2}_{cm}$ for solid solutions remains the same as for annealed alloys, and for pure iron is virtually zero. (Table 4). From that it follows that with hardening which occurs as a result of martensite transformation displacements of the third kind do not arise. Hardening here reaches approximately the same magnitude as with plastic deformation.

These facts allow us to conclude that the presence of displacements of the third kind (of a size which is observed in the measurement of the intensities of X-ray diffractions) is not necessary for the raising of the resistance to plastic deformation.

4. Thus, after scrutinizing the details of the microcrystal structure of metals and alloys in the hardened state, only the magnitude $\Delta a/a$ can be related to the hardness of the alloy in that state. Can one conclude from this that the displacements of the second kind are the main structure factor which determines the hardness of metals, and their magnitude the main factor which determines the magnitude of the resistance to deformation ? This conclusion is not justified.

To understand the role of the details of the microstructure in hardening, that is, in the increase in the resistance to plastic deformation. It is important to know the mechanism of the plastic deformation of metals. [36]. Existing experimental data has led to the following conceptions of the process of plastic deformation.

The gliding along crystallographic planes is represented as occurring not by simultaneous displacement of individual atomic layers but as a result of individual acts consisting in displacements of the same type of a group of atoms, which spread along certain directions in the lattice. Irrespective of the detailed conceptions of the nature and mechanism of such displacements of atoms the chief thing for this mechanism is that owing to the periodicity of the structure of crystals a relative displacement of atoms near one of the nodes of the lattice under the action of external forces makes it easier for similar displacements of atoms to occur near the neighbouring nodes. Such a consecutive process of the displacement of atoms, beginning in one place, can spread in certain directions for a great distance so long as the correct periodicity is preserved (e.g. the movement of dislocations). The process stops as soon as disturbances of the regular structure are met with block boundaries, displacements of the third kind, etc.). At any given moment of this consecutive displacement of atoms only the bonds of the shifting atom with its neighbours will take part in the resistance to deformation. Thus, only a small number of atoms will in plastic deformation take part simultaneously in the resistance to deformation. The places of disturbance of the regular crystal structure are the places where the acts of plastic deformation originate, but these same places are at the same time the areas where the spread of individual acts can stop.

The fewer such places there are, the smaller the number of elementary acts originating in the unit of time and the longer the path of their easy spread, the less the proportion of atoms which take part simultaneously in the resistance to deformation. On the contrary, the greater the number of disturbances, the greater are the number of acts originating in the unit of time and the shorter the path of their spread, the fewer the number of atoms which take part in each act, and the greater the number of atoms which take part in the resistance to the external forces.

This conception makes it possible to understand the small hardness of metals and alloys in the annealed state compared with the theoretical hardness calculated from the data on the strength of the interatomic bonds. Owing to the great size of the regions with the regular crystal structure the degree of simultaneity of the participation of the atoms in the resistance to deformation and, hence, the degree of utilization of the interatomic bonds, is small.

The submicroscopic inhomogeneity of the crystal structure which characterizes all hardened states conditions the heightenening of the degree of simultaneity of the work of the atoms and, hence, the heightened degree of the utilization of the interatomic bonds and the approximation to the theoretical hardness.

Disturbances of the regular periodicity of the crystal structure of the grains on account of the diminution of the mosaic blocks must from the standpoint described lead to an increase in the resistance to deformation. At the blocks boundaries elementary acts of plastic deformation can originate and their spread can be stopped. In this the degree of disorientation of the blocks must evidently play a part.

The diminution of the blocks can be regarded as one of the main crystallographic factors in the hardening of one or another metal or alloy as a necessary condition of hardening. The absolute magnitude of the attainable resistance to deformation depends, however, not only on the degree of diminution of the blocks. We have seen that the difference in the size of the blocks for different alloys in the hardened state is not great, yet their hardness characteristics may differ considerably. At the same time the displacements of the second kind also differ

VOL. 5 1957

greatly.

The magnitude $\Delta a/a$ characterizes the size of the inhomogeneous elastic deformation of the microregions of the alloy. In the case of hardening as a result of martensite transformation such elastically deformed regions are the little crystals (disks) of martensite. In plastic deformation these are possibly the elastically bent (glide disks. One may think that the difference in the magnitude of $\Delta a/a$ for the various alloys we have investigated is determined by the properties of the crystals of the solid solutions and in the first place by the elasticity of the microregions. From this standpoint the magnitude of $\Delta a/a$ observed for the state of hardening to "saturation" characterizes the elasticity of the microregions of the given metal or solid solution. For instance, in iron this is about 1.0×10^{-3}; for a solid solution of 0.1 per cent carbon in iron it already reaches a magnitude close to 3×10^{-3} and for martensite with 1.0 per cent carbon it reaches 8×10^{-3}. Greater values are not obtained for the given material because the little crystals of the solid solution of the given composition do not withstand greater stresses.

Starting from these conceptions the link between the hardness characteristics and the quantity $\Delta a/a$ can be explained in two ways.

One may suppose that the presence of great strains of the second kind (elastic deformation of the microregions) in itself is not the factor which conditions high resistance to deformation. The great magnitude of $\Delta a/a$ merely indicates the need for applying a greater mean stress to cause the emergence and spread of acts of plastic deformation in the lattice of the crystals of the given material. This can happen either on account of increased bonds or on account of a lowering of the average height of the peaks of stress or of a shortening of the duration of the acts. In that case, with one and the same size of the blocks, the resistance of the sample to deformation will be the greater the greater $\Delta a/a$.

From this point of view great hardness would be obtained also if by some means we could reduce the size of the blocks to a magnitude of 2 to 4×10^{-6} cm without at the same time creating elastic deformations in the microregions (bending of the glide disks or bends of the martensite disks).

One can also make another suggestion according to which not only the ability of the material to strongly resist plastic deformation in the microregions, but the very existence of a high elastic deformation in the glide disks or martensite crystals is important for the great hardness of the material. This can be so if the existence of microstrains leads to an increase in the degree of disturbance of the regularity of the crystal structure in the glide disks or martensite crystals. Such an increase in the magnitude and number of the disturbances is quite possible if one bears in mind that the elastic deformation of the microregions (the disks) consists of a large number of blocks. The thickness of the microregions is of the order of 10^{-4} cm, and that of the blocks 10^{-6}. In the elastic deformation of these regions an increase in the degree of disorientation of the blocks (a turning of the blocks is possible.) This should lead to an increase in the number of the incipient acts of plastic deformation and to a shortening of the paths of their spread, and consequently to a greater degree of simultaneity of the participation of the atoms in the resistance to the action of the external forces and a greater degree of utilization of the interatomic bonds.

In what measure the suggested conceptions on the role of the displacements of the second kind reflect the true state of affairs cannot be decided without further experiments.

5. We have so far discussed the question of the link between the defects of the second order with the hardness characteristics in the transition from one solid solution to the other. Both the resistance to deformation and the quantity $\Delta a/a$ change, however, more strongly when the degree of deformation is increased. The curves in Figs. 2, 3 and 4 show that the hardness and the magnitude $\Delta a/a$ change in the same way when the degree of deformation is increased.

Of the same description (first steep, then slower) is the change in the size of the blocks. Therefore, from the point of view expressed above, the conceptions on the nature of hardening, of the increase in the resistance to deformation in the process of plastic deformation, can first of all be attributed to the reduction of the blocks. The rapid increase in the magnitude of $\Delta a/a$ with the increase in the degree of deformation can be explained by the increase in the number of elastically deformed regions and the magnitude of the elastic deformation. With further plastic deformation the limit of elastic deformation for the given material is reached in certain microregions, the number of these regions increases all the time and reaches "saturation". The quantity $\Delta a/a$ which is measured in this process characterizes the properties of the crystals in the microregions. What magnitude of hardness is attained is from this point of view determined not by the existence of elastic deformations but by the properties of the crystals of the given material themselves the characteristic for which is the observed magnitude

VOL 5 195

of $\Delta a/a$. It is possible, however, as we have said above, that the existence of elastic deformations leads to an increase in the disorientation of the blocks and in this way makes its contribution to the hardening of metals.

In the curves of the hardness characteristics and the microstructure as functions of the degree of plastic deformation, after "saturation" at over 70 to 80 per cent deformation a further increase in the hardness is observed and a corresponding change in the characteristics of the microstructure, a further reduction of the blocks and increase in $\Delta a/a$, $\overline{u^2}_{cm}$. If the hardening of alloys is in the main attributed to the reduction of the blocks, one may think that under these conditions the increase in the "limit" of elastic deformation of the microregions is also due to this further diminution for the occurrence of special conditions are necessary.

We have seen that for all the alloys investigated and for tempered steels the limiting size of the diminution of the blocks is of the order of 2 to 4 x 10^{-6} cm, and that the further reduction of the blocks almost comes to a stop, although the plastic deformation continues. It is possible that we have here a case of a state of equilibrium at the given temperature and pressure, that is, that blocks of a smaller size become unstable and their dimensions are restored. In that case one can suggest that the limit of the blocks size for the given material must depend on the temperature and pressure at which the deformation occurs. A change in the conditions of deformation in a direction in which the size of the blocks can decrease should lead to an increase in hardening.

6. We have come to the conclusion that the quantity $\Delta a/a$ which corresponds to the plastic deformation at which the hardness characteristics and the microstructure already change little with the increase in the degree of deformation characterizes the elasticity of the crystals of the given material in the microregions, that is the elasticity of the glide disks or martensite crystals. It should be noted that the calculations from the quantities $\Delta a/a$ of the elasticity ($\sigma_s = E\Delta a/a$, where E is the Young's modulus) give a value close to the yield strength of the initial annealed material. This correspondence has already been noted for pure metals. [1]. The data given in Fig. 6 shows that this correspondence also holds for solid solutions. Comparison of the yield strength of the samples of hardened material (80 per cent deformation) with the elasticity in the microregions shows that as a rule the former is 3 to 3.5 time higher. Since the modulus of elasticity of plastically deformed metal is not higher

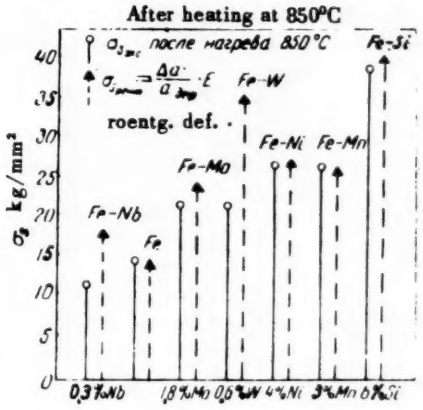

FIG. 6. σ_s for ferrite alloyed with various elements, calculated from X-ray data and from the results of the mechanical tests.

than the modulus of the annealed metal, this means that the elasticity of the whole sample (microvolume) is 3 to 3.5 times higher than the "limit" of elastic deformation in the microregions. Consequently, at stresses corresponding to the yield strength of the hardened material the mean interatomic distance in the direction of the applied force should change 3 to 3.5 times more than the limit of its change in the microregions before the application of the external force.

7. The magnitude of the yield strength of annealed iron and the corresponding magnitude $\Delta a/a$ of the limit of elastic deformation in the microregions, as we have seen, changes with the introduction into the iron of various alloy elements. One of the reasons for the raising of the yield strength can be the existence of static defects of the lattice caused by the presence of foreign atoms in the lattice. The elasticity in the microregions should then increase with the increase in the number of displaced atoms, since this is observed in the case of martensite crystals with varying carbon content.

The study of the data obtained in the present work on the action of different solute elements shows however, that the quantity $\overline{u^2}_{cm}$ is in no way a measure of the elasticity in the microregions. First of all, the presence in the solution of Ti and V, despite the presence of definite static lattice deformations, causes a lowering both of the yield strength and the elasticity in the microregions. It is, however, possible that the refining action of these elements plays a part here, leading to a lower-

VOL. 5 1957

ing of the quantity of solute gases and other admixtures. This conclusion can be confirmed by using much purer metals for the investigation then we had at our disposal for the present investigation.

Undoubtedly, besides the static lattice displacements the changes in the strength and nature of the interatomic bonds should also play a considerable part. Unfortunately, data on the change in the nature of the bonds are not available. Concerning the strength of the bonds, as we have seen, the measurements of the characteristic temperature of solid solutions indicates that in the ease of the deformed state their change is small.

Serious attention should be given to the fact that the characteristic temperature measured by X-ray photography for the deformed solid solutions differs considerably from that for the ones that were annealed at certain temperatures. This difference, as has already been pointed out earlier [32, 33], can be put down as due to the changes in the distributions of the solute elements in the lattice of the solid solution, that is, due to changes of the sequence in the distribution of the atoms. Thus, this fact indicates a disturbance of the sequence in the process of plastic deformation. That means that in the process of plastic deformation the displacement of the atoms occurs throughout the volume of the metal and not only along the boundaries of the glide disks or blocks.

CONCLUSIONS

The link between the microcrystal structure of solid solutions on the basis of α-iron in the hardened state and certain mechanical properties of these alloys was investigated. The hardening of the alloys was obtained by means of cold plastic deformation and as a result of the martensite mechanism of the $\gamma \rightarrow \alpha$ transformation.

To measure the properties of the crystals of α-iron in the micro-and submicroregions (the properties of the crystal lattice of the α solid solution) the iron was alloyed with various elements (Si, Ti, V, Cr, Mn, Co, Ni, Nb, Mo, W).

With the help of X-ray structure methods the following properties of the crystals of the phase in the submicroregions were determined:

(a) the static lattice displacements static displacements of atoms) caused by the presence of foreign atoms in the lattice;

(b) the dynamic displacements of the atoms with thermal oscillations and the characteristic temperature;

(c) the magnitude of the elastic deformation of the lattice caused by cold plastic deformation ($\Delta a/a$).

The following served as the characteristics of the microcrystal structure of the alloys in the hardened state: the size of the areas of coherent scattering of X-rays (the mosaic blocks, the displacements of the second kind (inhomogeneous microstrains) and the displacements of the third kind (the means squared static displacements of the atoms caused either by plastic deformation of phase transformation). The mechanical properties of the microvolumes were characterized by the hardness, the yield strength and the tensile strength.

The investigation led to the following results:

1. Characteristic for the alloys in the hardened state attained by means of cold deformation to a high degree or as a result of $\gamma \rightarrow \alpha$ martensite transformations is the small size of the areas of coherent scattering of X-rays. The size of these areas for almost all the alloys investigated is between 200 and 400 Å. The observable difference in the size of the blocks is close to the limits of the error of measurement. Yet the hardness characteristics change within very wide limits in going from alloy to alloy (H_V from 172 to 340; σ_s from 54 to 113 kg/mm²). Thus, the great difference in the resistance to deformation of the various alloys in the hardened state cannot be ascribed to the changes in the size of the blocks.

2. The presence of different elements in the solid solution has a large effect on the magnitude of the displacements of the second kind (inhomogeneous microstrains) both in the deformed and the annealed alloys. There is in this case a correspondence between the magnitude of the displacements of the second order and the hardness characteristics of the alloys in the hardened states.

3. As a result of plastic deformation to high degrees considerable displacements of the third kind occur. In the solid solutions investigated considerable static displacements of atoms take place in the alloys in the annealed state, which is conditioned by the presence in the lattice of the atoms of the solute elements; the magnitude

$$\sqrt{\overline{u^2_{cm}}}$$

varied from 0.058 to 0.120 Å. After cold deformation to a high degree (filings) the magnitude of

$$\sqrt{\overline{u^2_{cm}}}$$

rose approximately to one and the same level

(about 0.100 to 0.120) close to the level of the displacements of the third kind in cold deformed unalloyed iron. The greater the magnitude of

$$\sqrt{\overline{u^2}}_{cm}$$

for the "equilibrium" solid solution, the less this magnitude changed as a result of deformation.

4. After the quenching of alloyed iron to martensite the magnitude of the static displacements of the atoms did not increase. Thus, in alloys hardened by means of martensite transformation displacements of the third kind do not occur although the hardness characteristics are close to those of the cold deformed materials. This was particularly clearly seen in samples of pure iron quenched to martensite. Displacements of the third kind were not observed here, but the hardening, the size of the blocks and the displacements of the second kind were at the same level as in the case of cold deformed iron. Hence, the presence of displacements of the third kind, at all events of a size which can be observed with the usual intensity measurements of X-rays, is not necessary for the high resistance of the material to deformation.

5. Investigations of the microcrystal structure as a function of the degree of plastic deformation made on pure iron and certain solid solutions showed that with increasing degree of deformation the hardness, the displacements of the second and of the third kind increase, but the size of the blocks decreases. With that these characteristics change most rapidly at low degrees of deformation; in the region of 30 to 70 per cent deformation they change slowly. At higher degrees of deformation the rate of change of the characteristics once more increases. The behaviour of metals at very high degrees of deformation requires more detailed investigation.

6. The results obtained make it possible to conclude that the diminution of the areas of coherent scattering are a necessary condition for raising the resistance of metals to deformation (with the "gliding" mechanism of plastic deformation). The difference in the absolute magnitudes of the elastic characteristics for different metals and solid solutions is, however, conditioned not by the change in the size of these areas, but mainly by the difference in the properties of the crystals in the micro – and submicroregions (the nature and strength of the bonds, the static displacements and other disturbances of the regular periodicity of the lattice). The correspondence between the resistance to deformation and the magnitude of the displacements of the second kind which has been established in this paper should probably not be regarded as an indication of the great role of these defects for hardening. It may be thought that the magnitude of these defects (inhomogeneous elastic deformations of the microregions) are themselves conditioned by the properties of the small crystals of the given material. From this point of view the magnitude of the displacements of the second kind serves to gauge the elasticity of the microregions and may be regarded as a definite characteristic of the properties of the small crystals of the given substance. It is also possible that the observed displacements of the second kind in themselves have an effect on the resistance to deformation by causing an increase in the degree of disorientation of the blocks.

The experimental data obtained in the present paper on the connexion between the microstructure and the hardness of a material makes it possible to establish certain regularities of these phenomena and raises a number of new questions which it is important to clear up by further experiments for the understanding of the nature of hardness and hardening of metals and alloys.

Translated by B. Ruhemann

REFERENCES

1. H.D. Megaw and A.R. Stokes, *J. Inst. Metals* 71, 6, (1945).
2. W.A. Wood and W.A. Recninger, *J. Inst. Metals*, 16, 7, 571, (1949).
3. P.Gay and A. Kelly, *Acta Cryst.*, 50, 165, (1953).
4. B.M. Rovinskii, and L.M. Rybakov, *Izv. Akad. Nauk. SSSR, otd. tekh. nauk.* 10, (1952).
5. G.K. Williamson and R.E. Smalman, *Acta. Met.*, 7, 574, (1954).
6. G.V. Kurdyumov and L.I. Lysak, *Zh. tekh. fiz.*, 17, 9, 933, (1947).
7. R.A.J. Smith, *Iron and Steel*, 147-151, (1953).
8. M.P. Arbuzov, L.I. Lysak and E.G. Nesterenko, *Dokl. Akad. Nauk SSSR*, 90, 3, 375-377, (1953).
9. L.S. Moroz, *Zh. tekh. fiz.*, 24, 705, (1954).
10. G.V. Kurdyumov, *Zh. tekh. fiz.*, 24, 1254, (1954).
11. G.W. Brindley, *Proc. Phys. Soc.* Lond. 52, 117, (1940).
12. L.S. Moroz and T.E. Mingin, *Dokl. Akad. Nauk SSSR*, 93, 249, (1953).
13. V.A. Ilyina, V.K. Kritskaia and G.V. Kurdyumov, *(Problems of metallography and physics of metals)*, Metallurgizdat 2 Symposium 222, (1951).

VOL. 5 1957

14. V.I. Iveronova, *Trud. Inst. Krystallographic Akad. Nauk, SSSR.*, 10, 149, (1954).
15. V.A. Ilyina, E.Z. Kaminskii, V.K. Kritskaia and P.I. Entin, *Problems of metallography and physics of metals* 3, Symposium., 178, (1952).
16. V.I. Iveronova, A.A. Katznelson, *Dokl. Akad. Nauk. SSSR.*, 99, No. 3, (1954).
17. G.V. Kurdyumov, V.A. Ilyina, V.K. Kritskaia and L.I. Lysak, *Izv. Akad. Nauk SSSR., physical series*, 17, 297, (1953).
18. V.K. Kritskaia, G.V. Kudyumov and N.M. Nodia, *Zh. tekh. fiz.*, 2, (1955).
19. M.M. Shteinberg, *Steel*, 12, 1107, (1947).
20. M.M. Shteinberg, *Steel*, 9, 812, (1948).
21. G.R. Austin, *Trans. Amer. Soc. Metals.* 31, 321, (1943).
22. G.R. Austin, L.A. Luini and R.W. Lindsay, *Trans. Amer. Soc. Metals*, 35, 446, (1945).
23. A.P. Gulyayev and V.P. Emelina, *Steel*, 12, 1101, (1948).
24. A.P. Gulyayev and E.F. Turusova, *Zh. tekh. fiz.*, 20, 66, (1950).
25. A.P. Gulyayev and V.P. Emelina, *Steel*, 2, 139, (1947).
26. F.M. Jones, *Proc. Roy. Soc.*, 16, 166, (1938).
27. L.I. Lysak, *Problems of the physics of metals and metallography Akad. Nauk. Ukr. SS.R.* 45, (1954).
28. I.M. Roitman and Ya. B. Fridman, *The micromechanical method of testing metals*, (1950).
29. V.A. Ilyina, V.K. Kritskaia, G.V. Kurdyumov, and T.I. Stelletskaia, *Izv. Akad. Nauk. SSSR. physical series*, 20, 7, 723, (1956).
30. V.A. Ilyina and V.K. Kritskaia, *Dokl. Akad. Nauk, SSSR.*, 110, No. 5, (1946).
31. A. Kakhanovskaia, *Czechoslovak Physical Journal*, 4, 471, (1954).
32. V.K. Kritskaia, G.V. Kurdyumov and T.V. Stelletskaia, *Dokl. Akad. Nauk. SSSR*, 98, 63, (1954).
33. V.K. Kritskaia, G.V. Kurdyumov and L.I. Tikhonov, *Dokl. Akad. Nauk SSSR*, 102, 2, (1955).
34. G.V. Kurdyumov and M.D. Perkas, *Dokl. Akad. Nauk. SSSR.* 111, No. 4, (1956).
35. V.A. Ilyina, V.K. Kritskaia, G.V. Kurdyumov, Yu. A. Ocipyan and T.I. Stelletskaia, *Fiz. metal. metalloved.*, 4, No. 3. (1957).
36. M.V. Yakutovich, *Trud. Inst. Fiz. metal. Ural. fil. Akad. Nauk SSSR.*, 121, (1949).
37. G.V. Kurdyumov, M.D. Perkas and A.E. Shamov, *(Problems of Metallography and physics of metals)*, Metallurgizdat. 4, Symposium. (1955).
38. V.A. Ilyina and V.K. Kritskaia, *(Problems of metallography and physics of metals)*, Metallurgizdat., 4 Symposium., p. 412, (1955).

VOL
5
195

CALCULATION OF DIAGRAMS OF TRUE STRESSES OF A COLD-HARDENED METAL *

G.P. ZAITSEV

Western Siberian Branch Academy of Sciences U.S.S.R.

(Received 26 March 1956 – after shortening, 20 July 1956)

In this work is shown a method of constructing diagrams of small true stresses in cold – or work-hardened metal if its diagram in a non-work-hardened state and the extent of deformation suffered through cold-working are known.

VOL. 5 1957

1. The strength as determined by the mechanical properties of a work-hardened metal is associated, as known, only with the extent of cold deformation, and depends hardly at all on its specifically stressed condition. This makes it possible, from the true stress diagrams of an unhardened metal and the extent of cold plastic deformation, to construct the true stress diagrams of the same metal in a work-hardened condition.

A certain amount of plastic deformation may be imparted to a non-work-hardened metal during tensile testing as measured by the extent of elongation e_{xo} or from compression in a transverse section q_{xo}. The index (subscript) O here means the unhardened state.

It is possible to obtain precisely this form of deformation, and to divide it into two independent parts, of which one is associated with previous plastic deformation e_{pr} or q_{pr}, and the other with tensile deformation e_x or q_x by testing a previously deformed metal.

In accordance with the laws of addition of independent deformations, as expressed by elongations and compressions in a series of basic values [1] (we have):

$$e_{xo} = e_{pr} + e_x + e_{pr}e_x,$$
$$q_{xo} = q_{pr} + q_x - q_{pr}q_x, \qquad (1)$$

whence

$$e_x = \frac{e_{xo} - e_{pr}}{1 + e_{pr}},$$
$$q_x = \frac{q_{xo} - q_{pr}}{1 - q_{pr}}, \qquad (2)$$

If the given curve of true stresses $s - e$ of an unhardened metal is given, and we have thereon the the point X with co-ordinates e_{xo} and s_x, then on the curve of true stresses for the same metal in a work-hardened state the point X_1, corresponding to the same condition of hardness as also at point X, we shall have the co-ordinates $e_x - s_x$, wherein e_x is calculated from formula (1). The position is entirely similar also in using curves with co-ordinates $s - q$, only in calculating q_x formula (2) is used.

From formulae (1) and (2) it follows that, in strain hardening, with less uniform deformation of the metal under extension, i.e. with $e_{pr} < \delta_r$ and $q_{pr} < \psi_r$, the point X_1 will be placed more to the right of the ordinate axis. If $e_{pr} > \delta_r$ and $q_{pr} > \psi_r$ then the point X_1 is moved more to the left of the ordinate axis in the region of negative abscissae values. Here and subsequently the symbols for elongation and compression e and q will be represented respectively by δ and ψ.

On true stress diagrams of work-hardened metals the parts of the curves disposed more to the left of the ordinates axis give some idea of the plastic prehistory of the metal. The parts disposed more to the right of this axis show the behaviour of the hardened metal under test for extension (tensile test).

The true stress diagrams may be calculated from formulae (1) and (2) or even constructed by a purely graphic method.

For a graphic solution of the problem posed (Fig. 1), in the $s - e$ co-ordinate system, there must be drawn at first the supplementary straight line DK above the abscissae axis and spaced therefrom by a distance e_{pr}, and also there must be inserted at a supplementary origin O_1 at the left lower corner of the diagram at a distance from its abscissae axis equal to unity. Let there be the point X on the deformation curve of an unhardened metal.

By projecting this on the line DK and joining

* *Fiz. metal metalloved.*, 5, No. 3, 484-492, 1957.

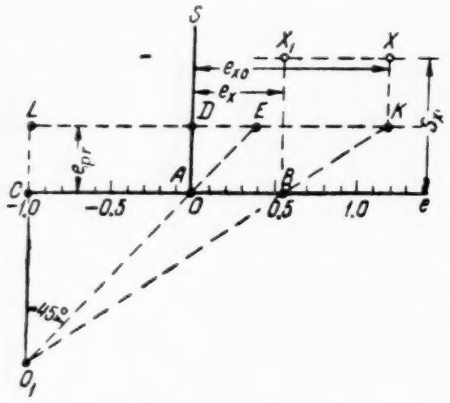

FIG. 1. Graphic method of constructing true stress curves of a work-hardened metal on the $s - e$ co-ordinates system.

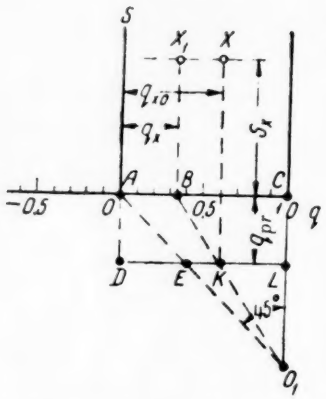

FIG. 2. Graphic method of constructing true stress curves of a work-hardened metal on the $s - q$ co-ordinates system.

points K and O_1 we find the point B. The interval (section) AB will also be abscissa for point X_1. Actually, from geometrical considerations we have:

$$\frac{BA}{AC} = \frac{KE}{EL} \quad \text{and} \quad \frac{BA}{AC} = \frac{DK - DE}{LD + DE}.$$

since

$$AC = LD = 1, \; DE = DO = e_{pr} \text{ and } DK = e_{x0},$$

we find that

$$BA = \frac{e_{x0} - e_{pr}}{1 + e_{pr}} = e_x.$$

To solve the problem in the system of co-ordinates $s - q$ it is necessary to extend the line DL (Fig. 2) below the abscissae axis to a distance therefrom of q_{pr}, and fix the pole O_1 in the lower right-hand corner of the diagram at a distance from the abscissae axis equal to unity.

We project on the line DL the point X lying on the curve $s - q$ of an unhardened metal, and thus obtain the point K which we connect to pole O_1. The line KO_1 intercepts on the abscissae axis the section AB equal to the abscissa of point X_1 of the diagram of an unhardened metal. From Fig. 2 it follows that

$$\frac{AB}{AC} = \frac{EK}{EL} = \frac{DK - DE}{DL - DE}.$$

Since

$$AC = DL = 1, \; ED = DO = q_{pr}, \; DK = q_{x0},$$

we have

$$AB = \frac{q_{x0} - q_{pr}}{1 - q_{pr}} = q_x.$$

Application of the rules just established for constructing diagrams of work-hardened metals is shown in Figs. 3 and 4, in an especially interesting case where the preliminary deformation, exceed its uniform elongation during work-hardening of the metal, i.e. $e_{pr} > \delta_{r0}$ and $q_{pr} > \psi_{r0}$. In this case the true breaking-down point s_b lies more to the left of the ordinates axis.

The co-ordinates of the point s_b on diagrams of a cold-hardened metal are

$$\delta_r = \frac{\delta_{r0} - e_{pr}}{1 + e_{pr}}, \quad \psi_r = \frac{\psi_{r0} - q_{pr}}{1 - q_{pr}}, \quad s = s_b.$$

The abscissae of points on diagrams of unhardened metal, the ordinates of which after cold-hardening will equal the yield point of a cold-hardened metal σ_s, are easily calculated from formulae (1) and (2), with $e_x = 0$ and $q_x = 0$. The abscissae in question equal

$$e_{x0} = e_{pr} \text{ and } q_{x0} = q_{pr}.$$

From geometrical considerations it follows that

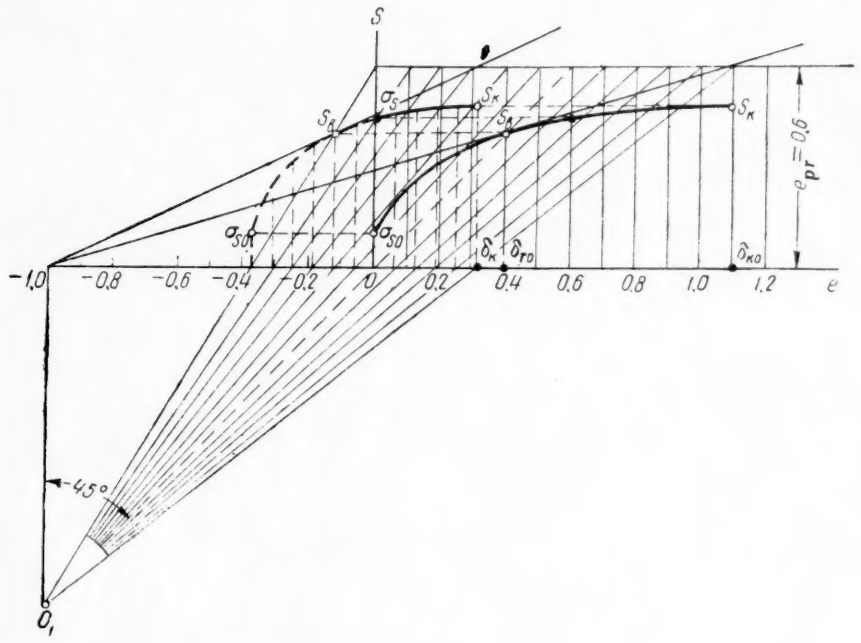

FIG. 3. Calculation of true stress diagram of a work-hardened metal on the $s - e$ co-ordinates system.

the angular coefficients tangent to point s_b of diagrams of cold-hardened and unhardened metal, in the co-ordinate systems $s - e$ and $s - q$, are respectively equal to [2]:

$$K_{\delta_r} = \left(\frac{ds}{de}\right)_{s_b} = \frac{s_b}{1+\delta_r}, \qquad (3)$$

$$K_{\psi_r} = \left(\frac{ds}{dq}\right)_{s_b} = \frac{s_b}{1-\psi_r}. \qquad (4)$$

where, if the point s_b lies more to the left of the ordinates axis, then

$$\delta_r = \frac{\delta_{r0} - e_{pr}}{1+e_{pr}} < 0 \text{ and } \psi_r = \frac{\psi_{r0} - q_{pr}}{1-q_{pr}} < 0.$$

The negative values of δ_r and ψ_r indicate that the capacity of the metal for uniform deformation was exhausted before the tensile test. The independence of the expressions for angular coefficients K_{δ_r} and K_{ψ_r} in respect to the point s_b shows that Kerber's rule is valid also in the case * when $e_{pr} > \delta_{r0}$ and $q_{pr} > \psi_{r0}$.

The rule indicated is given in the statement that the tangents to the curves of real stresses at the point s_b, in any given stage of cold-hardening of the metal, meet in one point, the co-ordinates of which are: in the system $s - e$, $s = 0$, $e = -1$, and then in the system $s - q$, $s = 2\,s_b$, $q = 1$. In the system of co-ordinates $s - q$ the tangents to point s_b intercept also the abscissae axis at a distance of $1 - 2\,\psi_r$ to the left of the co-ordinates base.

Whilst $e_{pr} < \delta_{r0}$ and $q_{pr} < \psi_{r0}$, by means of diagrams of true stresses, it is easy to determine graphically the values of the yield point $\sigma_b = P_{max}/F_0$. The proofs of the correctness of the structural details shown in Fig. 5 are not given here owing to their simplicity.

* In the generally known work of N.A. Shaposhnikov Mekhan. ispytan. metallov (The Mechanical Testing of Metals) it is erroneous to suppose that with $e_{pr} > \delta_{r0}$ and $q_{pr} > \psi_{r0}$ Kerber's rule does not hold.

VOL. 5 1957

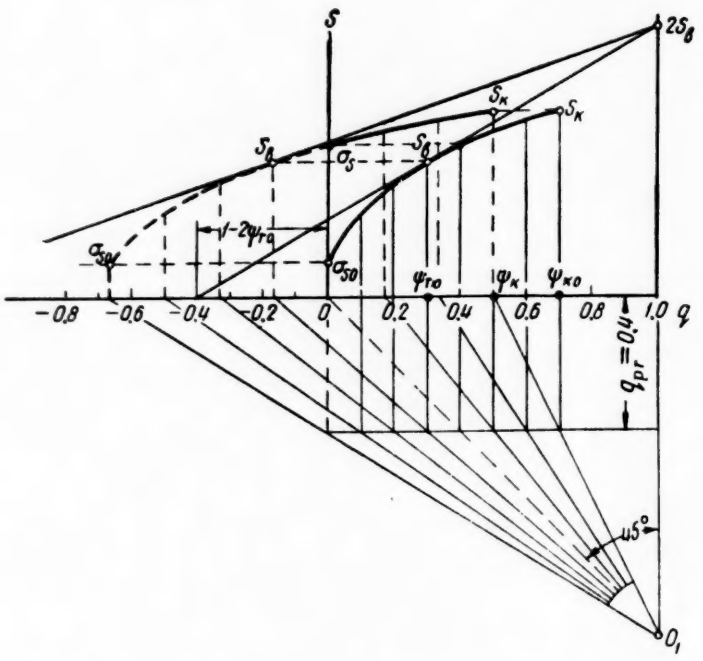

FIG. 4. Calculation of true stress diagrams of a work-hardened metal on the $s - q$ co-ordinates system.

Considerable interest both in theory and practice is attached to the relation of the ultimate tensile strength σ_s to the breakdown or yield point σ_b, and the ratio of tensile strength s_k to the true breakdown point s_b.

The author has previously shown that [4] for non-work-hardened metals

$$\frac{\sigma_{s0}}{s_b} \approx 0{,}02^{\psi_{r0}} \quad \text{or} \quad \frac{\sigma_{s0}}{\sigma_{b0}} \approx (1 + \delta_{r0}) \cdot 0{,}02^{\psi_{r0}}. \qquad (5)$$

The curves of these experimental relations are given in Fig. 6. In order to determine the ratios σ_s/σ_b and σ_s/s_b for work-hardened metals it is possible to use the graphs given in Figs. 3, 4, 6, permitting evaluation of σ_s and σ_b.

Since the curve of true stresses in the co-ordinate system $s - q$ to the right of point s_b passes very close to the tangent at point s_b of this curve, it is possible to assume that in this part of the curve $s - q$ coincides with the tangent. In this case, as the formula for the angular coefficient $K\psi_p$, we have, from geometrical considerations

$$\frac{s_k - s_b}{\psi_k - \psi_r} \approx K_{\psi_r} = \frac{s_b}{1 - \psi_r},$$

whence

$$s_k \approx s_b\left(1 + \frac{\psi_k - \psi_r}{1 - \psi_r}\right) = s_b(1 - \psi'_k), \qquad (6)$$

where

$$\psi'_k = \frac{F_r - F_k}{F_p}.$$

Here F_r and F_k are sectional areas of the testpiece at the moment of reaching stresses s_b and s_k.

Since

$$s_b \equiv \sigma_b(1 + \delta_r) = \frac{\sigma_b}{1 - \psi_p}$$

we have finally that

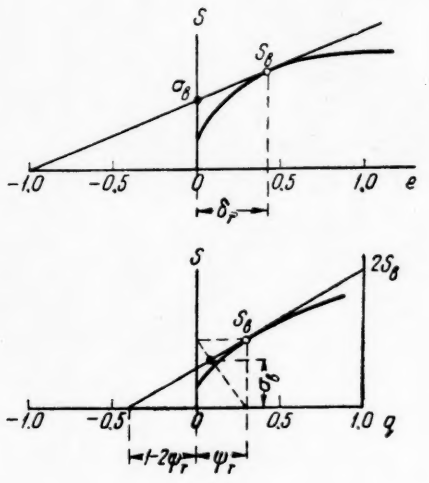

FIG. 5. Graphic expression of Kerber's rule and method of determining nominal (provisional) breaking point σ_s.

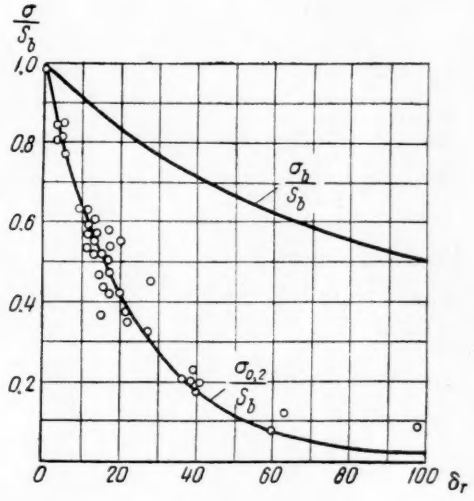

FIG. 6. Relation of ratios σ_b/s_b and $\sigma_{0,2}/s_b$ to uniform elongation σ_{r_0}.

$$\frac{s_k}{\sigma_b} \approx \frac{1-2\psi_r+\psi_k}{(1-\psi_r)^2} \text{ and } \frac{s_k}{\sigma_b} \approx (1+\delta_r)^2\left(\frac{1-\delta_r}{1+\delta_r}+\frac{\delta_k}{1+\delta_k}\right). \qquad (7)$$

M.P. Markovets [5], by mathematical treatment of the results of numerous experiments, found that, in two special cases:

$$\text{with } \psi_r = 15\% \quad s_k/\sigma_b \approx 1 + 1{,}35\,\psi_k,$$
$$\text{with } \psi_r = 30\% \quad s_k/\sigma_b \approx 0{,}8 + 2{,}06\,\psi_k.$$

From formula (7) it follows that

$$\text{with } \psi_r = 15\% \quad s_k/\sigma_b \approx 0{,}969 + 1{,}38\,\psi_k,$$
$$\text{with } \psi_r = 30\% \quad s_k/\sigma_b \approx 0{,}816 + 2{,}04\,\psi_k.$$

As can be seen above, approximate theoretical calculations with formula (7) agree very well with the experimental results of M.P. Markovets, so that formula (7), as being more generally universal, is preferable to the partial formula of M.P. Markovets.

According to the author mentioned the section of the ordinates axis intercepted by the tangent to the curve $s - q$ at the point s_b may be taken as approximately equal to σ_b. An accurate value for σ_b is given by the simple graphic construction shown in Fig. 5 or by the formula:

$$\sigma_b \equiv \frac{s_b}{1+\delta_r} \equiv s_b\,(1-\psi_r).$$

II. Let us consider how to construct true stress curves in the co-ordinate systems $s - \hat{e}$ and $s - \hat{q}$, where $\hat{e} = \ln(1+e)$ and $\hat{q} = \ln - q$), the "true" elongation and compression.

Differentiating the equation

$$P = sF,\ e = \frac{l}{l_0} - 1 = \frac{F_0}{F} - 1,\ q = \qquad \frac{F}{\quad}$$

we find that

$$\frac{dP}{P} = \frac{ds}{s} - \frac{de}{1+e} = \frac{ds}{s} - \frac{dq}{1-q}.$$

since $\hat{de} = \frac{de}{1+e}$ and $\hat{dq} = -\frac{dq}{1-q}$,

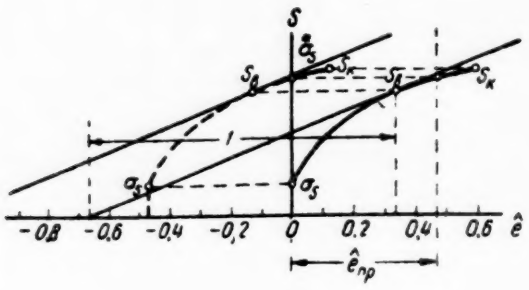

FIG. 7*. The $s - \hat{e}$ diagram.

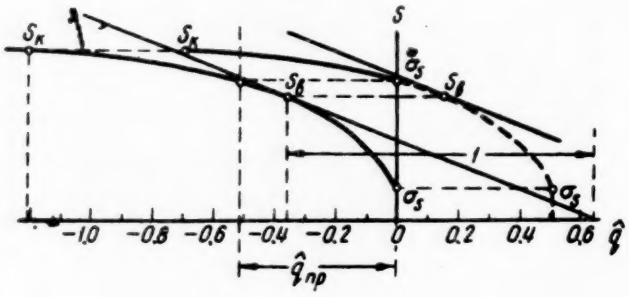

FIG. 8*. The $s - \hat{q}$ diagram.

we have

$$\frac{dP}{P} = \frac{ds}{s} - d\hat{e} = \frac{ds}{s} + d\hat{q}.$$

When the force P on the diagram $P - \Delta l$ reaches maximum $dP = 0$,

$$s = s_b, \quad \hat{e} = \hat{\delta}_r, \quad \hat{q} = \hat{\psi}_r,$$

where $\hat{\delta}_r = \ln(1 + \delta_r)$ and $\hat{\psi}_r = \ln(1 - \psi_r)$.

Therefore at the point s_b

$$\frac{ds}{s_b} - d\hat{e} = \frac{ds}{s_b} + d\hat{q} = 0.$$

Whence it follows that the angular coefficients of the tangents to point s_b on the diagrams $s - \hat{e}$ and $s - \hat{q}$ respectively equal

$$K_{\hat{\delta}_r} = \left(\frac{ds}{d\hat{e}}\right)_{s_b} = s_b \qquad (8)$$

$$K_{\hat{\psi}_r} = \left(\frac{ds}{d\hat{q}}\right)_{s_b} = -s_b \qquad (9)$$

* In Figs. 7 and 8 σ^*_s indicates the yield point of a cold-hardened metal.

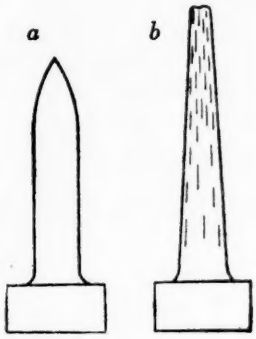

FIG. 9. Samples of (*a*) austenitic chromo-nickel steel and (*b*) of ferritic high chromium steel broken at a temperature of 1000°C.

VOL. 5 1957

Since, with increase of deformation in the metal, $\hat{e}$ increases from 0 to ∞, and $\hat{q}$ diminishes from 0 to $-\infty$, the curves $\hat{s} - e$ and $s - \hat{q}$ with the tangents thereto at the point s_b have the form shown in Figs. 7, 8.

Kerber's rule in these co-ordinate systems says that the tangent to point s_b intercepts the abscissae axis:

(*a*) at a distance equal to unity to the left of point s_b on the $s - \hat{e}$ diagram;

(*b*) at a distance equal to unity to the right of point s_b on the $s - \hat{q}$ diagram.

Since the true elongation and the true compression are subject to additive summation we have

$$\hat{e}_{x0} = \hat{e}_{pr} + \hat{e}_x \text{ and } \hat{q}_{x0} = \hat{q}_{pr} + \hat{q}_x,$$

where $\hat{e}_{x0}$ and $\hat{q}_{x0}$ are abscissae of point s_b on the curves for an unhardened metal, then $\hat{e}_{pr}$ and $\hat{q}_{pr}$ are measures of the preliminary cold deformation suffered by a metal under cold-hardening, and $\hat{e}_x$ and $\hat{q}_x$ are abscissae of the point X_1 on the diagrams of a work-hardened metal. The value of total deformation at points X and X_1 is the same.

It follows therefore that, in constructing a diagram for a work-hardened metal it is necessary, on the diagrams for an unhardened metal, to transfer the co-ordinate base at O to the point O_1 wherein:

(*a*) in the co-ordinate system $s - \hat{e}$ the point O_1 lies to the right of point O, and $OO_1 = \hat{e}_{pr}$;

(*b*) in the co-ordinate system $s - \hat{q}$ the point O_1 lies to the left of O, and $OO_1 = q_{pr}$.

The co-ordinate system $s - \hat{e}$ enters into the practical research of many investigators. Its disadvantage is the need involved of dealing with logarithmic values, and, as was shown, this is worth while owing to the simplicity of transition to different states of work-hardening.

III. In the practice of constructing real stress diagrams from experimental data it is necessary to take into account that the mechanical properties of a metal, in different sections of the testpiece, always vary somewhat. Therefore the true stress curves should be constructed for some one section or other of the sample. The true values for the mechanical properties of a metal in this section may be found through a true stress diagram only by conformity to the following recommendations:

(1) Before forming the neck, diameter measurements should be made in three or more sections of the gauge length of the sample. After locating the section in which development of the neck or notch begins it may be possible to settle the question: which of the above-named three sections is nearest to the neck thus formed, and determine which of several series of measurements made before forming the neck should be retained.

(2) If the point s_b is correctly chosen on the constructed true stress curve two conditions should be fulfilled:

(*a*) for the $s - e$ diagrams

$$K_{\delta_r} = \frac{s_b}{1 + \delta_r}, \qquad \sigma_b = \frac{s_b}{1 + \delta_r} \tag{10}$$

(*b*) for the $s - q$ diagrams

$$K_{\psi_r} = \frac{s_b}{1 - \psi_r}, \qquad \sigma_b = s_b (1 - \psi_r). \tag{11}$$

The simplest way of checking conformity to these conditions is by the graphic method in accordance with Fig. 5. The first condition is equivalent to Kerber's rule.

It is specially important to follow up the fulfilment of these conditions to see whether the uniform elongation or compression amounts to fractions of one per-cent, characterizing the tough constructional

alloy steels that receive hardening and low tempering treatment.

It should be pointed out that, in our case, with the $s - e$ and $s - q$ diagrams there are two vertical scales: that of the dimensionless values e_{pr} and q_{pr} and the stress scale s. It would be more convenient in practice and more correct from the point of view of theory to plot on the abscissae axis the dimensionless values s/s_b instead of the stresses s.

It should be pointed out that, in many cases, there are in nature also unknown to the researcher, relations or conformities that are more easily discoverable if, on the co-ordinate axes dimensionless complexes are plotted comprising, according to rules of analysis, definite dimensions [6,7] of physical values and physical constants that have been already investigated.

In conclusion it is necessary to dwell for a moment on the case where the broken sample has the appearance of two counter-stressed cones (Fig. 9). Here evidently there is no uniform deformation, any idea of a true breaking point s_b is inadmissible, true stress diagrams will have no special features or conformities peculiar to them.

Such an unusual picture of breakdown is characteristic of high chrome steels tested at high temperatures, especially of steels of the ferrite class. The high test temperature (about 1000°), as such, is not the cause of breakdown conicity in the samples, because ordinary carbon and austenitic chrome-nickel steels, tested at such temperatures, give a clearly indicated uniform elongation, i.e. beyond the limits of the neck the cylindrical form of the samples is retained.

The tapered or conical form of the samples of high chromium steels fractured at a high temperature is conditioned by the formation on their surface of a tough skin or scale. This scale at a high temperature is very hard and tough, exceeding that of the hot steel. The tough cylindrical film of scale covering the samples from the first moments of plastic deformation prevents reduction in diameter of the sample, as a result of which the usual picture of developing deformation is disturbed; sections of the sample contiguous to the neck are actively involved in the deformation, and in place of the neck tapered surfaces are formed. With an increasing degree of deformation the film loses its strength and begins to show longitudinal wrinkles or slight corrugations. It should be expected that, in a vacuum and in the absence of scale, high chromium steels will deform like other other metals.

It is interesting to note that, in vertically disposed parts (made of high chromium steel) of the heating elements of high temperature furnaces, the following feature is observed: the softening mass of metal under the action of its own weight slowly flows (creeps) within the surface film downward. In such case the film below is broken, but above it is contracted and forms wrinkles.

Translated by W.G. Cass

REFERENCES

1. G.P. Zaitsev, *Fiz. metal. metalloved.* 2, 1 (1956).
2. G.P. Zaitsev, *Fiz. metal. metalloved.* 5, 2 (1957).
3. N.A. Shaposhnikov, *Mekhan, ispyt. metallov (Mechan. testing of metals),* Mashgiz, (1951).
4. G.P. Zaitsev, *Symposium Trud. inst. stroit. mekhaniki, Akad. Nauk Ukr. S.S.R.* No. 10, (1949).
5. M.P. Markovets, *Diagrammy istinnyk naprazh. i razchet. na. prochn (True stress diagrams and strength calculations)* Oborongiz (1947).
6. A.I. Sedov, *Metody podobiya i raznomernosti v mekhanike (Methods of Similarity and Dimensional Difference in Mechanics,* Gostekhizdat. Moscow, (1954).
7. P.V. Brinkmen, *Analiz razmernosti (Dimensional Analysis)* United Scientific and Technical Publishing Houses, (1934).

THE EFFECT OF FROZEN-IN STRAINS OF THE CRYSTAL LATTICE ON THE MECHANICAL PROPERTIES OF ALLOYS OF ALUMINIUM WITH MAGNESIUM

I. DEPENDENCE OF THE YIELD STRENGTH AND TENSILE STRENGTH ON THE TEMPERATURE AND RATE OF DEFORMATION*

A.V. GRIN, V.A. PAVLOV and I.A. PERETURINA

Institute of Physics of Metals of the Urals Branch of the Academy of Science of the U.S.S.R.

(Received 11 August 1956)

The temperature dependence of the yield strength and tensile strength of pure aluminium and its alloys with magnesium in the temperature region of from 80 to 700°K was investigated, the rate of deformation varying 1000 times.

It was established that for pure aluminium in the temperature region up to 500°K the relation of the yield strength to the modulus of elasticity is virtually independent of temperature. At higher temperatures a more pronounced dependence on temperature was observed, which is linked with the deformation at the grain boundaries.

The strenghtening of alloys of aluminium by magnesium is due to the occurrence of frozen-in strains of the crystal lattice caused by the magnesium atoms. A strong effect on the yield strength by the diffusion processes which occur during the time of the deformation was observed.

VOL. 5 1957

INTRODUCTION

The many investigations that have been made into the mechanism of the plastic deformation of mono- and polycrystalline metals and alloys lead to the conclusion that plastic deformation does not occur simultaneously throughout the entire volume but begins in small areas of the crystal and then spreads along certain crystallographic planes and directions [1-3]. From this it follows directly that strength will be determined by the nature and strength of the inter-atomic bonds, by the properties and structures of those areas in which the plastic deformation originates or, in other words, by the nature of the "submicroscopic inhomogeneity of the crystal structure" [3-4]. If the number of inhomogeneities of the crystal structure is increased, plastic deformation begins at higher external stresses [3]. This increase in the strength of the crystal when the number of distortions of the crystal lattice is increased can be understood as an increase in the effectivity of the use made of the inter-atomic bonds [4].

Various kinds of diffusion processes which occur during the deformation also affect the behaviour of metals and alloys under load. Of the known diffusion processes which are caused by stresses one can name, e.g. uphill diffusion [5], the setting up of an anisotropic distribution of atoms [6], a change in the degree of order in alloys in the process of ordering [7], the separation of a solid solution [3, 13], diffusion into vacancies and intrusions into the interstices between the atoms, etc. The regularities of these diffusion processes can be studied with the help of observations of inelastic phenomena and they can be used to explain the behaviour of solid bodies under load.

At present it is accepted that diffusion processes only facilitate plastic deformation, lower the deforming stress, reduce the strains of the crystal lattice. There exist, however, experimental data which leads one to expect that diffusion which occurs under the effect of stress is during the time of deformation under certain conditions capable of raising the resistance to deformation [8]. Recently interesting data were published which shows that the ordinary concentration diffusion can be accompanied by the emergence of strains [9].

In the present paper the task is set of studying the effect of frozen-in strains of the crystal lattice which are caused by the atoms of the solute elements and of the diffusion processes which occur under the effect of stresses in plastic deformation on the mechanical properties.

Alloys of aluminium and magnesium were used for the investigation. As previous studies have shown [10, 11], there exist in these alloys considerable

* *Fiz. metal. metalloved.* 5, No. 3. 493-500, 1957

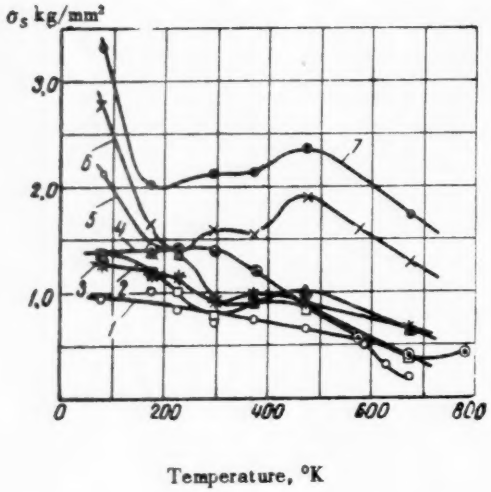

FIG. 1. Temperature dependence of the yield strength of aluminium and its alloys with magnesium at rate of elongation of 6.4×10^{-3} cm/sec:
1 – pure aluminium;
2 – aluminium with 0.02%;
3 – with 0.05%;
4 – with 0.1%;
5 – with 0.3%;
6 – with 0.5%;
7 – with 1.0% of magnesium.

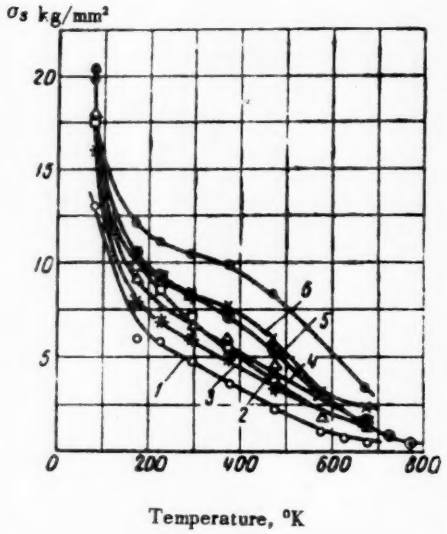

FIG. 2. Temperature dependence of tensile strength of aluminium and its alloys with magnesium at rate of elongation of 6.4×10^{-3} cm/sec:
1 – pure aluminium;
2 – aluminium with 0.02%;
3 – with 0.05%;
4 – with 0.1%;
5 – with 0.3%;
6 – with 0.5%;
7 – with 1.0% of magnesium.

frozen-in strains of the crystal lattice caused by the magnesium atoms, but the bonds do not change with the composition of the alloys. This combination of properties makes it possible to study the effect of frozen-in strains of the crystal lattice on the mechanical properties in a pure form.

METHOD OF EXPERIMENTS

Alloys were prepared from aluminium mark AB000 and electrolytic magnesium. From each cast wires of 3 mm diameter were drawn by pressing through a hole at a temperature of about 200°C which were then drawn at room temperature to about 2 mm diameter. Samples of 55 mm length were then cut from this wire for the study of the mechanical properties. The samples which were cold-hardened by the drawing were then annealed. The annealing temperature was so chosen that as a result of recrystallization the grains were in all alloys of the same linear size, about 0.1 mm.

The samples were deformed in a special machine [12] with automatic registration of the elongation pattern on a photographic film. From the elongation pattern the yield strength, the tensile strength and the full and uniform elongation were determined.

Pure aluminium, which contained admixtures of 0.01% magnesium, 0.0017% of iron, 0.0014% of silicon, 0.0011% of copper, and its alloys with 0.02, 0.05, 0.1, 0.3, 0.5 and 1.0% magnesium were investigated.

RESULTS OF EXPERIMENTS

In Figs. 1 and 2 are shown the curves of the dependence of the yield strength and the tensile strength on the temperature at a rate of elongation of 6.4×10^{-3} cm/sec for pure aluminium and its alloys with magnesium.

As Fig. 1 shows, for pure aluminium a simple dependence of the yield strength on the temperature is observed. The yield strength is lowered almost linearly with the temperature rising to 500°K, and then more rapidly.

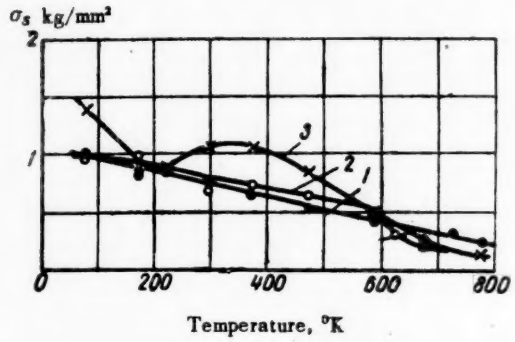

FIG. 3. Temperature dependence of the yield strength of pure aluminium at elongation rates of:
1 – 2 x 10^{-1} cm/sec;
2 – 6.4 x 10^{-3} cm/sec;
3 – 2 x 10^{-4} cm/sec.

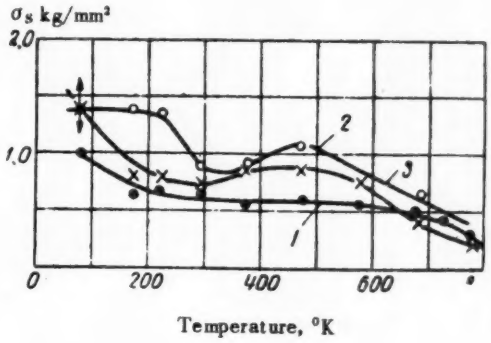

FIG. 4. Temperature dependence of the yield strength of an alloy of aluminium with 0.1% magnesium at elongation rates of:
1 – 2 x 10^{-1} cm/sec; 2 – 6.4 x 10^{-3} cm/sec;
3 – 2 x 10^{-4} cm/sec.

Even with the smallest additions of magnesium the temperature dependence of the yield strength already becomes more complex. The yield strength no longer changes uniformly with the temperature. There appears a maximum in the region of the temperature of 500°K and a pronounced rise in the yield strength at lower temperatures. With the rise in the concentration of magnesium the yield strength rises, the height of the maximum increases and the temperature dependence becomes more complex.

The tensile strength (Fig. 2) rises markedly with the increase in the magnesium concentration at all temperatures. On the curves of the dependence on temperature a weak maximum is to be seen at 400°K with high magnesium concentrations.

In Figs.3 to 5 are shown the curves of the dependence on temperature of the yield strength at three different rates of elongation for pure aluminium (Fig. 3), for the alloy with 0.1 per cent of magnesium (Fig. 4) and for the alloy with 0.5 per cent of magnesium (Fig. 5). Curve 1 was obtained with an elongation rate of 2 x 10^{-1} cm/sec, curve 2 with a rate of 6.4 x 10^{-3} cm/sec and curve 3 with a rate of 2 x 10^{-4} cm/sec.

Looking at Figs. 3 to 5 it is not difficult to discern the following regularity. In pure aluminium, with the lowest elongation rate, 2 x 10^{-4} cm/sec., a non-uniform dependence of the yield strength on the temperature with a maximum at 400°K and a rise in plasticity at 80°K appear. In the region of the temperatures where the maximum exists and anomalous dependence of the yield strength on the rate of deformation is observed which consists in the yield strength rising with decreasing rate of deformation. In discussing the regularities of plastic deformation for pure aluminium one must bear in mind that in its original state the pure aluminium already contained a number of admixtures, including about 0.01 per cent of magnesium. That the curve of the temperature dependence of the yield strength becomes complex at low rates of elongation is connected with the existence of these impurities.

With increased magnesium content the dependence of the yield strength on the rate of deformation becomes markedly complex. The curves of the temperature dependence for rates of deformation get twisted with one another which reflects the complex dependence of the yield strength on the temperature, the rate of deformation and the composition of the alloy. In alloys with high magnesium content the curves of the dependence on temperature of the yield strength are of a non-uniform description even at high rates of deformation. Thus, e.g. for an alloy with 0.1 per cent of magnesium the curve of the temperature dependence of the yield strength only at the highest rates of elongation lacks a maximum at 500°K and shows a weak rise at low temperatures, while the curves for the two lower rates are complex. In the alloy with 0.5 per cent magnesium the curves for all three rates of deformation have maxima. In all cases an anomalous dependence of the yield strength on the rate of deformation is observed. For the alloy with 0.1 per cent of magnesium, with the highest rate of deformation the yield strength proves to be lower than for pure aluminium over a fairly wide temperature region under the same conditions of deformation.

The tensile strength depends comparatively little on the rate of deformation in the case of pure

VOL. 5 1957

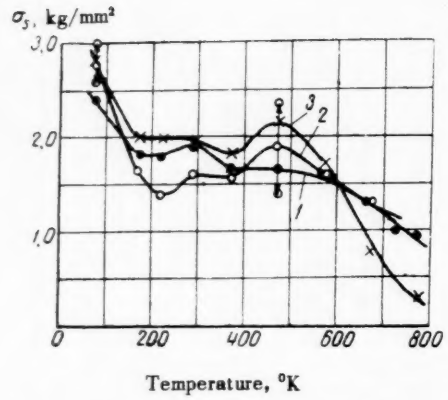

FIG. 5. Temperature dependence of the yield strength of an alloy of aluminium with 0.5% magnesium at elongation rates of:
1 – 2 x 10^{-1} cm/sec;
2 – 6.4 x 10^{-3} cm/sec;
3 – 2 x 10^{-4} cm/sec.

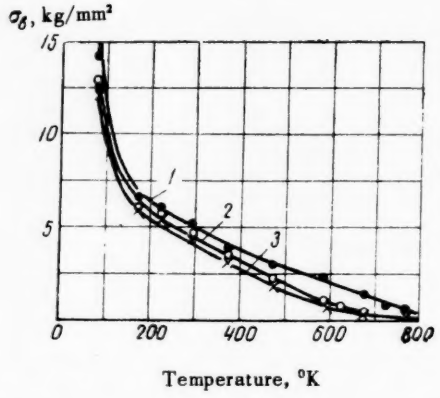

FIG. 6. Temperature dependence of the tensile strength of pure aluminium at elongation rates of:
1 – 2 x 10^{-1} cm/sec;
2 – 6.4 x 10^{-3} cm/sec;
3 – 2 x 10^{-4} cm/sec.

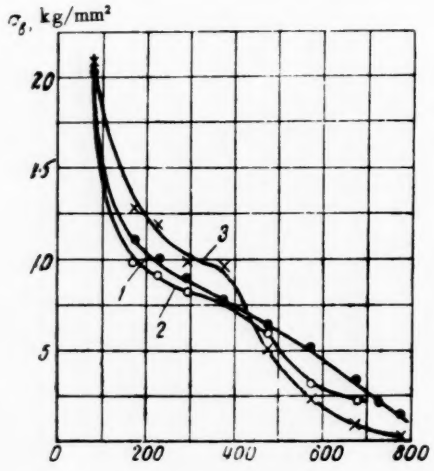

FIG. 7. Temperature dependence of the tensile strength of an aluminium alloy with 0.5% magnesium at elongation rates of:

1 – 2 x 10^{-1} cm/sec;
2 – 6.4 x 10^{-3} cm/sec;
3 – 2 x 10^{-4} cm/sec.

VOL
5
195

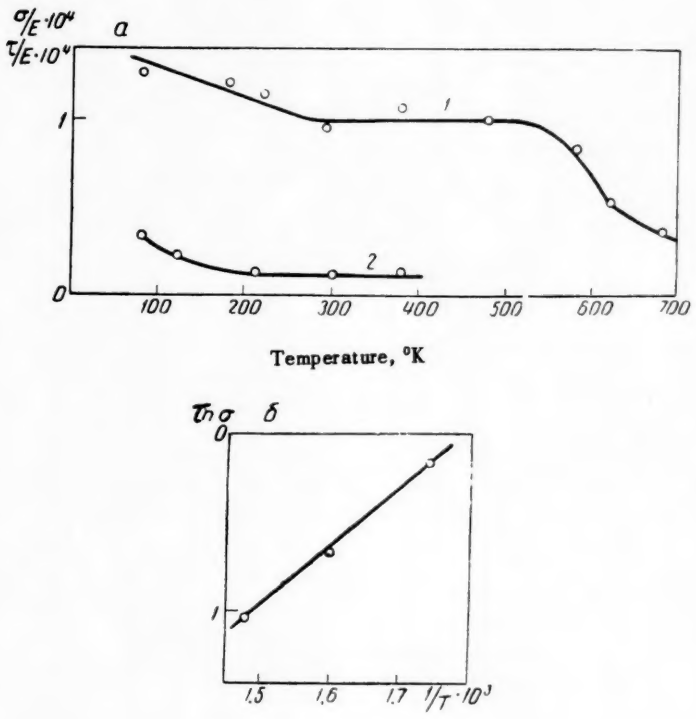

FIG. 8. *a* and *b*. 1 – polycrystal, 2 – monocrystal [21].

aluminium (Fig. 6) and of alloys with up to 0.3 per cent magnesium. In the alloys with 0.5 per cent of magnesium the effect of the rate of elongation is more marked, while in the temperature region between 80 and 400°K there is to be observed an anomalous dependence on the rate of deformation (Fig. 7).

DISCUSSION OF RESULTS

Measurements made of the mechanical properties of α-solid solutions of aluminium with magnesium when the temperature and the rate of deformation are varied over a wide range reveal a complex picture of the dependence of the mechanical properties of these alloys on the conditions of deformation and the composition of the alloy.

The temperature dependence of the yield strength for pure aluminium is the simplest. As one knows, the mechanical properties are determined by the inter-atomic bonds and the sub-microscopic structure of the crystal.[4] In order to take account of the effect of the change of the inter-atomic bonds with temperature on the temperature dependence of the yield strength it is useful to investigate the change in the relation of the yield strength to the modulus of elasticity with the temperature. In Fig. 8a the temperature dependence of the relation of the yield strength to the modulus of elasticity is shown for pure polycrystalline aluminium at a rate of deformation of 6.4×10^{-3} cm/sec, and for monocrystals of aluminium after the data of paper [21]. The figure shows clearly that for a fairly wide range of temperature this relation does not depend on the temperature; in other words, in that range of temperatures the change in the yield strength is conditioned mainly by the temperature change of the inter-atomic bonds.

The deviations from this regularity at low temperatures are apparently connected, as will be shown below, with the diffusion processes which occur during deformation. At high temperatures a stronger dependence of the yield strength on the temperature is observed, approximately following an exponential law (Fig. 8b). This part of the curve reflects the temperature dependence of the yield strength under

deformation along the grain boundaries. Microscopical investigation shows that at temperatures above 500°K a marked deformation along the grain boundaries is observed [16].

The alloying of aluminium with magnesium is accompanied by strengthening. In as much as in these alloys the inter-atomic bonds do not change with the composition of the solid solution, this strengthening is evidently connected with those defects of the crystal lattice which are caused by the atoms of magnesium.

At the same time the dependence of the mechanical properties on temperature and rate of deformation is more complex than in pure aluminium. In the curves of the temperature dependence of the mechanical properties maxima occur the size of which depends on the composition of the solid solution and the rate of deformation. All these regularities indicate that some kind of diffusion processes occur during deformation.

Maxima in the curves of the temperature dependence were first observed in the deformation of metastable solid solutions [3, 13]. In the region of the maxima an anomalous dependence of the mechanical properties on the rate of deformation was observed and the elongation patterns had a serrated appearance. Therefore, at present, when maxima are observed in the curves of the temperature dependence of the mechanical properties, their appearance is often explained by the precipitation from the solid solution during deformation of some small soluble admixtures.

Examining the established regularities in the changes of the mechanical properties of the investigated alloys it is not difficult to see that they have very much in common with those regularities which are usually observed in the deformation of metastable solid solutions. At the same time there are cases which are difficult to explain from this standpoint. Thus, e.g. maxima in the curves of the temperature dependence of the mechanical properties occur already at very low magnesium concentrations which lie far below the limit of saturation, when a dissociation of the solid solution is little likely.

There is however, at the present time a number of experimental data which show that the serrated appearance of the elongation pattern and the existence of slip planes are not peculiar to solid solutions [17, 18]. The majority of investigators explain all these phenomena by the interaction of the solute atoms with the defects of the crystal lattice, with dislocations. As the result of these interactions clouds of atoms of the admixtures in solution appear around the dislocations, which hinder the development of plastic deformation. These interactions change with temperature [19].

At present it is difficult to give completely definite conclusions on the problem of the diffusion processes which occur in plastic deformation under certain conditions and which affect plastic deformation in a certain way, since the study of these phenomena is still only in its beginnings. However, starting with the conception of dislocations and basing oneself on certain observations of internal stresses [14, 22, 23], one may suggest that when external stresses are applied a diffusion of the atoms of the admixtures may occur around the dislocations. These diffusion processes are accompanied by relaxation stresses and changes in the concentration of atoms in the cloud around the dislocation and can under certain conditions of deformation lead to a raised yield strength.

On the basis of the investigations of internal strains in alloys of aluminium and magnesium [14] one can suggest that the maximum of the yield strength which occurs in the temperature region of 500°K is conditioned by the diffusion of magnesium atoms.

The raising of the yield strength at low temperatures of deformation is connected with some kind of diffusion processes which have a low activation energy. In paper [15] on the investigation of the temperature dependence of the critical slip tension in monocrystals of brass a similar raising of the critical slip tension was observed at low temperatures. In that paper it is suggested that this raising is due to a large concentration of vacancies which emerge during the annealing of the alloy.

In paper [20] the effect of diffusion at the temperature of liquid air on the yield strength was observed in pure aluminium and in alloys with magnesium. The activation energy of the diffusion process in pure aluminium proved to be equal to 0.1. On the basis of this the authors suggest that at low temperatures a movement of the atoms which have penetrated into the interstices takes place to the dislocations, which leads to a raising of the deformation stress.

For the final decision of the question of the nature of the raised yield strength in alloys at low and high temperatures it is desirable that the study of the diffusion processes under the influence of tensions be continued over a wide range of temperatures.

CONCLUSIONS

1. For pure aluminium the temperature dependence

of the yield strength in the region of temperatures up to 500°K is in the main determined by the change in the inter-atomic bonds. At high temperatures a more pronounced dependence of the yield strength on the temperature is observed, which is apparently connected with deformations along the grain boundaries.

2. The strengthening of alloys of aluminium with magnesium is conditioned by the emergence of frozen-in strains of the crystal lattice caused by the atoms of magnesium.

3. Diffusion processes lead to a non-uniform dependence of the yield strength on the temperature, to an anomalous dependence on the rate of deformation, and make the dependence of the mechanical properties on the composition of the alloy and the conditions of deformation more complex. Maxima of the yield strength appear in the temperature region of 500 and a raising at 80°K which are connected with various kinds of diffusion processes occurring during the deformation under load.

Translated by B. Ruhemann

REFERENCES

1. E. Schmidt and B. Boas, *The plasticity of crystals, particularly of metals.* State United Publishing House of Science and Technology. (1938).
2. Ch. S. Barrett, *The Structure of Metals,* Metallurgizdat, (1948).
3. M.V. Yakutovich, *Trud. Inst. fiz.metalloved. Urals fil. Akad. Nauk* No. 12, p. 121, (1947).
4. G.V. Kurdiumov, *Problems of Metallurgy and the Physics of Metals; 4 collection of papers* p. 321, (1956).
5. S.M. Konobeevsky, *Zh. eksp. teor. fiz.* 13, 200, (1943).
6. K. Ziner, *Elasticity and Inelasticity of Metals; collection edided by S.V. Vonsovsky,* I.L., p. 119, (1954).
7. G. Gorsky, *Sow. Phys.* 8, 103, (1935).
8. V.A. Pavlov, *Dokl. Akad. Nauk SSSR,* 95, 1201, (1954).
9. V.I. Arkharov and S. Mardeshev, *Fiz. metal. metalloved.* 1, 517, (1955).
10. V.A. Pavlov, N.F. Kryuchko and I.D. Fedotov, *Fiz. metal. metalloved.* 3, 555, (1956).
11. N.I. Noskova, V.A. Pavlov and B.A. Yunikov, *Fiz. metal. metalloved.* 3, 557, (1956).
12. V.S. Averkiev, G.N. Kolesnikov, V.A. Pavlov and M.V. Yakutovich, *Zh. tekh. fiz.* 16, 349, (1946).
13. G.N. Kolesnikov, E.S. Yakovleva and M.V. Yakutovich, *Zh. tekh. fiz.* 19, (1949).
14. A.V. Grin and V.A. Pavlov, *Fiz. metal. metalloved.* 4, 103, (1957).
15. R.E. Sowison and F.A. Sherrill, *Acta Met.*, 4, 197, (1956).
16. E.S. Yakovleva, *Fiz. metal. metalloved.* 4, 141, (1957).
17. G.W. Ardley and A.H. Cottrell, *Proc. Roy. Soc.* A219, 328, (1953).
18. G.W. Ardley, *Acta Met.* 3, 525, (1955).
19. W. Louat, *Proc. Phys. Soc.* 69, 459, (1956).
20. F.D. Rosi and C.H. Mathewson, *Trans. Am. Inst. Min. met. Eng.,* 188, 1154, 1950.
21. A.R. Weswood and I. Broom, *Acta Met.* 5, 77, (1957).
22. T.S. Ke, *Metals Technol.* 15, No. 4, (1948).
23. W. Koster, L. Baugert and R. Hahn, Arch. Eisenhuttenw. 25, 269, (1954).

VOL. 5 1957

EFFECT OF MAGNESIUM ON THE MECHANISM OF PLASTIC DEFORMATION OF ALUMINO-MAGNESIUM ALLOYS*

V.I. SYUTKINA and E.S. YAKOVLEVA

Institute Fizika Metalov, Ural'sk fil. Akad. Nauk SSSR

(Received 15 October 1956)

The deformation mechanism of alumino-magnesium alloys has been studied. It is shown that the mechanism of plastic deformation changes with changes in magnesium content in the alloy. The strengthening produced by introduction of magnesium atoms into the alloy depends on changes in the mechanism of its deformation.

Metals under the action of sufficiently large external forces change their dimension in the retained form – they are plastically deformed. This process is accompanied by change in the mechanical properties of the metal. Change of properties is due to the fact that the transfer of matter produced by the external forces leads to breakdown of the true structure of the metal lattice. The method by which such movement of matter proceeds, with change in the structure of the metal caused during such transfer, has been called the mechanism of plastic deformation. Knowledge of deformation mechanism permits an understanding of the causes governing the mechanical properties of metals and of the changes taking place therein under deforming and alloying action. The effect of alloying on the mechanism of deformation has been studied only very slightly [1]. At the same time alloying is the principal method of imparting the required properties to an alloy. Alloying, in the general sense, causes changes in the bonding forces and a different kind of heterogeneity of structure in the alloy. The first directly produces change in mechanical properties of the substance, and the second through its effect on the mechanism of plastic deformation.

The mechanism of plastic deformation of semicrystalline alloys is much more complicated than the model forms devised for monocrystals. Complexity is introduced into the non-ideal structure of actual crystals by the presence in their grain boundaries also of foreign atoms. On application of external forces, owing to the existence of such type of disturbed structure, a very irregular distribution of stresses takes place in the alloys. As a result there is non-uniform and non-synchronized passing of deformation in the volume of the grains [2-5], which, in turn, may lead to initiation of new structural and concentrated irregularities in their structure [6, 7].

Study of the effect of alloying on the mechanism of plastic deformation of alloys rationally begins with the simplest case where alloying does not lead either to change in bonding forces in the alloy or to the appearance therein of new structural constituents. In this case differences in mechanism should be due to differences in amount and in mode of distribution of the alloying atoms in the alloy.

The present study was made with aluminium-magnesium solid solutions. It is known that, with these, within the limits of the α-solid solution, the bonding forces do not change with magnesium concentration [8]. Besides this the magnesium very markedly increases the parameter of the aluminium lattice [9], and therefore causes considerable static distortion therein. The effect of magnesium on the mechanical properties of solid solutions of aluminium-magnesium alloys has been studied in detail c.f. [10]. It was found that, within the limits of the α-solid solution, magnesium very appreciably, though non-uniformly with concentration, strengthens the alloy.

MATERIALS AND CONDITIONS OF TEST

Alloys of aluminium with magnesium were investigated, containing 0.00, 0.01, 0.04, 0.10, 0.30, 0.92 per cent magnesium, using as base aluminium of mark AV 000 with 0.0017 per cent iron, 0.0014 per cent silicon, 0.0011 per cent copper, and traces of zinc, magnesium, and manganese. Alloying was done with chemically pure electrolytic magnesium.

* *Fiz. metal. metalloved.*, 5, No. 3, 501-507, 1957.

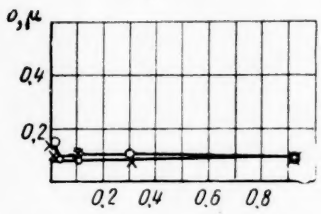

FIG. 1. Relation between value b of shear in slip track and magnesium content in alloys deformed up to 2 per cent at rate of 0.2 per cent/sec.
Rectilinear slip tracks; . — . T = 196°C,
X — X T = 18°C,
O — O 250°C

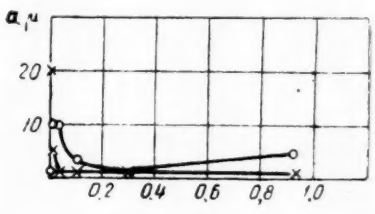

FIG. 2. Relation of distance a between slip tracks to magnesium content in alloys deformed to 2 per cent at rate of 0.2 per cent/sec;
rectilinear slip tracks;
temp as in Fig. 1.

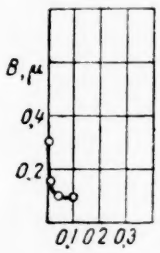

FIG. 3. Same as Fig. 1; curvilinear slip tracks.

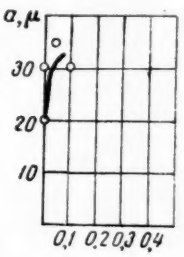

FIG. 4. Same as Fig. 2; curvilinear slip tracks.

Samples were in the form of strips 50 x 3.0 x 1.0 mm. Grain size in all the alloys was approximately the same. Average length was 0.1 mm. The tempered samples were electro-polished in an electrolyte consisting of two-thirds methyl alcohol and one-third nitric acid, after which they were extended at the rate of 0.2 per cent/sec. Elongation was done at temperatures of — 196, 18, and 250°C, on a machine for stretching thin specimens [11]. Moreover, at the temperature of 250°C all samples were subjected to a creep test at the rate of 4 x 10^{-3} per cent/hr. In the tensile tests these were made with two degrees of deformation : equal to 2 and 14 per cent elongation. For creep the samples were tested only with a 2 per cent elongation.

TEST PROCEDURE

Deformation mechanism was studied with the microscope, including form and distribution of traces of deformation appearing at the surface of the samples under tensile test. Moreover, with the aid of the light interference pattern the surface profile of the deformed alloys was also studied. According to displacement of the interference bands the vertical component of the deformation localized therein was determined on the deformation trace. The interference method permitted measuring the height of the profile with an accuracy of 0.02 μ in the case of a clear resolution (definition) of each individual trace under microscopic magnification of 320 x. The profile height in a trace and the distance between these deformation traces were accurately measured on the photographs taken of the most characteristic parts of the surface of the deformed alloys. Measurements were also made on grains in which the height of displacement in the deformation tracks was maximum.

EXPERIMENTAL RESULTS WITH ALLOYS DEFORMED TO 2 PER CENT

On the surface of all alloys deformed at — 196°C

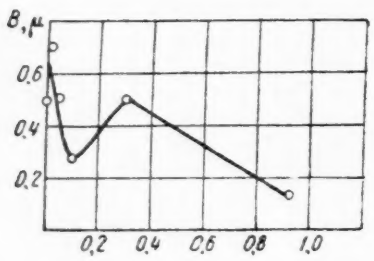

FIG. 5. Relation of displacement B at the grain boundaries to magnesium content in alloys deformed to 2 per cent at rate of 0.2 per cent/sec.

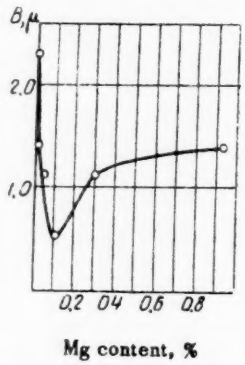

FIG. 6. Relation of displacement B at the grain boundaries to magnesium content in alloys stretched 2 per cent at rate of 4.10^{-3} per cent/hr 250°C.

could be seen a rather thick or dense pattern (lattice) of rectilinear unclearly exhibited traces of slip. The distance between traces was equal to about 1 μ. The amount of displacement in the slip trace was very small – much less than 0.1 μ. It was not possible accurately to measure the extent of this shift since the traces are only very indistinctly shown. Displacements of the interference bands on such traces blend together, so that the interference line is widened.

In the grains of the alloys deformed at 18°C there is also a pattern of slip indications. In this case the traces are more clearly visible; their distribution is more scattered and less uniform than at the temperature of – 196°C. With increase in the magnesium content of the alloy the space between the traces and magnitude of displacement in the slip trace are markedly reduced (Fig. 12a,f). and with a content of 0.04 per cent magnesium a picture is presented similar to those of alloys deformed at – 196°C. In a more highly alloyed alloy (0.92% Mg), besides a pattern or network of fine slip traces, there are coarser traces of deformation, the so-called deformation bands.

With alloys deformed at 250°C at the rate of 0.2 per cent the deformation picture differs strongly from those obtained at 18° and – 196°C. It is not the same also for alloys with different magnesium content. Thus, with pure aluminium the rectilinear slip traces are completely absent. In the alloys they are present, and the distances between the traces and the extent of displacement (shear) in the slip trace decline with increasing magnesium content.

Besides the rectilinear slip indications in individual grains of pure aluminium (Fig. 13a,b) and of alloys of low magnesium content (up to 0.1 per cent) there are curved traces, where the displacement decreases with increasing magnesium content. With highly alloyed alloys in individual grains there are clearly shown deformation bands (Fig. 13c,d). In addition to the deformation traces mentioned, there is in the the grains of alloys of all compositions, local displacement along the grain boundaries. The extent of the displacement decreases irregularly with increasing magnesium content. With this 0.1 per cent content displacement is minimum.

With alloys tested for creep at 250° and rate of flow of 4.10^{-3} per cent/hr there are no slip traces in the grains. Along the grain boundaries there is marked displacement (Fig. 13e,f). The magnitude of such displacement declines irregularly with the extent of alloying, and with a 0.1 magnesium content it is minimum.

In Figs. 1 to 6 are shown the relations between values of displacement localized in the slip indication, distance between these slip indications, and displacements along the grain boundaries, on the one hand, and magnesium content in the alloy, on the other.

EXPERIMENTAL RESULTS WITH SAMPLES DEFORMED UP TO 14 PER CENT

The surface of alloys of all compositions deformed at – 196°C was covered with a dense pattern of rectilinear traces of slip in one or two directions (Fig. 14a,b). The slip indications are more clearly visible than with the lower deformation stage.

VOL 5 195

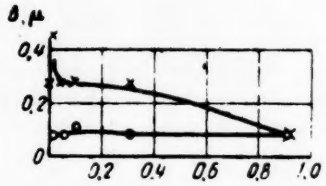

FIG. 7. Relation of value b of displacement in slip track to Mg content in alloys under elongation of 14 per cent at rate of 0.2 per cent/sec. Rectilinear slip tracks X – X T 18°C, O – O T is – 196°C.

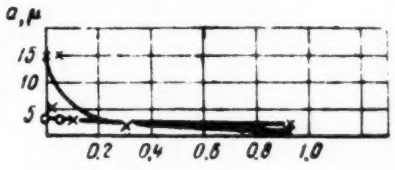

FIG. 8. Relation of distance a between slip tracks and Mg content in alloys under elongation of 14 per cent at rate of 0.2 per cent/sec- Rectilinear slip tracks X – X T is 18°C, O – O T is – 196°C.

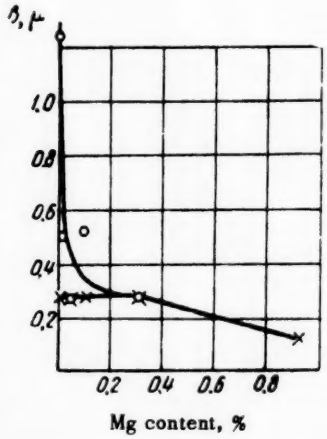

FIG. 9. Same as in Fig. 7, curvilinear slip tracks; X – X T is 18°C, O – O T 250°C.

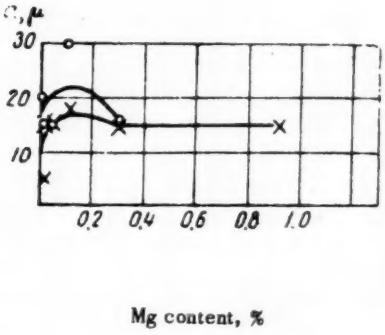

Fig. 10. Same as in Fig. 8; curvilinear slip tracks; X – X T 18°C, O – O T 250°C.

Distance between traces declines with increasing magnesium content, as also does displacement in the indications of slip. It is not possible accurately to measure the extent of displacement in this case, as the traces lie very close to each other. Besides this pattern of slip indications there are, in alloys of all compositions deformation bands. Within the limits of these bands deformation proceeds only along one plane of slip, but, with curvature of the bands, alon g several. With increased content of magnesium in the alloy the number of grains in which bands are formed also increases, and the height of the surface profile at the points where these bands appear is greater.

In alloys deformed at 18°C deformation proceeds very irregularly in the body of the grain. The appearance is noted of coarse rectilinear and curvilinear indications of slip (Fig. 14c,d). The extent of displacement in these slip traces declines with increasing content of magnesium. The distance between the rectilinear slip traces also declines. But that between the curvilinear slip traces varies considerably both within the limits of one grain and between several grains, and it was not possible to establish any uniform relation between such variation and magnesium content. In individual grains of the alloys deformation bands are to be seen, formed by coarse slip indications in one direction (Fig. 14 d).

Elongation to 14 per cent at 250°C proceeds with formation of coarse rectilinear and curvilinear slip indications in alloys of all compositions (Fig. 14 e, f). Particularly coarse slip traces appear with aluminium and weakly alloyed alloys. Displacement

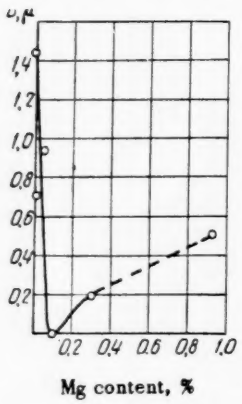

FIG. 11. Abs. content per cent. Relation of displacement B along the grain boundaries to Mg content in alloys under 14 per cent elongation at the rate of 0.2 per cent/sec, at 250°C.

in such slip indications with aluminium reaches 1.44 μ. Fine rectilinear slip tracks are observed only in individual parts of a grain. Along the grain boundaries there is marked displacement. The amount of displacement decreases non-uniformly with increase in magnesium content. With a 0.1 per cent magnesium content displacement is minimum. With aluminium only it is a maximum and reaches a value of 1.4 μ (Fig. 14 e). In an alloy containing 0.92 per cent magnesium, besides the aforesaid deformation traces, there are also deformation bands.

Displacement in individual bands reaches 0.27 μ. The bands are formed by coarse slip tracks of one direction (Fig. 14 f). The uniform regularity of change in deformation traces with magnesium content is shown in Figs. 7-11.

As a result of this work on deformation traces (tracks) in aluminium alloys it has been found that the presence of magnesium atoms in aluminium produces the following changes in these deformation traces:

1. Displacement in the trace and distance between slip traces or tracks are reduced.
2. Displacement along the grain boundaries is irregularly reduced.
3. The formation of curvilinear slip tracks is more difficult.
4. The tendency of the alloy to form deformation bands is enhanced.

With the observed regularities of change in deformation traces as a basis, it is possible to form some idea as to what changes in deformation mechanism are caused by the presence of magnesium atoms in aluminium.

Decrease of displacement in a trace and of distance between slip traces indicates that displacement or shear deformation includes most fully and uniformly the whole volume of the grain. Deformation on a microscopic scale proceeds more homogeneously.

Decrease in the amount of curvilinear slip tracks and in the extent of displacement along the grain boundaries indicates that the share of deformation taking place by atomic diffusion declines, but collectively, by displacement mechanism, it increases.

Increase in the amount of deformation bands in the grains shows that deformation on a macroscopic scale (within the limits of a single grain) takes place more heterogeneously.

DISCUSSION OF RESULTS OBTAINED

The more uniform distribution of deformation in the mass of the grain with the aluminium-magnesium alloys than with aluminium alone is conditioned by the fact that the magnesium atoms produce static distortion in the aluminium lattice, thus increasing the amount of heterogeneity in its structure. The existence of a heterogenous structure in crystals leads to irregular distribution of stresses in the body under load. Stresses together with heterogeneity facilitate the start of plastic deformation and determine the low value of yield point and strength in real crystals [2, 3]. With increase in the number of heterogeneities in the grains, produced by the presence of magnesium atoms, the number of places of incipient plastic deformation also increases, the coefficient of overstrain with heterogeneity declines. This is shown in an augmented number of slip tracks and in an increase in the mean effective strain required for deformation of the alloy [4, 5].

The distribution deformation between its mass and the boundary layer of a grain is changed with increased content of magnesium in the alloy. The share of deformation proceeding at the grain boundary declines irregularly with concentration of magnesium. This indicates a more intensive strengthening of the boundaries as compared with the mass of the grain in low-alloyed alloys than with alloys of larger magnesium content. This phenomenon may be explained by the irregular distribution of atoms of the alloying element in the alloy grain. The boundary layer of the grain in the alloy has a more distorted lattice than its mass, so that there are more of such distortions in which the presence of

VOL
5
195

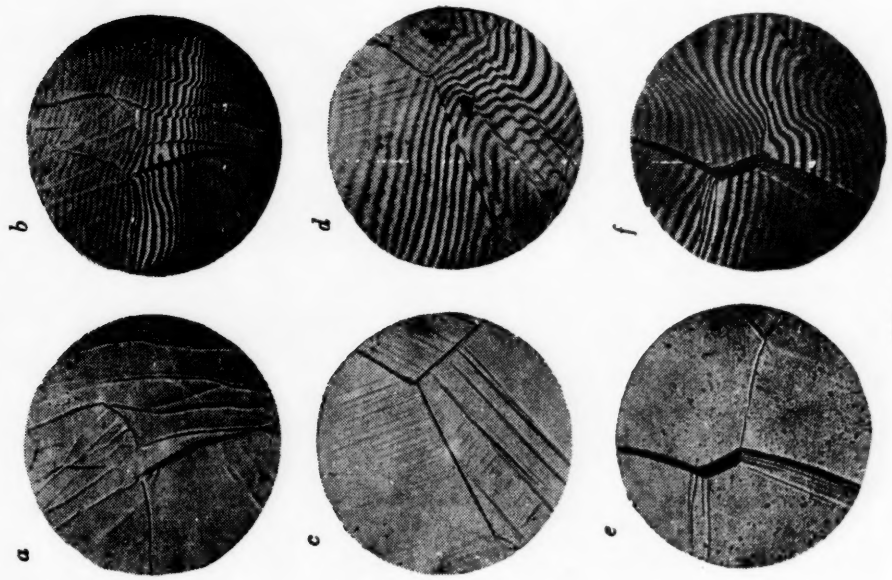

FIG. 13.

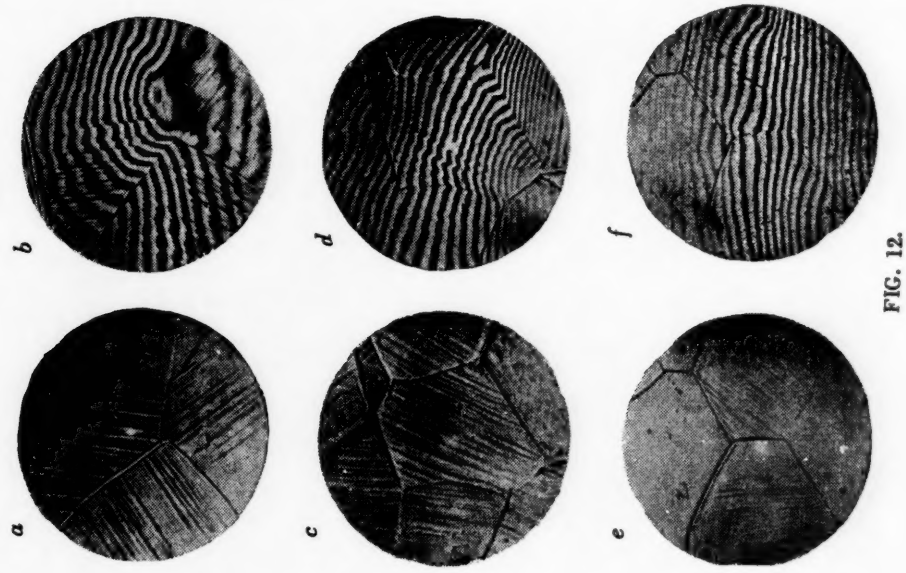

FIG. 12.

magnesium atoms leads to partial readjustment of the lattice [12]. The foreign atoms, so to speak, block distortions, make them less mobile [13], so that the grain boundaries of weakly alloyed alloys prove to be stronger than their mass. With the reduction of such distortions further enrichment of the boundaries is slowed up.

The blocking of lattice distortions by magnesium atoms is shown in the fact that, at a high temperature, the slip tracks, with increasing magnesium in the alloy, become more rectilinear. Temperature fluctuations indeed prove to be insufficient for

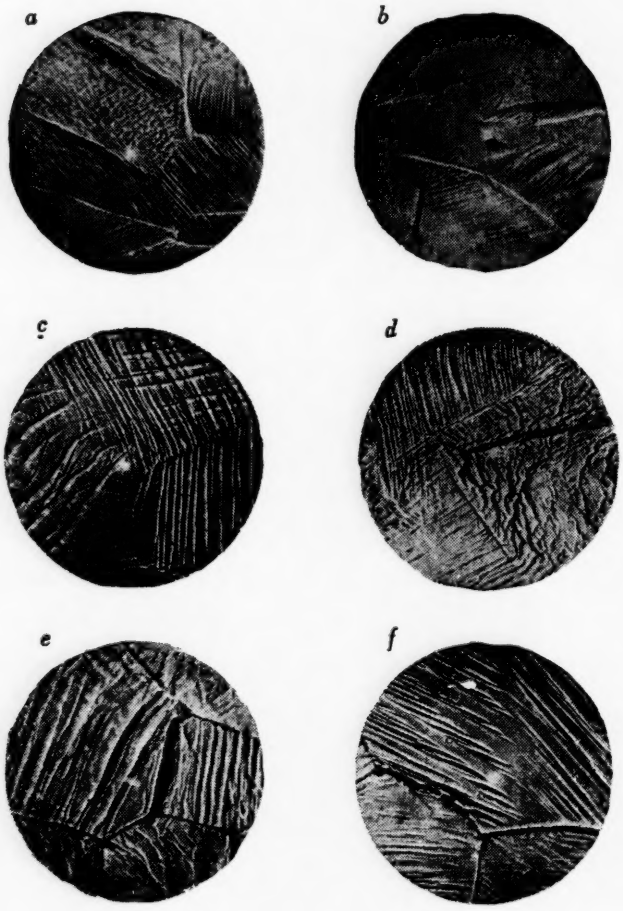

FIG. 14.

creating in the grains obstacles to rectilinear distribution of displacement.

Extension of the temperature range for the appearance of deformation bands in the direction of high temperatures is caused by increase in heterogeneous stresses in the grains, arising through their interaction. Magnesium strengthens the mass and the boundaries of the grains. This raises the elastic limit of the alloy and reduces stress relaxation at the grain boundaries, whereby heterogeneous stresses in the grains are increased and distribution of shear (displacement) is difficult. Moreover, heterogeneous stresses may induce in the grains processes of upward diffusion, leading to a lowering of stresses at points of incipient near deformation, with creation in the grains of concentrated heterogeneities, so that, for propagation of plastic deformation higher external strains are needed.

SUMMARY

The introduction of magnesium into aluminium changes the mechanism of plastic deformation of the alloy. The observed change of mechanism permits a revelation of the causes of the strengthening of aluminium due to the existence therein of magnesium atoms.

Alloying of aluminium with magnesium leads to more complete and uniform participation of the whole mass of metal grain in the process of plastic deformation, so that such deformation starts under higher external strains.

A part of the distorted lattice existing at the boundary and in the mass of the grain is blocked

by magnesium atoms. This reduces their mobility, so that the forces required for deformation of the alloy are increased. The amount of distortions at the boundary and in the mass of the grain is not the same, so that blocking of these distortions by magnesium leads to a more intensive strengthening of the boundaries as compared with the mass of the grain when the alloys magnesium content is low.

The heterogeneous stresses (strains) due to interaction of grains at their boundaries increase with increase in magnesium content. This hinders distribution of shear in the grain, i.e. augments the alloy's resistance to deformation. Moreover, these heterogeneous stresses may produce in the alloys processes of upward diffusion that hinder initiation and distribution of plastic deformation.

Translated by

REFERENCES

1. C. Jenkins and G.J. Mellor, *Iron and Steel Inst.* 132, 179, (1935).
   D. McLean and M. Fasmer, *J. Inst. Metals.* 83, 1558, (1954).
   T. Nagashima and T. Yamomoto, *Acta Met.* 4, 94, (1956).
   N.J. Millendore and J. Grant, *J. Metals*, 6, 975, (1954).
2. E. Shmid and V. Boas, *Plastichnost kristallov v osobennosti metallichesk. (Plasticity of crystals, especially metallic)*, *State United Publishing House of Science and Technology*, p. 239. (1938).
3. Ch. S. Barrett, *Struktura metallov (Structure of metals)*, Metallurgizdat, (1948).
4. M.V. Yakutovich, *Trud. Inst. fiz. met. Urals fil. Akad. Nauk*, 12 p. 12, (1947).
5. G.V. Kurdyumov, *Problemy metallovedeniya i fiz. metallov*, 4, 321, (1955).
6. S.O. Tsobkallo and V.V. Latsh, *Izv. Akad. Nauk SSSR*, ser. fiz. 17, 3, (1953).
7. S.T. Konobeevskii, *Zh. eksp. teor. fiz.* 13, 200, (1945).
8. W. Koster, Zeit. Metallk. 39, 1, (1948).
   V.A. Pavlov, N.F. Kryuchkov and I.D. Fedotov, *Fiz. metal. metalloved.*
   N.I. Noskova, V.A. Pavloc, and B.A. Yunikov, *Fiz. metal. metalloved.* 3, 3, (1956).
9. H. Axon, D. Phil and W. Hume-Rothery, *Proc. Roy. Soc.* 193, 24, (1948).
10. A.V. Grin, V.A. Pavlov and I.A. Pereturina, *Fiz. metal. metalloved*, (1957).
    I.I. Kornilov and L.I. Pryakhina, *Dokl. Akad. Nauk SSSR*, 87, 971, (1952).
    J.E. Dorn, P. Petrokowsky and F.E. Tietz, *J. Metals*, 2, 933, (1950).
    O.D. Sherby, R.A. Anderson and J.E. Dorn, *J. Metals*, 3, 643, (1951).
11. V.C. Averkiev, G.N. Kolesnikov, V.A. Pavlov and M.V. Yakutovich, *Zh. tekh. fiz.*, 16, 349, (1946).
12. V.I. Arkharov, *Trud. Inst. fiz. met. Urals fil. Akad. Nauk*, 8, 54, (1946).
13. A. Cottrell and B. Bilby, *Proc. Phys. Soc.* 62, 49, (1949).

VOL. 5 1957

THE EFFECT OF PHASE TRANSFORMATION IN A SOLID SOLUTION ON PLASTIC DEFORMATION

1. "UNIFORM" DEFORMATION*

N. F. SIUTKIN

Urals State University im A.M. Gor'kii

(Received 26 July 1956)

A study was made of the stepwise plastic deformation, in the "uniform" deformation range at various temperatures, of cylindrical testpieces made from an alloy of zinc with 20 per cent aluminium. It was found that the first steps in deformation occur almost at the very outset of the rectilinear portion of the rising section of the stress-strain diagrams, i.e. even in the range commonly averred to be "elastic". A possible mechanism is put forward for the occurrence of stepwise deformation.

INTRODUCTION

The process of plastic deformation in metals is intrinsically a non-uniform process, as can be seen, in particular, in the fact that when some metals and alloys are extended in certain temperature ranges, the deformation takes place in a series of sudden steps. In all these cases the diagrams have (in the obviously plastic range) a saw-tooth shape on the stress-strain curve. The phenomenological explanation of the interruptions in stress, observed on stress-strain diagrams when the deformation is stepwise, must be attributed to Davidenkov and Miroliubov [1].

It has been found by experiment, that stepwise deformation is most pronounced in alloys which constitute supersaturated solid solutions, when they are deformed in a temperature range corresponding to rapid breakdown. It has therefore been suggested that when supersaturated solid solutions are deformed, two interacting processes are superimposed, namely, plastic deformation proper and phase transformation [2].

The precipitating phase itself sets up non-uniform stresses within the solid solution, due to the difference in specific volumes between the precipitate and the matrix phases. These stresses allow further breakdown of supersaturated solid solution and the growth of particles which have already been precipitated. According to the views of Konobeevskii [3], the precipitating nuclei experience the effects of normal stresses only; in the solid solution lattice near the particles shear stresses are also developed, which can bring about plastic deformation if they are of sufficient magnitude.

It can be suggested that the interaction between phase transformation of this type and plastic deformation makes it possible to utilize the supersaturated state of the solid solution as a factor to increase the sensitivity of the experimental technique for studying both the initial and the later stages of plastic deformation in alloys, i.e. to examine as completely as possible the details and the shape of the stress-strain curve and to increase the accuracy of existing ideas on the mechanism of plastic deformation.

For this investigation we chose an alloy of zinc and aluminium, which possesses "super-ductility" [4] at elevated temperatures, i.e. in which one could expect the strongest interaction between phase transformation and plastic deformation. For comparison purposes, tests were carried out on the alloy in two conditions, quenched and aged.

In the present communication, data are given on stepwise plastic deformation during "uniform" elongation, i.e. up to the stage when a neck is formed.

PREPARATION OF TESTPIECES AND EXPERIMENTAL PROCEDURE

The material used for preparing the testpieces was 2 to 2.3 mm. diameter wire made from an alloy of technical pure zinc and aluminium (20% Al). The testpiece gauge length was 30 or 35 mm. The testpiece diameter was gauged to an accuracy of 0.01 mm.

The testpieces were water-quenched from a

*Fiz. metal. metalloved., 5, No. 3, 508-515, 1957.

FIG. 1. Stress-strain diagram for a quenched testpiece at 200°C. Strain rate 2 x 10^{-4} cm/sec.

temperature of 375°C, after holding for two hours. To ensure a constant period between the conclusion of quenching and the commencement of testing, each testpiece was quenched individually directly before testing.

The ageing of previously quenched testpieces was carried out with a stepwise reduction of temperature. With increasing annealing temperature, the holding time was increased. The total ageing time was 250 hours.

Testing was carried out on a tensile machine [5] at strain rates of 2 x 10^{-4} and 2 x 10^{-2} cm/sec and temperatures of 0,20, 100, 150, 200, 250, 300, 350 and 375°C. The testing temperature was maintained within an accuracy of ± 1°C. For the tests at 0°C, the electric furnace was replaced by a cryostat filled with a mixture of water and ice.

The photographic method used for recording the stress-strain diagrams made it possible to obtain a very fine line of any required density.

At each temperature and strain rate not less than three tespieces were pulled, as a rule. In all 92 diagrams were taken.

EXPERIMENTAL RESULTS

We have shown previously [6] that the fine detail of a stress-strain curve can only be recorded successfully on the diagram at a quite definite intensity of the light beam for each strain rate and temperature. Any change in the material affecting the velocity of the light beam across the photographic film, brings about a marked change in the blackening of the curve. A series of separate "points" and "teeth" is obtained on the diagram, characterizing the stepwise nature of the plastic deformation.

Fig. 1 shows a photograph of the diagram obtained on pulling quenched testpieces. Separate "points" and stress interruptions ("teeth") can be seen not only in the obviously plastic region but also in the rectilinear portion of the rising section. In all the diagrams it can be seen that the first jump takes place almost at the very outset of the rectilinear portion of the rising sections, i.e. in the strain range commonly averred to be "elastic", at stresses substantially below the so-called elastic limit. Measurements show that the difference in stress corresponding to two adjacent steps does not remain constant.

The stresses at which the first steps occur and the mean difference in stress corresponding to two adjacent steps, increase slightly with increasing strain rate.

With increasing testing temperature the number of steps on the rectilinear rising section of the stress-strain diagram falls off. Fig. 2 shows the relationship between stress at which the first step occurs and the testing temperature, for two strain rates on quenched testpieces. It can be seen from the graph that as the strain rate is increased and the temperature lowered the curve depicting the relationship between stress for the first step and testing temperature reaches higher values; at high temperatures, however, the stress for the first step is almost independent of strain rate. The stresses at which the first steps occur and the mean difference in stress corresponding to two adjacent steps, decrease with increasing testing temperature, reaching minimum values at 250°C.

As the maximum stress on the stress-strain curve is approached, the "jumps" assume a more pronounced stepped or saw-tooth nature, than on the rectilinear rising section and the curve takes on a distinct curvature.

The steps on the rectiliniear rising section for aged testpieces are considerably smaller and appear at higher stresses and temperatures.

It may be suggested that the appearance of steps

VOL. 5 1957

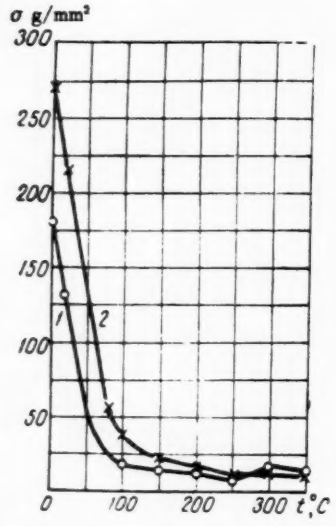

FIG. 2. Graph of variation with temperature of the stress corresponding to the occurrence of the first jump in quenched testpieces:
1 – strain rate 2 x 10^{-4} cm/sec;
2 – strain rate 2 x 10^{-3} cm/sec.

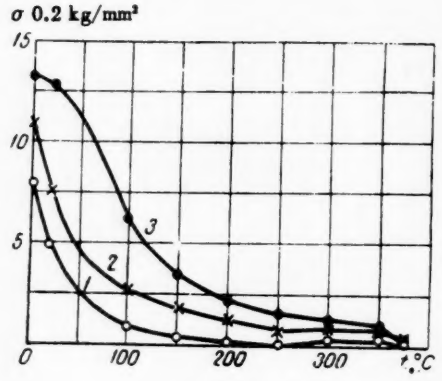

FIG. 3. Graph of variation with temperature of the resistance to strain for a constant strain of 0.2 per cent:
1 – quenched condition, strain rate 2 x 10^{-4} cm/sec;
2 – quenched condition, strain rate 2 x 10^{-2} cm/sec;
3 – aged condition, strain rate 2 x 10^{-2} cm/sec.

on the rectilinear rising section of the diagram is due to peculiarities in the testing machine used and is not connected with the behaviour of the material being strained. A "stepwise" form in the initial part of the diagram could be caused by: (1) oscillations in individual parts of the system used as a dynamometer (ring, spring, rotating mirror, etc,); (2) operational faults in the loading side of the machine (gear drives, friction clutch); (3) periodic changes in the intensity of the a.c. -supplied light source; (4) stepwise slipping of the tespiece in the shackles.

Experimental checks on these possibilities showed that the appearance of jumps on the rectilinear rising section of the stress-strain diagrams was in fact due to the properties of the alloy under investigation in this work and was unconnected with the peculiarities of the testing equipment used.

From the stress-strain diagrams for quenching and for aged alloys the following relationships were found:

(*a*) the resistance to strain against temperature at a constant value of 0.2 per cent strain (Fig. 3);

(*b*) the limiting strength (U.T.S.) against temperature (Fig. 4);

(*c*) the uniform elongation against temperature (Fig. 5). The final values of these parameters were found from the arithmetical averaging of the values found from each of the diagrams taken under the given conditions.

It can be seen from Fig. 3, that, for the quenched condition, the resistance to strain falls sharply with increasing temperature, reached a minimum at 250°C, beyond which it increases slightly up to 350°C and then falls again. Thus the resistance to strain increases somewhat on entering the solution range of the precipitate phase. On entering the solution range of the precipitate phase, i.e. above a temperature of 275°C, the resistance to strain increases relatively more at low strain rates than at high strain rates. From Figs. 2 and 3 it can be seen that the value of resistance to strain calculated according to the first step visible on the diagram, is about one-tenth the resistance to strain for 0.2 per cent strain, which corresponds to a proof stress σ 0.2.

For the aged condition, the resistance to strain again falls with increasing temperature, but differs from the corresponding quenched condition both in the magnitude of the change and in the absolute magnitude.

The curves depicting the variation in ultimate tensile strength with temperature for the quenched condition (Fig. 4) have the same general form as the curves depicting the variation in resistance to strain with temperature. For the aged condition, the ultimate tensile strength falls almost linearly with increasing temperature. The curves depicting the variation of ultimate tensile strength with temperature,

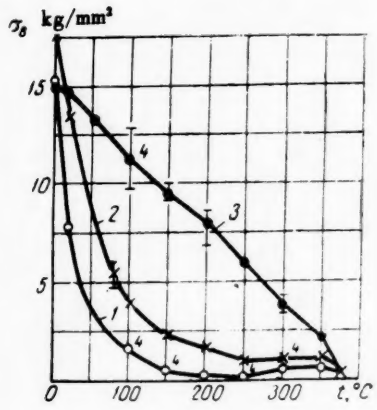

FIG. 4. Graph of variation with temperature of the ultimate tensile strength:
1 – quenched condition, strain rate 2 x 10^{-4} cm/sec;
2 – quenched condition, strain rate 2 x 10^{-2} cm/sec;
3 – aged condition, strain rate 2 x 10^{-2} cm/sec.

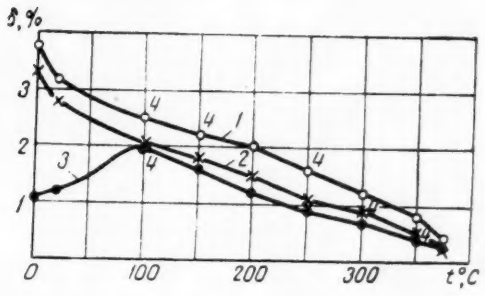

FIG. 5. Graph of variation with temperature of the uniform elongation:
1 – quenched condition, strain rate 2 x 10^{-4} cm/sec;
2 – quenched condition, strain rate 2 x 10^{-2} cm/sec;
3 – aged condition, strain rate 2 x 10^{-2} cm/sec.

VOL. 5 1957

for the quenched and for the aged conditions, actually coincide at a temperature of 375°C.

The uniform elongation for the quenched condition (Fig. 5) decreases almost linearly with increasing temperature. Thus, with increasing temperature, the maxima on the stress-strain diagrams are displaced in the direction of smaller strain values. For the aged condition, the uniform elongation increases up to temperatures of 100°C and then falls almost linearly.

DISCUSSION OF RESULTS

In a supersaturated solid solution, whatever the external stress influences, there occur processes of the formation of so-called "pre-transition" structure, which leads to breakdown of the solid solution. The occurrence of such formations is facilitated by non-uniformity in the crystal lattice, even if in small volumes of the crystal and possibly only in the presence of nucleation diffusion.

The precipitating phase sets up a state of non-uniform stress within the solid solution, due to the difference in specific volume between the precipitating phase and the matrix, the magnitude of the stresses depending on the dimensions of the precipitate nuclei. These stresses increase the nucleation diffusion and still further facilitate the nucleation and growth of new crystallization centres.

A real crystalline substance, particularly when polycrystalline, is very non-uniform as regards structure (inter-crystalline zones, mosaic structure, inclusions etc.). Therefore an applied external force sets up in a testpiece a condition of non-uniform stress, which also gives rise to nucleation diffusion of the dissolved component, as a result of which new centres of crystallization nucleate and grow. As the external force is increased, the diffusion process is speeded up and there is a corresponding increase in the number of precipitate particles forming and an acceleration in the rate of growth of those already formed.

In the precipitating crystallites of excess phase and the solid solution surrounding them normal and shear stresses are set up, which increase together with the precipitating particles. At each instant of time these stresses are superimposed upon the stresses set up by the applied load. Thus the precipitating crystallization centres and surrounding solid solution come under the influences of a resultant non-uniform stress field.

When the total resultant forces in the solid solution surrounding certain precipitating crystallites of excess phase reach the critical value, plastic strain – a jump – occurs. A diagram of a jump, based on ideas developed previously by Davidenkov, is illustrated in Fig. 6. The resistance to deformation drops immediately the jump is initiated (the portion *ab* on the dotted line) whereas the load drops considerably more slowly due to the terminal rigidity

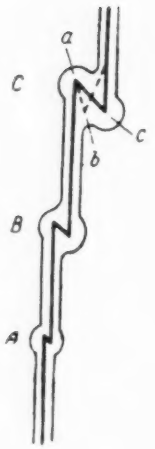

FIG. 6. Diagram of the change in resistance to strain and external load during the jumping process.

of the dynamometer and also to the inertia of the machine parts (the portion *ac* on the solid line). Consequently in the first phase of the jump, the deformation occurs at an accelerated speed and as a result the strain rate in the individual, quite small volumes in which plastic shear occurs, will be many times greater than the mean strain rate. Then the weakened resistance to strain is restored due to work-hardening, whilst the load continues to fall as the strain increases. The plastic deformation slows down and eventually stops. The elements of the testpiece volume in which strain has occurred in the jump process work-harden, and as a result there is a redistribution of stresses in the testpiece.

However, the stress redistribution causes new crystallization centres to form and those already precipitated to grow. When the load is increased further, the internal stresses begin to increase, together with the elastic strain on the testpiece. Conditions again arise in which the resultant stresses in the solid solution surrounding certain precipitated crystallites of excess phase reach the critical value and another jump is propagated. This process repeats itself until plastic strain can be transferred to weaker areas along the testpiece length.

Fig. 6 shows on an enlarged scale the shape of the rectilinear rising portion of the diagram in the form in which it is recorded by the light signal. This shape shows that when the magnitude of the jump is small (*A*) the light signal moving along the full line, leaves a trace in the form of a point, when the jump is large (*B*), in the form of a step, and when considerably larger (*C*), in the form of a break. Hence it follows that the stress also falls when small-strain jumps occur, but the fall is not discernible on the diagram because of its insignificant magnitude.

If, during the jump, plastic deformation occurs near a relatively few crystallization centres (i.e. when the total amount of plastic strain is relatively small) the recording method used may not register the occurrence of this jump on the stress-strain curve, which may be the case particularly in the earliest stages of deformation. It follows from what has been said that purely elastic deformation of the testpiece only takes place from the start of the test until the first jump appears, and, since the latter may not always register, it is impossible to establish an elastic limit and a physical yield point, and these concepts can be classed as purely conditional.

The appearance of the first jumps in the rectilinear upward section of the stress-strain diagram is conditioned by the rate of decomposition of the given supersaturated solid solution and by the time which has elapsed between quenching and starting the test. The amount and speed of transformation during ageing depend on temperature and on the alloy composition, with respect to major constituents and impurities.

It can be taken that the critical resultant stress at a given testing temperature is more or less constant. Therefore, with increasing external load, the critical resultant stress is reached at lower values of the stress due to precipitation of the new phase and near larger and larger numbers of nucleating centres of crystallization. Consequently, plastic strain will also take place in an increasing volume of the solid solution, as the load is increased. The increase in the amount of plastic strain associated with an individual jump causes a sharper drop in resistance to strain and in the load during the jump; this also determines the shape of the steps at the end of the rectilinear rising section, particularly as the maximum stress on the diagram is approached.

As the strain rate is increased, the increase in the rate of growth of the crystallization centres, and consequently of the stresses set up by them, is on a smaller scale than the increase in the rate of growth of the stresses set up by the load. Therefore the resultant stresses reach the critical value at smaller stresses due to the precipitating phase, but at higher external stresses (work-hardening due to strain rate) which are also recorded on the diagram

VOL 5 195

whilst the jumps are taking place.

Increase of the temperature, like that of the applied load, accelerates the processes of nucleation and growth of the crystallization centres, which leads to an increase in the stresses due to the precipitating phase; at the same time the crystal lattice bonds are weakened, thus lowering the value of the critical resultant stress. As a result of this, the resultant stresses in the solid solution near the precipitating crystallization centres reach the critical value at lower loads.

Increase in the strain rate also has a less pronounced effect, as the rate of increase of internal stresses due to the precipitating phase becomes much greater.

In the temperature range in which the precipitating phase goes back into solution, the same mechanism of jump formation takes effect: when a testpiece, not under load, is heated up to temperatures below that at which the precipitating phase dissolves, a certain number of crystallization centres form in the material of the testpiece as a result of the breakdown of supersaturated solid solution. On entering the solution range, the number of particles decreases. The dissolution process reduces the stresses in the particles and the solid solution surrounding them, whereas the load increases them. Therefore the resultant stresses reach the critical value at somewhat higher loads. With increasing strain rate the stresses near the crystallization centres, due to the precipitating phase are reduced to a less extent by dissolution, and correspondingly the external loads at which the first jumps are exhibited, are somewhat lower than at the lower strain rate (see Fig. 2).

For testpieces in the aged condition the mechanism of jump formation remains the same. During ageing (not under load) breakdown occurs in a considerable volume of the testpiece, but because of coagulation only a relatively small number of crystallization centres is precipitated. The remainder of the solid solution only breaks down when the temperature is raised and under the influence of a load. Thus, at low temperatures jumps only occur in accordance with the number of crystallization centres already precipitated during ageing, whereas at higher temperatures they also occur in accordance with the breakdown of the residue of supersaturated solid solution remaining after ageing. In order for the resultant stresses in the solid solution near the precipitating crystallization centres, which stresses are substantially reduced during ageing by diffusional relaxation, to reach the critical value, a higher external load must be applied to the tespiece. This means that, up to comparatively high loads, the testpiece extends elastically, and jumps are therefore only exhibited at the end of the rectilinear rising section of the stress-strain diagram and in the region adjacent to the maximum load.

The critical value of resistance to plastic deformation in a super-saturated solid solution is overcome by a resultant stress, namely the stress caused by the action of the external load and the stresses set up by precipitation of the new phase. As the loading is increased the process of nucleation and growth of crystallization centres is accelerated, and consequently the stresses they produce are increased. Therefore the average difference in load corresponding to two successive jumps decreases, i.e., there is a decrease in the increment of that part of the resistance to deformation of the testpiece, which is overcome by the external load. The effective work-hardenability of the alloy falls off as the jumps succeed each other. By "effective work-hardening" is meant that part of the work-hardening which is due to the action of external forces. When the increment of effective work-hardening becomes insignificant, the deformation loses stability and becomes localized in one point along the testpiece length; the process of step-wise deformation is also intrinsically altered. This amount corresponds to the attainment of the maximum load in the stress-strain diagram plotted in nominal stress-elongation co-ordinates.

The ultimate tensile strength characterizes that part of the maximum resistance to plastic deformation of the alloy, during "uniform" plastic deformation, which is overcome by the external load. With increasing temperature, the ultimate tensile strength falls, not only because of weakening of the bonds in the inter-crystalline zones and the crystal lattice, but even more because of the formation of new phase, which leads to redistribution of the resultant stresses. Therefore the drop in ultimate tensile strength with increasing temperature takes place more rapidly in specimens in the quenched condition than in those in the aged condition, in which the phase transformation has already occurred.

CONCLUSIONS

1. The occurrence of stepwise deformation has been experimentally established in that stage of the extension process which is depicted on ordinary stress-strain diagrams (in the co-ordinates $P - \Delta l$) as a rectilinear rising portion of the curve, i.e. in the strain range normally averred to be "elastic", at stresses substantially below the so-called

VOL. 5 1957

elastic limit.

2. Study of the changes in exposure density on various parts of nominal stress-elongation diagrams obtained by photographic recording, facilitates a more detailed elucidation of the fine structure of stress-strain curves.

3. Examination of the fine structure of the early part of stress-strain curves for quenched alloys facilitates a more precise picture of the mechanism underlying the interaction between the breakdown processes in supersaturated solid solutions and plastic deformation.

4. The critical value of resistance to plastic deformation in age-hardening alloys is overcome by the resultant of two stresses, namely (1) the stress due to the action of the external load and (2) the stresses set up during precipitation of the new phase. The relationship between these two types of stress depends on the structure of the alloy, the mean strain rate of the testpiece and the testing temperature.

5. The elastic limit and the physical yield point are macroscopic, i.e. average, concepts, whereas it is only possible to speak of a true elastic or yield limit in the case of uniformly distributed deformation over all the micro-volumes of the material under test, since plastic deformation occurrs very early, well within the "elastic" range.

Translated by E. Bishop

REFERENCES

1. N.N. Davidenkov and I.N. Miroliubov, *Zh. tekh. fiz.*, 6, 60 (1936).
2. G.N. Kolesnikov, E.S. Iakovleva and M.V. Iakutovich, *Zh. tekh. fiz.*, 19, 347 (1949).
3. S.T. Konobeevskii, *Zh, eksp. teor. fiz.*, 13, 200 and 418 (1943).
4. A.A. Bochvar and Z.A. Sviderskaia, *Izv. Akad. Nauk SSSR, otd. tekh. nauk*, 9, 821 (1945).
5. V.S. Averkiev, G.N. Kolesnikov, V.A. Pavlov and M.V. Iakutovich, *Zh. tekh. fiz.*, 16, 1349 (1946).
6. N.F. Siutkin, *Dokl. Akad. Nauk SSSR*, 91, 83 (1953).

VOL 5 195

ON THE ACCELERATION OF THE AGEING PROCESS IN ALLOYS OF ALUMINIUM WITH MAGNESIUM UNDER THE INFLUENCE OF SMALL ADMIXTURES OF SILVER AND ZINC

ON THE QUESTION OF THE CAUSES OF THE EFFECTS OF SMALL ADMIXTURES ON THE KINETICS OF THE AGEING OF ALLOYS III*

V.I. ARKHAROV, I.P. BERENOVA and L.M. MAGAT

Urals State A.M. Gor'kii Institute, Sverdlovsk Branch, V.N.I.I.M.

(Received 17 July 1957)

VOL. 5 1957

AIM OF THE PAPER AND FORMULATION OF THE PROBLEM

The ageing of alloys, which is made use of in practice as a method of controlling the physical properties of technical materials, is subject to the influence of admixtures. This effect is in turn used in practice to regulate the ageing process and to control the properties of the alloys thereby. The choice of admixtures for these purposes is in the main made on an empirical basis. For a scientifically well founded approach to this problem it is necessary to study the effect of admixtures on the separation of supersaturated solid solutions.

There are grounds for supposing that this mechanism is complex and is by no means confined to a simple change of the degree of supersaturation of the solid solution by the admixture which is the third component [1]. Apparently, it is possible for internal adsorption to occur on pre-transitional formations at the stage of the preparation of the supersaturated solid solution for separation. Moreover, in the zones of adsorption the pre-transitional processes are not the same as without adsorption. The effect of the third component (the admixture) on the ageing process through the change of the degree of supersaturation or through internal adsorption is of quite a different physicochemical nature; therefore the regulation of this effect and the qualitative and quantitative composition of the admixture will, of course, be quite different depending on the mechanism of the effect of the different elements which make up the composition of the alloy. From this flows directly the need for the detailed examination of the question of the effect of the admixtures of the third component of the solubility of the supersaturating component in the ageing alloy. In the absence of a sufficiently pronounced change in solubility the effect of the admixture on the ageing process must be connected with internal adsorption.

Previously this question has been investigated in relation to ageing alloys of the type of the solid solution of copper in aluminium with admixtures of zinc or silver [1-3], and conclusions were derived as to the affinity of these admixtures to solid solutions on an aluminium basis and on the adsorptional nature of their effect on the separation of the supersaturated solid solution of Cu in Al. Conclusions on the affinity of the admixtures Zn and Ag to Al were also obtained in paper [4].

For the further investigation of this problem alloys on the basis of the binary system Al-Mg were selected; this system forms the basis for many technically important ageing alloys. As admixtures, Zn and Ag were chosen, for which on the basis of what has been said earlier one may suppose an affinity to aluminium as the solvent. In paper [5] the accelerating effect of small admixtures of Zn on the ageing of Al-Mg solutions was observed.

METHOD OF INVESTIGATION AND DESCRIPTION OF EXPERIMENTS

The alloys were made from aluminium of 99.97 per cent and 99.99 per cent purity, magnesium of 99.91 per cent, zinc of 99.91 per cent purity and electrolytic silver, in porcelain crucibles under a layer of a smelted mixture of 50 per cent NaCl and 50 per cent KCl, at an oven temperature of about 850°C. The magnesium was introduced into the alloys in the form of a ligature prepared in advance; zinc and silver were introduced directly, after melting down the alloys were carefully stirred with a porcelain stick. The weight of each ingot was about 7 – 10 g; from every smelt 2 – 3 samples were prepared.

For the investigation of the effect of additions of zinc and silver on the ageing process of a solid

* *Fiz. metal. metalloved.* 5, No. 3, 516-526, 1957.

TABLE 1. Chemical composition of alloys (per cent weight of the alloyed elements, remainder aluminium)

Alloy No.	Magnesium	Zinc	Silver
1	8.0	—	—
2	8.0	0.5	—
3	8.0	1.0	—
4	8.0	—	0.5
5	8.0	—	1.0
6	10.0	—	—
7	10.0	0.2	—
8	10.0	1.0	—
9	10.0	—	0.2
10	10.0	—	1.0

TABLE 2. Chemical composition of alloys (per cent weight of the alloyed elements, remainder aluminium)

Alloy No.	Magnesium	Zinc	Silver
1	10	—	—
2	10	0.2	—
3	10	1.0	—
4	10	—	0.2
5	10	0.2	0.2
6	10	1.0	0.2

TABLE 3. Chemical composition of alloys (per cent weight of alloyed elements, remainder aluminium)

No.	Magnesium	Zinc	No.	Magnesium	Zinc	No.	Magnesium	Silver
1	3.6	—	13	6.2	1	26	5.0	0.5
2	6.2	—	14	6.4	1	27	5.7	0.5
3	7.3	—	15	7.7	1	28	6.5	0.5
4	10.0	—	16	10.0	1	29	7.1	0.5
5	11.0	—	17	13.0	1	30	3.6	1.0
6	13.0	—	18	2.0	2	31	6.0	1.0
7	5.0	0.5	19	4.0	2	32	6.2	1.0
8	5.5	0.5	20	5.3	2	33	7.7	1.0
9	6.4	0.5	21	6.0	2	34	10.0	1.0
10	6.9	0.5	22	8.0	2	35	13.0	1.0
11	11.0	0.5	23	9.0	2	36	11.0	0.5
12	3.6	1.0	24	12.0	2			
			25	14.0	2			

solution of magnesium in aluminium, alloys were prepared (from aluminium of 99.97 per cent purity) of the compositions set out in Table 1. Besides, the following ternary and quaternary alloys from aluminium of 99.99 per cent purity were prepared (Table 2).

To determine the solubility of magnesium in aluminium in the presence of zinc or silver the following alloys were prepared from aluminium of 99.97 per cent purity (Table 3).

Finally, alloys were prepared for which the lattice constants of phase T and of the α solid solution were determined (Table 4).

After casting all samples were deformed and annealed for 10 to 20 hr at a temperature of 450°C for homogenisation. The annealing was interrupted two or three times and the alloys were additionally deformed. After annealing the alloys were quenched in water.

The effect of zinc and silver on the process of separation of the supersaturated solid solution of magnesium in aluminium was investigated by means of the X-ray analysis of the lattice constant of the solid solution at consecutive stages of ageing. From this data curves were constructed with the lattice constant and the time of ageing at a given temperature as co-ordinates.

For the study of the effect of additions of zinc and silver on the solubility of magnesium in aluminium curves of the dependence of the lattice constant

TABLE 4. Chemical composition of alloys (per cent weight of alloyed elements, remainder aluminium)

Alloy No.	Magnesium	Zinc
1	5.0	4.0
2	6.3	6.0
3	7.6	4.0

of the solid solution on the magnesium content were constructed.

After quenching the surface of the samples was cleaned by polishing and the deformed surface removed by etching. The samples on which the ageing process was observed were after quenching and etching once more annealed for 10-15 min, again quenched in water and etched.

The second variant excluded the possibility of the deformation affecting the surface layer (in case it had not been completely removed by etching) on the course of the ageing process. The value of the lattice constant was the same for both variants of the treatment.

The ageing process was conducted with interruptions for X-raying the samples, while the state of the sample was fixed by quenching. The samples were only etched to remove the surface layer since it was found that the lattice constant in these cases does not change with increasing distance from the surface of the sample.

The samples were X-rayed by the method of back-reflection in a KROS-1 camera. Copper radiation was used and the measurement made on the lines (511) – (333) K_{α_1}. The distance sample-film was measured by exposing a standard (pure aluminium). The temperature of the sample during exposure was 20 ± 2°C. The error of measurement of the lattice constant was ± 0.0004 Å, except for diffraction patterns with diffuse lines (at certain stages of ageing) for which the accuracy was of the order of ± 0.001 Å.

The lattice constant of the T-phase was determined from Debye photographs taken of the surface in an Ivensen-type camera with chrome radiation. For the measurement the line (530) K_α was used. The position of this line was determined with the help of a measuring microscope relative to the line (111) K_β of the solid solution, the constant of which for the same samples was determined by the method of back-reflection. The accuracy of the measurement of the constant of phase T was ± 0.03 Å.

The effect of additions of zinc on the ageing process was studied at temperatures of 250 and 300°C. At 250°C samples of alloys of the following compositions were subjected to ageing: Al + 8% Mg, Al + 8% Mg +0.5% Zn and Al + 8% Mg + 1.0% Zn; at 300°C: Al + 10% Mg, Al + 10% Mg + 0.2% Zn and Al + 10% Mg + 1.0% Zn.

The time of ageing at 250°C was up to 45 hr, at 300°C up to ten hr.

The curves of the dependence of the lattice constant of the solid solution on the magnesium content were constructed for the sections of constant zinc contents 0.5, 1.0 and 2.0 per cent at temperatures of 450 and 300°C.

At the temperature of 300°C the samples which had been quenched from 450°C and deformed were kept for 5 hr and then quenched. After taking the X-ray photograph, the samples were for a second time kept at the temperature of 300°C for 5 hr and once more X-rayed. The lattice constant of the solid solution did not change within the limits of the error of measurement when the time was increased from 5 to ten hr. The constant of the T-phase was measured on samples kept for 5 hr at 300°C and quenched in water.

RESULTS OF THE EXPERIMENTS WITH Al-Mg-Zn ALLOYS

The relation between the lattice constant of the solid solution and the time of ageing at 250°C obtained for alloys of Al + 8% Mg with additions of zinc is graphically represented in Fig. 1.*) In Fig. 2 the analogous curve for alloys with 10% Mg and a temperature of 300°C is shown.

The initial points represent the value of the constant for alloys quenched from the single-phase region and thus provide a control for the magnesium content of the samples, since in small quantities zinc does not affect the lattice constant of the solid solution within the limits of the error of measurement. As can be seen from Fig. 1, the course of the curves for the two samples of Al + 8% Mg, the constant of which in the quenched state differs by 0.0021 Å (which corresponds to a difference in magnesium content of 0.45 per cent) coincide within the limits of error. In other words, a change of the supersaturation by 0.5 per cent Mg does not materially affect the rate of separation.

* In Figs. 1, 2, 6, 7, 8 within each group signs, different signs correspond to different smelts and samples.

VOL. 5 1957

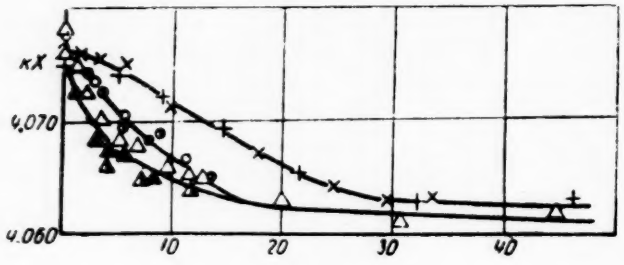

FIG. 1. Change of lattice constant of solid solution with time at 250°C ageing temperature

+ — × Al+8% Mg; • — ○ Al+8% Mg+0.5% Zn; ▲ — △ Al+8% Mg+ +1% Zn.

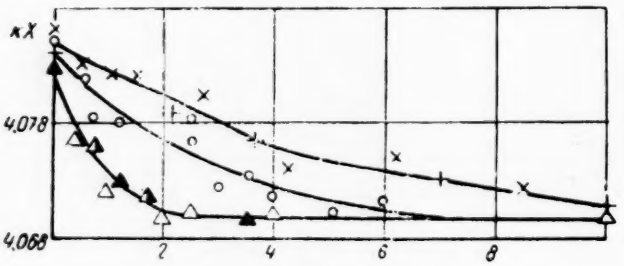

FIG. 2. Change of lattice constant of solid solution with time at 300°C ageing temperature

×—+ Al + 10% Mg, ○—• Al+10% Mg + 0.2% Zn; ▲—△ Al+ +10% Mg+1% Zn.

As can be seen from the figures, additions of zinc considerably accelerate the process of separation, which can be judged from the rate at which the two curves approximate the constant level which corresponds to the approximation of the solid solution to the state of equilibrium. This effect increases with increased zinc content and is more clearly expressed at 300°C than at 250°C. At the temperature of 250°C, 1% Zn at first accelerates the separation 4 to 5 times, then the difference between the alloys with and without zinc gradually evens out. At 300°C the alloy with 1% Zn reaches the state of equilibrium already after 2 hr, while the alloy without zinc does not even reach it after 10 hr. One should also note that the values of the lattice constant for alloys with additions of zinc and without zinc come very close at the later stages.

In Fig. 3 the dependence of the lattice constant of the solid solution on the magnesium content is represented.

If for binary alloys at 300°C a straight, horizontal branch is observed, which intersects the inclined branch at an angle, for alloys containing zinc the horizontal branch begins to bend low even before the intersection with the inclined branch. This bending increases with increasing zinc content. The point of intersection of the two inclined branches moves with increased zinc content in the direction of lower magnesium content.

The results of the measurement of the lattice constant of the *T*-phase and the values of the constant of the solid solution for the same alloys are entered

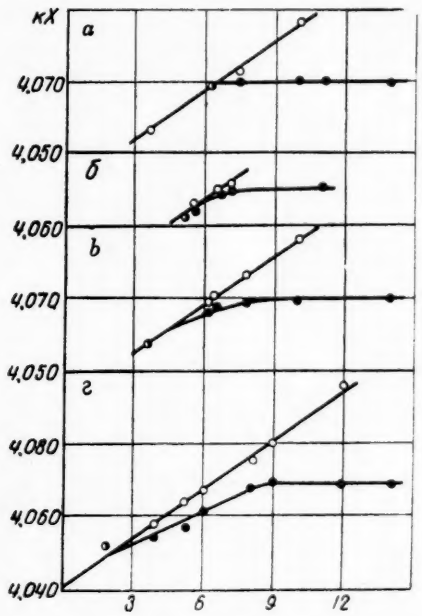

FIG. 3. Dependence of lattice constant of solid solution on concentration of the alloys:

а — Al+Mg; *б* — Al+Mg+0,5% Zn; *в* — Al+Mg+1% Zn; *г* — Al+Mg+2% Zn. ○ — 450° C. ● — 300° C.

TABLE 5. Value of the lattice constant of the *T*-phase and the solid solution at 300°C.

No.	Alloy composition	Lattice constant of *T*-phase, Å	Lattice constant of solid solution, Å	Position of alloy in the isothermal section
1	Al + 3.6% Mg + 1% Zn	—	4.0575	Region $\alpha + T$ (connodal I in Fig. 5)
2	Al + 1% Mg + 2% Zn	—	4.0552	
3	Al + 5% Mg + 4% Zn	14.23	4.0556	
4	Al + 6.3% Mg + 6% Zn	14.26	4.0563	
5	Al + 5% Mg + 0,5% Zn	—	4.0625	Region $\alpha + T$ (connodal II in Fig. 5)
6	Al + 6% Mg + 2% Zn	14.32	4.0616	
7	Al + 7.6% Mg + 4% Zn	14.33	4.0636	
8	Al + 8% Mg + 2% Zn	14.43	4.0682	Region $\alpha + \beta + T$
9	Al + 9% Mg + 2% Zn	14.42	4.0705	

VOL. 5 1957

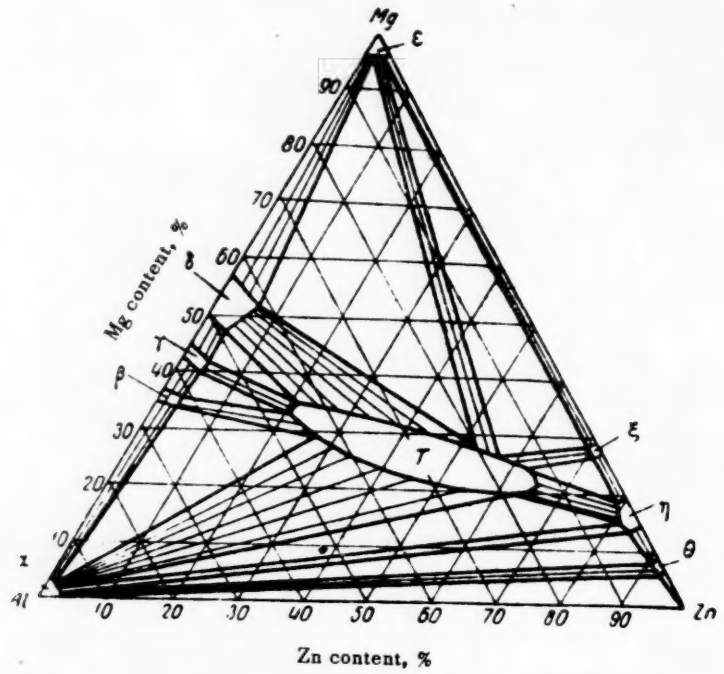

FIG. 4. Scheme of distribution of phase regions at low temperatures after Koester [6]

in Table 5.

DISCUSSION OF THE RESULTS OF THE EXPERIMENTS

The accelerating effect of the admixtures of zinc on the separation of supersaturated solid solution of Mg in Al may be caused either by greater supersaturation or by internal adsorption. In the latter case the mechanism of the effect can be represented as follows. On the periphery of the pre-transitional formations (of the zones of increased magnesium content still coherent with the mother solution) a zone enriched with zinc is formed. This enriching can have two consequences:

(1) at such a high concentration of zinc the limit of magnesium concentration in the solid solution may prove to be lowered considerably and the pre-transitional zone of magnesium enrichment should therefore be precipitated more rapidly, disrupting the cohesion with the mother solid solution: this would mean an accelerating effect of the admixture on the growth of the crystals of the phase that is being precipitated;

(2) through the enriched zone the diffusion of magnesium atoms can proceed more rapidly from the environment to the pre-transitional formation and then (after the disruption of the cohesion with the solid solution) to the small crystal of the phase which is being precipitated; this would mean an accelerating effect of the admixture on the growth of the nucleus of the phase which is being precipitated.

First of all one must find out whether the accelerating effect of zinc on the ageing of the alloy Al-Mg is due to the increase in the general supersaturation. In order to establish to what extent and in which direction an addition of zinc alters the solubility of magnesium in aluminium one must look at the diagram of the ternary system Al-Mg-Zn. This diagram has been studied by a number of authors whose results in the main coincide. A difference is noted in the configuration of the region of the α-solution formed on the basis of aluminium and in the configuration of the region of the T-solution formed on the basis of a ternary chemical compound.

Fig. 4 shows the schematic distribution of the phase regions at low temperatures according to Koester [6]. As can be seen from the diagram, on the aluminium and magnesium side there are regions of solid solutions; on the zinc side the solubility is very small and therefore the homogeneous phase is

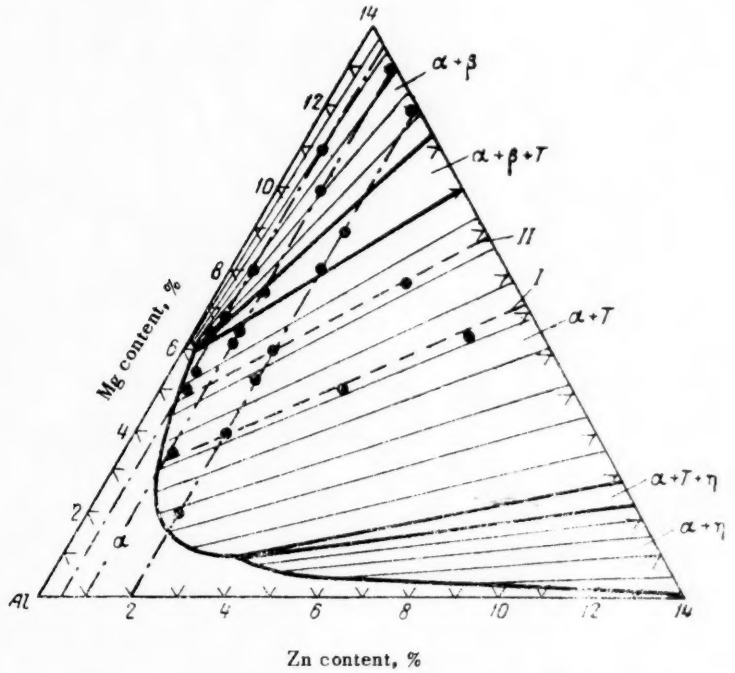

FIG. 5. Isothermal section at 300°C after Fink and Willey [11].
Points mark alloys that have been investigated

identical with pure zinc.

On the Al-Mg side three single-phase regions can be recognised, which according to Kawakami [7] include the chemical compounds Al_8Mg_5, Al Mg, Al_3Mg_4; on the Mg-Zn side there are the regions of homogeneity ξ, η and Φ formed on the basis of the chemical compounds MgZn, $MgZn_2$, $MgZn_3$.

Besides the above mentioned regions, there is the extensive region of the homogeneous phase T, formed on the basis of the ternary chemical compound Al-Mg-Zn.

A number of investigators have come to the conclusion that this compound has the formula $Al_2Mg_3Zn_3$ and has a volume centered cubic lattice. Laves, Loberg and Witte [8] give the lattice constant as 14.16 Å; according to Riederer [9] the constant of the phase T changes within the limits of the homogeneous region from 14.29 Å to 14.71 Å.

At low temperatures the region of homogeneity of the α-solid solution is relatively small. When the temperature is raised, it expands considerably as a result of the increased solubility of magnesium and zinc.

The limits of the α-solid solution have been studied by many authors [10-13]. As a result of their work certain differences of opinion on the quantitative analysis have appeared concerning the position of the limit between the regions α and $(\alpha + T)$. However, the picture of this part of the ternary diagram obtained by all these observers is qualitatively the same to the extent to which we need it for the discussion of our results. This picture is presented on Fig. 5 after the data of [11].

At high magnesium contents and low zinc contents the effect of zinc on the solubility of magnesium is inconsiderable. This is so because the isotherms of of the solubility in the region $(\alpha + \beta)$ approach the side of the concentration triangle under angles of nearly 60°; thus a slight change in the zinc concentration in the alloy leads to a similarly small change in the magnesium concentration in the solid solution.

In alloys lying in the region of equilibrium $(\alpha + T)$ a change in the zinc concentration leads to a comparatively large and disproportionate change in the magnesium concentration in the α-solution.

In alloys with small magnesium concentration even a considerable change in the zinc content does not lead to a material change in the magnesium concentration in the α-solution because the isotherms of solubility in that part of the diagram run almost parallel with the side of the triangle.

For binary systems the limit of solubility at a

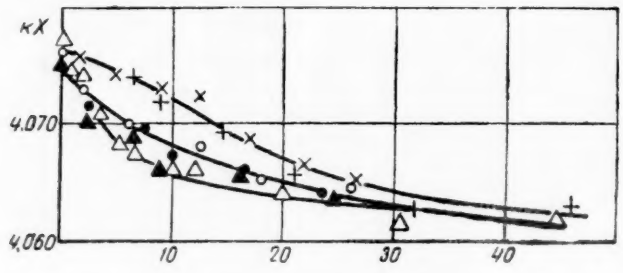

FIG. 6. Change of lattice constant of solid solution with time at 250°C ageing temperature

+ — × - - - - Al + 8% Mg; ○ — • Al + 8% Mg + 0.5% Ag; — ▲ — Al + + 8% Mg + 1% Ag.

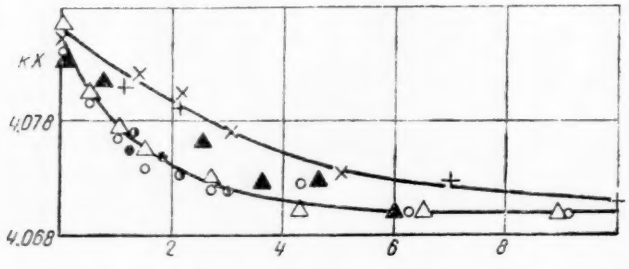

FIG. 7. Change of lattice constant of solid solution with time at 300°C ageing temperature

× — + Ag + 10% Mg; ○ — • Al + 10% Mg + 0.2% Ag; ▲ — △ Al + 10% Mg + 1% Ag.

given temperature is determined from the graph $\alpha = \phi(c)$, which consists of an inclined and a horizontal branch.

For ternary systems the graph can have a similar form only if as a result of the addition of the third component the composition of the solid solution supersaturated to the limit remains constant. This can happen in two cases:

(1) if the concentration of the ternary alloys changes in such a way that an immediate transition from the single phase to a three-phase region occurs, that is if the line of change of the alloy composition passes through the summit of the three-phase triangle; in that case the composition of the solid solution will remain constant in the limits of the three-phase region; or,

(2) when the line of change of the alloy composition in going through the two-phase region coincides with the direction of one of the connodals.

If at the transition into the two-phase region the line of change of the composition intersects with the connodals and the composition of the solid solution supersaturated to the limit changes proportionally (which is shown by the straightness of the line of the isotherms of solubility), then in the graph, beginning with the point of supersaturation to the limit, the straight line changes direction. If the isotherm is curved, then the second branch of the graph will also be curved.

If the composition of the alloys is changed within

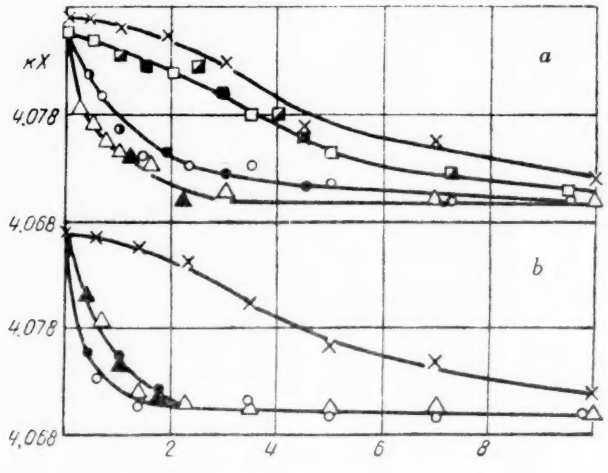

FIG. 8. Change of lattice constant of solid solution with time at 300°C ageing temperature

a) ×—+Al+10% Mg; ○—■ Al+10% Mg+0.2% Zn; ○—● Al+10% Mg+0.2% Ag; ▲→△ Al+10% Mg+1% Zn;
b) ×—Al+10% Mg; ▲— Al+10% Mg+0.2% Ag+0.2% Zn; ○—● Al+10% Mg+0.2% Ag+1.0% Zn.

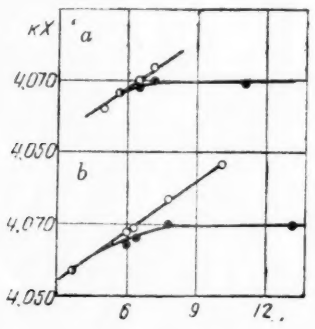

FIG. 9. Dependence of lattice constant of solid solution on the concentration in the alloys:

a—Al + Mg + 0.5% Ag; *b*—Al + + Mg + 1.0% Ag.
○—450° C; ●—300° C.

broader limits, where the transition from the single-phase to the two-phase and then into the three-phase region is made, the graph $a=\phi(c)$ consists of three sections.

The third section is a horizontal straight line and characterizes the constancy of the solid solution when the medium concentration of the alloy is changed within the limits of the three-phase region.

With our alloys, at certain constant zinc concentrations the magnesium content changed. As shown in Fig. 5, the line of change of composition of the alloys with 0.5, 1.0 and 2.0% Zn goes from the single-phase region a through the two-phase region $(a + T)$

and the three-phase region ($\alpha + T + \beta$) into the two-phase region ($\alpha + \beta$).

Under the scheme indicated, it would appear that on our graphs there ought to be observed a fourth section: after the third straight horizontal section there should follow a fourth curved section, in as much as the alloys in their composition go from a three-phase region into a two-phase region. However, such a section was not observed in our graphs. The lattice constant of the solid solution remained constant and corresponding to the constant of the solution supersaturated to the limit for the three-phase region.

This can be explained by the isotherms of solubility being very short in the region ($\alpha + \beta$), and the difference in the composition of the α-solution and the value of the lattice constant being within the limits of error of the measurements.

The results of the measurement of the lattice constant of phase T and the solid solution which is in equilibrium with it show that the lattice constants of both phases in the alloys examined increase regularly with the increase of the magnesium content in the phases. Along the connodal in the region ($\alpha + T$) the lattice constant of the α-phase remains virtually constant (see Table 5, Fig. 5, connodals I, II).

Our data shows (Fig. 1, 2) that the addition of zinc to the amount of 0.2 and 0.5 per cent increases the rate of ageing. Even stronger is the effect of the addition of 1% Zn, especially at the temperature of 300°C.

It follows from a study of the isothermal sections [11] that additions of up to 1% Zn to the alloy with 10% Mg alters the magnesium content in the solid solution at 300°C within a limit of 0.3 per cent; the same additions of zinc to the alloy with 8% Mg changes the magnesium content in the solid solution at 250°C by less than 0.2 per cent. As was shown above (see Figs. 1 and 2), the change in the degree of supersaturation of the solid solution within such limits does not have a noticeable effect on the rate of separation. Thus, the observed accelerating effect of additions of zinc on the ageing process of solid solution of magnesium in aluminium cannot be explained by a change in the solubility of magnesium in aluminium in the presence of zinc, i.e. by a change in the general supersaturation.

It must be concluded that this effect is connected with the internal adsorption of zinc the possible mechanism of which effect on ageing has been indicated above.

ADDITIONAL INVESTIGATION OF AGEING IN THE SYSTEMS Al-Mg-Ag AND Al-Mg-Zn-Ag

The effect of silver on the ageing of a solid solution of magnesium in aluminium was investigated by the same method as the effect of zinc at 250° and 300°C.

The curves obtained are shown in Figs. 6 and 7. Additions of 0.2 to 0.5 per cent of silver considerably accelerate the separation. The further increase in the silver content (to 1.0 per cent) gives a slightly greater effect.

The curves of the dependence of the lattice constant of the solid solution on the magnesium content in the presence of silver (Fig. 9) have the same aspect as the analogous curves for the Al-Mg alloys with additions of zinc. Evidently, they can be given the same explanation.

It was also interesting to investigate the combined effect of zinc and silver on the process of separation of a supersaturated solution of magnesium in aluminium. This effect was studied at 300°C on alloys with 10% Mg (see Table 2). The results are shown in Fig. 8. The combined effect of 0.2% Zn and 0.2% Ag is almost additive; for an alloy with 0.2% Ag and 1.0% Zn this is not the case.

CONCLUSIONS

(1) By measuring the change in the lattice constant of a separating solid solution with the time of ageing it has been established that admixtures of 0.2% to 1% of Zn and Ag accelerate the ageing of Al-Mg alloys.

(2) The analysis of the experimental data on the solubility of Mg in Al in the presence of admixtures of Zn, together with data found in the literature on the phase diagram of the ternary system Al-Mg-Zn, shows that the observed acceleration of ageing cannot be attributed to an increase in the general supersaturation of the solid solution with magnesium in the presence of small additions of zinc (this only increases by 0.2 to 0.3% Mg); evidently, a considerable role in this acceleration is played by the internal adsorption of zinc on the periphery of the pretransitional formations in the separating solid solution and further on the periphery of the small crystals of the excess phase which are being precipitated. The case is similar with the effect of admixtures of Ag.

(3) In the discussion on the question of the mechan-

ism of the effect of small admixtures of a third component on the kinetics of the separation of a supersaturated binary solid solution it is necessary to take account of the nature of the course of the isotherms and connodals in the phase diagram of the corresponding ternary system. Significant here is not the degree of solubility which corresponds to the intersection of the straight line which runs through the point of the composition of the ternary alloy parallel to the side of the concentration triangle with the boundary of the region of the solid solution, but that which corresponds to the intersection of the connodal going through the point of the composition of the alloy with the isotherm which limits the phase region including the composition of the alloy. If this isotherm is intersected by the side of the concentration triangle under an acute angle and is very long, then even a small admixture can noticeably alter the supersaturation of the solid solution. If the angle of intersection of the isotherm with the side of the triangle is large, but the isotherm is short, then even a considerable admixture effects little change in the supersaturation of the ageing alloy. In the second case the change in the kinetics of ageing under the influence of admixtures may be caused by internal adsorption.

Translated by B. Ruhemann

REFERENCES

1. V.I. Arkharov and N.N. Skorniakov, *Trud. Inst. Fiz. met. Urals fil. Akad. Nauk U.S.S.R.* 91, (1955).
2. L.M. Magat and N.I. Noskova, *Fiz. metal. metalloved.*, 1, 307, (1955).
3. V.I. Arkharov and N.I. Noskova, *Fiz. metal. metalloved.*, 2, 472, (1956).
4. V.I. Arkharov, I.P. Berenova and N.A. Kozina, *Dokl. Akad. Nauk SSSR.*, 98, 207, (1954).
5. C.W. Perryman and G.B. Brook, *J. Inst. Metals* 79, 19, (1951).
6. W. Koester and W. Dullenkopf, *Z. Metallk.*, 28, 365, 309, (1936).
7. M. Kawakami. Quot. M. Hansen, *Structure of binary alloys.* State United Publishing House of Science and Technology, (1941).
8. F. Laves, K. Loberg and H. Witte. *Metallwirtschaft.* 14, 793, (1935).
9. K. Riederer, *Z. Metallk.* 28, 312, (1936).
10. V.I.Mikheeva, *The chemical nature of very strong alloys of aluminium with magnesium and zinc.* Izd. Akad. Nauk. U.S.S.R. (1947).
11. L. Fink and L.A. Willey, *Trans. Am. Inst. Mining Met. Engs. Metals. Div.* 124, 78, (1937).
12. E. Butchers, A.T. Little, G. Raynor and M.A.W. Hume-Rothery, *J. Inst. Metals*, 69, 209; 415; 423; 467, (1943).
13. M.I. Zamotorin, *Trud. Leningrad Polytech. Inst.* 180, (1955).

VOL. 5 1957

STUDY OF THE PROPERTIES AND STRUCTURE OF INVAR ALLOYS ALLOYED WITH MOLYBDENUM, CHROMIUM, AND NIOBIUM*

A.Z. IVANUSHKINA and B.G. LIVSHITS

Institute of Precision Alloys All Union Central Scientific Research Institution

(Received 26 February 1957)

It has been shown [1] by electrical resistance and dilatometry methods that with the introduction of molybdenum into alloys of Permalloy composition Ni_3Fe the ordering effects are suppressed, and with a Mo content above 1 per cent they take the opposite sign. Thus, with prolonged low temperature annealing of hardened samples of composition Ni_3Fe + 2-6% Mo their electrical resistance increases, as also the volume. Other properties too are changed.

It was suggested [1] that the introduction of molybdenum into the composition of the solid solution Ni_3Fe makes it heterogeneous at low temperatures. Such a condition of the solid solution was named by Thomas [2] the *K*-condition. Thomas revealed the anomalous change in electrical resistance in Nichrome and other alloys used in electrical resistances. The hypothesis was put forward [1] that such heterogeneity of the solution is the result of the variable affinity of molybdenum (in other alloys, some other transitional metal) with iron and nickel. The contrary view was expressed [3,4] that the change in properties of the molybdenum-containing Permalloy under heat treatment is due to ordering of the solid solution. The same has been said in regard to Nichrome [5]. Therefore it was of interest to study the introduction of transitional metals in those ferro-nickel alloys where, without addition of a third component, an ordering effect is absent. In this connexion Invar was a very suitable alloy. The alloying of Invar with transition metals was interesting also from another point of view. It could be expected that, by such means, it would be possible to lower the temperature coefficient of the modulus of elasticity of Invar, a matter suggested by practical problems.

All the test alloys, except No. 8, comprised solid solutions, as shown by the phase equilibrium diagrams of the systems Fe-Ni-Mo and Fe-Ni-Cr and results of structure study. Alloy 8 was two-phase.

Experimental melts were obtained in the high-frequency induction furnace. From bars of 3.2 mm diam. dilatometric testpieces were prepared, also samples for measurement of electrical resistance, microhardness, and for micro-structural analysis. For heat treatment the heating was done in a hydrogen furnace or under a vacuum of 10^{-3} mm Hg col. Temperature of the furnace was controlled with the aid of an automatic potentiometer together with a Chromel-Alumel thermo-couple accurate to within ± 5°. Hardening was effected by quenching in iced-water.

For studying the effect of cold deformation on the electrical resistance of the alloys, bars were chosen with different initial diameters (from 10 mm to 3.2 mm), and drawn down to a diameter of 3.2 mm, which made it possible to obtain various degrees of reduction – from 0 to 90 per cent.

Electrical resistance of the alloys was measured with a double Thomson bridge on the UTV-2 apparatus. The dilatometric tests of the alloys were made with the Chevenard dilatometer by the differential method, using a Pyros sample as standard. The microhardness of the alloys after various heat treatments was measured on the PMT-3 apparatus. Fracture tests were made on samples 120-130 mm long and 3.2 mm diam. on the rupturing machine of the "Shopper" type with 1000 kg range. The gauge length in determining relative elongation was 30 mm.

TESTS WITH SINGLE-PHASE ALLOYS Nos. 1 TO 7

In order to study the internal transformations in the alloys their properties and microhardness were tested after quenching in water from 950°, cooling from 950° for a week at the rate of 5°/hr (anneal), and after quenching in water from 950° with subsequent anneal at 500° for 10 or more hr.

By rapid cooling from 950° (quenching) the high temperature atomic-structural state of the alloys was established, and the low temperature state by annealing and the extended tempering at 500°.

* *Fiz. metal. metalloved.* 5, No. 3, 527-535, 1957.

The chemical composition of the test alloys is given in Table 1.

TABLE 1.

No. of alloy	Chemical composition percentage								
	C	Ni	Mo	Cr	Nb	Mn	Si	S	P
1	0.020	36.30	trace	trace	—	0.19	0.018	0.008	0.002
2	0.025	36.80	0.97	trace	—	0.28	0.047	0.014	0.002
3	0.020	36.30	2.10	trace	—	0.24	0.050	0.015	0.004
4	0.020	35.30	3.88	trace	—	0.32	0.10	0.013	0.009
5	0.020	35.85	6.20	trace	—	0.34	0.050	0.014	0.011
6	0.025	35.4	8.15	trace	—	0.35	0.080	0.019	0.009
7	0.025	36.6	trace	3.20	—	0.29	0.12	0.010	0.007
8	0.025	36.0	0.41	trace	5.5	0.31	0.88	0.008	0.004

VOL. 5 1957

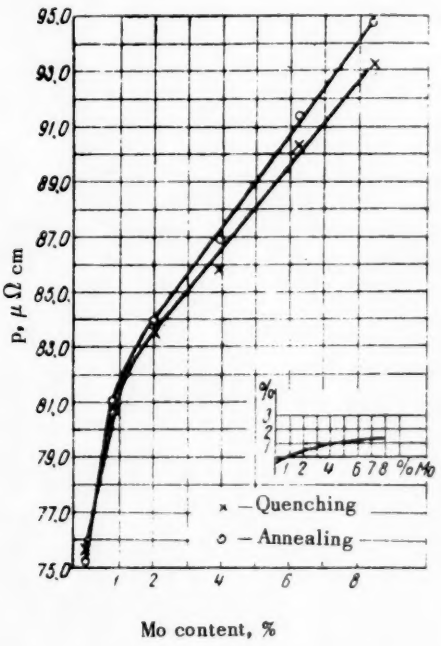

FIG. 1. Change in specific electrical resistance in relation to composition of alloy under anneal at 500° for 10 hr; initial state, quenched from 950°. Mo content %; x is quenching, o is anneal.

In Fig. 1 are shown the changes in specific electrical resistance of the alloys in relation to molybdenum content after quenching and after quenching with subsequent annealing at 500° for 10 hr. The difference in specific electrical resistance of quenched and annealed alloys increases uniformly with increase in the molybdenum content. The maximum difference is obtained with an alloy containing 8 per cent molybdenum. The increase in electrical resistance after anneal may be explained by some special process taking place in the test alloys. Evidently this process is analogous to that occurring in the

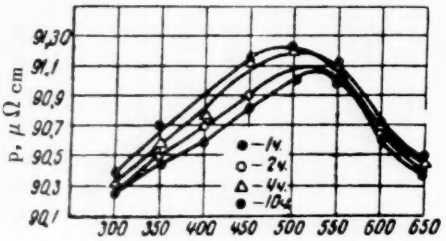

Annealing temperature °C

FIG. 2. Change in electrical resistance of alloy 6 with annealing temperature.
Annealing temperature °C time: 1, 2, 4, 10 hr.

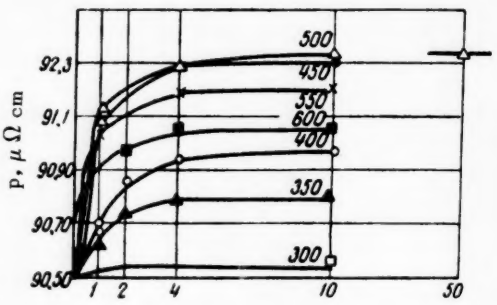

Annealing time, hr

FIG. 3. Change in electrical resistance of alloy quenched from 950° (6% Mo) with time at different temperatures. Annealing time in hours.

alloys Ni_3Fe + Mo, NiCr and others.

In order to determine the temperature range in which the process takes place that is responsible for the rise in electrical resistance of alloys alloyed with molybdenum, these alloys were annealed at different temperatures.

In Fig. 2 is shown the change in specific resistance of an alloy in relation to the annealing temperature after different holding times. Electrical resistance in relation to temperature of anneal varies according to the curve, with maximum approximately at 500°. Annealing at a temperature below 300° does not involve any change in specific electrical resistance. The value of the maximum increases with increasing molybdenum content. At 650° the resistance, as a result of annealing, has nearly its initial value (as after hardening).

With extension of the holding time the value of the maximum increases and is displaced towards the lower temperatures. Such transformation kinetics testifies to the fact that the process is one of diffusion.

In Fig. 3 are shown the changes in electrical resistance of alloys quenched from 950° in water in relation to holding time at different temperatures. The resistance tends towards a definite value characterizing a stable condition of the alloy. With rise in temperature up to a definite level (500°) the limiting value increases, but with a further rise in temperature it declines. The most marked change in electrical resistance is to be seen in the initial stage of the process, and afterwards the resistance asymptotically approaches the limiting value. The process occurring by diffusion is difficult at a temperature below 400° owing to kinetic factors.

The activation energy of the process which was calculated from data of electrical resistance change, approximately corresponds in magnitude to that of ordering and other diffusion processes. In the case of alloy No. 5 the activation energy equalled 57,400 cal/g. atom, and with alloy No. 6 it was 53,600 cal/g. atom.

It is known [1, 2] that if, through creation of the *K*-condition, electrical resistance of the alloys rises, then cold deformation leads to disruption of the *K*-condition and lowers the electrical resistance of the alloys.

In the given case the resistance of samples containing 8% Mo, after anneal at 500° and deformation at 90 per cent fell by 3.3 per cent.

The subsequent low temperature heat treatment of the deformed samples leads to restoration of the condition disturbed by deformation, that is manifested in a new rise in the electrical resistance of the deformed samples. This is evident from Table 2 where the changes in specific electrical resistance of the deformed alloys (deformation up to 90 per cent resulting from heat treatment at 500° are shown.

In the annealing of deformed alloys containing no molybdenum electrical resistance decreases with time, indicating some removal of work-hardening. Of alloys containing 1 per cent molybdenum the electrical resistance hardly changes at all. With those containing more than 2 per cent the electrical resistance increases with time, and this increase is greater the larger the Mo content in the alloy. The effect obtained through annealing the deformed alloys is nearly twice as great as that obtained in annealing hardened alloys (with the same temperature and holding time). This indicates that the structural condition corresponding to higher electrical resistance of the molybdenum-containing alloys, as a

VOL
5
195

TABLE 2. Specific electrical resistance microhms/cm

No. of alloy	after deformation	After annealing at 500° for			
		1 hr	4 hr	10 hr	50 hr
1	76.86	76.55	72.26	76.03	75.05
2	81.10	81.18	81.20	81.23	—
3	84.07	84.58	84.74	84.75	—
4	86.19	87.48	87.70	87.74	—
5	89.00	90.71	90.95	91.04	91.14
6	91.80	94.19	94.52	94.61	94.73

result of preliminary cold deformation, is removed in greater measure than with hardening.

The testpieces hardened from 950° (for establishing the low temperature state with statistically disordered disposition of atoms) were subjected to dilatometric study.

In Fig. 4 are shown the differential heating and cooling curves of the test alloys. From Fig. 4a it can be seen that in heating alloy No. 1 up to 260° there is a loss of magnetic properties (Curie point). On the heating curve this is shown in a sharp change in the thermal coefficient of expansion, as a result of which its direction is changed. The cooling curve of alloy No. 1 lies on the heating curve, and at room temperature no residual change of volume is observed. This indicates the absence in the alloy of any kind of transformations other than magnetic. The heating curves of alloys 2 and 4 (Fig. 4 b, c) nearly coincide with the heating curve of alloy No. 1.

The cooling curve of alloy No. 2 nearly coincides with the heating curve. The cooling curve of alloy No. 4 lies somewhat below the heating curve, indicating the presence of very slight compression due to heating and cooling.

After heating the hardened alloy samples Nos. 5 and 6 and cooling them at the rate of 150°/hr down to room temperature a residual reduction in length was observed (Fig. 4 d, e). The heating curves lie above the cooling curves. Moreover, on the heating curve of alloy No. 6 there is compression at 450-500°. Further heating of this alloy leads to expansion, with another coefficient.

In the alloy alloyed with chromium a residual change in volume is not observed, and this agrees with results of measurement of electrical resistance.

Thus, from the differential curves it is evident that, with rise in molybdenum content there is residual compression which is greater the larger the Mo content in the alloy.

Experiments at different temperatures showed that the greatest change in volume is observed in the temperature range 400-500°. These results agree very well with those obtained from measurements of electrical resistance.

The method of determining microhardness was used for measuring the hardness of the grain interior in the phase of interest to us, so that the grain boundaries in this case played no part.

In Fig. 5 are shown the changes in microhardness of a hardened alloy with 8% Mo in relation to annealing temperature after holding for 10 hr. The microhardness increases in proportion to Mo content in the ferro-nickel solid solution. The maximum change in microhardness observed in an alloy with 8 per cent molybdenum amounted to 12 per cent. The relation between hardness of the iron-nickel-molybdenum alloys and annealing temperature has the same form as that in the case of specific electrical resistance.

In Fig. 6 are shown the changes in microhardness of quenched alloys after the following treatment: 950° cooling for two weeks. From the diagram it is clear that, in the first place, the microhardness of alloy No. 1, containing no Mo, changes little with heat treatment, and, in the second place, the greater the Mo content in the solid solution the greater is the difference in hardness between the as-quenched and the annealed samples.

Thus, with creation of the *K*-condition, the microhardness of iron-nickel-molybdenum solid solutions is increased. The same applies also to the yield strength.

The difference in values of yield strength after quenching and annealing at 500° for 30 hr is proportional to the Mo content and reaches 4 per cent for an alloy containing the maximum amount of Mo (8%).

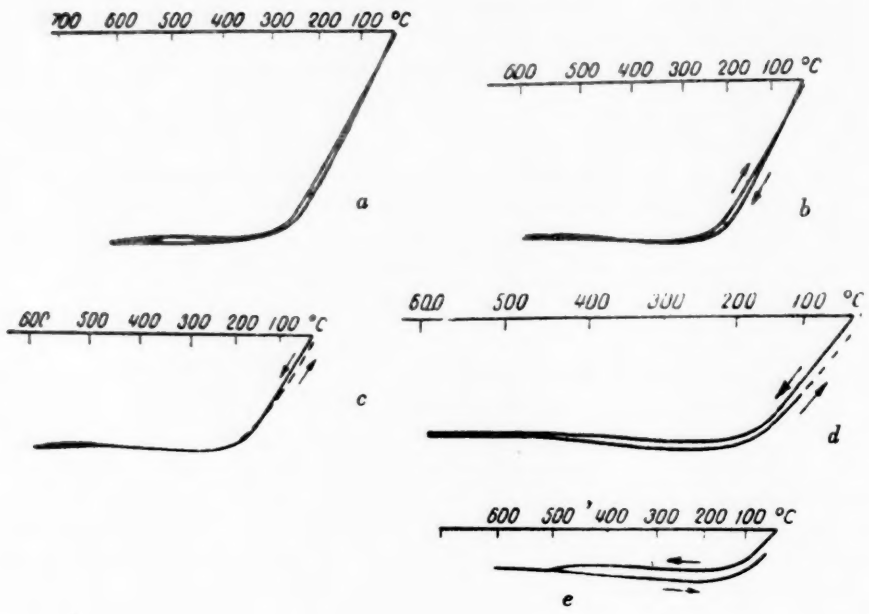

FIG. 4. Heating and cooling curves of sample on "Chevenard" dilatometer. Heating and cooling rate, 150°/hr.

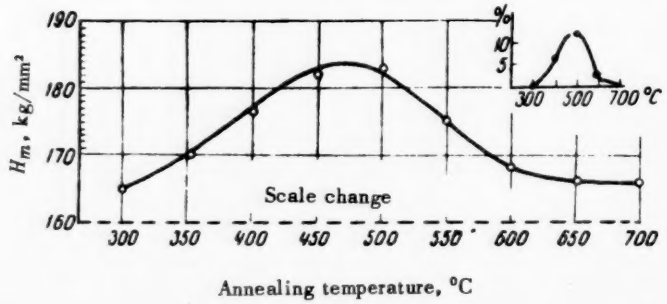

FIG. 5. Change in microhardness of alloy 6 in relation to temperature of anneal.

Due to the effect of molybdenum in considerable measure the temperature coefficient of the modulus of elasticity is changed (Table 3) as was found by the method of torsional oscillations.

Heat treatment has little effect on the atomic-structural state of alloy No. 1, since annealing raises the temperature coefficient of the modulus of elasticity by only 3.5 per cent. Heat treatment produces considerable change in the structural condition of alloys Nos. 5 and 6, for here reduction in the modulus of elasticity is 36-40 per cent.

STUDY OF THE TWO-PHASE ALLOY

In discussing the question of the *K*-condition as if it were a special solid solution state, it was suggested that the appearance of the *K*-condition is a process of pre-precipitation in two-phase alloys containing a small amount of the second phase. On heating such an alloy after quenching, according to this

TABLE 3.

No of alloy	Heat treatment		Change in temperature coefficient %
	Hardening	Annealing	
1	$+490 \cdot 10^{-6}$ deg^{-1}	$+507 \cdot 10^{-6}$ deg^{-1}	3,5
5	$+353 \cdot 10^{-6}$ »	$+220 \cdot 10^{-6}$ »	36
6	$+278 \cdot 10^{-6}$ »	$+170 \cdot 10^{-6}$ »	40

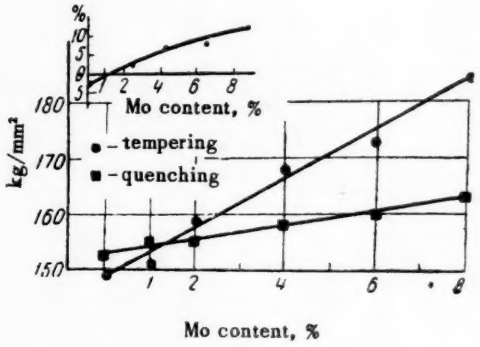

FIG. 6. Change in microhardness of ferro-nickel alloys, with 36 per cent nickel in relation to molybdenum content.

view, a process of pre-separation begins, which is completed by a submicroscopic precipitation of the second phase, or is not completed at all by actual precipitation with a rise in temperature, since the alloy transforms into a homogeneous state, as is explained by the low temperature of limiting solubility. In order to check this suggestion the two-phase alloy No. 8 containing 5.5 per cent niobium was tested. The alloy comprised grains of the solid solution and small amounts of the second phase (probably iron niobide). The second phase was only slightly dissolved on heating up to 900°.

After slow cooling from 950° (for a week) the electrical resistance of this alloy was appreciably higher than after quenching from this temperature.

In order to determine the temperature range in which this rise in electrical resistance occurs the resistance was measured for alloy No. 8 after annealing at different temperatures from 300 to 650°.

From consideration of Fig. 7 we see that electrical resistance in relation to annealing temperature changes in accordance with a peaked curve. Even at 300° there is a noticeable rise in resistance; at 400° the resistance continues to increase, and around 500° reaches maximum. With extension of holding time the effect (change in specific electrical resistance) is enhanced.

The experiments have shown that the nature of the change in specific electrical resistance with time under low temperature treatment of hardened Fe-Ni-Nb alloys is the same as with Fe-Ni-Mo alloys, i.e. electrical resistance, increasing with time, tends towards a limiting value which depends on the temperature.

The effect of deformation on specific electrical resistance was also studied. The results obtained showed that deformation of a hardened alloy leads to a decline in its electrical resistance; but the subsequent low temperature anneal evidently produces a restoration of the *K*-condition, disturbed by deform-

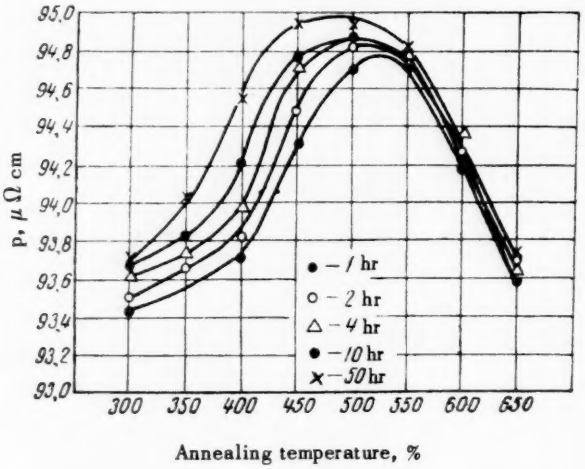

FIG. 7. Relation of specific electrical resistance of a ferro-nickel alloy with niobium to annealing temperature.

ation, as manifested by the fresh rise in electrical resistance.

The results of dilatometric tests agree very well with those for electrical resistance. On heating a hardened sample maximum compression was noted in the same temperature range (400-500°) as the maximum value for electrical resistance.

The results of microhardness measurements for alloy No. 8 also indicate that a maximum change in microhardness is observed for annealing of a hardened alloy in the temperature range 400-500°. In this case the yield strength rises by 6 per cent.

From the results presented it is obvious that all the changes arising through heat treatment are due to changes in the structure of the solid solution. In this connexion the changes in properties under work hardening are particularly convincing. If there had been solution or precipitation of the second phase, then this would have taken place and already existing crystals of the second phase, and properties would have changed as in ordinary ageing. Electrical resistance should have been reduced with ageing and hardly changed at all with work hardening. Thus, the suggestion that the creation of the *K*-condition is the result of the breakdown of the solid solution (in two-phase low temperature alloys) cannot be accepted as correct.

DISCUSSION OF RESULTS AND SUMMARY

The phenomena revealed in alloys Fe-Ni-Mo and Fe-Ni-Nb may be explained from consideration of the following hypothesis:

The heterogenous structure of a solid solution may be represented to us as atomic agglomerations which, in their average composition, differ from the average composition of the solid solution. Evidently the atoms of molybdenum (and possibly also of iron) from the agglomerations referred to from through statistical disorder. The creation of atomic agglomerations may be the cause of a supplementary scattering of conduction electrons and thus bring about a rise in electrical resistance as a result of low temperature anneal up to 500°. A rise in temperature above 500° acts in the same way as cold hardening, i.e. brings about a reabsorption of these agglomerations and leads to the formation of a statistically homogeneous (ordered) solid solution. The transition from a heterogeneous structure to a statistical arrangement of atoms in the lattice of the solid solution proceeds gradually. Obviously for each temperature there is a corresponding definite degree of heterogeneity. Rise in specific electrical resistance, reduction in volume, increase in strength characteristics under low temperature anneal, and also a lowering of electrical resistance under deformation, all indicate the formation, in the ferro-nickel alloys alloyed with molybdenum, of a special structural condition, differing both in respect to high temperature (statistical arrangement of atoms) and to ordered condition. The condition referred to may be called "internal phase heterogeneity". This designation, more than any other, reflects the essential nature of the process.

VOL 5 195

VOL. 5 1957

Change in properties of the iron-nickel-molybdenum and iron-nickel-niobium solid solutions, accompanied by internal phase heterogeneity, is similar to the change in properties under natural ageing and in the initial stage of the artificial ageing of aluminium-copper supersaturated solid solutions.

An effect was also discovered by Konobeevskii [6] and by Rovenskii [7], after anneal of work-hardened copper solutions that these authors explained in terms of atomic segregation. The process they disclosed differed from creation of a *K*-condition in that, for its manifestation, the existence of a heterogeneous stressed state is necessary. During the annealing of a heterogeneously stressed solid solution diffusion will take place therein leading, not to an equalising of concentrations, but to a segregation of the components forming the solid solution; wherein the atoms with large radius tend to be displaced to the layer where deformation occurs by extension, whilst the atoms with smaller radius may be displaced to the layer where compression deformation takes place; as a result of which chemical heterogeneity is also introduced. Such type of diffusion is named by Konobeevskii "ascending diffusion". In creation of the *K*-condition a preliminary cold-hardening is not inevitable. The *K*-condition is stable at a low temperature and is produced by slow cooling in the furnace or by anneal after hardening. Probably the heterogeneity of solid solutions under consideration is due to the formation of zones of the Guinier-Preston type.

In conclusion it is necessary to formulate the distinguishing characteristics of the *K*-condition or "internal phase heterogeneity".

1. The kinetics of formation of the *K*-condition shows that it is established by means of diffusion, as in ordering or the usual ageing.

2. The process goes on within the solid solution without precipitation of the second phase from the lattice, differing from the lattice of the original solution. In this way the *K*-condition process itself suggests ordered arrangement.

3. The formation or disappearance of the *K*-condition is accompanied, as is the case with other phase transformations, by absorption and evolution of heat, a volume effect, change in hardness, in strength limits of elastic and other properties.

4. Electrical resistance changes in the opposite direction to the change occurring on ordering. In the creation of the *K*-condition (in slow-cooling or annealing resistance increases, and in quenching or work-hardening (after slow cooling or anneal it decreases).

5. The introduction of a third component into a binary alloy that is tending to ordered arrangement (for example Ni_3Fe) at first reduces or eliminates such order; but with increasing concentration of the third component it initiates, and, with further increase in this concentration, strengthens the *K*-condition, as manifested by a change in all the physical properties of the alloy [1]. If the alloy is not in ordered arrangement (e.g. Fe + 36% Ni) then introduction of the third component brings about the *K*-condition and strengthens this in proportion as it enters more and more into the alloy structure. In both cases considerable strengthening results from the introduction of only a few atomic percents of the third component. In this the *K*-condition differs essentially from the usual ordered arrangement, where the introduction of a third component may merely weaken the effect of order through concentrated disorder.

6. The *K*-condition, as Thomas has stated, manifests itself in alloys containing transitional elements. Obviously the effect in question is governed by chemical (electronic) interaction of the atoms of the components which causes their regrouping in the lattice. The possibility is not excluded that affinity of components may lead to atomic segregation.

Translated by W.G. Gass

REFERENCES

1. B.G. Livshits and M.P. Ravdel', *Dokl. Akad. Nauk SSSR*, 93, 6, (1953).

2. H. Thomas, *Z. Metall.*, 41, 6, (1950).

3. R. Bosworth and Boothby, *J. Appl. Phys.* 18, 2, 173, (1947).

4. E. Josso, *Rev. Met.*, No. 10, (1950).

5. A. Taylor and G. Hinton, *J. Inst. Metals.*, 169, (1952).

6. S.T. Konobeevskii, *Zh. eksp. teor. fiz.*, 13, 200, (1943).

7. G.M. Rovenskii, *Trud. All-Union Scientific Research Institute of Aviation Materials*, (1946).

EXCESS VACANCIES IN AN ELECTROLYTIC METAL*

Ya. E. GEGUZIN
Kharkov State University

(Received 31 October 1956)

Reliable experiments [1-3] have shown that the coefficient of self-diffusion of the atoms in distorted crystal lattices (D_{ai}) is significantly greater than that determined on specimens whose lattices are free from distortions (D_{ao}), and this is especially clearly shown by specimens of galvanic origin. Agglomeration experiments on compressed electrolytic powders have shown [1] that the coefficient of self-diffusion can be increased by a factor of 2 to 3 in comparison with an "equilibrium" value. The cause of this predominance of D_{ai} over D_{ao} is a natural consequence of the mechanism of self-diffusion in the lattice and of the properties of a distorted lattice structure.

If self-diffusion is regarded as being accomplished by a "vacancy" mechanism, the relation between the coefficient of diffusion of the atoms (D_a) and the coefficient of diffusion of the vacancies (D_v) can be written [4] as:

$$D_a = \xi D_b ,$$

where ξ is the concentration of vacant sites in the lattice. (1) is applicable with equal correctness both to objects with distorted lattices and to "equilibrium" objects, if the general mechanism of self-diffusion for these objects is assumed to be a "vacancy" mechanism: according to this, the elementary act of changing the position of an atom in a crystal lattice, consists of its transition from an occupied site to a neighbouring unoccupied one.

Pines [2, 5] has expressed the opinion that the "healing" of a distorted lattice which takes place at high temperatures is accompanied by the appearance of excess vacancies whose presence effects a considerable increase in the coefficient of self-diffusion. This hypothesis allows a semi-quantitative description of the kinetics of the shrinkage in volume of "active" powder compacts. If the concentration of vacancies in a metal with a distorted lattice (ξ_i) at increased temperatures actually exceeds the concentration of vacancies in the "equilibrium" metal (ξ_o), it can be assumed that the excess vacancies will coagulate with the resulting formation of macroscopic pores (negative crystals). This postulated effect is analogous to the formation of macroscopic pores when volatile components are expelled from an alloy, but with the difference that in a metal with a distorted lattice, the excess vacancies appear as a result of the removal of the distortion, and in the alloy, as a consequence of the removal of the atoms of the volatile component.

Observations have been made of a fine porosity appearing after annealing crystals with a distorted lattice.

Garber and his co-workers [10] have observed the appearance of pores when optically inhomogeneous crystals of rock salt are annealed.

Bunin and Pogrebnoi [13] have observed the coagulation and subsequent healing of fine pores formed when quenched steel is annealed.

We have used an electrolytic metal because our aim was to observe the development of diffusion porosity, and diffusion experiments have shown that in such metals $D_{ai} \gg D_{ao}$, and this is a basis for supposing that there is a considerable supersaturation of vacancies in the metal lattice ($\Delta \xi = \xi - \xi_o$).

The coagulation of excess vacancies is obviously not the only way in which ξ_i may approach ξ_o. The excess vacancies could be replaced by displaced atoms, but this would not exclude the coagulation process.

It is natural to suppose that the rate of the coagulation of the excess vacancies under isothermal conditions should depend on the amount of their supersaturation in the metal, and so experimental determination of the kinetics of this process can be used to judge the amount of excess vacancies.

The amount of supersaturation of a crystal lattice by vacancies can be determined not only from the kinetics of their coagulation (discharge of vacancies into a flux inside the specimen) but also from the kinetics of the volume compression of the specimen

* *Fiz. metal. metalloved.* 5, No. 3, 536-544, 1957.

resulting from the discharge of vacancies at the external boundaries. Volume compression is most easily observed on porous specimens obtained from the compaction of "active" electrolytic powders, that is from a study of the kinetics of agglomeration.

This paper, then, is concerned with the problem of excess vacancies in an electrolytic metal, based on experimental data for the kinetics of their coagulation and the volume compression (agglomeration) of porous powder compresses.

THE FORMATION OF MACROSCOPIC PORES

Preliminary experiments with electrolytic copper carried out* in order to follow the formation of macroscopic pores when a metal with a strongly distorted lattice is annealed.

The copper was obtained from an acid galvanic bath by deposition on to a copper plate whose surface had been rubbed with finely dispersed graphite so that the layer deposited could be easily removed from the substrate. The specimens were obtained at a current density $\sim 5 A/dm^2$.

The specimen were annealed for one hour at temperatures of 500, 700 and 900°C in order to develop the macroscopic pores. The annealing was carried out in a vacuum furnace. Fig. 1 shows the original structure of the specimens and typical structures observed after annealing. The photographs demonstrate that the formation of the macroscopic pores is an evident fact. The dark regions are proved to be pores by control experiments in which the indentor of a microhardness tested (PMT-3) penetrated in these places. The photographs also show that annealing at much higher temperatures leads to the appearance of coarse pores. Most of the pores are situated at the grain boundaries, and pores between the grains have boundaries determined by the mutual orientation of the enclosing grains. When a pore is situated within a single grain its shape is determined by the orientation of the grain relative to the plan of the section [6].

In many cases, the pores disposed between the grains appear to be the cause of separation of neighbouring grains along a considerable part of the surface between them. The grain marked with a cross in Fig. 1c is an example of this. A natural consequence of the separation of grains is the difficulty of intergranular *recrystallization as is shown by the experiments which follow. Back reflection X-ray photographs showing the lines (331) and (420) (Fig. 2) were taken of specimens which had undergone various amounts of annealing at 1000°C. Comparison with the corresponding microstructures (Fig. 3) demonstrates that intra-granular collective recrystallization leading to coarsening of the mosaic blocks [5] takes place very quickly, there being practically no coarsening of grains on further annealing.

We have also observed the formation of macroscopic pores in electrolytic nickel.

The situation of the pores at the intergranular boundaries is in agreement with a previous conclusion [7] that there is little probability of the spontaneous formation of negative crystal nuclei in a lattice and that they are mostly generated at "impurities" to the number of which they are related, and at the boundaries between grains. Experiments thus show that macroscopic pores are formed when electrolytic metals are annealed and that these pores are mostly situated at the boundaries between the grains.

A porosity similar to that described appears when the cuprous oxide in a specimen of cast copper is reduced. Although this process is not completely excluded in the case of electrolytic copper, it obviously cannot determine the kinetics of the phenomena described. Careful metallographic control showed no cuprous oxide in our experiments and the amount of hydrogen in the electrolytic copper was small [14]. We have also observed the formation of porosity on annealing a copper which had been obtained at the very small current density $\sim 0.12 A/dm^2$.

SUPERSATURATION OF A METAL BY VACANCIES FROM THE RATE OF THEIR COAGULATION

The experimental data on the kinetics of the growth of macroscopic pores can be used to estimate the supersaturation of the metal by vacancies. To follow the rate of growth of the pores, three series of isothermal annealing at 500, 750 and 1000°C were undertaken with subsequent metallographic investigation of the structure of the annealed specimens.

The maximum duration of annealing at 500°C was

* M.I. Plastik-Kapinus (student) assisted in some of these experiments.

* We have in mind the unification of neighbouring grains by recrystallization as distinct from crystallization within the original grain (intra-granular recrystallization).

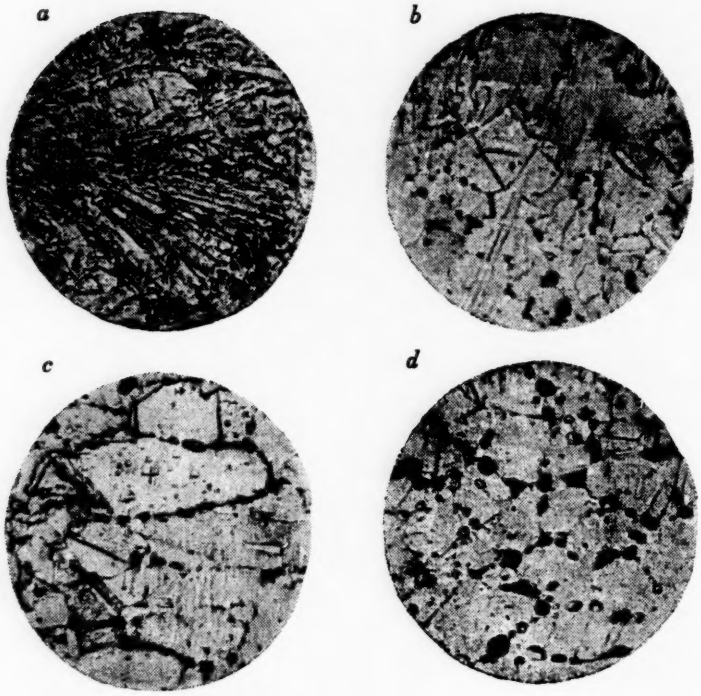

FIG. 1. Photomicrographs of structures of electrolytic copper after annealing at various temperatures:
a — original condition;
b — $T = 500°C$, $t = 60$ min;
c — $T = 700°C$, $t = 60$ min;
d — $T = 900°C$, $t = 60$ min x 600.

20 hr, at 750°C 12 hr, and at 1000°C 10 hr. A series of typical structures observed on specimens which had been annealed at 1000°C is shown in Fig. 3. The size of the pores obviously increases with the time of annealing and the total number decreases because of the disappearance of the smaller sized pores. Both observations testify that the fine pores are "devoured" by the coarser simultaneously with the coagulation of surplus single vacancies.

The results of the metallographic study of the structure of the specimens which have undergone isothermal annealing of a given duration, can be used to construct curves of dependence of the average linear size of the pores as a function of the annealing time, which are shown as the curves $L(t) = \phi(t^{1/2})$ in Fig. 4. In the field of view of the metallographic section there could always be distinguished a group of coarse pores of approximately the same size and a group of definitely much finer pores. The pores of the first group were used in the determination of $L(t)$.

It can be shown that Zener's formula [8] determining the dependence of the linear dimension of the precipitate growing from a supersaturated solution (in the solid phase), is applicable to the case of coagulation of surplus vacancies in a distorted lattice, when written in the form [8, 9]:

$$L(t) \simeq K(\Delta\xi)^{1/2} (D_{vi} t)^{1/2}, \qquad (2)$$

where

$$K \cong 1; \quad \Delta\xi = \xi_i - \xi_0; \quad D_{vi}$$

D_{vi}, is the coefficient of diffusion of vacancies in a distorted lattice; t, time. (2) gives an approximate expression which can be used to evaluate the supersaturation of the metal by vacancies:

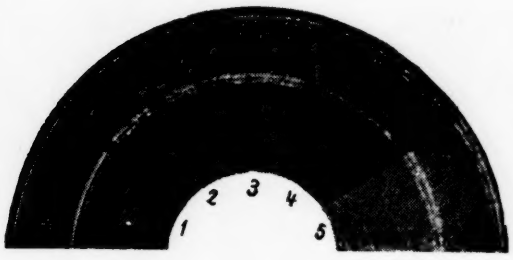

FIG. 2. X-ray diffraction diagrams obtained from specimens after deposition (1) and after annealing at 1000°C for different lengths of time [2-5]:
1 – original condition;
2 – t = 0 min;
3 – t = 30 min;
4 – t = 90 min;
5 – t = 9000 min.

VOL. 5 1957

$$\Delta\xi \simeq \frac{1}{D_{vi}}\left[\frac{d}{dt^{1/2}} L(t)\right]^2 \qquad (3)$$

Direct application of (3) does not seem possible since data as to the value D_{vi} are lacking. It is however, possible to estimate the value of D_{vi} from the relation between D_a and D_v in (1).

According to (1), D_{ai} is generally greater than D_{ao} in the following cases:

1) $\xi_i = \xi_0$, $D_{vi} \gg D_{b0}$;

2) $\xi_i \gg \xi_0$, $D_{vi} = D_{b0}$;

3) $\xi_i > \xi_0$, $D_{vi} > D_{b0}$.

The first case (that is, $\Delta\xi = \xi_i - \xi_o = 0$) is excluded because it is inconsistent with the facts of the formation of macroscopic pores and their growth with time. In the second and third cases, $\Delta\xi \neq 0$, and so they can take place. Having nothing from which to estimate the coefficient of diffusion of vacancies in a distorted lattice, we shall further suppose that $D_{vi} = D_{vo}$, that is, that a unique cause of the increase of the coefficient of diffusion of atoms in a distorted lattice is the excess of ξ_{oi} over ξ_o, that is that the second case takes place. Generally speaking it is natural to suppose that the energy barrier for the supersaturation of vacancies is lower in a distorted lattice than in a lattice in equilibrium (third case), but it is easy to show that the considerable increase in the coefficient of diffusion of atoms in a distorted lattice which has been observed (by a factor of 2 to 3) can be the result of the lowering of the energy barrier for supersaturation of vacancies to only a small extent. We shall therefore assume that

$$D_{vi} = D_{vo} = \frac{D_{ao}}{\xi_o}. \qquad (4)$$

and from (3) and (4) thus find an expression for the relative supersaturation by vacancies of a metal with a distorted lattice.

$$\frac{\Delta\xi_0}{\xi} \simeq \frac{1}{D_{ao}}\left[\frac{d}{dt^{1/2}} L(t)\right]^2 \qquad (5)$$

Using the experimentally determined dependencies $L = \phi(t^{1/2})$ to find $d/dt^{1/2}\, L(t)$ and the data for the coefficient of diffusion of atoms in a specimen of copper with an undistorted lattice from [11], the time dependence of the relative supersaturation at a given temperature can be determined, and is shown in Fig. 5 in the form of a graph with co-ordinates $\ln \Delta\xi/\xi_0$ and $\ln t$. These curves show that an extremely great supersaturation whose value decreases with time takes place at the beginning of the isothermal treatment. With increase of the temperature of the isothermal annealing, the supersaturation becomes less. It is, therefore, to be borne in mind that the

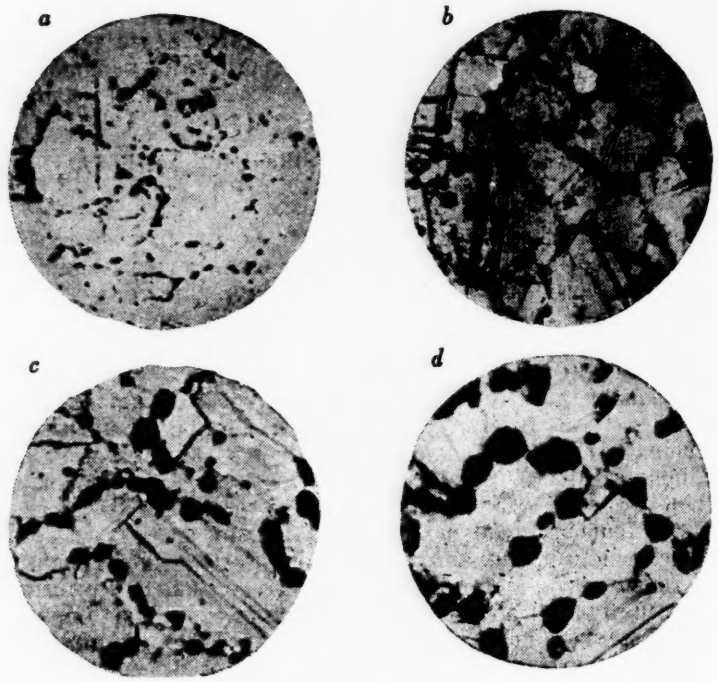

FIG. 3. Microstructures of electrolytic copper after annealing for different times at $T = 1000^{\circ}$C:
$a - t = 5$ min;
$b - t = 30$ min;
$c - t = 90$ min;
$d - t = 900$ min; x 600.

curves in Fig. 5 do not correspond to a strictly isothermal procedure, since the supersaturation could in practice, have decreased at the time taken by the specimen to reach the stipulated temperature.

In discussing these phenomena we concur with Pines in assuming that the surplus vacancies which coagulate into macroscopic pores when an electrolytic metal is annealed are the result of "healing" a distorted lattice. Strictly speaking in the case of an electrolytic metal still another "source" of additional vacancies can be suggested. Since the density (not X-ray) of the electrolytic metal in its original state is a little less than the density of the worked and annealed metal, it follows that the galvanic metal has little cracks and pores of various sizes. With increasing temperature, the pores of smallest size will "evaporate" with subsequent condensation of the surplus vacancies formed by the "evaporation" into pores of greater size. The "devouring" of the fine pores by the coarse will thus be accompanied by an enrichment of the lattice by single vacancies. According to this mechanism, the surplus vacancies appear not as the result of the "healing" of the micro-distorted lattice, but as a consequence of the "healing" of microscopic cracks and pores. It can, however, be easily shown that the latter "source" of surplus vacancies has a negligibly small capacity and cannot provide the supersaturation observed. Actually, the surplus concentration of vacancies in the neighbourhood of pores of radius r is determined by the relation [12] $\Delta\xi/\xi_0 = 2\sigma/r.\ \delta^3/kT$, where σ is the surface tension, δ the lattice parameter. Assuming that $\sigma \simeq 10^3$ erg/cm^2 and $\delta = 3 \times 10^{-8}$ cm, at 1000°C, $\Delta\xi/(\xi_0) \simeq 1$ can be achieved by the presence of pores with $r \simeq 10^{-7}$ cm, supersaturation $\Delta\xi/(\xi_0) \simeq 10^3$ cm, can take place at $\simeq 10^{-10}$cm which is absurd. Thus the marked supersaturation which has been observed, supports the idea that surplus vacancies are formed as a result of "healing" of a micro-distorted crystalline lattice.

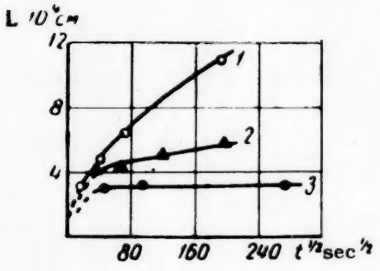

FIG. 4. Curves showing the dependence of the average grain size on the time of isothermal annealing:
1 – 1000°C;
2 – 750°C;
3 – 500°C.

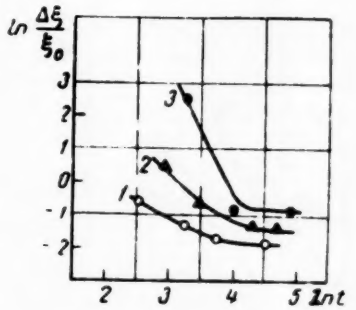

FIG. 5. Curves showing the dependence $\ln \Delta\xi/\xi_0 = \phi(\ln t)$ from pore coagulation data:
1 – 1000°C;
2 – 750°C;
3 – 500°C.

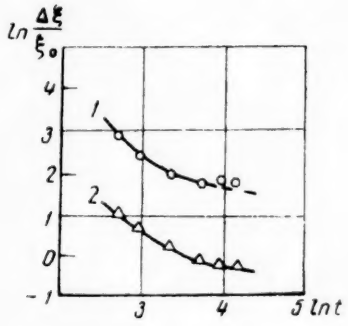

FIG. 6. Curves showing the dependence $\ln \Delta\xi/\xi_0 = \phi(\ln t)$ from shrinkage of the compress:
1 – T = 750°C;
2 – T = 1000°C.

SUPERSATURATION OF A METAL BY VACANCIES BY SHRINKAGE

The supersaturation by vacancies of the lattice of electrolytic copper can be estimated independently from considerations of the kinetics of the volume compression (agglomeration) of porous powder compresses. In agreement with the diffusion theory of agglomeration, the time dependence of the linear shrinkage of porous compresses under isothermal annealing is described by the following equation:

$$d\left(\frac{\Delta L}{L_0}\right) \simeq \frac{8}{3}\pi \frac{N\sigma\delta^3}{kT} D_{ai}(t)\, dt, \qquad (6)$$

where N is the number of pores in unit volume, $D_{ai}(t)$ is the coefficient of self diffusion of atoms varying with time and connected with the relief of the distortion. From (6) (1) and (4) a formula can be easily obtained establishing a relationship between the relative supersaturation of the lattice by vacancies ($\Delta\xi/\xi_0$), the equilibrium coefficient of self diffusion and the rate of linear contraction of the compact ($d/dt\ (\Delta L/L_0)$)

$$\frac{\Delta\xi}{\xi_0} \cong \frac{3}{8\pi} \frac{kT}{\sigma\delta^3 N D_{a0}} \cdot \frac{d}{dt}\left(\frac{\Delta L}{L_0}\right)\Big|_{T=\text{const}} - 1. \qquad (7)$$

To determine the relative supersaturation the

powder lattice by vacancies using (7) the time dependence of the linear contraction of the compact has to be found experimentally. We undertook the relevant experiments using compact of electrolytic copper powder obtained from an acid bath at a current density $\sim 20 A/dm^2$.

The dimensions of the powder particles were $\sim 2 - 3 \times 10^{-3}$ cm, the porosity of the compress $\eta =$ 30 per cent.

To find $\Delta\xi/\xi_0$ from (7) N must be known and it can be estimated only as to its order. If L is the linear dimension of the powder particles N can be estimated by using the formula

$$N \simeq 10 \frac{1}{L^3},$$

in which the factor 10 takes into account the fine porosity, the "seam" pores arranged along the junctions of the particles. In this case, $N \simeq 10^9$.

The number of pores can be estimated approximately from (7) only when the first term is large in comparison with unity. To find $\Delta\xi/\xi_0$ we made use of the results of dilatometer experiments which had been carried out at 750°C and 1000°C, but not at 500°C because at this temperature the shrinkage effect was very small and masked by secondary phenomena. The compact was annealed in vacuo. The curves $\Delta L/L_0 = \phi(t)$ obtained experimentally were used to construct curves of the dependence $\Delta\xi/\xi_0 = \psi(t)_{T=\text{const}}$, which are represented as the graphs $\ln \Delta\xi/\xi_0$, $\ln t$ in Fig. 6. Qualitatively, the course of the time dependence of the supersaturation found from agglomeration experiments is similar to analogous curves based on the coagulation of vacancies (see Fig. 5). That the absolute value of $\Delta\xi/\xi_0$ for powders exceeds the supersaturation in a massive layer by a factor of 1.5 to 2 is in good agreement with the fact that the diffusion "activation" of an electrolytic metal increases with increase of the anode current by which the metal was obtained. The experiments described in this section therefore confirm and supplement the information as to the value of $\Delta\xi/\xi_0$ obtained from experiments on the growth of pores.

RESULTS

1. Macroscopic pores (negative crystals) appear when electrolytic copper is annealed.

2. The pores are mainly situated along the grain boundaries, and this appears to be the reason for the difficulty of intergranular recrystallization in an electrolytic metal.

3. The kinetics of pore growth have been traced at three temperatures.

4. Experimental data of the kinetics of pore growth have been used to evaluate the supersaturation of the lattice by vacancies.

5. The relative supersaturation by vacancies of electrolytic copper powders has been estimated from data obtained from agglomeration experiments on powder compresses.

6. The values found for the supersaturation and the kinetics of change of $\Delta\xi/\xi_0$ with the time of annealing are in agreement with the ideas [2, 5] that surplus vacancies in a crystal lattice are the result of "healing" of a micro-distorted lattice.

Translated by J. Agrell

REFERENCES

1. Ya. E. Gegusin, V.M. Makhonin and B. Ya. Pines, *Uchen. zap. Kazan. Gosudarst. Univ.* 4, (1953).
2. B. Ya. Pines and Ya. E. Geguzin, *Zh. tekh. fiz.* 23, 11, (1953).
3. E.F. Chaikovskii, *Thesis, Kazan. Gosudarst. Univ.* (1956).
4. Ya. I. Frenkel, *Vvedenie v teoriya metallov (Introduction to the theory of metals)* (1948).
5. B. Ya. Pines, *Uspekhn Fiz. Nauk.* 52, 4, (1954).
6. Ya. E. Geguzin, *Dokl. Akad. Nauk SSSR*, 100, 2, (1955).
7. Ya. E. Geguzin, Rost kristallov *(Crystal growth). Trud. Vsesoyuz. soveshch. po rostu kristallov* Moscow, pp. 91-98, (1957).
8. C. Zener, *J. Appl. Phys.*, 20, 20, (1949).
9. A. Accary, *C.R.Acad. Sci., Paris*, 240, 5, 519, (1955).
10. R. I. Garber, V.S. Kogan and L.M. Polyakov, *Fiz. metal. metalloved.* 4, No. 1, (1957).
11. G. Gohen and G. Kuczinski, *J. Appl. Phys.*, 21, 12, (1950).
12. B. Ya. Pines, *Zh. tekh. fiz.* 16, 6, (1946).
13. K.P. Bunin and E.N. Pogrebnoi, *Izv. Akad. Nauk SSSR, otd. tekh. nauk.* 12, (1955).
14. A.T. Vagramyan and Z.A. Solov'eva, *Metody issledovaniya elektroosazhdeniya metallov (Methods for studying the electrodeposition of metals).* Akad.Nauk,Moscow, (1956).

VOL 5 195

LETTERS TO THE EDITOR

CONTRIBUTION TO THE THEORY OF SURFACE TENSION IN LIQUID METALS*

P. S. ZYRIANOV

S. M. Kirov's Uralsk Politechnical Institute

(Received 26 March 1957)

VOL. 5 1957

An attempt to elucidate the temperature dependence of surface tension in liquid metals starting only on the basis of the electron gas properties is clearly doomed from the beginning. The reason is that the temperature dependence of any particular physical property of a metal is determined primarily by the thermal motion of the ions, while the characteristics of a degenerated electron gas depend on temperature to an insignificant degree only.

Frenkel identifies the surface tension in metals with the energy of the binary electric layer in the surface. Starting with this model, a calculation was made [1-3] of the surface tension of metals, referring to the temperature of absolute zero since no account was taken of the thermal motion of the ions. A consideration of the thermal motion of ions leads to the presence of fluctuations in the electric field strength of the binary layer. The intensity of fluctuation increases with increasing temperature and when the electric field strength amplitude becomes comparable with that of the electric field intensity in the binary layer, the surface tension disappears, that is, the binary electric layer itself disappears and the metal is transformed into vapour.

The purpose of the present article is to amplify Frenkel's model in such a way that due account is taken of the thermal motion of the ions.

It will be shown in what follows that there exist surface thermal oscillations of ions having an amplitude which decreases exponentially as a function of the depth below the metal surface. The role of such oscillations reduces to the fact that they lower (diminish) the effective width of the binary electric layer. If we denote by σ_0 the surface tension at the temperature $T = 0°K$, and by σ surface tension at $T > 0°K$, then $(\sigma_0 - \sigma) = \sigma_T$ represents the reduction in the binary electric layer energy (or a reduction in surface tension) which results from the thermal oscillation of the surface ions. Our problem reduces therefore to finding σ_T as a function of temperature and of the constants characterizing a given metal.

Certain small oscillations in the ion density (fluctuations) caused by thermal motion, will be defined by a system of linearized equations from hydrodynamics of charged liquids:

$$\Delta\varphi + \frac{1}{\rho_0}\frac{\partial \rho}{\partial t} = 0 \qquad \text{(continuity equation)},$$

$$\Delta\Phi + 4\pi\frac{\varepsilon}{M}\rho = 0 \qquad \text{(Poisson's equation)},$$

$$\frac{\partial\varphi}{\partial t} + \frac{\varepsilon}{M}\Phi + \frac{u_0^2}{\rho_0}\rho = 0, \qquad \text{(Bernoulli-Evler equation)}, \qquad (1)$$

in which:

$$\rho_0 = n_0 M, \quad \varepsilon = ze, \quad \rho = \rho' - \rho_0,$$

n_0 is mean ionic density, ϵ – charge, M – ionic mass, ρ – deviation of density from the equilibrium value,

$$u_0^2 = \frac{1}{M}\left(\frac{\partial p}{\partial \rho}\right)_{\rho=\rho_0}$$

the velocity of sound in metal, p – pressure, existing mainly due to the degenerated electron gas. In case of full degeneration, we have according to [4] that:

$$u_0^2 \approx \frac{2}{3} z\frac{E_0}{M}$$

(E_0 = Fermi's boundary energy). Variations in the

---

* *Fiz. metal. metalloved.* 5, No. 3, 545-547, 1957.

electron gas density can be ignored since, for the well known reasons [5], they cannot be brought about in a metal by the thermal motion.

The system of equations (1) has a solution of the type:

$$\varphi = \int_{-\infty}^{+\infty} \varphi_\omega \exp\{i\omega t + i\kappa_\omega x\}\, d\omega \qquad (2)$$

with dispersional equation

$$\kappa_\omega^2 = \left(\omega^2 - \omega_0^2\right)\frac{1}{u_0^2}, \qquad (3)$$

where

$$\omega_0^2 = 4\pi n_0 \frac{\varepsilon^2}{M}.$$

With $\omega^2 < \omega_0^2$, equation (3) gives imaginary values of k_ω and solutions (2) die down exponentially. For simplicity reasons we shall now consider the problem in the case of the semi-space where $x > 0$.

In this case, for surface oscillations we have that:

$$\nabla\varphi = v = \int_{-\omega_0}^{+\omega_0} \dot{y}_\omega \exp\{-\kappa_\omega x\}\, d\omega,$$

$$\rho = \int_{-\omega_0}^{+\omega_0} \kappa_\omega y_\omega \exp\{-\kappa_\omega x\}\, d\omega - \nabla\Phi = E = \frac{4\pi e}{M}\rho_0 \int_{-\omega_0}^{+\omega_0} y_\omega \exp\{-\kappa_\omega x\}\, d\omega, \qquad (4)$$

wherein,

$$y_\omega = -\frac{M}{4\pi\varepsilon} E_\omega^0 \exp\{iat + i\beta_\omega\}$$

and $\exp\{i\beta_\omega\}$ is the phase multiplier, while β_ω is a real number. By means of these equations it is now possible to construct Hamilton's function for small oscillations:

$$H = \int_{-\omega_0}^{+\omega_0} \left(\frac{P_\omega^2}{2M} + \frac{M\omega^2}{2} Z_\omega^2\right) \rho_{\omega_0}\, d\omega, \qquad (5)$$

wherein,

$$\omega_0 y_\omega = Z_\omega, \quad P_\omega = M\dot{Z}_\omega, \quad \rho_{\omega_0} = \frac{zn_0}{\omega_0 \kappa_\omega} -$$

is the density of surface oscillators. Under the conditions of thermodynamic equilibrium and when $\chi T > h\omega_0$ (χ – Boltzman's constant), we have that:

$$\overline{y_\omega^2} = Z_\omega^2/\omega_0^2 = \varkappa T/M\omega^4 \qquad (6)$$

We shall now calculate σ_T. According to what has been said above:

$$\sigma_T = \frac{1}{8\pi}\int_0^\infty E^2 dx. \qquad (7)$$

By putting the value of E from (4) into equation (7) and after averaging for all the possible phases β_ω, we get that:

$$\sigma_T = \frac{M}{4\pi}\omega_0^3 Z n_0 \int_0^{\omega_0} y_\omega^2 \frac{d\omega}{\kappa_\omega}. \qquad (8)$$

Since

$$k_\omega^{-1} = u_0(\omega^2 - \omega_0^2)^{-1/2},$$

the region where $\omega \sim \omega_0$ to σ_T will be of most importance. The values of the interval will be of correct order if y_ω^2 will be substituted by $y_{\dot{\omega}}$ in equation (8), which corresponds to the thermodynamic equilibrium in equation (6) and is taken for $\omega = \omega_0$. This leads to the following equation:

$$\sigma_T = u_0\omega_0^2 M Z n_0 \overline{y_{\omega_0}^2} \int_0^{\omega_0} \frac{d\omega}{\left(\omega^2 - \omega_0^2\right)^{1/2}}.$$

The last interval equals $\pi/2$, and consequently:

$$\sigma_T = \frac{\pi}{2} Z \frac{u_0 n_0}{\omega_0} \varkappa T.$$

The temperature coefficient of surface tension becomes equal to:

$$\frac{\partial \sigma}{\partial T} = -\frac{\partial \sigma_T}{\partial T} = -\frac{\pi}{2} Z \frac{u_0 n_0}{\omega_0} \varkappa. \qquad (9)$$

In equation (9), it is possible to pass from ω_0 to the Debye's characteristic temperature θ_D. A relationship is given between θ_D and the frequency ω_0 in [5]:

$$\theta_D = \frac{\hbar \omega_0}{\varkappa \sqrt{2}}$$

By making use of this relationship, equation (9) can be put into the following form:

$$\frac{\partial \sigma}{\partial T} = -\frac{\pi \hbar}{\sqrt{8}} \frac{u_0 n_0}{\theta_D}.$$

The above equation gives results that are in satisfactory agreement with experimental data (see table). In the table data are given for u_0 for the alkali metals as calculated theoretically from the equation

$$u_0 \approx \frac{2}{3} Z \frac{E_0}{M},$$

and similar data for other metals are obtained by experiment. In the case of mercury, both u_0 and θ_D were determined experimentally. If one remembers that in the case of mercury the number of shared electron per atom is less than one, the agreement with experimental values is improved.

The author expresses his gratitude to V.M. Elenski for his evaluation of the problems discussed in this work.

Translated by H. Cygielski

REFERENCES

1. Ya. I. Frenkel, *Zh. russk. Fiz. khin. obshch.*, 49, 100, (1917).

2. Ya. I. Frenkel, *Zh. russk. fiz. khim. obshch.* 5a, 5, (1918).

3. Ya. I. Frenkel, *Z. Physik.*, 51, 332, (1928).

4. V.P. Silin, *Zh. eksp. teor. fiz.*, 23, 649, (1952).

5. P.S. Zyryanov, *Zh. eksp. teor. fiz.*, 29, 193, (1955).

6. Zhirov, *Trud. All-Union Scientific Research Institute of Aviation Materials*, 14, 99, (1937).

7. Drath Sauerwals, *Z. Anorg. Chem.*, 154, 79, (1926); 162, 301, (1927).

8. Erwing Harkins, *J. Amer. Chem. Soc.*, 42, 2539, (1920).

TABLE 1.

Metal	$n_0 \cdot 10^{-22}$, cm^3	$u \cdot 10^{-5}$ cm/sec	$\omega_0 \cdot 10^{-13}$ sec^{-1}	$\partial\sigma/\partial T$ theoretical	$\partial\sigma/\partial T$ exper.
Na	2.6	3.0	4.4	0.04	0.05 [5]
K	1.4	5.8	2.4	0.07	0.06 [5]
Ag	5.9	2.6	3.0	0.11	0.13 [6]
Au	5.9	2.1	2.2	0.12	0.10 [6]
Sn	3.7	2.5	2.3	0.08	0.09 [6]
Pb	3.3	1.23	1.6	0.05	0.08 [6]
Hg	4.0	1.2		0.4	0.22 [7]

VOL. 5 1957

ON THE THEORY OF EXCITONIC DISPERSION AND LIGHT ABSORPTION*

V. I. CHEREPANOV and V. S. GALISHEV
A.M. Gorkii's Uralsk State University

(Received 11 March 1957)

In work [1], a consideration was made of the excitonic light absorption for case of the absolute zero temperature. The calculations were done by the method of perturbation theory in representation of the second quantization, on the basis of a generalized Frenkel's model of the excitonic excited states [2].

In the present note, the results are given of further calculations of the absorption and dispersion of light, as caused by the excitonic states in a crystal. As distinct from work [1], the calculations were based on the density matrix method [3, 4], applied to the second quantization concept. This enabled a study of not only light absorption but also a simultaneous consideration of its dispersion, as well as a measurement of the dielectric permeability ϵ.

The dispersion equations for the conductance σ and for the dielectric permeability ϵ is in the following form:

$$\sigma(\nu) = \frac{e^2 nh}{24\pi^2\mu^2\nu} \int \theta_0(q)\, \vec{\nabla}_q \theta_1(q)\, dq|^2 \cdot |a(0)|^2 \cdot \delta(\nu_1 - \nu), \qquad (1)$$

$$\epsilon(\nu) = 1 + 4\pi a(\nu) = 1 + 4\pi \left[\frac{e^2 hn}{24\pi^4\mu^2\nu^2} \cdot \frac{\nu_1}{\nu_1^2 - \nu^2} \cdot \right.$$

$$\left. \cdot |\theta_0'(q)\, \vec{\nabla}_q\, \theta_1(q)\, dq|^2 \cdot |a(0)|^2 - \frac{e^2 h}{4\pi^2\mu\nu^2} \right]. \qquad (2)$$

For meaning of symbols see ref. [1].

Thus, the expression for conductance fully coincides with the equation (4, 6) in ref. [1], and differs from the corresponding expression (148,25) in Seitz's book [5] in that the multipler $|a(0)|^2$ is independent of the light frequency. The expression for the dielectric permeability can be compared with the corresponding Seitz equation (148, 27). It follows from this comparison that, in this case, the difference lies in the presence of an identical multiplier in the quantized part of the dielectric permeability. In a special case when $a(0) = 1$, (see our equation (2)) passes also into the Seitz formula (148, 27).

Translated by

REFERENCES

1. S.V. Vonsovskii, V.I. Cherepanov and V.S. Galishev, *Fiz. metal. metalloved.*, 4, (1957).

2. V.S. Galishev and S.V. Vonsovskii, *Fiz. metal. metalloved.*, 3, 395, (1956).

3. M.I. Sergeev, *Zh. eksp. teor. fiz.*, 8, 948, (1938).

* *Fiz. metal. metalloved.* 5, No. 3, 547-548, 1957.

4. A.V. Sokolov
Zh. eksp. teor. fiz., 25, 341, (1953).

5. F. Seitz, *Sovremennaya teoriya twerdogo tela (Modern theory of solid bodies)*. Gostekhizdat, (1949).

VOL.
5
1957

CONTRIBUTION TO SPIN WAVE STATISTICS*

M. S. SVIRSKII and B. Kh. ISHMUKHAMETOV
Metal Physics Institute, Uralsk Branch of the Academy Nauk SSSR

(Received 21 May 1957)

It is postulated in work [1] that spin waves conform to Fermi statistics. The basis for this postulate, was an analysis of the accurate solution of secular equations for a linear chain as put forward by Bethe [2] Frank [1], by changing the region of the ϕ phase determination to $0 \leqslant \phi \leqslant \pi$, instead of

$$-\frac{\pi}{2} \ll \varphi \ll \frac{\pi}{2},$$

as used by Bethe, improved Bethe's result to the effect that the spin function of spin waves was found not only to disappear under conditions of coincident wave numbers but also to be antisymmetric with respect to these numbers. Furthermore, as distinct from Bethe, according to whom the number of solutions with real wave numbers is less than the general number of solutions (for $n = 2$, $\frac{1}{2} N (N-3)$ instead of $\frac{1}{2} N (N-1)$ solutions), the region of ϕ determination as chosen by Frank leads, as it were, to a coincidence of the wave numbers mentioned above. On the basis of the above considerations Frank concluded that spin waves obey Fermi statistics.

The inconsistency of Frank's arguments becomes apparent during an analysis of the cause of the disappearance of states with identical wave numbers, which results in the additional condition that

$$2a_{n,\,n+1} = a_{n,\,n} + a_{n+1,\,n+1}, \qquad (1)$$

introduced in order to transform the secular equations for neighbouring left spins into equations for the non-neighbouring left spins. It is exactly because of this condition that there follows such a relationship between the coefficients c_1 and c_2 of the wave function:

$$a_{n_1,\,n_2} = c_1 exp\,[i\,(k_1 n_1 + k_2 n_2)] + c_2 exp\,[i\,(k_2 n_1 + k_1 n_2)] \qquad (2)$$

which leads to antisymmetry with respect to the wave numbers k_1 and k_2 and to the disappearance of $a_{n,n}$ when $k_1 = k_2$.

The introduction of an additional condition (1) appears as an artificial procedure on the basis of which it would be unwise to make any deductions as to the statistical behaviour of the system. It is sufficient to point out that, in their physical sense, the coefficients $a_{n,n}$ should equal zero since they represent the amplitudes of the probability of the existence of two left spins in one and the same atom, which is prohibited by the Pauli exclusion principle. From this point of view, there is a contradiction in the condition as given by equation (1), since we have that the right hand side is zero and on the left side of the equation there is the factor $2a_{n,\,n+1}$, which generally speaking is different from zero. Therefore, in solving the problem regarding the existence of states with identical wave numbers, it is necessary to use a procedure involving no such additional condition as given in equation (1). A direct consideration of the secular equations:

$$2\varepsilon a_{n_1,\,n_2} = a_{n_1,n_2} - a_{n_1-1,\,n_2} + a_{n_1,\,n_2} - a_{n_1+1,\,n_2} + a_{n_1,n_2} - a_{n_1,\,n_2-1} + a_{n_1,\,n_2} - a_{n_1,\,n_2+1} \qquad (3)$$

$$2\varepsilon a_{n_1\,n+1} = a_{n,\,n+1} - a_{n,\,n+2} + a_{n,\,n+1} - a_{n-1,\,n+1} \qquad (4)$$

shows that they are capable of a simultaneous

---

* *Fiz. metal. metalloved.* 5, No. 3, 548-550, 1957.

solution with identical wave numbers γ in both spin waves, namely:

$$a_{n_1, n_2} = c\, exp\,[ik\,(n_1 + n_2)] \qquad (5)$$

represents a solution of equations (3) and (4) when $k = 0$, to which corresponds an energy level with $\epsilon = 0$,

Thus, the secular equations themselves admit of an accurate solution corresponding to a state with identical wave numbers. Frank's argument in favour of the spin waves obeying Fermi statistics is thereby refuted.

It should be remarked that the solution when $k_1 = k_2 = 0$ was derived not only without assuming the artificial additional condition as given in equation (1), but that this condition does not apply to its derivation and the conclusions drawn from it with regard to the symmetry properties a_{n_1, n_2} are inadmissible. In reality, if an attempt is made to obtain a solution in the form given in equation (2) from expression (1), it follows that:

$$\frac{c_1}{c_2} = \frac{i\left(\cos\frac{k_1 + k_2}{2} - exp\left(i \cdot \frac{k_1 - k_2}{2}\right)\right)}{-i\left(\cos\frac{k_1 + k_2}{2} - exp\left(-\,i \cdot \frac{k_1 - k_2}{2}\right)\right)}, \qquad (6)$$

which leads to the interminable ratio of $c_1/c_2 = 0/0$ if $k_1 = k_2 = 0$, and therefore no definite conclusions with regard to the relationship between c_1 and c_2 should be based on this ratio and, furthermore, no deductions should also be made in this case as to the symmetry of the wave function.

The above remarks show contradictions in Frank's considerations based on equations (1) and (2). In fact, in calculating the number of solutions, Frank included also the case when $\chi = 0$, where

$$k = k_1 + k_2 = 2\pi\nu/N. \qquad (7)$$

But when $\chi = 0$, if follows from equation (7) that, on the one hand:

$$k_1 = -\,k_2, \qquad (8)$$

and, on the other one, it follows from the equations:

$$k_1 N = 2\pi\chi_1 + 2\varphi\,(k_1,\ k_2). \qquad (9)$$

$$k_2 N = 2\pi\chi_2 \quad 2\varphi\,(k_1,\ k_2), \qquad (10)$$

and

$$(k_1 + k_2)\,N = 2\pi\,(\chi_1 + \chi_2) \qquad (11)$$

that

$$\chi_1 \quad -\chi_2. \qquad (12)$$

Furthermore, when $\chi = 0$, we are dealing with an even number and hence, according to Frank, the maximum value of χ_1, which equals $\chi/2-1$, will in this case be:

$$\chi_1 = -\,1 \qquad (13)$$

Let us now take into account that, on the basis of equation (6), $k_1 k_2$ and ϕ are combined in the following relationship:

$$2\cot\varphi\,(k_1,\ k_2) = \cot\frac{k_1}{2} - \cot\frac{k_2}{2}. \qquad (14)$$

From equation (14) it follows, if use is made of equations (8), (9) and (10) and due attention paid to expressions (12) and (13), that:

$$\cot\varphi\,(k_1,\ k_2) = \cot\,(-\,\pi/N + \varphi\,(k_1,\ k_2)/N), \qquad (15)$$

and hence if Frank's region of ϕ determination is used we get that:

$$\varphi\,(k_1,\ k_2) = \pi. \qquad (16)$$

On substituting (16) into expressions (9) and (10) we obtain, bearing in mind equations (12) and (13), that:

$$k_1 = k_2 = 0, \qquad (17)$$

which contradicts Franks postulate regarding the absence of levels with identical wave numbers. However, this level should not be ignored since the number of solutions becomes less than $\frac{1}{2}\,N\,(N-1)$.

Thus it is shown, both independently of the additional condition (1) and within the framework of Frank's approach, that there exist energy states with identical wave numbers. And hence it follows that the statistics of spin waves cannot be of the Fermi statistics type.

The presence of Bose level at the bottom of the energetic spectrum should affect radically the statistical behaviour of the spin excitation system even in the case when Pauli's exclusion principle embraces all the higher energy levels. A system of this kind will behave at low temperatures as a Bose system.

In connexion with the above, we consider that one is perfectly justified to use Bose statistics for representing the properties of the spin wave system.

The present study was made at the suggestion and guidance of the corresponding Member, Akad. Nauk SSSR, S.V. Vonsovskii, to whom the authors express their gratitude.

Translated by H. Cygielski

REFERENCES

1. D. Frank, *Z. Physik*, 146, 615, (1956).

2. G. Bethe and A. Zommerfeld, *Elektronnaya teoriya metallov (Electronic Theory of Metals)*, Gostekhizdat p. 280, (1938).

VOL
5
195

THEORY OF STARK EFFECT IN EXCITONS. PART I*

G. G. TALUTS and S. A. SHULYATEV

Metal Physics Institute, Uralsk Branch Academy Nauk U.S.S.R.

(Received 7 July 1957)

In the present note a consideration will be made of the effect exerted by a uniform external electric field $\vec{E}$ on the spectrum of excitonic excitations [1, 2] in a semiconductor with a crystalline atomic lattice.

The starting Hamiltonian system of electrons has, in terms of the secondary quantization, the following form:

$$H = H_0 + H_1, \qquad (1)$$

wherein,

$$H_0 = \sum_{mm'nn'} L(mn,\ m'n')\, a^+_{mn}\, a_{m'n'} + \sum_{mm'nn'} (\vec{E}\vec{d}_{mn\,m'n'})\, a^+_{mn}\, a_{m'n'},$$

$$H_1 = \frac{1}{2} \sum_{\substack{m_1 \neq m_2,\ m_2' \neq m_1' \\ n_1 n_2\ n_1'\ n_2'}} F\left(m_1 n_1\ m_2 n_2,\ m_1' n_1'\ m_2' n_2'\right) a^+_{m_1 n_1} a^+_{m_2 n_2} a_{m_2' n_2'} a_{m_1' n_1'}.$$

In the above, we have that L and F are matrix elements of the additive and binary types, respectively, and

$$\vec{d}_{mn\,m'n'} = e \int \varphi_n(r - m)\, \vec{r}\, \varphi_{n'}(r - m)\, dr.$$

Wannier's function [3] was chosen as a function according to which the expansion is carried out.

In obtaining from equation (1) the excitonic excitations, use is made of the following simplifications:

a) only one excited state is considered, and therefore $n = 0,1$;

b) only weak excitations are considered, that is

$$\overline{a^+_{m_1} a_{m_1}} \ll \overline{a^+_{m0} a_{mn}},$$

c) the condition is assumed of homopolarity,

$$a^+_{m0}\, a_{m0} + a^+_{m1}\, a_{m1} = 1;$$

d) the exchange effect is ignored and therefore the excitation energy is independent of the electron spin.

By making the above assumptions, the Hamiltonian system becomes considerably simplified. A still further simplification of the system can be achieved by its diagonalization by means of a series of basic transformations. Isolation of excitonic excitations is realised by means of operators [2]:

$$b^+_m = a^+_{m1}\, a_{m0},\quad b_m = a^+_{m0}\, a_{m1}.$$

The operators b^+_m and b_m correspond roughly to the variable relationships in Bose's statistics.

As a result of the above transformations, the following equation is obtained for the energy of an elementary excitonic excitation:

$$E(k) = \{W^2 + 2WG_k\,(|C_{k01}|^2 + \Phi M_k)\}^{1/2}, \qquad (2)$$

where,

$$W^2 = [A_1 - A_0 + E\,(d_{11} - d_{00})]^2 + 4\,(E\,d_{01})^2$$

---

* *Fiz. metal. metalloved.* 5, No. 3, 550-552, 1957.

VOL. 5 1957

In the above equation we have that:

$$A_n = L\ (mn,\ mn)$$

is the energy of electron in state n,

$$\vec{d}_{nn'} = \int \varphi_n(\xi)\, e\vec{\xi}\, \varphi_{n'}(\xi)\, d\xi,$$

$$M_k = C_{-k00}\, C_{k01} + C_{k00}\, C_{-k01} - C_{-k11}\, C_{k01} - C_{k01}\, C_{k11},$$

$$C_{knn'} = N^{-\frac{1}{2}} \int \varphi_n(\xi)\, exp\,(-lk\xi)\, \varphi_{n'}(\xi)\, d\xi,$$

$$\Phi = \frac{1}{2} \arccos\{[A_1 - A_0 + \vec{E}\,(\vec{d}_{11} - \vec{d}_{00})]/W\},$$

G_k is the Fourier component of centre interaction between electrons and N is the electron density.

The energy equations obtained above are correct in the presence of weak fields defined by the condition that:

$$2\,(\vec{E}\vec{d}_{01}) \ll A_1 - A_0 + \vec{E}\,(\vec{d}_{11} - \vec{d}_{00}).$$

It should be remarked that in the case when $G_k = 0$, the expression (2) leads to the well known results for the Stark effect regarding the interaction of atoms.

If $d_{00} = d_{01} = 0$, then in the case of weak fields, we have that:

$$E(k) = A_1 - A_0 - \frac{2\,(\vec{E}\vec{d}_{01})^2}{A_1 - A_0} + G_k |C_{k01}|^2 + 2G_k M_k \frac{(\vec{E}\vec{d}_{01})}{A_1 - A_0}. \qquad (3)$$

From equation (3) it is clear that the consideration of the interelectronic interaction leads to the appearance of a linear effect in addition to the quadratic one, that is, to a reduction in the order of the Stark effect. A comparison of our results with those arrived at in the work of Gross [4] will be given in a subsequent article.

Of a certain interest is also the degenerated case ($A_1 = A_0$) if an account is taken of the interelectronic interaction ($G_k \neq 0$) while $d_{00} = d_{11} = 0$. Here, we are concerned not with the energy of excitons (since, in general, such transitions are forbidden by the selection principles), but instead with a splitting of the electronic level in an external field. In this case, we have that:

$$E_k = \left\{4\,(\vec{E}\vec{d}_{01})\left[(\vec{E}\vec{d}_{01}) + G_k\left(|C_{k01}|^2 + \frac{\pi}{8} M_k\right)\right]\right\}^{1/2} \qquad (4)$$

In the absence of interaction ($G_k = 0$), we get the normal Stark effect for hydrogen:

$$E = 2\,(\vec{E}\vec{d}_{01}).$$

It is clear from equation (4) that the interelectronic interaction leads to the appearance of more complex relationships in function of the field, and it has, generally, an order lower than the linear one.

Thus, an interelectronic interaction results in lowering of the Stark effect order by comparison with that of the Stark effect in non-interacting atoms.

Translated by H. Cygielski

REFERENCES

1. Ya. I. Frenkel, *Phys. Rev.*, 37, 17, (1931).
2. V.S. Galishev and S.V. Vonsovskii, *Fiz. metal. metalloved.* 3, 395, (1956).
3. G.H. Wannier, *Phys. Rev.*, 52, 191, (1937).
4. E. Gross, *Izv. Akad. Nauk SSSR*, ser. fiz., 20, 89, (1956).

THE *S-D* EXCHANGE MODEL OF TRANSITION METALS*

A. A. BERDYSHEV and Iu. A. IZIUMOV
A.M. Gorki's Urals State University

(Received 11 April 1957)

In the *s-d* exchange model of transition metals [1] it is usual to consider only one *d*-electron per atom, whereas in reality there are several of them. Within the framework of the homopolar model, Moller [2], and then in a greater detail Pakhomov and Kondorski [3], considered the case of several *d*-electrons, while the last authors derived a small exponential correction to the known $T^{3/2}$ law of spontaneous magnetizability at low temperatures. However, the important *s-d* exchange interaction was not taken into consideration in the above investigations.

If it is assumed in the *s-d* exchange model that there are several (z) *d*-electrons per atom, then the operator of the *s-d* electrons system will have the following form:

$$H = U + H_d + H_{sd} + H_s,$$

$$H_d = \sum_{n_1\nu_1 n_2\nu_2}{}' J(n_1\nu_1; n_2\nu_2)\left\{\left(b^+_{n_1\nu_1} b_{n_1\nu_1} - b^+_{n_1\nu_1} b_{n_2\nu_2}\right) + \right.$$

$$\left. + \left(b^+_{n_1\nu_1} b^+_{n_1\nu_1} b_{n_1\nu_1} b_{n_2\nu_2} + b^+_{n_1\nu_1} b^+_{n_2\nu_2} b_{n_1\nu_1} b_{n_1\nu_1} - 2 b^+_{n_1\nu_1} b^+_{n_2\nu_2} b_{n_1\nu_1} b_{n_2\nu_2}\right)\right],$$

$$H_{sd} = \sum_{\nu=1}^{z}\left\{-\frac{1}{N}\sum_{nk_1k_2} \exp\left[i\vec{n}(\vec{k}_2 - \vec{k}_1)\right] I_\nu(\vec{k}_1, \vec{k}_2)\left[\left(b_{n\nu} a^+_{k_1} a_{k_2}(-) + \right.\right.\right.$$

$$\left. b^-_{n\nu} a_{k_1}(-) a^+_{k_2}\right) + b^+_{n\nu} b_{n\nu}\left(a^+_{k_1}(-) a_{k_2}(-) - a^+_{k_1} a_{k_2}\right)\left.\right]\left.\right\},$$

$$H_s = \sum_k\left[\varepsilon_k a^+_k a_k + \varepsilon_k - \sum_{\nu=1}^{z} I_\nu(\vec{k}, \vec{k})\, a^+_k(-) a_k(-)\right],$$

$$\varepsilon_k = L(\vec{k}, k) + N\sum F(0, \vec{k}; 0, \vec{k}),$$

wherein, U – an additive constant; $L(\vec{k}, \vec{k})$ is the specific energy of the 4*s*-electron [1,4];

$$F\nu(o, \vec{k}; o, \vec{k})$$

is the Coulomb energy of the 3*d*-electrons interaction with the 4*s*-electron having an impulse of $\vec{k}$ while the interacting 3*d*-electron is in the ν orbit;

$$J(\vec{n}_1\nu_1; n_2\nu_2)$$

is the interval of the *s-d* interaction of the 3*d*-electron orbit ν with the $\vec{k}_1$ and $\vec{k}_2$ states of the 4*s*-electrons; $b_{n\nu}$ and a_k, $a_k(-)$ are operators of the secondary quantizations of the Bose and Fermi statistics, respectively. A calculation of the energy spectrum of the weakly excited states of the system can be carried out by the method given [3], while the magnetizability determination can be made by the method described [4]. If such calculations are carried out, we get that in the case when

$$z = 2,\ M = \left(1 + \frac{b}{c}\right) M_d,$$

where the constant b and c have the same meaning as in work [4] and

$$M_d = M_0\left\{1 - \lambda_1 T^{3/2}\sum_{n=1}^{\infty}\frac{e^{-\alpha n}}{n^{3/2}} - \lambda_2 T^{3/2} e^{-\frac{I_0}{kT}}\right\}, \quad 1, 2 = \quad (1)$$

* *Fiz. metal. metalloved.* 5, No. 3, 552-553, 1957.

VOL. 5 1957

$$\left(\frac{k}{4\pi n}\right)^{3/2}\left[\frac{1}{2}(J_{11}+$$

$$+J_{22})\pm J_{12}\Big]^{-3/2},\quad I_0=z\left(J_{12}^0+nJ_{12}\right),$$

$$z=\frac{2zb^2}{ckT};\quad M_0=zN\mu_0,$$

n is the number of neighbours,

$$J_{ik},\ J_{ik}^0$$

are exchange integrals of d-orbits of neighbouring atoms and of one and the same atom, respectively. If

$$J_{ik}=J \text{ and } J_{ik}^0=J_0,$$

then in a general case z-d electrons,

$$\lambda_2=0,\quad \text{and}\quad \lambda_1=2\left(\frac{k}{4\pi znf}\right)^{3/2},$$

Two cases should be distinguished in considering the series given in equation (1): one of large and another of small values of a. Turov [4] studied the case of large values and showed that then the s-d exchange interaction leads to the appearance of an exponential relationship between M and T. In the opposite case when $a \ll 1$, the dependence $M(T)$ is completely different. In investigations of Turov [5] and in those of Kittel and Mitchell [5], concerning the ferromagnetic resonance, certain assumptions were made regarding the value of the s-d exchange integral: it was shown that the factor b has in all probability a value of the order of 10^{-15} to 10^{-14} ergs. If it is assumed that $b = 10^{-15}$, and that the limiting Fermi energy is $c \approx 10^{-12}$ ergs, then, at a temperature of the order of several degrees K (the lowest temperature at which the s-d exchange model is still applicable without taking into consideration the magnetic interaction) we get that $a \approx 0.05$, and at higher temperatures the value of a is still lower. At $a \ll 1$, we find by means of the Euler-MacLauren integration method that:

$$\sum_{n=1}^{\infty}\frac{e^{-sn}}{n^{3/2}}=2{,}61-3{,}6a^{1/2}+1{,}46a-0{,}1a^2+\ldots$$

(which agrees with the results derived in the work [6] concerning the representation of the Bose-Einstein intervals in the form of series). Then,

$$M_d=M_0\left\{1-\left(\frac{T}{\theta}\right)^{3/2}-1{,}95\left(\frac{zb^2}{ck\theta}\right)^{1/2}\frac{T}{\theta}+\right.$$

$$\left.+1{,}48\frac{zb^2}{ck\theta}\left(\frac{T}{\theta}\right)^{1/2}+\ldots-2(z-1)\exp-\left(\frac{zI_0}{kT}\right)\right\},$$

and hence, if it is assumed that

$$\theta\approx 10^3\ ^\circ\mathrm{K},\ z=1$$

$$M_d=N\mu_0\left\{1-\left[\frac{T}{\theta}\right]^{3/2}+\right.$$

$$\left.+0{,}02\left[\frac{T}{\theta}\right]-1{,}2\cdot 10^{-4}\left[\frac{T}{\theta}\right]^{1/2}+0\left(\frac{\theta}{T}\right)^{1/2}\right\}.$$

Of necessity, the values given for the coefficients define their order only. The remaining members of the series, which were ignored, have values lower than 10^{-6} at any temperature $T \geq 1^\circ\mathrm{K}$.

Thus, the consideration of a weak s-d exchange interaction

$$(I_{sd}\approx 10^{-15}\text{ to }10^{-14})$$

leads to the appearance of an additional linear member in the temperature dependence of spontaneous magnetizability of a ferromagnetic material, and this can be responsible for some deviations from the

$$T^{3/2}\ \text{law}\ (\lesssim 10\%),$$

thereby improving the agreement with practical results.

Translated by H. Cygielski

REFERENCES

1. S.V. Vonsovskii, *Zh. eksp. teor. fiz.* 16, 981, (1946);
   S.V. Vonsovskii and E.A. Turov,
   Zh. eksp. teor. fiz. 25, 419, (1935);
   S.V. Vonsovskii and A.A. Berdyshev,
   Izv. Akad. Nauk SSSR, Ser. Fiz., 18, 328, (1954).
2. C. Moller, *Z. Physik.* 82, 559, (1933).
3. A. Pakhomov and E.N. Kondorskii,
   Dokl. Akad. Nauk SSSR, 93, 431, (1953).
4. E.A. Turov, *Zh. eksp. teor. fiz.* 25, 352, (1953).
5. E.A. Turov, *Izv. Akad. Nauk SSSR*, Ser. Fiz., 19,
   462, (1955);
   C.K. Kittel and A.N. Mitchell, *Fiz. metal. metalloved.*,
   (1957) Phys. Rev., 101, 1611, (1956).
6. I.E. Robinson, *Phys. Rev.*,
   83, 678, (1951).

VOL.
5
1957

THE EFFECT OF SHORT RANGE ORDER ON THE ELECTRICAL RESISTANCE OF ALLOYS IN THE STATE OF ORDERING*

A. F. POLESIA and B.N. FINKELSHTEIN

Dnepropetrovsk State University Metal Physics and Metallography Institute of Ts.N.I.I.Ch.M.

(Received 18 February (1957)

At present, the theory of the electrical resistance of ordering alloys, in which due consideration is given to the far order correlation between the atoms, is developed sufficiently fully. Smirnov [1] obtained within the framework of the mono-electron theory, a most general expression for the dependence of the residual electrical resistivity on the degree of far order and on the composition of a $A-B$ type binary alloy having any desired stoichiometric ratio between the centres of the A and B atoms. The expression obtained was also confirmed for the poly-electrons theory [2].

Much less attention has been given to the near order calculations. In particular, no quantitative evaluation has been made of the effect of near order correlation between atoms on the electrical resistivity. An evaluation of this kind can be carried out within the framework of the mono-electron theory. For this purpose, in the calculation of the matrix elements of the excitation energy $V_{kk'}$, there is introduced into the expression for the electrical resistivity [3]:

$$\rho - \alpha T = 4K \int_0^{\pi} |V_{kk'}|^2 (1 - \cos\theta) \sin\theta d\theta, \qquad (1)$$

in addition to prior probabilities

$$P_j^{(m)}$$

also a posterior probability:

$$P_j^{(m)}(k) \cdot (j, k = A, B).$$

In equation (1), K is a constant, k and k' are wave vectors of an electron before and after collision, respectively; Θ is the angle between these vectors; V is the excitation energy and α is the temperature coefficient of electrical resistivity.

In cases of the body-centred, and a simple cubic lattice, the expressions

$$P_j^{(m)}$$

have the following values [4].

$$\begin{aligned} P_A^{(m)} &= c_1 + (-1)^m q\eta, \\ P_B^{(m)} &= c_2 - (-1)^m q\eta, \end{aligned} \qquad (2)$$

wherein, c_1 and c_2 are constants for the atoms A and B; η – far order; q is equal c_1 if $c_1 < 1/2$ and $q = c_2$ if $c_1 \geqslant 1/2$.

In order to arrive at a correct relationship between the prior probabilities

$$P_j^{(m)}$$

and the posterior ones in the case of a body-centred and a simple cubic lattices, it is necessary to introduce eight probabilities

$$P_j^{(m)}(k),$$

satisfying the following relationships:

$$\begin{aligned} &P_A^{\beta}(A) + P_A^{\beta}(B) = 1; \quad P_B^{\alpha}(A) + P_B^{\alpha}(B) = 1, \\ &P_B^{\beta}(A) + P_B^{\beta}(B) = 1; \quad P_A^{\alpha}(A) + P_A^{\alpha}(B) = 1, \\ &P_A^{\alpha} \cdot P_A^{\alpha}(A) = P_A^{\beta} \cdot P_A^{\beta}(A); \quad P_A^{\alpha} \cdot P_A^{\alpha}(B) = P_B^{\beta} \cdot P_B^{\beta}(A), \\ &P_B^{\alpha} \cdot P_B^{\alpha}(B) = P_B^{\beta} \cdot P_B^{\beta}(B); \quad P_A^{\beta} \cdot P_A^{\beta}(B) = P_B^{\alpha} \cdot P_B^{\alpha}(A). \end{aligned} \qquad (3)$$

In the above expressions, α and β are centres occupied in a fully ordered state by the atoms A and B.

Using the procedure as given in work [5], and with the help of the posterior probabilities

$$P_j^{(m)}(k)$$

---

* *Fiz. metal. metalloved.* 5, No. 3, 554-556, 1957.

it is now possible to determine the correlation coefficient $\epsilon^{(mn)}$ between atoms situated in the centres m and n of the lattice

$$(m = m_1 + m_2 + m_3);$$

$$\varepsilon(m, n) = u(1 + ve^{im\pi})\gamma^{|m-n|}e^{i(m-n)\pi},$$

if $|m - n|$ is an even number;

$$\varepsilon(m, n) = u\sqrt{1 - v^2}\,\gamma^{|m-n|}e^{i(m-n)\pi}$$

if $|m - n|$ is odd, while:

$$|m - n| = |m_1 - n_1| + |m_2 - n_2| + |m_3 - n_3|,$$

$$\gamma = \frac{c_1^2(\sigma - \eta^2)}{u\sqrt{1 - v^2}}, \quad \text{if} \quad c_1 < \frac{1}{2};$$

$$\gamma = \frac{c_2^2(\sigma - \eta^2)}{u\sqrt{1 - v^2}}, \quad \text{if} \quad c_1 > \frac{1}{2}; \qquad (4)$$

$$u = c_1c_2 - q^2\eta^2, \quad v = \frac{(c_1 - c_2)q\eta}{u}$$

If $\epsilon^{(m,n)}$ is known, it is possible to calculate those members of the expression for the matrix elements of the excitation energy which depend on correlation between the atoms

$$|V_{kk'}|^2 = \frac{1}{N^2}|V_A^{kk'} - V_B^{kk'}|^2 \sum_m p_A^{(m)} \cdot p_B^{(m)} + \frac{1}{N^2}|V_A^{kk'} -$$

$$- V_B^{k'}|^2 \sum_{m \neq n}\sum \varepsilon^{(m,n)} exp\, i(\varphi_i,\ m_i - n_i)\ \varphi_i = (\vec{k} - \vec{k'},\ \vec{a_i}). \qquad (5)$$

When equation (4) is taken into consideration, it is easy to integrate equation (5). After integration, the expression obtained is then substituted in equation (1), which is then followed by its expansion into a series according to γ and considering only the quadratic terms. Integration in function of the angle θ is carried for a specific case of β-brass crystal lattice of stoichiometric composition. In doing so it is assumed that the electron scattering is isotropic and that the electron density is $3/a^3$, where, a is the β-brass crystal lattice constant. By carrying out the above indicated operations, we get that:

$$\rho - \alpha T = K(1 - \eta^2)(1 - 1{,}365\,\gamma + 0{,}506\gamma^2). \qquad (6)$$

In order to compare with experimental data the relationship obtained for variation of the residual electrical resistivity in function of the degree of ordering, use will be made of the approximate expression for near order:

$$\sigma = \eta^2 + \frac{\omega}{2}(1 - \eta^2)^2, \qquad (7)$$

where,

$$\omega = \frac{U}{\kappa T},$$

and U is the energy of displacement. This expression is very accurate for temperatures close to the Curie point temperature. In Fig. 1 is drawn the curve [7]

$$\frac{\rho - \alpha T}{\rho_0} = \qquad (II)$$

$$= (1 - \eta^2)\,\frac{1 - 1{,}365\,\frac{\omega}{2}(1 - \eta^2) + 0{,}506\,\frac{\omega^2}{4}(1 - \eta^2)^2}{1 - 1{,}365\,\frac{\omega_0}{2} + 0{,}506\,\frac{\omega_0^2}{4}},$$

as calculated from equation (6), in addition to Smirnov's formula curve

$$\frac{\rho - \alpha T^{[7]}}{\rho_0} = (1 - \eta^2) \qquad (III)$$

as well as the experimental curve [6]

$$\frac{\rho - \alpha T}{\rho_0} \qquad (I)$$

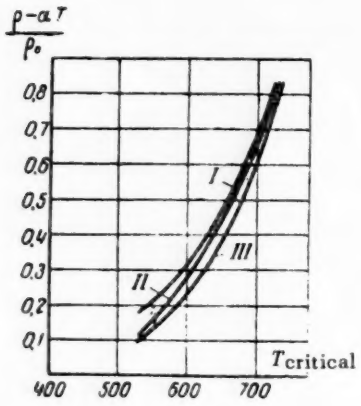

FIG. 1.

ρ_0 represents variation in the electrical resistivity of the alloy during its transition from a fully ordered state to the state of full disorder at a temperature higher than the Curie point temperature. It is clear from Fig. 1 that in the temperature interval within which the approximate expression (7) is correct, the curve II represents extremely well the variation in the alloy resistivity with far order changes. The deviations from the experimental curve do not exceed 2 – 3 per cent, whereas a similar deviation for curve III reaches 10 – 12 per cent.

The analysis, carried out in the present article, regarding the effect of the near order on the electrical resistivity of an ordering alloy enables us to conclude that the deviation of Smirnov's curve from the experimental data is due to the fact that its derivation was made without taking into account the near order correlation between atoms.

Translated by H. Cygielski

REFERENCES

1. A.A. Smirnov, *Zh. eksp. teor. fiz.*, 17, 743, (1947).
2. M.A. Krivoglaz and Z.A. Matysina, *Zh. eksp. teor. fiz.*, 16, 46, (1955).
3. G. Bete and A. Sommerfeld, *Elektronnaya teoriya metallov (Electronic theory of metals), United Scientific and Technical Press*, (1938).
4. A.A. Polesya and B.N. Finkelshtein, *Problemy metallovedeniya i fizyki metallov (Problem in metallurgy and metal physics)*, in print.
5. Iu. N. Obraztsov, *Zh. eksp. teor. fiz.*, 8, 593, (1938).
6. J.M. Cowley, *Phys. Rev.*, 77, 669, (1950).

ON DETERMINATION OF THE PONDEROMOTIVE FORCE OF INTERACTION BETWEEN MAGNET AND A FERROMAGNETIC MATERIAL *

V. L. SHMARTS

(Received 18 February 1957)

An exact calculation of the force of interaction between a magnet and a ferromagnetic part is important for the theory of magnetic thickness gauges, since in this theory an approximate only calculation of the point interaction force between the "magnetic charges" [1] is incapable of elucidating the dependence of the force of interaction on the structure of the ferromagnetic material.

In the present communication the basic concepts are given of calculating the force of interaction with the help of magneto-static methods developed by Grinberg [2].

For convenience of calculations, let the magnet be considered to be in the form of a sphere, of radius r_0, with magnetic permeability μ_1, which is magnetized with a uniform field of

$$\vec{H}_0 \quad (H_0 = H_{0z} = \vec{H}_0).$$

The other component (ferromagnetic) is considered to be flat and to fill with its ferromagnetic mass of permeability μ_3, the semi-space $Z < 0$. Let a non-magnetic medium (of magnetic permeability $\mu_2 = 1$), consisting of a cover and of a layer of air surrounding the magnet, exist between the magnet and the ferromagnetic element.

If the ferromagnetic parts are absent, the potential of the magnet ψ_1, and that of the non-magnetic medium ψ_2, are in the form of Lorentz's potentials:

$$\psi_1 = \psi_1^*(X, Y, Z) = -\frac{3}{\mu_1 + 2} H_0 Z; \quad \psi_2 = \psi_2^*(X, Y, Z) = \\ = -H_0 Z + \frac{(\mu_1 - 1) H_0^3 r_0 (Z - Z_0)}{(\mu_1 + 2)(X^2 + Y^2 + Z^2)^{3/2}} \tag{1}$$

In the presence of ferromagnetic elements, whose potential is denoted by ψ_3, all the three potentials, which satisfy Laplace's equation, should according to Lebedev [3], be in the following form:

$$\psi_1 = \psi_1^* + \\ + \sqrt{2\cosh\beta - 2\cos\alpha} \sum_{n=0}^{\infty} a_n \exp\left[-\left(n + \frac{1}{2}\right)\beta\right] p_n(\cos\alpha),$$

$$\psi_2 = \psi_2^* + \\ + \sqrt{2\cosh\beta - 2\cos\alpha} \sum_{n=0}^{\infty} \left\{C_n \exp\left[-\left(n + \frac{1}{2}\right)\beta\right] + \right. \\ \left. + d_n \exp\left[(\beta - 2\beta_0)\left(n + \frac{1}{2}\right)\right]\right\} p_n(\cos\alpha), \tag{2}$$

$$\psi_3 = -\frac{H_0 \sinh\beta}{\mu_3(\cosh\beta - \cos\alpha)} + \\ + \sqrt{2\operatorname{ch}\beta - 2\cos\alpha} \sum_{n=0}^{\infty} b_n \exp\left[(\beta - 2\beta_0)\left(n + \frac{1}{2}\right)\right] P_n(\cos\alpha).$$

Here, α, β and ϕ are bipolar co-ordinates associated with Dekart's relationships:

* *Fiz. metal. metalloved.* 5, No. 3, 556-558, 1957.

$$X = \frac{\bar{c}\sin\alpha\cos\varphi}{\cosh\beta - \cos\alpha};$$

$$Y = \frac{\bar{C}\sin\alpha\sin\varphi}{\cosh\beta - \cos\alpha};\quad Z = \frac{\bar{c}\sinh\beta}{\cosh\beta - \cos\alpha}$$

In these co-ordinates, the cover thickness is:

$$X^0 = \bar{c}\left(\coth\beta_0 - \frac{1}{\sinh\beta_0}\right).$$

The coefficients a_n, b_n, c_n and d_n of Lezhander's polynominals p_n are determined from the conditions of potentials continuity and from induction in the boundary between the magnet and the non-magnetic medium (boundary equation $\beta = \beta_0$), and also from induction in the boundary between the steel and cover (equation: $\beta = 0$).

$$\begin{gathered}(\psi_1)_{\beta=\beta_0} = (\psi_2)_{\beta=\beta_0};\ \mu_1\left(\frac{\partial\psi_1}{\partial\beta}\right)_{\beta=\beta_0} = \mu_2\left(\frac{\partial\psi_2}{\partial\beta}\right)_{\beta=\beta_0}.\\ (\psi_2)_{\beta=0} = (\psi_3)_{\beta=0};\ \mu_2\left(\frac{\partial\psi_2}{\partial\beta}\right)_{\beta=0} = \mu_3\left(\frac{\partial\psi_3}{\partial\beta}\right)_{\beta=0}.\end{gathered} \tag{3}$$

In order to simplify further calculations, a_n, b_n, c_n and d_n will be expanded into a power series (with the accuracy to

$$\frac{1}{(\mu_1-1)^k}):$$

$$a_n = S_0\sum_{k=0}^{\infty}\frac{a_n^{(k)}}{(\mu_1-1)^k};$$

$$b_n = S_0\sum_{k=0}^{\infty}\frac{b_n^{(k)}}{(\mu_1-1)^k};$$

$$c_n = S_0\sum_{k=0}^{\infty}\frac{C_n^{(k)}}{(\mu_1-1)^k};$$

$$d_n = S_0\sum_{k=0}^{\infty}\frac{d_n^{(k)}}{(\mu_1-1)^k}\quad\left(S_0 = -\frac{\mu_1-1}{\mu_1+2}H_0 r_0\right) \tag{4}$$

From the boundary conditions, a system of equations is derived which enables the determination of the k-th order expansion components

$$a_n^k,\quad b_n^k,\quad c_n^k,\quad \text{and}\quad d_n^k$$

from those of the $(k-1)$-th order, thus solving the problem in question:

$$a)\ a_n^{(k)} = c_n^{(k)} + d_n^{(k)};$$

$$\begin{aligned}b)\ &(n+1)\left(a_{n+1}^{(k)} - d_n^{(k)}\right)\exp\left(-2\beta_0\right) - n\left(a_n^{(k)} - a_{n-1}^{(k)}\right) =\\ &= 2(n+1)\left(d_n^{(k-1)} - d_{n+1}^{(k-1)}\right)\exp\left(-2\beta_0\right) -\\ &- 2n\left(d_{n-1}^{(k-1)} - d_n^{(k-1)}\right) - 2\operatorname{sh}\beta d^{(k-1)};\end{aligned} \tag{5}$$

$$c)\ \sum_{n=0}^{\infty} d_n^{(k)}\exp - (2n+1)\beta_0 = 0;$$

$$d)\ C_n^{(k)} = -\gamma\exp\left[-(2n+1)\beta_0\right]\left(A_n^{(k)} + d_n^{(k)}\right) =$$

$$= \exp\left[-(2n+1)\beta_0\right]\left(b_n^{(k)} - A_n^{(k)} - d_n^{(k)}\right)$$

Here the free members A_n^k equal:

$$A_n^{(0)} = A_n;\ A_n^{(k)} = 0\ (\text{при } k \neq 0); \tag{6}$$

$$\psi_2^* = \sqrt{2\operatorname{ch}\beta - 2\cos\alpha}\sum_{n=0}^{\infty} A_n\exp$$

$$\exp\left[(\beta - 2\beta_0)\left(n+\frac{1}{2}\right)\right]P_n(\cos\alpha);$$

VOL 5 195

$$A_n = S_0[\cosh\beta_0 - (2n+1)\sinh\beta_0]; \quad \gamma = \frac{1-\mu_3}{1+\mu_3}.$$

The following expressions for the coefficients

$$\bar{d}_n^0:$$

can be derived from the equations system (5):

$$\bar{d}_0^{(0)} = \frac{1}{S_0} A_0^{(0)} + d_0^{(0)} =$$

$$= \frac{\sum_{n=0}^{\infty} \frac{2n\sinh\beta_0 \exp -(2n+1)\beta_0}{1+\gamma\exp[-(2n)+1\beta_0]}}{} = S' + 0(\beta) \quad (S' \neq S(\mu_3)), \tag{7}$$

$$d_n^{(0)} = \sum_{n=0}^{\infty} \frac{1+\gamma e^{-\beta_0}}{1+\gamma\exp[-(2n+1)\beta_0]}$$

$$= \frac{1}{S_0} A_n^0 + d_n^0 = \frac{(\gamma e^{-\beta_0}+1)\bar{a}_0^0 + 2n\sinh\beta_0}{1+\gamma\exp[-(2n+1)\beta_0]} \approx \bar{d}_0^{(0)} + 0(\beta)$$

In case of thin coverings

$$\beta \ll \frac{1}{\mu_3} (\beta \to 0), \quad \bar{d}_0^0 \quad \text{and} \quad d_n^0$$

are practically independent of μ_3.

Other relationships obtain for the components of the first and higher orders of approximation

$$d_n^{(k)}$$

Thus, in case of

$$d_n^{(1)}$$

we get:

$$d_n^1 = \frac{\bar{d}_n^{(0)}}{1+\gamma e^{-\beta}} \approx \mu_3 d_n^{(0)}. \tag{8}$$

The force of interaction $\vec{F}$ is determined using Maxwell's formula:

$$\vec{F} = \frac{1}{4\pi}\int\left[\vec{H}_2(\vec{H}_2\vec{n}) - \frac{1}{2}(\vec{H}_2)^2\vec{n}\right]dS. \tag{9}$$

(The integral is taken for the external surface of the spherical magnet).

$$H_{2Z} = -\frac{\partial\psi_2}{\partial Z}.$$

A simple calculation (with an accuracy up to

$$\frac{1}{(\mu_1-1)^2}$$

gives for $\vec{F}$ the following expression in the form of a combination of the coefficients

$$\bar{d}_n^0 \quad \text{and} \quad d_n^1:$$

$$\vec{F} = F_Z = -\frac{\gamma S_0^2}{2}\left[K(\beta_0) + \frac{\mu_3}{\mu_1-1} G(\beta_0)\right]. \tag{10}$$

Here,

$$K(\beta_0) = \sum_{n=0}^{\infty}\left[(2n+1)\bar{d}_n^{(0)} d_n^{(0)} - 2(n+1)\bar{d}_n^{(0)}\bar{d}_{n+1}^{(0)}\right]$$

$$\exp\left[-(4n+2)\beta_0\right] \neq \chi_1(\mu_3),$$

$$\frac{\mu_3}{\mu_1-1} G(\beta_0) = \sum_{n=0}^{\infty}\left[(2n+1)\bar{d}_n^{(0)}\bar{d}_n^{(1)} - 2(n+1)\right.$$

$$\left. d_n^{(0)} d_n^{(1)} + \bar{d}_{n+1}^{(0)} d_{n+1}^{(1)}\right)\Big] \exp[-(2n+1)\beta_0].$$

The effect of structure is defined by the second term in equation (10):

$$\frac{\mu_3}{\mu_1 - 1} G\beta_0,$$

which depends on the structure-sensitive factors μ_3 and μ_1.

Two cases are of practical importance:

1. When $\mu_1 \ll \mu_3$. This condition occurs in thickness gauges with permanent magnet of the Vinokurski [4] MT-2 type. The magnets for these instruments are made of alloys with low magnetic permeability values (Alnico, Magnico). As it is clear from equation (10), the role of the structure-sensitive term gains in importance during the use of such instruments (and therefore, their readings depend considerably on structural variations and on the method used for heat treatment of the steel, since μ_3 varies with it).

2. When

$$\mu_1 \gg \mu_3.$$

This conditions occurs in electromagnetic thickness gauges, the cores of which are made of materials having a high magnetic permeability (Armco, Permalloy). The readings of these instruments depend little on the magnetic permeability values of the instrument components and the same applies to the effect of structure and method of heat treatment. Practical experience [5], including also measurement tests data obtained at the national instrument calibration institute M.T.D.A.Z. using an instrument of our construction, proved also the industrially important advantage of the electromagnetic instruments.

Translated by H. Cygielskii

REFERENCES

1. N.S. Akulov, *Vestnik metallopromyshlennosti*, (1940).
2. G.A. Grinberg, *Izbrannye voprosy matematicheskoi teorii elektricheskikh i magnetnykh yavlenii (Selected problems in the mathematical theory of electrical and magnetic phenomena)*, Moscow-Leningrad, (1948).
3. N.N. Lebedev, *Spetsyalnyie funktsii, (Special functions)*, (1949).
4. S.A. Vinokurskii, Vestnik mashinos roenia, 5, (1953).
5. S.V. Yakubovich, *Ispytaniya lakokrasochnykh materialov i pokrytii (Investigations of varnish colours and films)*, (1952).

THE EFFECT OF PRESSURE ON THE YOUNG'S MODULUS OF CERTAIN METALS*

A.D. EKHLAKOV, V.A. GLADKOVSKII and K.P. RODIONOV
Institute of Metal Physics of the Urals Branch of the Academy of Sciences of the U.S.S.R.

(Received 15 May 1957)

Investigation of the effect of high pressure on the variation in Young's modulus of various materials is not only of interest theoretically in defining more closely our theories concerning bonding forces in a material, it is also of great practical value, especially for certain fields of contemporary geophysics.

Hitherto no direct measurements have been made under pressure of Young's modulus as this presents technical difficulties [1]. The attention of investigators has thus been in the main directed towards studying the shear modulus. The variation with pressure in the shear modulus of metals was first studied using the static method by Bridgman [2], and a little later using the dynamic method [3-5].

In order to measure the change with pressure in Young's modulus E we designed and built special high-pressure equipment (up to 5,000 kg/cm² hydrostatic pressure, by means of which the pressure coefficient of Young's modulus could be measured directly using the static method. The principle of operation of the equipment is the variation in the rigidity of cantilevered test beam on the application of hydrostatic pressure. The rigidity was measured from the change in the angle of inclination of the test beam from the angle through which the high-pressure chamber must be turned in order to restore the initial deflexion of the test beam. Then for a constant deflexion of the beam the bending momment is directly proportional to the angle of rotation of the chamber. A detailed description of the equipment will be given in a later article.

The variation in Young's modulus with pressure was studied for metals (electrotechnical aluminium and copper with 0.05 – 0.15 per cent impurity contents, and medium-carbon 50 steel) of which the variation with pressure in the shear modulus G and the bulk modulus K were known from experiments. The test specimens were made in small batches of 5 – 6 units and were annealed at appropriate temperatures with subsequent slow cooling with the furnace.. The medium selected to convey high pressure to the specimen was a mixture of kerosine and transformer oil, the compressibility of which was also determined using the equipment.

The results of the experiments into the direct measurement of the coefficient of Young's modulus up to 4000 kg/cm² at room temperature are given in Table 1. The experimental

$$\frac{1}{E_0}\frac{dE}{dp}$$

values given are mean values of separate measurements made on three specimens. The measurements were made at 100 kg/cm² intervals both on increase and decrease in pressure. The maximum deviation of the measurements of the pressure coefficient of Young's modulus according to scatter of the experimental points was 10 per cent at a pressure of 4000 kg/cm², that is no more than 0.5 per cent of the Young's modulus itself.

The experimental data concerning the variation in the coefficient of Young's modulus with pressure obtained by means of direct measurement may be compared with calculated values of

$$\frac{1}{E_0}\frac{dE}{dp},$$

employing for this purpose experimental data available in the literature concerning the change with pressure of the bulk modulus K and the shear modulus G, and the well-known relationship between the elastic constants of an isotropic solid:

$$E = \frac{9KG}{3K+G}, \qquad (1)$$

that is valid in the case of small deformations (i.e. for not very large pressure intervals or for materials of low compressibility).

* *Fiz. metal. metalloved.* 5, No. 3, 559-561, 1957.

VOL. 5 1957

TABLE 1.

Material	$\frac{1}{E_0}\frac{dE}{dp}$ (10^6cm²/kg)	
	According to equation (2)	Experimental data
Aluminium	7,15	7,2
Copper	2,69	4,3
Steel	2,24	2,3

Differentiating equation (1) and bearing in mind that in the range of pressures up to 5,000 kg/cm² it is possible with sufficient accuracy for practical purposes to substitute for the real values

$$\frac{1}{E}\frac{dE}{dp}, \quad \frac{1}{G}\frac{dG}{dp},$$

$$\frac{1}{K}\frac{dK}{dp} \quad \text{and} \quad \frac{G}{K}$$

their usual values

$$\frac{1}{E_0}\frac{dE}{dp}, \quad \frac{1}{G_0}\frac{dG}{dp}$$

$$\frac{1}{K_0}\frac{dK}{dp} \quad \text{and} \quad \frac{G_0}{K_0},$$

finally for the coefficient of Young's modulus we get:

$$\frac{1}{E_0}\frac{dE}{dp} \approx \frac{1}{3+\frac{G_0}{K_0}}\left(3\frac{1}{G_0}\frac{dG}{dp}+\frac{G_0}{K_0}\frac{1}{K_0}\frac{dK}{dp}\right), \quad (2)$$

where

$$\frac{1}{G_0}\frac{dG}{dp} \quad \text{and} \quad \frac{1}{K_0}\frac{dK}{dp}$$

are the coefficients of the shear and the bulk moduli respectively.

The relationship of the bulk modulus to the pressure can be calculated using Bridgman's semi-empirical formula that applies to many solids in the range of pressures up to 10,000 kg/cm²

$$-\frac{\Delta V}{V} = ap - bp^2, \quad (3)$$

where a and b are material constants, of the orders of magnitude 10^{-7} cm²/kg and 10^{-12} cm⁴/kg² respectively; p is the pressure (in kg/cm²).

From equation (3) in the zero approximation we get

$$\frac{1}{K_0}\frac{dK}{dp} \approx -a+\frac{2b}{a}. \quad (4)$$

The necessary experimental data concerning the magnitude:

$$E_0,\ K_0,\ G_0,\ \frac{1}{G_0}\frac{dG}{dp} \quad \text{and} \quad \frac{1}{K_0}\frac{dK}{dp}$$

for calculation according to equation (2) are given in Table 2. A comparison of the experimental values of the pressure coefficient obtained by us

$$\frac{1}{E_0}\frac{dE}{dp}$$

with the values calculated according to equation (2)

TABLE 2.

Material	a, [1] 10^7 cm²/kg	b, [1] 10^{13} cm⁴/kg²	E_0, [3] 10^{-6} kg/cm²	G_0 [3] 10^{-5} kg/cm²	$K_0\,10^{-6}$ kg/cm²	$\frac{1}{G_0}\frac{dG[6]}{dp}$ 10^6 cm²/kg	$\frac{1}{K_0}\frac{dK}{dp}$ 10^6 cm²/kg
Aluminium	13.40	3.44	0.72	2.67	0.74	7.61	3.74
Copper	7.16	1.04	1.30	4.77	1.39	2.71	2.18
Steel	5.83	0.80	2.13	8.26	1.70	2.36	2.11

is shown in Table 1. As will be seen from this table, in the range of pressures up to 4,000 kg/cm² the experimental data agree satisfactorily with the results obtained according to equation (2). The lack of agreement of the data for copper is evidently due to the fact that the modulus of normal elasticity of copper depends very extensively on the conditions of heat treatment of the specimens, that we were not able to reproduce accurately in our experiment owing to the absence of the necessary information in the literature [3-6].

Translated by R. Hardbottle

VOL. 5 1957

REFERENCES

1. P. Bridgman, *Recent work in the field of high pressures. Foreign Literature Publishing,* (1948).
2. P. Bridgman, *Proc. Am. Acad. Arts Sci.,* 63, No. 10: 401, (1929).
3. F. Birch, *J. Appl. Phys.,* 8: 129, (1937).
4. D. Lazarus, *Phys. Rev.,* 76, No. 4: 545, (1949).
5. D. Hughes and J. Kennel, *J. Appl. Phys.,* 26, No. 11: (1955).
6. F. Birch, *J. Appl. Phys.,* 9: 279, (1938).
7. A. Smith, *Phil. Mag.,* 44, No. 352: 453, (1953).

THE THERMODYNAMICS OF THE FERROMAGNETIC STATE AT LOW TEMPERATURES*

M.I. KAGANOV and V.M. TSUKERNIK

Physico-technical Institute of the Academy of Sciences of the U.S.S.R.

(Received 12 December 1956)

1. The thermal capacity of solids at low temperatures generally consists of several components, corresponding to several branches of the energy spectrum of the solid. Thus for example the thermal capacity of a metal at low temperatures:

$$C = \alpha T^3 + \beta T, \qquad (1)$$

where αT^3 is the component connected with the spin section of the thermal capacity and βT is that connected with the electronic section. For ferromagnetic metals, according to Bloch's theory [1] to expression (1) must be added $\gamma T^{3/2}$ – the spin thermal capacity. In the experimental determination of each component the problem arises naturally of separating them, which is very difficult, since the measurements are made in a comparatively narrow temperature interval. It is especially difficult in the case of ferromagnetic metals, where it is difficult to distinguish $T^{3/2}$ from T. The problem arises therefore of finding a parameter which when it changes will have different effects on each of the components in the expression for the thermal capacity. When the system contains a magnetic branch of the energy spectrum, the natural parameter is the magnetic field H which at $\mu H \gg T$† "freezes" the spins, the result of which the spin (magnetic) portion of the thermal capacity falls exponentially. In this case the electronic section of the thermal capacity hardly changes provided that the fields taken are not too high [2].

$$T \ll \mu H \ll \zeta_0$$

(ζ_0 is Fermi surface energy, the latter inequality is practically always found, $\zeta/\mu \sim 10^8$ oersteds).

This method of separating the magnetic section of the thermal capacity* involves measurements at low temperatures and in strong magnetic fields (at $H = 10^4$ oersteds,

$$\mu H \simeq 1^\circ\mathrm{K}),$$

so that it is necessary to study the thermodynamics of the ferromagnetic state at very low temperatures and in high magnetic fields.

2. In order to calculate the thermodynamic potential Ω, we employ the energy spectrum of spin waves that was first obtained by Holstein and Primakoff [3] from microscopical observations, and then by Herring and Kittel [4] phenomenologically on the basis of Landau and Lifshits' equations [5].

Indicating the spin wave energy by ϵ and its wave vector by $\vec{k}$, then

$$\epsilon = \sqrt{(\mu H + \theta_c a^2 k^2)^2 + 4\pi\mu M_0 (\mu H_0 + \theta_c a^2 k^2)}\,\sin\varphi. \qquad (2)$$

Here θ_c is a constant of the dimensions of energy coinciding in order of magnitude with the Curie temperature, M_0 is the magnetic saturation moment, a is a lattice constant, ϕ is the angle between $\vec{k}$ and $\vec{M}_0$; we assume that the external magnetic field $\vec{H}_0$ runs along $\vec{M}_0$; no account is taken of the magnetic anisotropy energy; the constant μ coincides in order of magnitude with a Bohr magneton. In the consecutive phenomenological theory the constants μ and Θ_c must be determined by experiment.

As we know

$$\Omega = T \sum_{\vec{k}} \ln\left(1 - e^{-\frac{\epsilon}{T}}\right). \qquad (2a)$$

---

* *Fiz. metal. metalloved.* 5, No. 3, 561-563, 1957.

† Bor's magneton, T = temperature in units of energy.

* In order to measure the spin thermal capacity C_S the thermal capacity of a ferromagnetic material must be measured at $H = 0$ (C_0) and at $H \to \infty$, i.e. at $MH \gg T$. Then $C_S = C_0 - C_\infty$.

Or, turning from summation to integration according to sections we get

$$\Omega = -\frac{V}{6\pi^2 a^3}\int_0^{\pi/2}\sin\varphi d\varphi\int_{\varepsilon_0}^{\infty}\frac{(ak)^3 d\varepsilon}{e^{\varepsilon/T}-1}, \qquad (3)$$

where V is the volume of the ferromagnetic body,

$$\varepsilon_0 = \sqrt{(\mu H_0)^2 + 4\pi\mu^2 M_0 H_0 \sin^2\varphi}. \qquad (3a)$$

Since the chemical potential of spin wave gas is zero, then the thermodynamic potential Ω coincides with the free energy F.

Employing (2) and (3), we get

$$F = -\frac{TV}{6\pi^2 a^3}\left(\frac{T}{\theta_c}\right)^{3/2}\int_0^{\pi/2}\sin\varphi d\varphi\int_0^{\infty}\frac{\left[\sqrt{\beta^2\sin^4\varphi + x^2} - (\beta\sin^2\varphi + \eta)\right]^{3/2} dx}{e^x - 1}, \qquad (4)$$

$$\sqrt{\eta^2 + 2\eta\beta\sin^2\varphi}$$

where

$$\beta = \frac{2\pi\mu M_0}{T}; \quad \eta = \frac{\mu H_0}{T}. \qquad (5)$$

Knowing the free energy, we get the thermal capacity, the magnetic moment and all the thermodynamic magnitudes that are of interest to us

$$C_V = -T\frac{\partial^2 F}{\partial T^2}; \quad M = -\frac{\partial F}{\partial H}\Big|_{H=0} + M_0. \qquad (6)$$

The following are the final results for the different limiting cases:

(*a*) There is no magnetic field ($\eta = 0$).

$$C_V = \frac{15}{32}\frac{\zeta(5/2)}{\pi^{3/2}}\frac{V}{a^3}\left(\frac{T}{\theta_c}\right)^{3/2}; \qquad (7)$$

$$M_0 - M(T) = \frac{\zeta(3/2)}{8\pi^{3/2}}\mu\frac{V}{a^3}\left(\frac{T}{\theta_c}\right)^{3/2};$$

II. $T \ll 2\pi\mu M_0$.

$$C_V = \frac{147}{64}\frac{\zeta(7/2)}{\pi^{3/2}}\frac{V}{a^3}\frac{T}{2\pi\mu M_0}\left(\frac{T}{\theta_c}\right)^{3/2}, \qquad (8)$$

$$M_0 - M(T) = \frac{\pi}{48\sqrt{2}}\mu\frac{V}{a^3}\left(\frac{T}{2\pi\mu M_0}\right)^{1/2}\left(\frac{T}{\theta_c}\right)^{3/2}.$$

(*b*) large magnetic fields ($\mu H_0 \gg T$).

I. $\mu H_0 \gg T$, $2\pi\mu M_0$,

$$C_V = \frac{1}{8\pi^{3/2}}\frac{V}{a^3}\left(\frac{\mu H_0}{\theta_c}\right)^{3/2}\left(\frac{\mu H_0}{T}\right)^{1/2} e^{-\frac{\mu H_0}{T}}; \qquad (9)$$

II. $T \ll \mu H_0 \ll 2\pi\mu M_0$,

$$C_V = \frac{V/a^3}{32\sqrt{2}\,\pi^{3/2}}\left(\frac{T}{\theta_c}\right)^{1/2}\frac{\mu H_0}{\theta_c}\frac{H_0}{2\pi M_0} e^{-\frac{\mu H_0}{T}} \qquad (10)$$

Thus the thermal capacity is exponentially low at

$$(\mu H_0 \gg T.$$

It is difficult at present to speak of comparison of the considerations made here with experiment. The thermal capacity did not, so far as is known, change in the magnetic field. The spin past of the thermal capacity was determined from the relation-

ship of the thermal capacity to the temperature [6-8]. The author of the last work was able to show that in the temperature interval 1.8 – 4.2°K the thermal capacity of magnetite is given to a good approximation by a binominal of the type

$$\alpha T^3+\beta T^{3/2}.$$

In conclusion the authors wish to thank L.D. Landau, A.I. Akhizer and V.G. Bar'yakhtar for useful discussion, and also B.G. Lazarev for his comments on the results obtained.

Translated by R. Hardbottle

REFERENCES

1. F. Bloch, *Z. Physik*, 61, 206, (1930).
2. I.M. Lifshits and A.M. Kosevich, *Zh. eksp. teor. fiz.* 29, 732, (1955).
3. T. Holstein and H. Primakoff, *Phys. Rev.*, 58, 1098, (1940).
4. C. Herring and C. Kittel, *Phys. Rev.* 81, 869, (1951).
5. L. Landau and E. Lifshits, *Phys. Z. Sowjet*, 8, 157, (1935).
6. W.H. Keesom and B. Kurrilmeyer, *Physica* 6, 364, 401, 633, (1939).
7. J.S. Kouvel, *Phys. Rev.* 102, 1489, (1956).

VOL
5
195

ON THE NATURE OF EXPANSION OF CAST IRON CASTINGS PRIOR TO FINAL CONTRACTION*

V.P. CHERNOBROVKIN

Metallurgical Institute of the Urals Branch of the Academy of Sciences of the U.S.S.R.

(Received 15 April 1957)

If liquid metal is poured into a casting mould the external dimensions of the casting increase first of all, and then after a certain time has elapsed they decrease. For better observation of this phenomenon investigators usually pour the metal into a horizontal mould and determine the change in length of the casting. The initial increase in length is termed the expansion prior to final contraction.

The question of the nature of expansion of metals prior to final contraction has so far not been explained [1, 2].

From special investigations we found that there are three reasons for the expansion of cast iron castings prior to final contraction [3]. The first is due to an increase in the volume of cast iron through the formation in it of an austenite-graphite eutectic. The second is due to thermal expansion of the outer shell of the casting during removal by the mould of the heat of overheating and of crystallization of the metal. The third reason is due to the growth of graphite inclusions in the outer shell of the casting during solidification of the liquid metal enclosed in this shell.

These reasons explain the difference in the effects of various factors on the expansion prior to final contraction of cast iron poured into a casting mould.

We will consider several examples [4].

1. On pouring cast iron into metal and sand (green, dry and preheated) moulds, the maximum expansion prior to final contraction is observed in specimens cast into a green mould, and the minimum in specimens cast into preheated and metal moulds.

On liquid cast iron being cooled in a preheated mould over a long period, no firm shell is formed that is capable of changing the dimensions of the casting. At first, through decrease in temperature, the volume of the liquid cast iron decrease and its level in the pouring gate falls. Then, on the formation in the cast iron of austenite-graphite crystals, its volume increases although this increase in volume does not result in an increase in the length of the casting while the cast iron is in the liquid-solid condition.

It is interesting to note that during this solidification period it is possible that the level of the cast iron in the pouring gate may not even rise. The fact is that owing to heating of the mould its diameter, and thus the volume of the hollow enclosing the cast iron, is increased. Since the volume of the hollow of the mould increases simultaneously with the volume of the cast iron, then through compensation of one volume by the other, the level of the cast iron in the mould remains unchanged.

This explanation is confirmed by the fact that the diameter of specimens of grey cast iron cast into preheated moulds exceeds that of specimens cast into green moulds.

On further crystallization, on the formation of a firm shell, simultaneously with rise in the volume of the cast iron the length of the casting also starts to increase. However by this time a considerable proportion of the graphite is being precipitated, and since it exhibits an insignificant expansion prior to final contraction only a small amount of graphite will affect the change in the length of the casting.

This explanation is based on the fact that, on cast iron being cooled in a preheated sand mould almost all the graphite, both in the centre of the casting and in its outer layers, forms in a liquid medium. In a preheated mould solidification takes place throughout the entire volume without the formation first of a solid shell: thus the occurrence of expansion prior to final contraction due to thermal expansion of a shell is excluded in this case. The position is different on casting cast iron in a green sand mould. In this case owing to considerable heat transfer a thin solid shell soon forms. Then, on the sand immediatly in contact with the metal losing its moisture and starting to heat up, there is a sharp decrease in the heat removal and the process of successive solidification throughout the entire volume. Now the temperature of the outer shell rises (if the metal had a

* *Fiz. metal. metalloved.* 5, No. 3, 563-564 , 1957.

high temperature on being poured) and, owing to thermal expansion of the outer shell the dimensions of the casting increase first of all.

Moreover, during the eutectic arrest of the centre of the casting, through its heat of crystallization the outer shell is annealed, resulting in considerable growth of the graphite inclusions contained in the shell; considerable expansion prior to final contraction is observed therefore in castings made in green moulds.

On pouring cast iron into a metal mould solidification takes place gradually in thin layers whose temperature is constantly falling, so that linear contraction of the casting begins almost immediatly after the metal has been poured into the mould. In this case the extensive cooling of the rapidly-growing shell prevents it from heating up. Extensive development of graphite formation is also possible, since this process requires time and high temperatures. Under these cooling conditions these processes do not become developed, therefore expansion prior to final contraction is either entirely absent or insignificant in cast iron poured into a metal mould.

2. With increasing carbon and silicon contents in cast iron expansion prior to final contraction increases to a certain limit, after which, despite the growth of graphite in the cast iron, it decreases.

This is explained as follows:-

During solidification of the cast iron casting, in its outer shell part of the graphite forms in a liquid medium (C_{lm}) and part in a solid medium (C_{sm}). With increasing silicon content in the cast iron the expansion prior to final contraction grows while ever the C_{sm} is increasing. On a certain silicon content in the cast iron being reached the C_{sm} starts to fall (here C_{lm} increases), and the expansion prior to final contraction falls accodingly.

3. In specimens cast from cast iron (3.8 – 3.9% C; 1.2 – 1.3% Si) treated at a low temperature with magnesium, after introducing ferrosilicon into it the expansion prior to final contraction falls, whereas in specimens treated with magnesium at a high temperature, on the other hand, it rises. In the first case, after adding ferrosilicon to the cast iron the amount of C_{sm} falls, in the second after adding ferrosilicon it increases. This is also the reason for the difference in the effect of the ferrosilicon on the expansion prior to final contraction of specimens cast from cast iron treated with magnesium at high and low temperatures.

4. The next experimental fact requiring explanation is that expansion prior to final contraction is greater, the greater the diameter of the cast specimen.

In a specimen of large diameter cast into a green mould, a thinner solid shell is obtained at the start of solidification of the centre than in a specimen of low diameter. Far more of the heats of overheating and of recrystallization passes through the thin shell of the first specimen than through the thick wall of the second, so that the thermal expansion of the first specimen is greater than that of the second.

For this same reason the graphitization processes in the outer shell of the first specimen are more than in the second. Thus expansion prior to final contraction occurring as a result of the first and the second reasons will be greater in a specimen of large diameter than in one of small diameter.

5. In investigating specimens cast from white iron and from light metals it was found that with rise in the temperature of casting the metal the expansion prior to final contraction also increases. In the same cases, on pouring the metal into a mould at a low temperature, no prior expansion is observed. This is explainable by the fact that prior expansion of these specimens depends solely on the thermal expansion of their shell, that is greater the more heat of overheating there is in the metal, i.e. the higher the pouring temperature.

It follows from the above that expansion prior to final contraction depends not only on the properties of the metal but also on those of the casting. It varies with the nature of solidification of the melt, the pouring conditions, the condition of the mould, the temperature of the metal, the dimensions and shape of the mould etc. In the case of cast iron it also depends on the graphite forming in the outer shell of the casting.

Translated by R. Hardbottle

REFERENCES

1. A.A. Bochvar, E.A. Sviderskaya and E.K. Korbut, *Izv. Akad. Nauk SSSR, otd. tekh. nauk*, 4, 409, (1947).
2. A.A. Bochvar and N.I. Novikov, *Izv. Akad. Nauk SSSR, otd. tekh. nauk.*, 2, 220, (1952).
3. V.P. Chernobrovkin, *Izv. Akad. Nauk SSSR, otd. tekh. nauk.*, No. 4-5, 106, 172, (1957).
4. V.P. Chernobrovkin,
   New Method of controlling the properties of cast iron during melting and casting
   (Novyi metod kontrolya svoistv chugunov po khodu plavki i zalivki).
   Mashgiz (1956).

THE DIFFUSION OF SILICON IN TRANSITION METALS*

G.V. SAMSONOV and L.A. SOLONNIKOVA

Institute of Powder Metallurgy and Special Alloys, Akad. Nauk U.S.S.R.

(Received 22 January 1957)

The transition metals form compounds with silicon, which are characterized by high electrical conductivity [1], ability to transform to the superconducting state [2], metallic lustre and other properties inherent in metals.

From the crystal chemistry viewpoint, the silicides are substitutional phases [3], in contrast to the carbides and nitrides, which are interstitial phases, and the borides, the crystal lattices of which include, besides certain features of interstitial phases, linear and layer elements of structure which are typical of silicides.

Investigations of the physical properties of silicides are of interest with a view to clarifying the features of electron structure of these compounds.

In the work, a study was made of the diffusion of silicon into certain transition metals (Ti, Nb, Ta, Cr, Mo, W, Fe, Co, Ni), in order to establish the values of activation energy for the formation of the corresponding silicide phases.

Cylindrical specimens were impregnated from a solid-phase bath, composed of silicon powder with activating additions. The thickness of the silicon-saturated layers was determined on etched microsections of end faces.

To determine the phase constitution of the layers, cuttings were taken from the specimen, of smaller thickness than that of the layers, and subjected to X-ray and chemical analysis. As a result it was found that the layers on all the metals consist of the disilicide. The results were manipulated to determine the diffusion constants by the method generally adopted for reactive diffusion [4].

Values found for the activation energy in (cals/mole) are shown in the table, in comparison with the activation energies for the diffusion of B, C and N in the same metals according to data [4, 5, 7].

From the data in the Table it follows that the energies of activation for the formation of silicide phases by diffusion are the lowest, although on formal grounds one would expect them to be the highest, if one starts from the proposition that silicon has the largest atomic radius (1.18 A) as compared with the atomic radii of B, C and N (0.91, 0.77 and 0.71 A respectively). As follows from the Figure, the values of activation energy increase in inverse ratio to the ionization potentials of the metalloids, which characterize their ability to contribute electrons to the general electron mass distributed within the positively charged framework.

Thus, the determining factors for the activation energies for formation of this type of phase are, in the first place, not dimensional but purely electronic factors.

In spite of the low activation energies for the formation of silicide phases, the silicides have relatively low values of physical properties, compared with the borides, carbides and nitrides. This can be explained as follows: whereas the refractory carbides and nitrides [8], and in part the borides also [9] are structurally interstitional phase types, the silicides, as stated above, are typical substitutional phases. In the borides, carbides and nitrides the shear strains caused by hardness measurements and also occurring during the process of melting, are hindered by the "wedging" effect of the metal atoms. In the case of the silicides which have graphite-type lattices with a weak bond between layers in the lattice [10], shear strain is made considerably easier.

Therefore the melting points of the silicides are frequently of the same order as, and even lower than the melting points of the corresponding metals and of silicon, whilst the hardness does not exceed 1000-1500 kg/mm², whereas for the borides, carbides and nitrides, it reaches values of 2000-3000 kg/mm² [11, 12]

Translated by E. Bishop

* *Fiz. metal. metalloved.*, 5, No. 3, 565-566, 1957.

VOL. 5 1957

TABLE 1

Transition metal	Diffusing element			
	Si (present work)	B (ref. 4)	C (ref. 5)	N (ref. 7)
Ti	5.690	9.150	17.500	33.800
Zr	—	—	17.300	39.200
Nb	11.720	14.130	18.900	25.400
Ta	6.040	16.900	19.300	39.400
Cr	10.250	20.520	26.000	—
Mo	9.470	14.300	34.400	—
W	5.780	20.400	39.500	—
Fe α	2.900	21.160	32.000 [4]	31.1000
Fe γ	25.170			
Co	13.090	33.400	39.850	—
Ni	24.950	—	32.200 [4]	

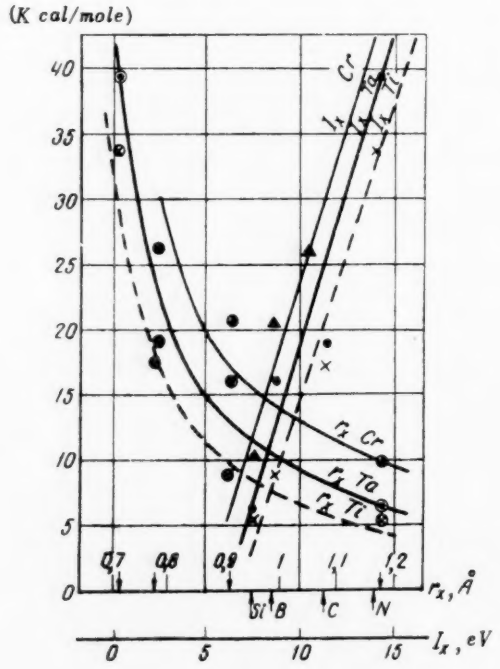

FIG. 1. Relationships of activation energies for the formation of phases with the same metal, to the atomic radii and ionization potentials of the metalloids.

REFERENCES

1. G.V. Samsonov, *Zh. tekh. fiz.*, 26, 716, (1956).
2. G.V. Samsonov and V.S. Neshpor, *Zh. eksp. teor. fiz.*, 30, 1143 (1956).
3. Ya. Umanskii and G.V. Samsonov, *Zh. fiz. khim.*, 30, 1526 (1956).
4. G.V. Samsonov, *Dokl. Akad. Nauk SSSR*, 93, 859, (1953).
5. G.V. Samsonov and V.P. Latysheva, *Fiz. metal. metalloved.*, 2, 303, (1956).
6. P.L. Gruzin, Yu. P. Polikarpov and M.A. Shumilov, *Zavodok. lab.*, 21, 417, (1955).
7. E. Gulbransen and K. Andrews, *J. Metals*, 187, 746, (1949); 188, 596, (1950).
8. G.V. Samsonov, *ISFKHA Akad. Nauk SSSR*, 27, 97, (1956).
9. G.V. Samsonov and L.Ya. Markovskii, *Uspekhi Khim.*, 25, 130, (1956).
10. G.B. Bokii, *Vvedenie v Kristallokhimiyu (Introduction to Crystal Chemistry)*, MGU (1954).
11. G.V. Samsonov, *Dokl. Akad. Nauk SSSR.*, 86, 329, (1952).
12. A.E. Koval'okii and L.A. Petrova, *Mikrotverdost' (Microhardness), Acad. Sci. USSR*, (1950).

VOL.
5
1957

THE NATURE OF ETCH-FIGURES IN AN AGEING Al-Zn-Cu ALLOY*

N.N. BUINOV and T.V. SHCHEGOLEVA
Institute of Metal Physics, Urals Filial, Academy of Sciences USSR

(Received 11 April 1957)

It is known from published data [1, 2], that the etch figures on crystals of different materials are associated with the emergence at the surface of screw and edge dislocations. In an electron microscope study of an Al-Zn-Cu alloy which had previously been rolled and homogenization annealed, we have observed spiral etch figures of roughly cubic form (Figs. 1 and 2). After partially ageing the alloy (without producing marked ordering) there can be seen on the steps of the etch figures clear bright marks (Fig. 2) which correspond either to Guinier-Preston zones or to particles of a precipitate phase.

The spirals which can be seen cannot be associated with dislocations having a unit Burgers vector. On the basis of the features of the oxide replica technique used for the examination in this case, it can be assumed that etch steps can only be observed in the electron microscope if the screw dislocations have a Burgers vector of not less than about 15–20 Å. In fact in our case the Burgers vector is apparently equal to some hundreds of Angstrom units. This follows both from analysis of stereoscopic photographs and from the excellent way in which the steps are revealed by means of the oxide replicas. Hence it can be concluded that each etch figure is associated with the emergence at the alloy surface of some large or gigantic screw dislocations, parallel to the cubic axes of the crystal. (In connexion with the observation in CaF_2 of helicoidal dislocations [5] it appeared possible to associate the spiral figures with helicoidal and prismatic dislocations). At the same time, at the midpoint of each side of the etch figure there generally emerges not one but several (most frequently three) screw dislocations of the same sign. However, the complexity of certain spiral etch figures gives grounds for assuming that in a number of cases dislocations of opposing signs emerge at the midpoints of the sides.

Thus, despite existing theoretical ideas [2], to the effect that there are no grounds for assuming the existence of large dislocations in metals, gigantic dislocations are observed. Such dislocations in metals having a Burgers vector of several hundred Angstrom units, have only previously been observed by Amelinckx [3] and Steiberg [4]. The first of these examine crystals of gold, grown by deposition from solution on an NaCl seed crystal, and the second, crystals of titanium, produced electrolytically. In both cases the phenomenon of gigantic screw dislocations was attributable to the special conditions, e.g. growth from alien crystals. Amelinckx pointed out that in his experiments the gold crystals could either have inherited the screw dislocations from the seed crystal of common salt, or have developed them because of the large discrepancy between the gold and NaCl crystal lattices. In our experiments special conditions of this type are apparently excluded.

Translated by E. Bishop

REFERENCES

1. P.B. Hirsch, *Progr. in Metal Phys.*, 6, 236, (1956).

2. A. Dzh. Forti, *Neposredstvennoe nablyudenie dislokatsii v Kristallakh (Direct observation of dislocations in crystals)*, Metallurgizdat (1956).

3. S. Amelinckx, *Phil. Mag.*, 43, 562, (1952).

4. M.A. Steinberg, *Nature*, 1704, 1119, (1952).

*Fiz. metal. metalloved., 5, No. 3, 566-567, 1957.

VOL
5
195

5. W. Bontinck, *Phil. Mag.*, 2, 561, (1957).

FIG. 1.

FIG. 2.

VOL.
5
1957

ERRATA*

In the last issue of the journal (vol. 5, No. 2) the photographs in Fig. 1 (*d*) and 1 (*e*) (page 237) in the article "About the domain structure of the strongly coercive alloy manganese-bismuth" by Ya. S. Shur, E.V. Shtol'ts, G.S. Kandaurova and L.V. Bulatova have been wrongly laid out due to a typographical error. The left-hand portions of Figs. 1 (*d*) and 1 (*d*) should be turned through 180°, placing them so that they should correspond to the right-hand portions of the Figs. (i.e. by lettering). On page 238, Fig. 3 (*a*) should also be turned through 180°, placing it analogous to Fig. 3 (*b*).

* Translated from the original Russian.

VOL
5
195

VOL.
5
1957